

**INVESTIGATION OF THERMAL SEMICONDUCTORS FOR ADAPTIVE HEAT
MANAGEMENT IN BUILDINGS**

by

Wesley Andrew Knotts

B.S. in Mechanical Engineering, University of Pittsburgh, 2008

Submitted to the Graduate Faculty of
the Swanson School of Engineering in partial fulfillment
of the requirements for the degree of
Master of Science in Mechanical Engineering

University of Pittsburgh

2010

UNIVERSITY OF PITTSBURGH
SWANSON SCHOOL OF ENGINEERING

This thesis was presented

by

Wesley Andrew Knotts

It was defended on

April 26, 2010

and approved by

Laura A. Schaefer, Ph. D, Associate Professor of Mechanical Engineering Department

Bong J. Lee, Ph. D, Assistant Professor of Mechanical Engineering Department

Thesis Advisor: William W. Clark, Ph. D, Professor of Mechanical Engineering Department

Copyright © by Wesley A. Knotts

2010

INVESTIGATION OF THERMAL SEMICONDUCTORS FOR ADAPTIVE HEAT MANAGEMENT IN BUILDINGS

Wesley A. Knotts, M.S.

University of Pittsburgh, 2010

Much focus has been recently placed on improving the energy efficiency of buildings through improved insulation in order to lower both energy consumption and carbon emissions worldwide. A new type of building insulation, smart insulation, shows great potential for lowering the heating and cooling energy usage of buildings by turning off the insulation whenever certain outside environmental conditions exist where it would be beneficial to remove the insulation. The specific type of smart insulation proposed is a thermal semiconductor that can be actuated to switch between a thermal conductor and a thermal insulator depending on the temperature gradient across the insulation. After careful examination of many different potential concepts thermal semiconductors, two main concepts involving contacting/non-contacting aluminum fins which allow or break a thermal conduction path and an inflatable honeycomb-like structure were chosen for fabrication and testing. Within these two main concepts, several different designs were developed and tested using an insulation test chamber constructed to reproduce the conditions the smart insulation prototypes would encounter in an real-world building setting. Once the experiment testing was completed, the different smart insulation devices were compared against each other and to a benchmark insulation test piece composed of conventional building insulation to evaluate their performance. Finally, a theoretical, finite element model was formulated for the testing of one of simplest smart insulation prototypes to better understand the results of the experimental testing and to examine other designs for smart insulation that were not experimentally tested.

TABLE OF CONTENTS

ACKNOWLEDGEMENTS	XIX
1.0 INTRODUCTION AND LITERATURE REVIEW	1
1.1 THE POTENTIAL OF SMART INSULATION	5
1.2 THERMAL SEMICONDUCTOR	6
1.3 EXISTING VARIABLE INSULATION DEVICES AND CONCEPTS.....	6
1.3.1 Thermal Semiconductors	7
1.3.2 Thermal Semiradiators.....	24
1.3.3 Thermal Semiconductors	29
1.4 POTENTIAL ENERGY CONSERVATION OF SMART INSULATION	37
1.4.1 Department of Energy Simulation of Smart or Active Insulation Systems	37
1.4.2 Why Further Study of Variable Thermal Resistance Insulation is Needed	42
1.4.3 High-Value Smart Insulation Building Applications	44
2.0 SMART INSULATION CONCEPT DEVELOPMENT AND FABRICATION.....	46
2.1 SMART INSULATION COMMON FEATURES.....	46
2.2 SHIFTING ALUMINUM FINS THERMAL SEMICONDUCTOR DEVELOPMENT	47
2.2.1 Shifting Aluminum Fins Thermal Semiconductor Concept	47
2.2.2 Shifting Aluminum Fins Thermal Semiconductor Design	49
2.2.3 Shifting Aluminum Fins Thermal Semiconductor Fabrication	53
2.3 VARIATIONS OF THE SHIFTING FINS THERMAL SEMICONDUCTOR.....	58
2.3.1 Using Foam Insulation in Spaces between the Fins Instead of Air	58
2.3.2 Using Silver- and Silicone-based Thermal Grease to Improve Thermal Conduction	60
2.3.3 Back-to-Back Aluminum Plates with Fins Concept	62

2.3.4	Variations of Shifting Aluminum Fins Thermal Semiconductor Modeled in ANSYS	64
2.4	INFLATABLE HONEYCOMB-LIKE STRUCTURE THERMAL SEMICONDUCTOR DEVELOPMENT	67
2.4.1	Inflatable Honeycomb-like Structure Thermal Semiconductor Concept...67	
2.4.2	Inflatable Honeycomb-like Structure Thermal Semiconductor Design.....70	
2.4.3	Reflectix Inflatable Thermal Semiconductor.....71	
2.4.4	NOVUS Inflatable Thermal Semiconductor.....76	
2.4.5	Variations of the Inflatable Thermal Semiconductor.....81	
3.0	INSULATION TEST CHAMBER FABRICATION AND EXPERIMENTAL SET-UP	83
3.1	SMART INSULATION TEST CHAMBER DEVELOPMENT.....	84
3.1.1	Insulation Test Chamber Interior Design.....84	
3.1.2	Insulation Test Chamber Overall Design and Fabrication.....88	
3.2	EXPERIMENTAL DATA ACQUISITION AND TESTING SET-UP	95
3.2.1	Temperature Measurement	95
3.2.2	Thermocouple Placement.....96	
3.2.3	Temperature Measurement Data Acquisition	99
3.2.4	Kapton Heater Equipment and Temperature Control of Bottom Air Space.....100	
3.2.5	Final Experimental Set-up	102
3.3	INSULATION TEST CHAMBER PERFORMANCE TEST.....	104
3.4	EXPERIMENTAL TESTING PARAMETERS.....	107
3.5	POLYISOCYANURATE FOAM INSULATION TEST PIECE	110
4.0	SMART INSULATION EXPERIMENTAL RESULTS AND DISCUSSION.....	113
4.1	SHIFTING FINS THERMAL SEMICONDUCTOR EXPERIMENTAL RESULTS.....	114
4.1.1	Basic Shifting Fins Thermal Semiconductor Testing Results	114
4.1.2	Shifting Fins Thermal Semiconductor with Insulation between Fins Testing Results.....122	
4.1.3	Shifting Fins Thermal Semiconductor with Thermal Greases Testing Results.....130	
4.1.4	Back-to-Back Aluminum Plates Thermal Semiconductor Testing Results.....132	

4.1.5	Folding Fins with Vertical Contact Testing Results.....	140
4.2	EMPTY CHAMBER CONSTANT TEMPERATURE TEST	145
4.3	INFLATABLE THERMAL SEMICONDUCTOR EXPERIMENTAL RESULTS.....	147
4.3.1	Reflectix Inflatable Thermal Semiconductor Testing Results	147
4.3.2	NOVUS Inflatable Thermal Semiconductor Testing Results	155
4.3.3	NOVUS Inflatable Thermal Semiconductor with Aluminum Plates Testing Results.....	162
4.4	DISCUSSION OF SMART INSULATION EXPERIMENTAL RESULTS	172
5.0	MODELING OF SHIFTING FINS THERMAL SEMICONDUCTOR WITH INSULATION BETWEEN THE FINS	175
5.1	DEVELOPMENT OF THE SHIFTING FINS PROTOTYPE TRANSIENT FINITE ELEMENT MODEL.....	176
5.1.1	Modeling of Shifting Fins Prototype with Thermal Contact Resistance Added.....	176
5.1.2	Meshing of Shifting Fins Prototype with Insulation between Fins.....	179
5.1.3	Modeling of Hot Side Air Space in Insulation Test Chamber	181
5.1.4	Modeling of Cold Side Air Space in Insulation Test Chamber	190
5.1.5	Thermal Boundary Conditions of FEA Model of Shifting Fins Prototype.....	194
5.2	RESULTS OF THE TRANSIENT FINITE ELEMENT MODELING OF THE SHIFTING FINS PROTOTYPE.....	196
5.3	OTHER VARIATIONS OF THE SHIFTING FINS PROTOTYPE MODELED	201
5.3.1	Shifting Fins with Side Contact Device Theoretical Model	201
5.3.2	Folding Fins with Vertical Contact Device Theoretical Model.....	206
5.3.3	Folding Fins with Side Contact Device Theoretical Model.....	213
6.0	CONCLUSION AND FUTURE WORK.....	218
6.1	CONCLUSION.....	218
6.2	FUTURE WORK.....	220
	BIBLIOGRAPHY	221

LIST OF TABLES

1	Energy Savings for Best Passive Insulation Case over Reference Case [23]	40
2	Energy Savings for Best Active Insulation Case [23].....	40
3	Yearly Cost Savings in 1990 using Best-Case Active Insulation System in Structure (Yearly Cost Savings not adjusted for inflation) [23].....	41
4	Smart Insulation Prototype Testing Experimental Set-up Electronic Equipment.....	104
5	Basic Shifting Fins Thermal Semiconductor Prototype Experimental Results.....	119
6	Shifting Fins Prototype with Insulation between the Fins Experimental Results	126
7	Back-to-Back Plates with Outward Facing Fins Thermal Semiconductor Experimental Results.....	138
8	Folding Fins Thermal Semiconductor Experimental Results	143
9	Reflectix Inflatable Thermal Semiconductor Experimental Results.....	151
10	NOVUS Inflatable Thermal Semiconductor Experimental Results.....	159
11	NOVUS Inflatable Thermal Semiconductor with Aluminum Plates Experimental Results	167
12	Material Properties used in Finite Element Analysis of Shifting Fins Device.....	179
13	Hot Side Air Space Convection Coefficients for Constant Temperature Boundary Condition.....	186
14	Hot Side Convection Coefficients for Constant Heat Flux Boundary Condition	189
15	Convection Coefficients used for Hot Side Air Space in FEA of Shifting Fins Device.....	190
16	Cold Side Air Space Convection Coefficients.....	194
17	Shifting Fins Prototype with Insulation between the Fins Theoretical Results	200
18	Shifting Fins with Side Contact Device Theoretical Results	205

19	Convection Coefficients for Air Gap in Folding Fins with Vertical Contact Device	210
20	Folding Fins with Vertical Contact Device Theoretical Results.....	212
21	Folding Fins with Side Contact Device Theoretical Results.....	216

LIST OF FIGURES

1	Overall U.S. Energy Consumption and Building Consumption Breakdown [1]	1
2	Comparison between Conventional and Smart Insulation for Sunny Winter Day Case.....	3
3	Comparison between Conventional and Smart Insulation for Clear Summer Evening Case.....	4
4	Conceptual Sketch of a Variable Conductance Roof Panel [2]	8
5	Invention Patented by Bovenkerk for a Variable Thermal Conduction Device using a metal hydride [5]	9
6	Hydrogen Gas Released vs. Hydride Temperature for Patent [5].....	10
7	Thermal Conductivity vs. Hydrogen Gas Pressure Measured for Patent [5].....	10
8	Invention Patented by Theodore Xenophou for a Variable Thermal Conduction Device using a Vacuum Pump [6].....	11
9	Sectional View of TA-CC3 Prototype [7].....	12
10	Measured Converter Cooldown of TA-CC3 Prototype [7].....	13
11	Side-View Drawing of FSTA VCI Enclosure Prototype [8]	14
12	Thermal Conductivity vs. Gas Pressure for Invention Patented by Honeywell International, Inc. [9].....	15
13	Vapor Pressure vs. Temperature for Invention Patented by Honeywell International, Inc. [9]	16
14	First Invention Patented by Riordan for a Variable Thermal Conduction Device Using a Temperature-Responsive Bimetallic Element [10].....	17
15	Second Invention Patented by Riordan for a Variable Thermal Conduction Device Using a Temperature-Responsive Bimetallic Element [10].....	18

16	Third Invention Patented by Riordan for a Variable Thermal Conduction Device Using a Thermally Expansive Medium [10].....	18
17	Invention Patented by Potter for a Variably Insulating Portable Heater/Cooler [11].	20
18	Invention Patented by Laing for an Inflatable Insulation Device [12]	22
19	Insulator State of Smart Thermal Insulation System by Al-Nimr, Asfar, and Abbadi [14].....	23
20	Conductor State of Smart Thermal Insulation System by Al-Nimr, Asfar, and Abbadi [14].....	24
21	Principle of the VARES Radiator [16]	26
22	OHP System of the VARES Technology [16].....	27
23	VARES Technology Demonstrator Model (TDM): VARES Radiator Connected to Copper Electronics Simulator [16]	28
24	How Liquid Crystal Panels of Smart Greenhouse Work [17].....	29
25	Invention Patented by Ingeborg and Nickolaus Laing for a Variable Convection Insulation [19]	30
26	Invention Patented by Davis and Strohlein for an Inflatable Heat Barrier [20].....	31
27	Diagram of the Thermodiode Employed in the Experimental Study [22]	32
28	How Changing the Inclination Angle of the Fluid Loops Changes the Direction of Effective Heat Flow [22]	34
29	Indoor Test Results for a Radiation Flux of 800 W/m ² : a) Heating Phase; (b) Cooling Phase [21]	35
30	Temperature Variations of the Thermodiode Module under Reverse-Biased for a Radiation Flux of 800 W/m ² [21].....	36
31	Flow Chart of Simulation Process for Passive and Active Insulation System Structures [23]	38
32	Contacting/Non-contacting Aluminum Fins Thermal Semiconductor Concept	48
33	Schematic Showing How Screws are Used to Join Aluminum Fins and Plates	50
34	CAD Drawing of Shifting Fins Thermal Semiconductor Prototype in its Insulating Configuration	52
35	CAD Drawing of Shifting Fins Thermal Semiconductor Prototype in its Conducting Configuration	53

36	Schematic that Illustrates How Small Air Gaps can Result from Different Fin Heights during Fabrication	55
37	CAD Model of Shifting Fins Prototype with Screw Holes Added	56
38	Bottom Piece of Shifting Fins Smart Insulation Device Prototype	57
39	Shifting Fins Thermal Semiconductor Prototype Conducting Configuration.....	57
40	Shifting Fins Thermal Semiconductor Prototype Insulating Configuration	58
41	Bottom Piece of Shifting Fins Thermal Semiconductor Prototype with Foam Insulation between Fins	59
42	Shifting Fins Thermal Semiconductor Prototype with Foam Insulation between Fins in its Insulating State.....	60
43	Schematic Diagram of the Effects of Thermal Contact Resistance at the Interface between Two Surfaces [27]	61
44	Application of Silver-Based Thermal Grease to the Bottom Fins of the Shifting Fin Prototype.....	62
45	Back-to-Back Aluminum Plates with Fins Device in its Conducting Configuration.....	63
46	Back-to-Back Aluminum Plates with Fins Device in its Insulating Configuration	64
47	Insulating and Conducting States of Fins Shifting with Side Contact ANSYS Model.....	65
48	Insulating and Conducting States of Fins Fold in with Vertical Contact ANSYS Model	66
49	Conducting State of Fins Fold in with Side Contact ANSYS Model	67
50	Inflatable honeycomb-like Structure Thermal Semiconductor Concept.....	68
51	2-D Side-View Schematic of Inflatable Honeycomb-like Structure for Thermal Semiconductor Concept	69
52	Side-View of One Layer of Reflectix Building Insulation	72
53	Top-View of One Layer of Reflectix Building Insulation	72
54	Reflectix Inflatable Thermal Semiconductor Prototype in its Insulating Configuration	73
55	Close-Up View of Reflectix Inflatable Thermal Semiconductor in its Insulating State.....	73
56	Reflectix Inflatable Thermal Semiconductor Prototype in its Conducting Configuration.....	75
57	Close-Up View of Reflectix Inflatable Thermal Semiconductor in its Conducting State	75

58	Side-by-Side Comparison of Reflectix Inflatable Thermal Semiconductor Inflated and Deflated Prototypes	75
59	Top-View of One Layer of NOVUS Packaging Material.....	78
60	NOVUS Inflatable Thermal Semiconductor Prototype in its Insulating Configuration	79
61	Close-Up View of NOVUS Inflatable Thermal Semiconductor in its Insulating State.....	79
62	NOVUS Inflatable Thermal Semiconductor Prototype in its Conducting Configuration	80
63	Close-Up View of NOVUS Inflatable Thermal Semiconductor in its Conducting State	80
64	Side-by-Side Comparison of NOVUS Inflatable Thermal Semiconductor Inflated and Deflated Prototypes.....	81
65	NOVUS Inflatable Thermal Semiconductor Prototype with Aluminum Plates for Compression in its Insulating State.....	82
66	NOVUS Inflatable Thermal Semiconductor Prototype with Aluminum Plates for Compression in its Conducting State.....	82
67	Bottom Air Space of the Smart Insulation Test Chamber with Kapton Heater Heat Source	86
68	Insulation Test Chamber Interior with Smart Insulation Prototype Inserted	87
69	Front Wall of Insulation Test Chamber showing Seven Layers Bonded Together	89
70	Side-View of Final Insulation Test Chamber Fabricated showing How Individual Walls Fit Together	91
71	Front-View of Final Insulation Test Chamber Fabricated showing How Individual Walls Fit Together.....	91
72	L-shaped Metal Angle Bracket Applied to Corner of Front Removable Wall	92
73	Process of How Front Removable Wall is used to Open and Close Test Chamber.....	93
74	Process of How Top Removable Wall is used to Open and Close Test Chamber.....	94
75	Locations of Thermocouple Holes: a) Front Thermocouple Hole; b) Top Thermocouple Hole.....	94
76	Final Fabricated Insulation Test Chamber with Front and Top Removable Walls Closed....	95
77	Hot Side Air Space Thermocouple Placement	97
78	Cold Side Air Space Thermocouple Placement.....	98

79	Reflectix Inflatable Smart Insulation Prototype Showing the General Thermocouple Placement on the Hot and Cold Sides of the Smart Insulation Devices	99
80	Top View of the Experimental Set-up Electronic Equipment	103
81	View of the Overall Experimental Set-up for the Insulation Test Chamber	103
82	Largest Gap in Insulation Test Chamber between Front Removable Wall and Front Frame for Potential Greatest Heat Losses	106
83	Chamber Thermal Efficiency Test Results	106
84	Final Fabricated Benchmark Insulation Test Piece.....	111
85	Plot of Benchmark Insulation Test Piece Constant Temperature Test	112
86	Basic Shifting Fins Smart Insulation Prototype in Test Chamber	114
87	Shifting Fins Smart Insulation Prototype Plates' Thermocouple Placement	115
88	Basic Shifting Fins Thermal Semiconductor Prototype Conducting State, Constant Temperature Test	117
89	Basic Shifting Fins Thermal Semiconductor Prototype Insulating State, Constant Temperature Test	117
90	Basic Shifting Fins Thermal Semiconductor Prototype Conducting State, Constant Heat Flux Test.....	118
91	Basic Shifting Fins Thermal Semiconductor Prototype Insulating State, Constant Heat Flux Test.....	118
92	Comparison between Basic Shifting Fins Prototype Conducting and Insulating States for Constant Temperature Tests	120
93	Comparison between Basic Shifting Fins Prototype Conducting and Insulating States for Constant Heat Flux Tests.....	121
94	Shifting Fins Smart Insulation Prototype with Foam Insulation between Fins in Test Chamber.....	123
95	Shifting Fins Thermal Semiconductor Prototype with Insulation between the Fins Conducting State, Constant Temperature Test	124
96	Shifting Fins Thermal Semiconductor Prototype with Insulation between the Fins Insulating State, Constant Temperature Test	124
97	Shifting Fins Thermal Semiconductor Prototype with Insulation between the Fins Conducting State, Constant Heat Flux Test.....	125

98	Shifting Fins Thermal Semiconductor Prototype with Insulation between the Fins Insulating State, Constant Heat Flux Test.....	125
99	Comparison between Shifting Fins Thermal Semiconductor with Insulation Between the Fins Conducting and Insulating States for Constant Temperature Tests	127
100	Comparison between Shifting Fins Thermal Semiconductor with Insulation between the Fins Conducting and Insulating States for Constant Heat Flux Tests.....	128
101	Conducting State Comparison between Shifting Fins Thermal Semiconductors with Air or Foam Insulation between the Fins	129
102	Insulating State Comparison between Shifting Fins Thermal Semiconductors with Air or Foam Insulation between the Fins	130
103	Back-to-Back Plates with Fins Smart Insulation Prototype in Test Chamber	132
104	Back-to-Back Plates with Fins Smart Insulation Prototype Plates' Thermocouple Placement.....	134
105	Back-to-Back Plates with Fins Thermal Semiconductor Prototype Conducting State, Constant Temperature Test.....	135
106	Back-to-Back Plates with Fins Thermal Semiconductor Prototype Insulating State, Constant Temperature Test	136
107	Back-to-Back Plates with Fins Thermal Semiconductor Prototype Conducting State, Constant Heat Flux Test	136
108	Back-to-Back Plates with Fins Thermal Semiconductor Prototype Insulating State, Constant Heat Flux Test.....	137
109	Comparison between Back-to-Back Plates with Fins Conducting and Insulating States for Constant Temperature Tests	137
110	Folding Fins with Vertical Contact Insulating State Device in Insulation Test Chamber ...	141
111	Folding Fins Thermal Semiconductor Insulating Configuration, Constant Temperature Test	142
112	Folding Fins Thermal Semiconductor Insulating Configuration, Constant Heat Flux Test.....	143
113	Comparison between the Conducting and Insulating States of the Folding Fins Thermal Semiconductor for the Constant Temperature Tests	144
114	Empty Insulation Test Chamber Constant Temperature Test	146
115	Reflectix Inflatable Smart Insulation Prototype in Chamber	148

116	Reflectix Inflatable Thermal Semiconductor Prototype Conducting State, Constant Temperature Test.....	149
117	Reflectix Inflatable Thermal Semiconductor Prototype Insulating State, Constant Temperature Test	149
118	Reflectix Inflatable Thermal Semiconductor Prototype Conducting State, Constant Heat Flux Test	150
119	Reflectix Inflatable Thermal Semiconductor Prototype Insulating State, Constant Heat Flux Test.....	152
120	Comparison between Reflectix Inflatable Prototype Conducting and Insulating States for Constant Temperature Tests.....	152
121	Comparison between Reflectix Inflatable Prototype Conducting and Insulating States for Constant Heat Flux Tests	153
122	NOVUS Inflatable Smart Insulation Prototype in Chamber	156
123	NOVUS Inflatable Thermal Semiconductor Prototype Conducting State, Constant Temperature Test.....	157
124	NOVUS Inflatable Thermal Semiconductor Prototype Insulating State, Constant Temperature Test	157
125	NOVUS Inflatable Thermal Semiconductor Prototype Conducting State, Constant Heat Flux Test	158
126	NOVUS Inflatable Thermal Semiconductor Prototype Insulating State, Constant Heat Flux Test.....	160
127	Comparison between NOVUS Inflatable Prototype Conducting and Insulating States for Constant Temperature Tests.....	160
128	NOVUS Inflatable Prototype with Aluminum Plates in Chamber Experimental Set-up.....	162
129	NOVUS Inflatable Thermal Semiconductor with Aluminum Plates Prototype Conducting State, Constant Temperature Test	163
130	NOVUS Inflatable Thermal Semiconductor with Aluminum Plates Prototype Insulating State, Constant Temperature Test	164
131	NOVUS Inflatable Thermal Semiconductor with Aluminum Plates Prototype Conducting State, Constant Heat Flux Test.....	164
132	NOVUS Inflatable Thermal Semiconductor with Aluminum Plates Prototype Insulating State, Constant Heat Flux Test.....	165
133	Comparison between NOVUS Inflatable Prototype with Aluminum Plates Conducting and Insulating States for Constant Temperature Tests	165

134	Comparison between NOVUS Inflatable Prototype with Aluminum Plates Conducting and Insulating States for Constant Heat Flux Tests.....	166
135	Conducting State Comparison between NOVUS Inflatable Thermal Semiconductors with or without Aluminum Plates	169
136	Insulating State Comparison between NOVUS Inflatable Thermal Semiconductors with or without Aluminum Plates	169
137	Back-to-Back Aluminum Plates Constant Temperature Test	171
138	Comparison of Fins-Related Prototype ΔT Values to Ideal Smart Insulation Case.....	172
139	Comparison of Inflatable Prototype ΔT Values to Ideal Smart Insulation Case.....	173
140	Conducting State of Shifting Fins Prototype Constructed in FEA Software	177
141	Insulating State of Shifting Fins Prototype Constructed in FEA Software.....	178
142	Close-Up View of Air Spaces Added at Interface between Contacting Fins.....	178
143	Shifting Fins Prototype Mesh at Interface between Upper Fins and Top Plate of Device...	181
144	Schematic of How Hot Side Air Space Heating is applied to Shifting Fins Device.....	183
145	Areas of Hot Side Plate over which 1-D Link Elements Act.....	183
146	Hot Side Air Space and Shelf Conditions Applied to Hot Side Plate in FEA Model.....	184
147	How LINK32 and LINK34 elements represent Cold Side Air Space in FEA Model.....	192
148	Cold Side Air Space Conditions Applied to Cold Side Plate in FEA Model.....	193
149	Final Thermal FEA Model of Shifting Fins Prototype with Insulation between Fins in Test Chamber Set-up.....	196
150	Comparison of Theoretical and Experimental Results for Conducting State of Shifting Fins Prototype with Insulation between Fins	198
151	Comparison of Theoretical and Experimental Results for Insulating State of Shifting Fins Prototype with Insulation between Fins	199
152	Conducting State of Shifting Fins with Side Contact Device Constructed in FEA Software	202
153	Insulating State of Shifting Fins with Side Contact Device Constructed in FEA Software	202
154	Shifting Fins with Side Contact Device Theoretical Results for Conducting State.....	203

155	Shifting Fins with Side Contact Device Theoretical Results for Insulating State.....	204
156	Conducting State of Folding Fins with Vertical Contact Device Constructed in FEA Software	206
157	Insulating State of Folding Fins with Vertical Contact Device Constructed in FEA Software	207
158	How LINK32 and LINK34 elements Modeled Conduction and Convection across Air Gap.....	208
159	Folding Fins with Vertical Contact Device Theoretical Results for Conducting State.....	211
160	Folding Fins with Vertical Contact Device Theoretical Results for Insulating State	211
161	Conducting State of Folding Fins with Side Contact Device Constructed in FEA Software	214
162	Folding Fins with Side Contact Device Theoretical Results for Conducting State	215

ACKNOWLEDGEMENTS

First, I would like to thank my advisor Dr. William Clark and my co-advisor Dr. Laura Schaefer. Dr. Clark has been an excellent advisor over the course of my project, and I have had a very good experience working under him in the Vibration and Control Lab at the University of Pittsburgh. Dr. Schaefer provided me valuable research experience to prepare me for my graduate work in the form of undergraduate research and a summer research internship in the area of thermoacoustics.

Besides my two advisors I would also like to thank several other individuals at the University of Pittsburgh who greatly assisted me over the course of my thesis project. First, I would like to thank Dr. Changki Mo for all of his help during the smart insulation project. Changki helped greatly during the development of the prototypes, the test chamber, and the experimental set-up, while also providing me with a great deal of previous literature for smart insulation concepts. Next, I would also like to thank Andy Holmes, the supervisor of the student machine shop for the Swanson School of Engineering, for all of his help and advice during the fabrication of prototypes in the student machine. In addition to the people mentioned at the University of Pittsburgh, I would also like to thank two teachers I had in high school, Mr. Phil Carey, and Mr. Pete Karpyk for getting me excited about science and engineering.

Finally, I would like to thank my family for their love and support during my undergraduate and graduate studies. My mother, father, and brother have always encouraged me to do my very best and have gone above and beyond to help me greatly during my time in the School of Engineering at the University of Pittsburgh. I would also like to thank my late grandfather for providing me with the inspiration to become a mechanical engineer during my time in high school and college.

1.0 INTRODUCTION AND LITERATURE REVIEW

Improving the energy efficiency of buildings has been one of the main focuses in recent years toward lowering energy consumption and carbon emissions in both the United States and worldwide. As shown in Figure 1, in the United States, buildings account for nearly 40% of overall energy consumption. Within building energy consumption, heating and cooling loads account for 42% and 29% of residential and commercial building energy consumption respectively, resulting in much effort placed toward improvements in the implementation of conventional insulation materials.

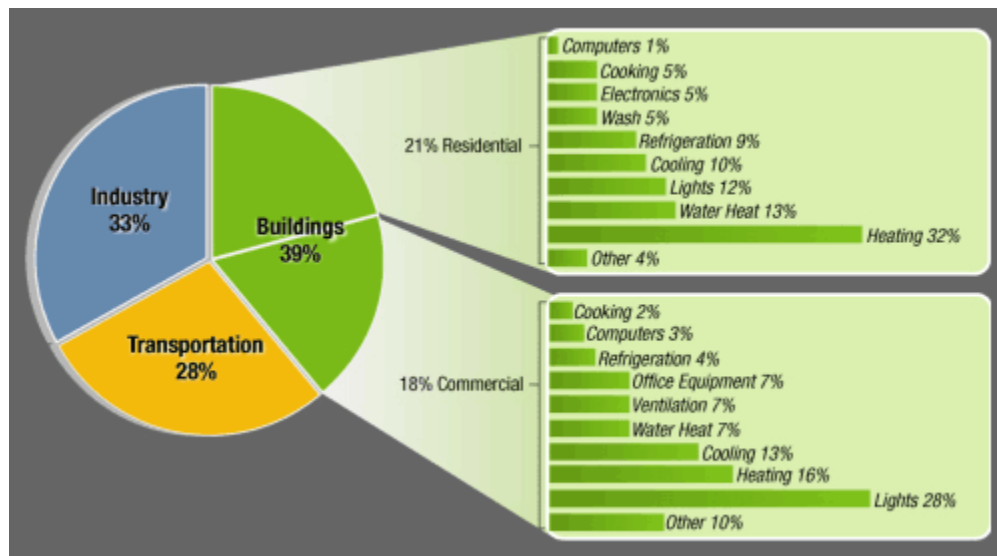


Figure 1: Overall U.S. Energy Consumption and Building Consumption Breakdown [1].

The main purpose of conventional insulation is to passively prevent heat transfer in either direction between the building interior and the cold outside environment, to maintain a desired temperature gradient over the insulation at all times. For example, during a cold winter night, conventional insulation helps to maintain the temperature difference between the warm building interior and the cold outside environment, helping to reduce the load on the building's heating system. Most conventional insulation materials today make use of the fact that static air is a poor conductor of heat, so their volumes are made primarily of air to eliminate conduction. Because convection currents in air can greatly increase the total heat transfer, insulators divide the air into many small volumes to practically eliminate convection. In general, the only existing ways to improve the energy efficiency of conventional insulation are through either developing higher R-value insulation or insulating to the maximum amount that can be cost-justified [2]. The main focus of this thesis is to look to the field of smart materials and structures to begin the development of a new type of insulation materials, smart insulation, to lower building heating and cooling loads.

The basic idea behind smart insulation is that certain temperature gradients occur for buildings where it would be beneficial to remove the insulation and allow some heat transfer to flow between the interior of the building and the outside walls or ambient environment. By acting as an active component instead of passive conventional building insulation, smart insulation is able to switch between low and high heat transfer states to take advantage of these cases. Two main cases that illustrate times where little or no building insulation would be advantageous would be the sunny winter day and cool summer evening cases.

During the winter in most areas of the United States, it would usually be beneficial to have building insulation with a very low thermal conductivity to maintain the interior building space at temperatures much warmer than the cold outside environment. In the afternoon of a sunny winter day, however, thermal radiation can cause heat to build up on the building walls and in the attic to temperatures much higher than the interior building space. If the building insulation could be "turned off" to allow heat to flow across it, the thermal radiation could be used to help heat the building interior, lowering building

energy consumption. Figure 2 shows a comparison between conventional and smart building insulation for the sunny winter day case. Conventional insulation blocks the flow of the thermal radiation from the walls and attic to the interior of the building, resulting in any beneficial heating from the thermal radiation being lost. On the other hand, smart insulation is able to "turn off" the insulator state allowing the thermal radiation to transfer heat to the building interior and lower heating costs.

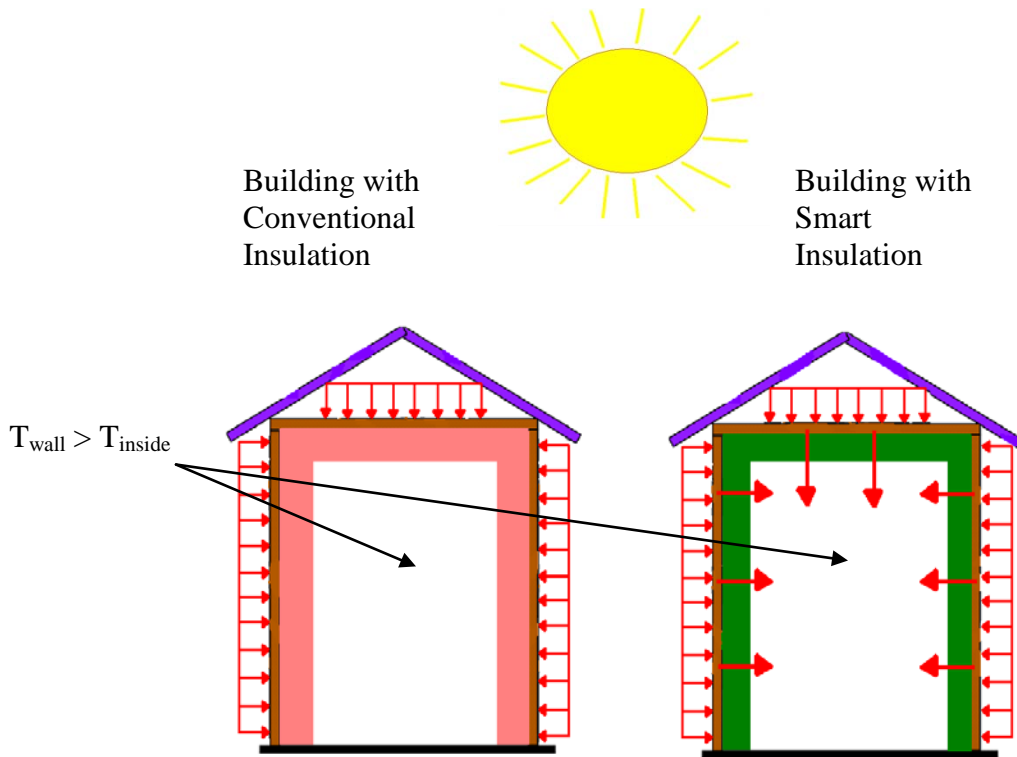


Figure 2: Comparison between Conventional and Smart Insulation for Sunny Winter Day Case.

For the second case during the summer in most areas of the United States, it would also be beneficial most of the time to have very low thermal conductivity insulation to maintain the interior building space at temperatures cooler than the hot outside environment. In the evening or at night on a clear summer day, however, the outside temperature can drop rapidly to a cooler, comfortable temperature. Sometimes, homeowners try to take advantage of this effect by opening windows or using whole-house fans to allow

air to transfer heat from the building interior to the cooler outside environment, but often homeowners will continue to use their centralized air conditioning system instead of taking advantage of the cool outside environment. If the building insulation could be "turned off" to allow heat to transfer from the building interior to the outside environment, it would have a similar effect to opening windows except on a much larger level, since it would be like "taking the attic off" or "taking the walls off" of the building. Unlike opening windows, however, smart insulation would only transfer heat and not air between the building interior and outside environment, which would allow the comfortable humidity level of the conditioned air inside of many buildings to be maintained, while preventing very humid or very dry air from transferring from the outside environment into the building as with windows. Figure 3 shows a comparison between conventional and smart building insulation for the cool summer evening case. Conventional insulation blocks heat from flowing from the interior of the building to the cooler outside environment, resulting in any beneficial cooling being lost. On the other hand, smart insulation is able to "turn off" the insulator state allowing the heat to transfer from the building interior to the outside environment, lowering cooling costs.

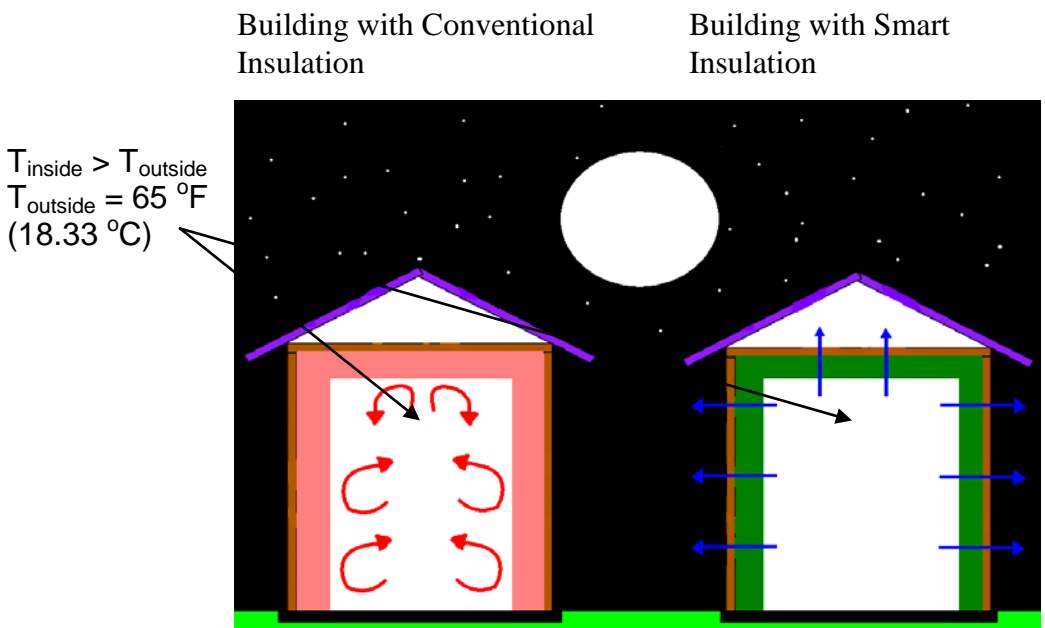


Figure 3: Comparison between Conventional and Smart Insulation for Clear Summer Evening Case.

1.1 THE POTENTIAL OF SMART INSULATION

Smart insulation that can change from an insulator to a conductor when a beneficial temperature gradient exists between the building interior and outside environment would help to greatly lower heating and cooling loads for both residential and commercial buildings. From studies conducted by Neeper and McFarland for the U.S. Department of Energy, it was found that the potential exists for solar energy to supply almost all space heating needs in the continental United States [3]. For both of their studies, an example small rectangular building with 1200 ft² (111.48 m²) of floor and projected horizontal roof area and 8 ft. (2.44 m) high walls, a heating load of 7200 Btu/DD (degree-day), R-20 ft² F-hr/Btu (3.52 m² K/W) building insulation, and double-glazed windows were utilized. [4]. Using the example building with a worst-case heating scenario of the month of January for very cold or cloudy locations, Neeper found that the insolation on the roof alone exceeded 80% of the building's heating load, and the insolation on the south wall alone exceeded 50% of the building's heating load at all locations [4]. Even in the coldest month in severe climates of the continental U.S., the insolation on the roof and walls of the example building far exceeded the heating requirements. If smart insulation can switch to its conductor state at times to take advantage of this insolation, it is easy to see how buildings' heating costs and energy consumption can be significantly reduced. In addition, although the environmental cooling resource would not be able to completely supply all of the cooling needs of buildings in the continental U.S., Neeper and McFarland did conclude that the environment provides sufficient resources to potentially supply half of all cooling loads in the continental U.S. [4]. Therefore, smart insulation that can take advantage of the environmental cooling resource would be able to significantly reduce building' cooling costs and loads. Now that the potential benefits of smart insulation have been illustrated, the following sections will examine several of the ideas, concepts, and devices that have been previously developed involving smart or variable insulation.

1.2 THERMAL SEMICONDUCTOR

In developing a type of smart insulation that could switch between low and high heat transfer states, conduction was chosen as the main method of heat transfer. Smart insulation must be able to switch between a low and high thermal conductivity state whenever it is necessary to inhibit or allow heat transfer by the application by an external trigger. This makes smart insulation analogous to the thermal equivalent of an electric semiconductor in that it must be able to switch between low and high conductivity states upon stimulation by an external trigger, such as a current or voltage. The concepts that were developed in this thesis were thus classified as thermal semiconductors because of their similarity to electrical semiconductors. In extension of the concept of a thermal semiconductor, previous concepts for variable insulation developed that are able to switch between low and high heat transfer states as well using other methods of heat transfer were classified as thermal semiradiators and thermal semiconductors, since for them convection and radiation heat transfer can be inhibited or allowed by application of an external trigger as well.

1.3 EXISTING VARIABLE INSULATION DEVICES AND CONCEPTS

Many different concepts have been previously proposed for variable insulation devices, but only a few of the concepts have advanced to the next phase of actual fabrication and experimentation. The concepts are divided into three different types of variable insulation systems according to whether their primary mode of heat transfer is conduction, radiation, or convection: thermal semiconductors, thermal semiradiators, and thermal semiconductors.

1.3.1 Thermal Semiconductors

Thermal semiconductor devices that can switch between an insulator state and a conductor state have many possible applications, including use as smart building insulation. Potter and Tuluca provided an example of how a variable conductance insulation might be applied to the roof of a building, for situations such as the sunny winter day case, as shown in Figure 4 [2]. Transparent convection suppression is used to ensure that any solar heating captured by the absorbed/radiator surface is transferred to the interior of the building and not convected back out to the likely colder outside environment [2]. A very efficient absorber/radiator surface is necessary to make sure as much of the thermal radiation imparted on the roof is captured as possible [2]. Finally, a thermal storage medium is included in the design so that solar heat captured can be stored and utilized at later times [2]. When it is not beneficial for high heat transfer across the insulation, the variable conductance insulation can be switched to its insulator state. The following sections present a survey of the different types of thermal semiconductor concepts previously developed [2].

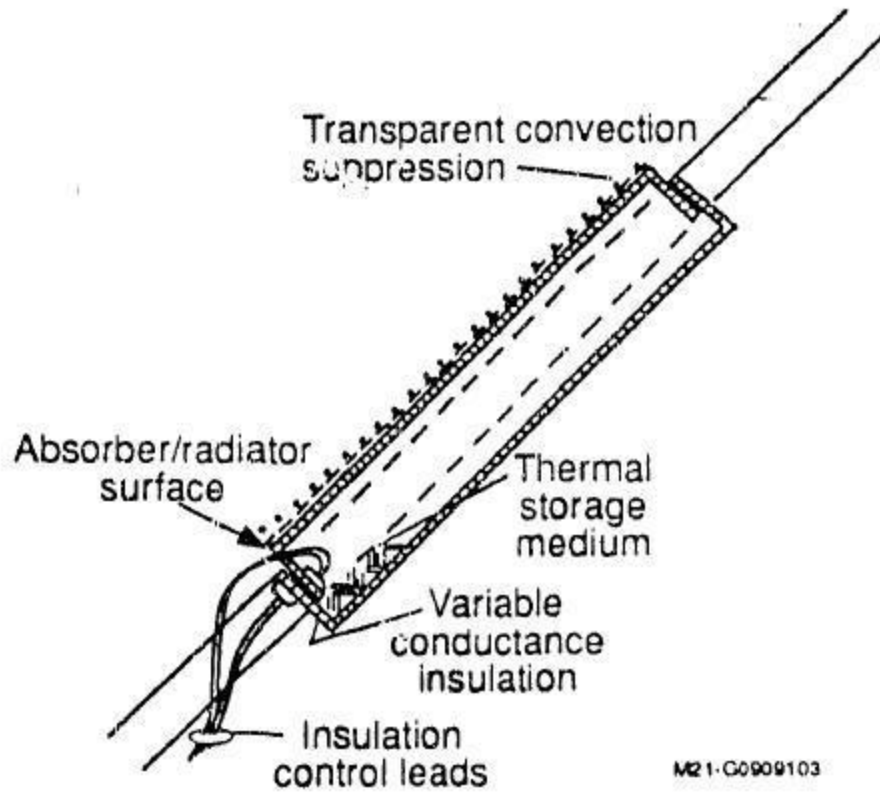


Figure 4: Conceptual Sketch of a Variable Conductance Roof Panel [2].

Vacuum Insulation with Variable Gaseous Conduction

Many different devices have been previously proposed for thermal semiconductors, but most of them fall into three or four general concepts. The first concept involves an insulation space that can change between containing a near vacuum, which would have a very low thermal conductivity, to containing a much higher thermal conductivity gas. The first person to file a patent for this idea was Bovenkerk in 1965 [5]. His proposed device, which is shown in Figure 5, consists of a metal hydride filled appendage given by items 15-17 in Figure 5, connected to an evacuated insulation panel given by items 10-14 [5].

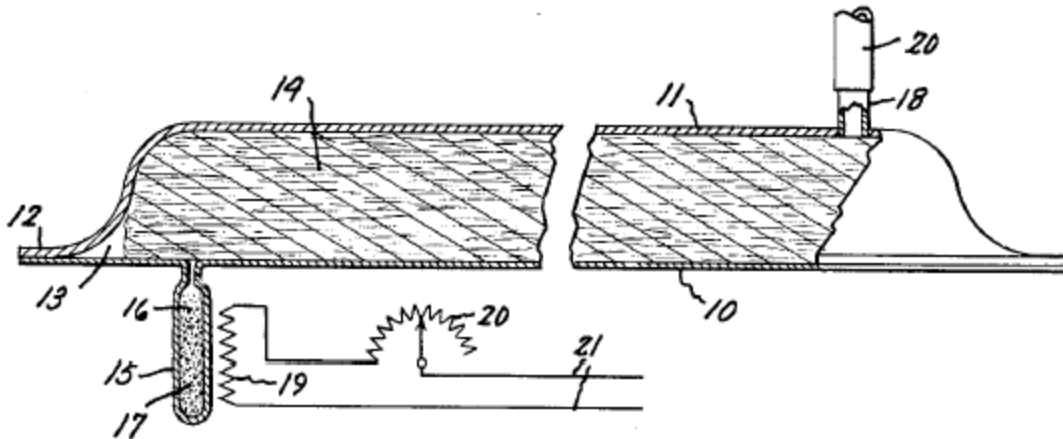


Figure 5: Invention Patented by Bovenkerk for a Variable Thermal Conduction Device using a metal hydride [5].

As the metal hydride is heated in the device by a heating element, a chemical reaction causes hydrogen gas to be released into the near vacuum of the insulation panel. Hydrogen gas was utilized because its thermal conductivity is much greater than other known gases, and hydrides are able to absorb and release large amounts of hydrogen to vary thermal conductivity over a large range [5]. As the metal hydride temperature increases, the amount of hydrogen gas released to the insulation panel also increases, which in turn causes the thermal conductivity of the insulation panel to increase as given in Figures 6 and 7 from the patent [5]. When the metal hydride's temperature is decreased, the metal hydride reabsorbs the hydrogen gas in the insulation panel, causes the gas pressure in the panel to decrease, reducing the thermal conductivity of the panel. Hence, by controlling the temperature of the metal hydride, the thermal conductivity and heat transfer of the insulation panel can be controlled [5].

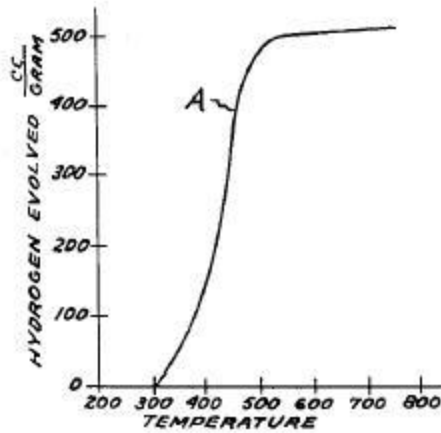


Figure 6: Hydrogen Gas Released vs. Hydride Temperature for Patent [5].

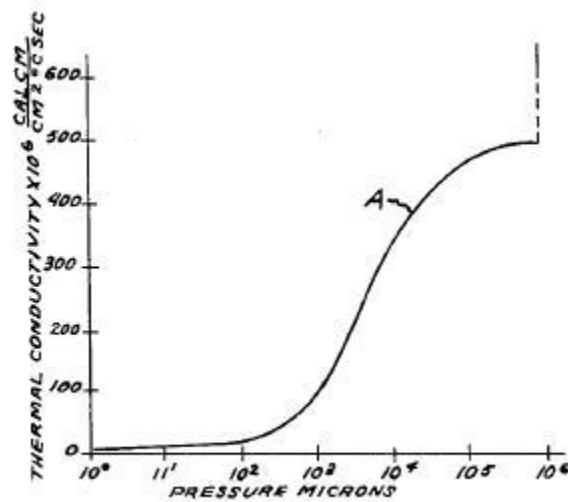


Figure 7: Thermal Conductivity vs. Hydrogen Gas Pressure Measured for Patent [5].

Another patent by Xenophou in 1976 uses an even simpler method for a variable thermal gaseous conduction system by varying the degree of vacuum between the inner and outer walls of buildings using a vacuum pump [6]. The system involves a cellular structure of stiffening members made up of

interconnecting strips extending between the panels that will hold their spacing when placed under vacuum conditions to prevent structural collapse [6]. Air can be pumped in and out of the cellular structure using holes within the structure and a vacuum pump [6]. Two diagrams of the variable insulation system proposed are shown in Figure 8 where items 7-9 in the diagram make up the vacuum pump [6]. Within the system, whenever heat transfer needs to be inhibited between the building interior and outside environment, the vacuum pump will be used to decrease the air pressure of the space between the walls to a very low level so that the thermal conductivity of the space will be very low [6]. When heat transfer is desired between the building interior and the outside environment, the air pressure of the space between the walls will increase toward normal pressure conditions, increasing the thermal conductivity of the space [6].

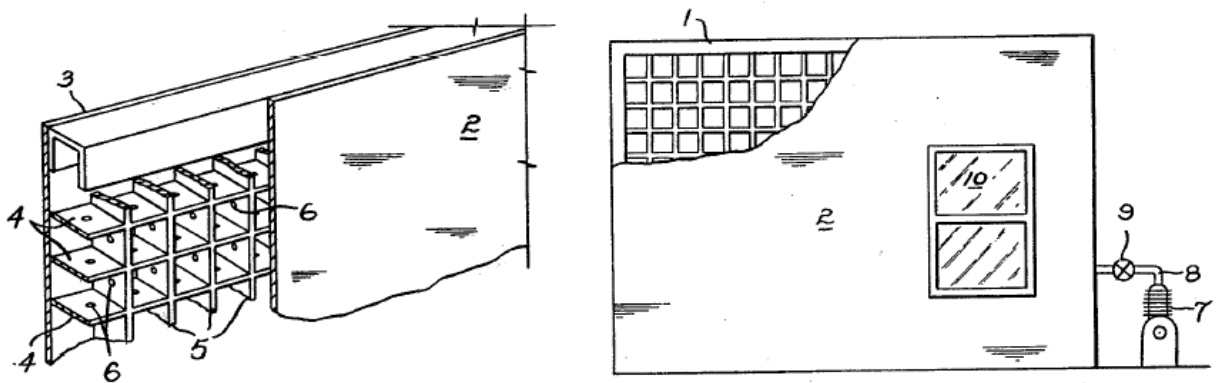


Figure 8: Invention Patented by Xenophou for a Variable Thermal Conduction Device using a Vacuum Pump [6].

By the mid-1990s variable conductance insulation involving the metal hydride concept was being developed for implementation in several different types of devices outside the field of building insulation. A joint study in 1995 between the National Renewable Energy Laboratory and the Chrysler Corporation focused on the use of variable conductance insulation (VCI) based on the metal hydride concept for the thermal management of an automotive catalytic converter [7]. In an effort to lower United States vehicle

emissions, VCI was utilized to solve the problem of cold-start emissions, which occur when a vehicle is first started, and the catalyst of the catalytic converter is at temperatures below its maximum effectiveness [7]. Similarly to the patent proposed beforehand, when the engine of the vehicle is running, the metal hydride is electrically heated to allow hydrogen gas to be released into the vacuum insulation to increase the thermal conductivity of the VCI [7]. The excess heat from the exhaust gases can then be rejected from the catalytic converter, preventing its overheating [7]. Later on, when the engine is turned off, the metal hydride decreases in temperature, which allows hydrogen gas to be reabsorbed from the vacuum insulation, lowering the thermal conductivity. This allows the catalytic converter to retain heat from when the engine is in operation to prevent cold-start emissions when the engine is first restarted [7]. To evaluate the reduction in emissions from use of a VCI, the authors of the study constructed several prototypes. The TA-CC3 prototype of a catalytic converter utilizing VCI shown in Figure 9 was installed in a Dodge Neon for FTP emissions testing [7].

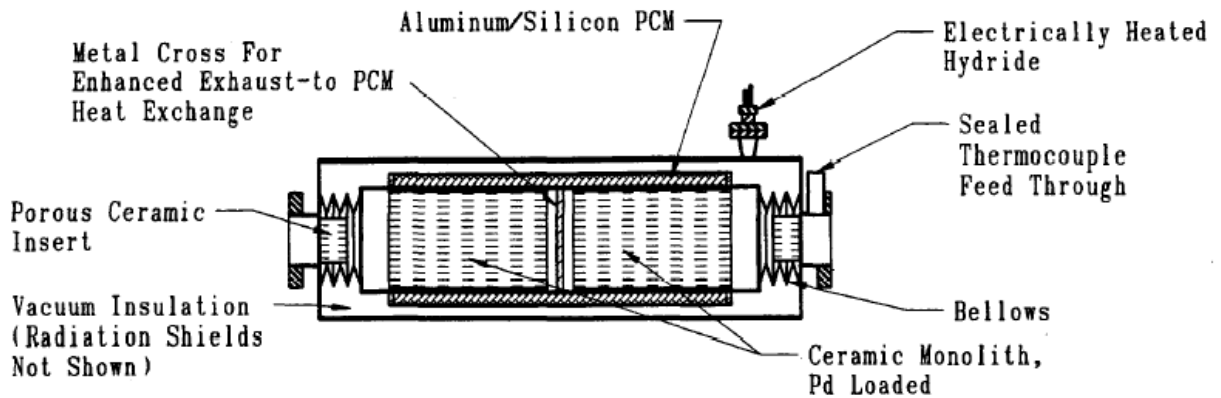


Figure 9: Sectional View of TA-CC3 Prototype [7].

First, a cooldown test was conducted in the study to evaluate the heat retention ability of the TA-CC3 prototype with the results given in Figure 10 [7].

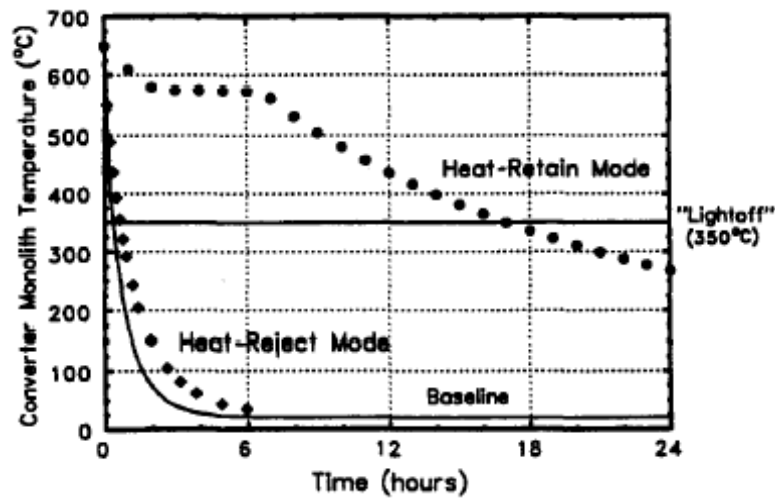


Figure 10: Measured Converter Cooldown of TA-CC3 Prototype [7].

When the insulation of the catalytic converter prototype has a high conductivity in its heat-reject mode, the prototype cools off very quickly like the baseline catalytic converter without varying thermal conductivity insulation [7]. When the insulation of the prototype has a low conductivity in its heat-retention mode, the catalyst is able to stay above its temperature for full effectiveness, its lightoff temperature, for up to 17 hours [7]. Emissions testing later showed that FTP-cycle cold-start CO and HC vehicle emissions were decreased by 52% and 29% following a 23-hour cold-soak at 27 °C [7].

Yet another automotive application for a VCI device involving a metal hydride was also pursued by Burch, Parish, and Keyser for the National Renewable Energy Laboratory for the thermal management of electric-vehicle batteries [8]. To achieve their optimum performance and durability, most electric-vehicle batteries require some thermal control to regulate heat transfer to their surroundings [8]. When the batteries are in normal operation or rapid recharge, high heat rejection from the battery is needed to prevent overheating, and when the batteries are not in operation or are in slow charges, high heat retention is necessary to prevent the stored energy from escaping [8]. By using the same type of VCI mentioned before in several patents and studies consisting of a metal hydride and a vacuum space, the thermal conductivity of the batteries' insulation can be varied by more than 100:1 between very low and very high

conductivity states [8]. For the study two full-scale prototypes of a VCI enclosure for batteries were designed and tested by the National Renewable Energy Laboratory to analyze its thermal management performance [8]. One of the two prototypes developed can be seen below in Figure 11 [8].

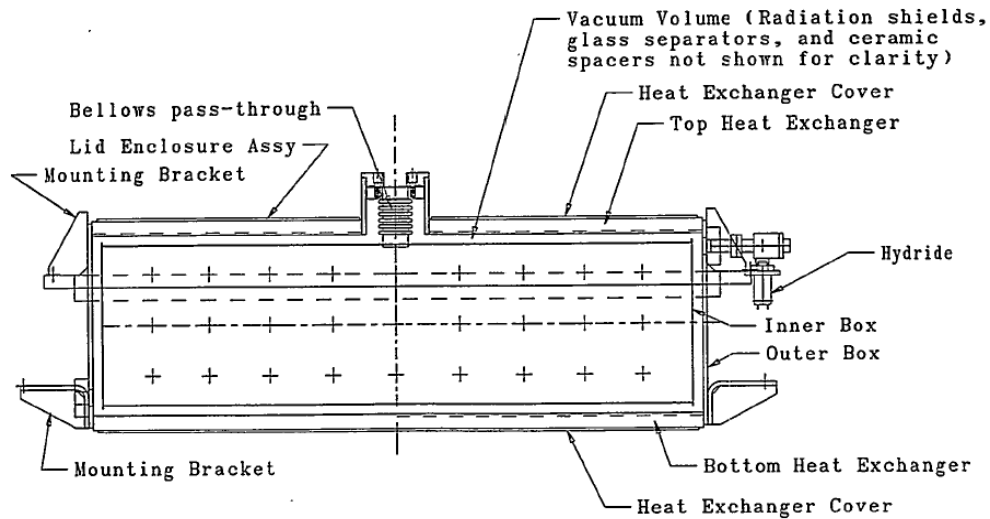


Figure 11: Side-View Drawing of FSTA VCI Enclosure Prototype [8].

The thermal conductivity of the VCI of the prototypes was shown to be able to vary from 0.12 W/m^2K to 13 W/m^2K from the results of experimental testing [8]. This shows that the batteries' insulation can be varied from a very low thermal conductivity when high heat retention is needed to a very high thermal conductivity when high heat rejection is needed [8].

Another variation on the concept of varying thermal conductivity by changing the pressure of a gas was given in a patent by for a variable thermal resistor system in 2008 by Eickhoff and Zhang [9]. Their variable conductance system is designed to be a passive system to maintain a device at a constant desired temperature [9]. Instead of using hydrogen gas in conjunction with a metal hydride to insulate their system, the vapor of a low pressure solid or liquid is utilized in a few mm-size gap between the device itself and a hermetically sealed shell surrounding the device [9]. The interior surface of the gap is coated

with either a low vapor pressure solid or liquid substance [9]. As the temperature of the device increases, the vapor pressure of the "low vapor pressure material" will increase, which will also increase the thermal conductivity of the gap due to gaseous conduction [9]. As shown below in Figures 12 and 13, over a temperature range of $-40\text{ }^{\circ}\text{C}$ to $85\text{ }^{\circ}\text{C}$, the gap's thermal conductivity can vary by up to five orders of magnitude [9].

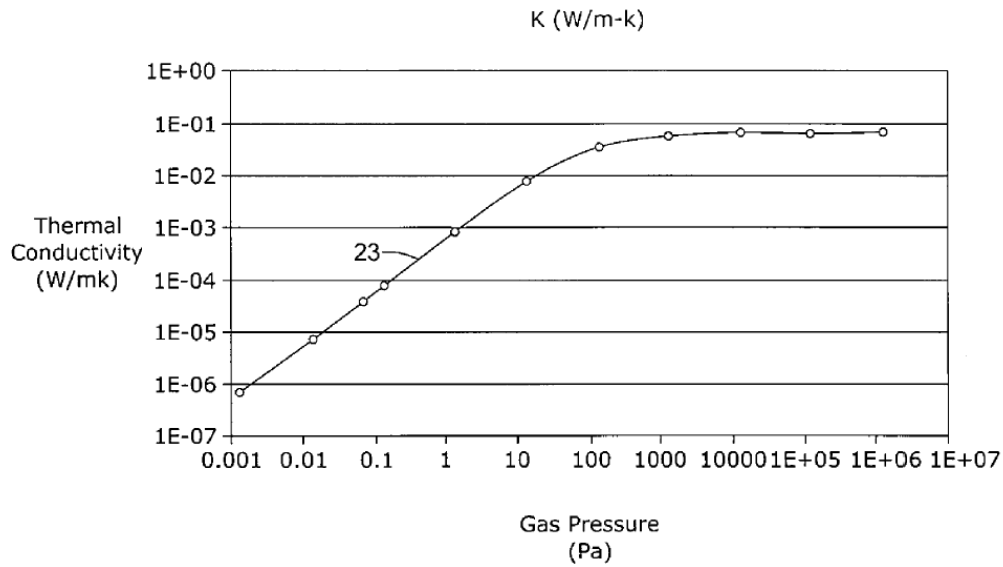


Figure 12: Thermal Conductivity vs. Gas Pressure for Invention Patented by Honeywell International, Inc. [9].

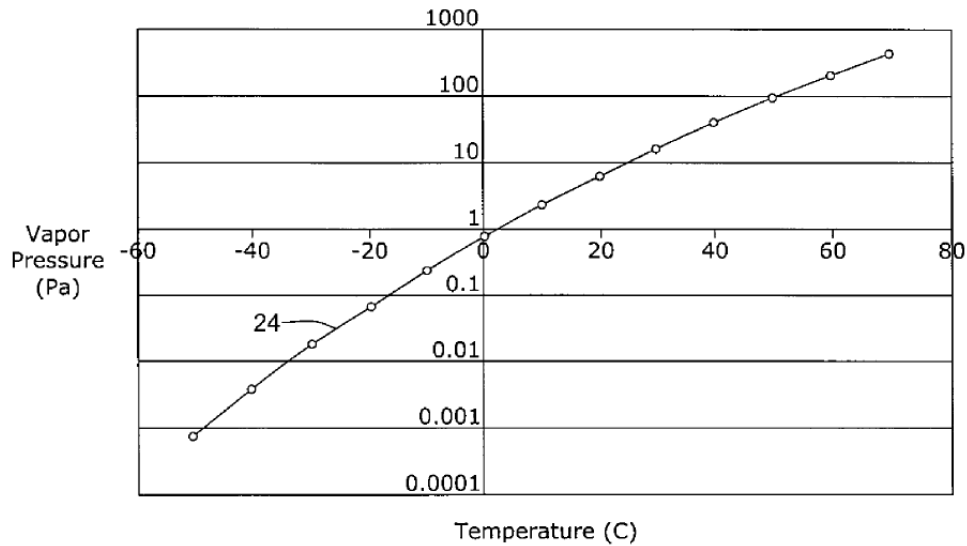


Figure 13: Vapor Pressure vs. Temperature for Invention Patented by Honeywell International, Inc. [9].

Bimetallic Switch Thermal Semiconductors

The second concept found in several patents for a thermal semiconductor involved the use a temperature-responsive bimetallic element. A bimetallic element consists of two metals with different thermal coefficients of expansion fused together. As the temperature of the bimetallic element increases, one of the metals will expand faster than the other one, causing the bimetallic element to bend to the side with the lower thermal coefficient of expansion. From the research, it appears that the second concept never evolved past the patent stage to actual fabrication and experimentation. In 1965, Riordan was the first to patent this idea with several different devices of this type designed to control the operating temperature of electronic component packages by controlling the heat transfer between the package and an attached heat sink [10]. The first device found in the patent uses a temperature-responsive bimetallic element attached to the heat sink and placed in a gap containing a gas or liquid between the heat sink and the electronic component package as shown in Figure 14 [10]. The device is designed so that as the temperature of the heat sink increases, the bimetallic element will bend toward the electronic component package to decrease the width of the gap, which will increase the heat transfer by conduction across the gap [10]. Later when

the temperature of the heat sink decreases, the bimetallic element will bend back to its original position to decrease the width of the gap and consequently the conductive heat transfer [10].

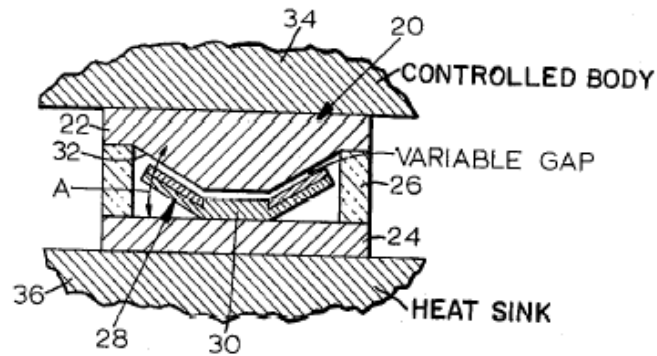


Figure 14: First Invention Patented by Riordan for a Variable Thermal Conduction Device Using a Temperature-Responsive Bimetallic Element [10].

The second device proposed in the patent also involves a temperature-responsive bimetallic element, but in this device the effective contact area between the bimetallic element and the electronic component package is varied instead of gap width [10]. When the heat sink of the device is at low temperatures, the effective contact area between the heat sink and the package will be very low, resulting in very low conductive heat transfer as shown in Figure 15 [10]. Then, as the temperature of the heat sink increases, the bimetallic element will bend toward the electronic component package, causing more of the bimetallic element to come into contact with the package, increasing the effective contact area and conductive heat transfer [10].

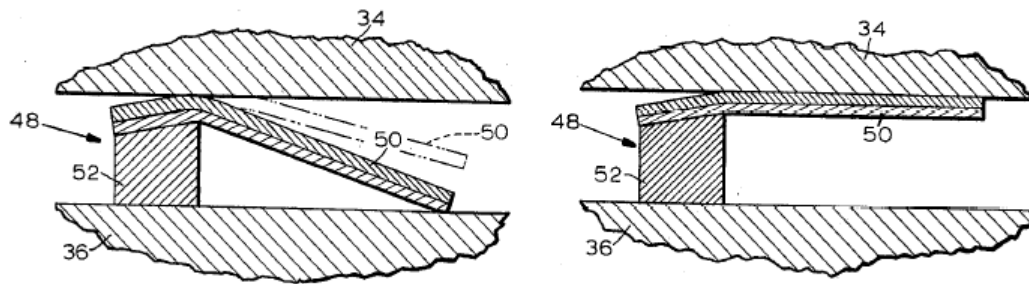


Figure 15: Second Invention Patented by Riordan for a Variable Thermal Conduction Device Using a Temperature-Responsive Bimetallic Element [10].

The third and final device proposed in the patent involved an expandable bellows containing a thermally expansive material that is connected to a heat sink by a thermally conductive material on one end as shown in Figure 16 [10]. On the other end of the bellows is a gap containing a low conductivity material between the electronic component package and the bellows itself [10]. As the temperature of the heat sink increases, the thermally expansive material will cause the bellows to expand toward the package, decreasing the width of the gap, which will increase the conductive heat transfer of the device [10]. When the temperature of the heat sink decreases, the bellows will contract, increasing the width of the gap and decreasing the conductive heat transfer [10].

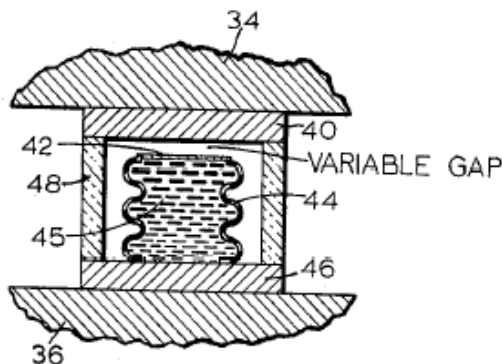


Figure 16: Third Invention Patented by Riordan for a Variable Thermal Conduction Device Using a Thermally Expansive Medium [10].

Another much more recent patent by Potter in 1998 offers several different ideas for variable insulation devices that switch between low and high heat transfer states, including a device shown below in Figure 17 that utilizes both the temperature-responsive bimetallic element concept and the metal hydride with vacuum insulation concept [11]. In the device bimetallic laminate switches that are outwardly convex in shape are used inside of a vacuum insulation panel to create thermal short circuits for very high conductive heat transfer when desired [11]. When the bimetallic switches are at low temperatures, they will remain separated from the other sidewall, resulting in an insulator state for the variable insulation panel. As the temperature of the bimetallic switches increases either passively by the wall or environmental temperature increasing or actively through the use of a heating element near the switch in or on the sidewall, the bimetallic switch will reach a point where it will "snap" from being convex in shape to concave in shape [11]. Once this happens, a metal-to-metal contact between the sidewalls will be created resulting in a thermal short circuit with very high conductive heat transfer [11].

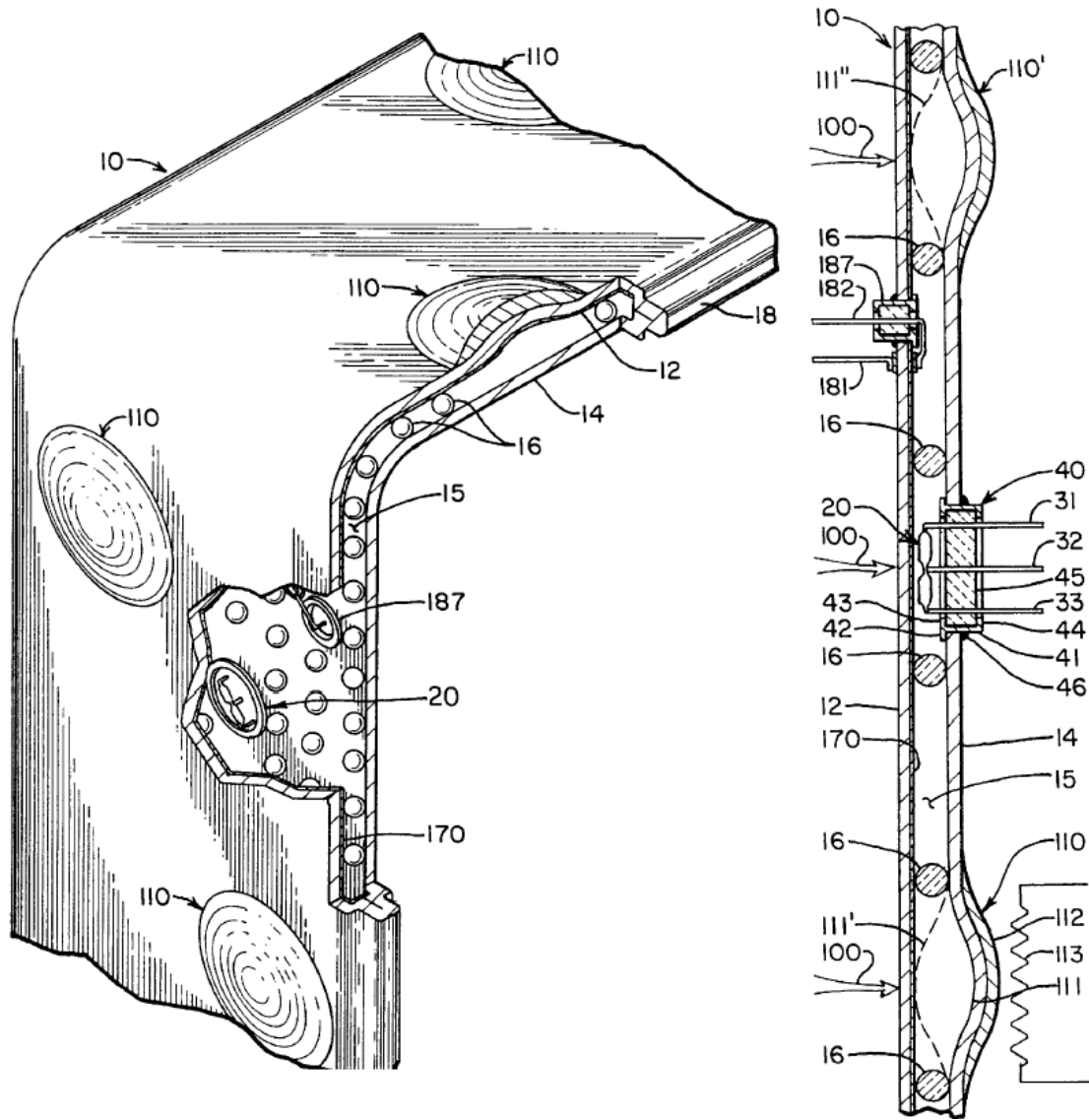


Figure 17: Invention Patented by Potter for a Variably Insulating Portable Heater/Cooler [11].

In addition to the bimetallic laminate switches, the device patented by Potter also incorporates the metal hydride ideas described previously [11]. Between the two sidewalls of the device, glass-like spacers are used to maintain a vacuum without allowing the insulation panel to structurally collapse [11]. The main advantage of the metal hydride/vacuum insulation system patented by Potter over the ones mentioned previously is that for an active control system it only requires heating or power to change the device from an insulator to a conductor and vice versa, without any power being required to maintain the

variable insulation panel in either of the two states [11]. This is done by using a permeable hydrogen gate in conjunction with the metal hydride [11]. To change the insulation panel from an insulator to a conductor, the metal hydride and the hydrogen gate are both heated to allow hydrogen gas to be released from the metal hydride and pass through the gate to the insulation panel [11]. Once enough gas has been released to obtain the desired thermal conductivity, the heating of the metal hydride and gate is stopped. For the other devices mentioned before, as the temperature of the metal hydride cooled, the hydrogen gas would be reabsorbed, causing the thermal conductivity of the insulation panel to decrease [11]. With the invention by Potter, however, the hydrogen gate feature is not permeable at low temperatures, so the hydrogen gas cannot pass through the gate to the metal hydride to be reabsorbed [11]. Thus, the hydrogen gate feature keeps the hydrogen gas pressure in the insulation panel at a high level, allowing the insulation panel to remain in its conductor state without requiring constant heating or power [11].

Inflatable Insulation

Next, the third type of VCI found in the literature was inflatable insulation type devices. The first one to patent the concept was Laing with his idea for a building insulation panel with controllable heat insulation [12]. The panel consists mainly of two walls with inflatable honeycomb-like ducts between them [12]. One wall is designed to be fixed and face the building interior, while the other wall of the panel is moveable facing either the building exterior or a heat storage element [12]. When high thermal conductivity is desired for the insulation panel, the ducts are left deflated, resulting in very small separation distance and air present between the walls [12]. Later on, when low thermal conductivity is necessary for the insulation panel, the ducts are inflated with air or a gas, increasing the separation distance between the walls of the panel and decreasing the conductive heat transfer [12]. Normally, convection of the air in the ducts would cause high convective heat transfer, but the honeycomb structure of tiny air pockets of the flexible ducts inhibits convection [12]. A schematic of the invention found in the patent by Laing is shown below in Figure 18.

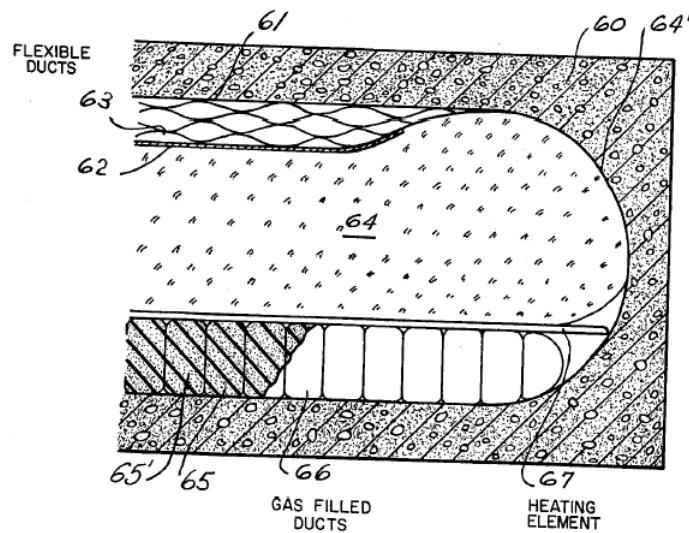


Figure 18: Invention Patented by Laing for an Inflatable Insulation Device [12].

A few years after the patent by Laing, another group at IBM in the 1970s also came up with an idea for an inflatable VCI device found in an IBM technical disclosure bulletin from 1979 [13]. Their device also consisted of a collapsible and inflatable honeycomb structure that could go from very high to very low thermal conductivity and vice versa by inflating and deflating the structure [13]. By using a honeycomb structure, convection was also prevented by trapping air in tiny pockets where it cannot circulate [13].

Other Types of Thermal Semiconductors

The final thermal semiconductor concept in a paper by Al-Nimr, Asfar, and Abbadi was very recent and unique. The basic idea of their smart insulation system involves two storage tanks of fluids both connected to a slab wall containing both fluids separated by a movable partition [14]. One of the fluids is a high conductivity fluid, such as water, while the other fluid is a low conductivity fluid, such as an inert gas like argon [14]. When conditions require that the system be in its insulator state, low conductivity fluid would be pumped from its storage tank into the slab wall, moving the partition and resulting in the

slab wall consisting of most or all low conductivity fluid [14]. The same procedure would occur except with the high conductivity fluid and its tank if the system needed to be in its conductor state [14]. The authors of this paper calculate the ratio of heat transfer for the system's conducting state compared to its insulating state was 200:1 [14].

The authors of the paper developed both active and passive designs for their smart thermal insulation system [14]. The active system consisted of pumps and valves to control the flow of the two fluids to and from their tanks with sensors and a differential temperature controller to control the heat transfer over the slab wall [14]. Their second design involved a piston-type device that made use of a saturated liquid's transition between vapor and liquid to pump the fluids between the slab walls and tanks in accordance with temperature changes in the environment to regulate heat transfer [14]. A schematic of their active system design proposed in its insulating and conducting states can be seen below in Figures 19 and 20.

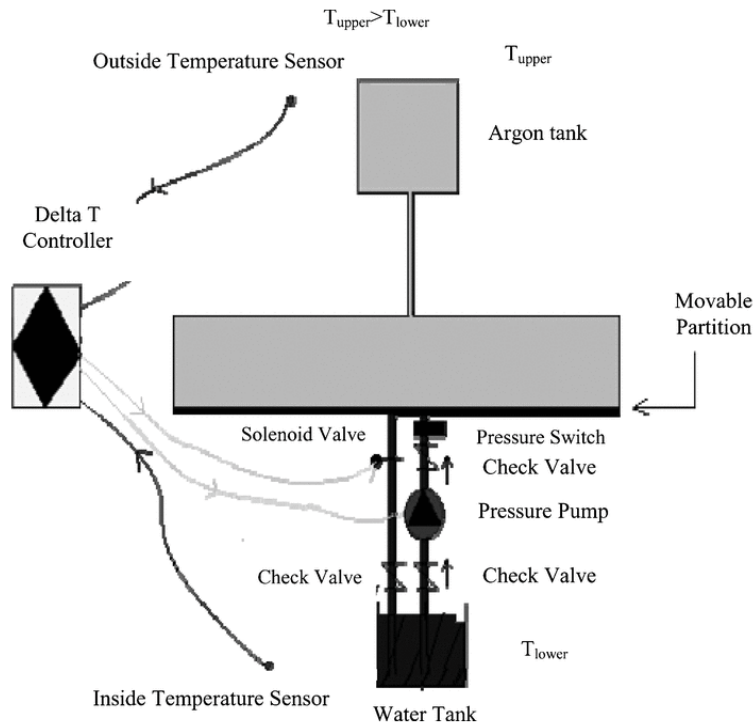


Figure 19: Insulator State of Smart Thermal Insulation System by Al-Nimr, Asfar, and Abbadi [14].

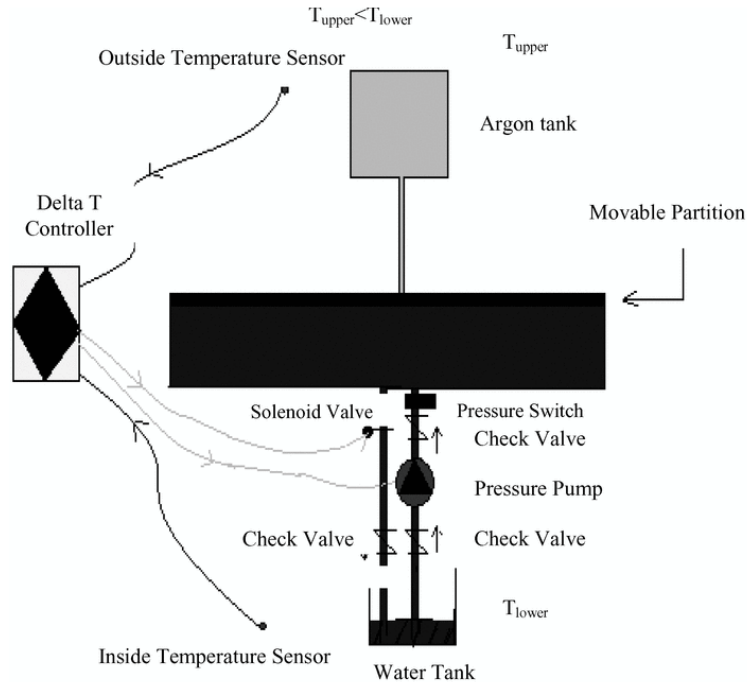


Figure 20: Conductor State of Smart Thermal Insulation System by Al-Nimr, Asfar, and Abbadi [14].

1.3.2 Thermal Semiradiators

Not only conduction has been used as the method of heat transfer for smart insulation devices that have been developed previously. Several smart insulation devices that can switch between high radiation or convection heat transfer and an insulator state have also been designed. Only a few types of thermal semiradiator devices have been proposed compared to variable conductance systems, and they will be described in the following sections.

Variable Emissivity Thermal Semiradiators

The first type of thermal semiradiator device relies on a variable emissivity material coating on the external surfaces of a device that varies with either the surface temperature or with an applied electric potential. The authors of a 2002 paper in the Japanese Journal of Applied Physics proposed a Smart

Radiation Device (SRD) that uses a variable infrared emissivity material on the external surfaces of spacecrafts to control the heat transfer between the spacecrafts and the exterior space environment [15]. The material, $\text{La}_{1-x}\text{Sr}_x\text{MnO}_3$, utilized for the SRD has an emissivity that can vary substantially at the metal-insulator transition temperature to change the material from a low emissivity metal at low temperatures to a high emissivity material at high temperatures [15]. By bonding the material in the form of thin and light ceramic tiles to the outside surfaces of spacecraft, the material effectively serves as smart insulation for the spacecraft that can switch between an insulator state and a high radiation heat transfer state when necessary to regulate the temperature of the spacecraft [15].

Another author who proposed using a variable emissivity material as variable insulation in a device was Potter, who included the idea in his patent in addition to his metal hydride and bimetallic switch concepts [11]. In his system the variable emissivity material coating would be applied to one of the sidewalls in the insulation panel shown in Figure 17 [11]. Either thermochromic or electrochromic materials would be used for the variable emissivity coating [11]. Thermochromic materials work like the variable infrared emissivity materials in that their emissivities change with temperature. As the temperature of the material increases either passively or actively through the use of a heating element, the emissivity of the material will increase, giving high radiation heat transfer across the insulation panel designed by Potter [11]. On the other hand, electrochromic materials' emissivity changes in response to an applied electric potential [11]. By applying an electric potential through an active smart insulation system to the material, its emissivity will increase proportionally to the length of time the potential is applied, while changing the direction of the electric potential applied to the material will decrease its emissivity [11]. Electrochromic materials show great promise for use as thermal semiradiators in smart insulation systems.

Other Types of Thermal Semiradiators

Another type of smart insulation developed involving radiation heat transfer is the unique VARES (VARiable Effective Surface Radiator) technology developed by the National Aerospace Laboratory of

the Netherlands as a lightweight alternative for conventional thermal switches and pumped loops used on Mars rovers for temperature control [16]. Unlike the previous thermal semiradiator devices that varied material emissivity to control radiation heat transfer, the VARES technology relies on varying the radiator's effective radiation surface area to control the radiation heat transfer between the Mars rover and the outside environment of the Martian surface [16]. An illustration showing how the VARES technology is used to vary the effective surface area of the radiator and thus radiation heat transfer is shown below in Figure 21 [16].

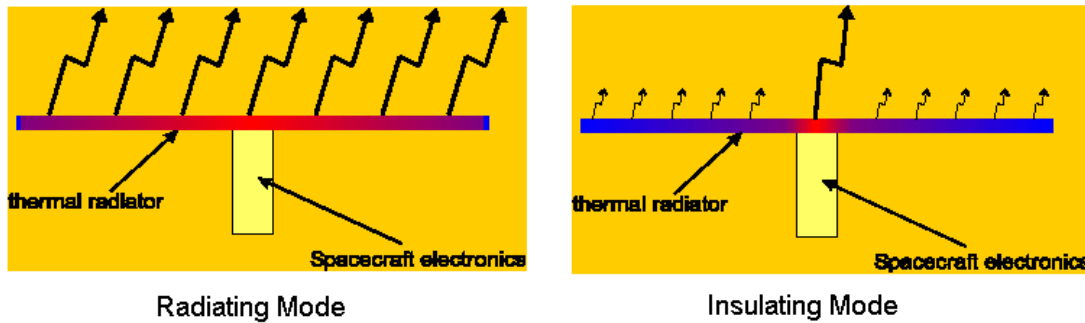


Figure 21: Principle of the VARES Radiator [16].

The VARES system can switch between two different heat transfer states: radiating and insulating [16]. During periods of time when the electronics inside the Mars rovers are operating and causing high temperatures at the center of the spacecraft and radiator, high radiation heat transfer is needed to reject the spacecraft's excess heat to the cold exterior environment [16]. An oscillating heat pipe (OHP) system, consisting of small diameter tubing containing both the working fluid and its own vapor is used to transfer heat when the system is in radiating mode, from the center of the radiator near the spacecraft's electronics outward over the entire radiator surface area [16]. The fluid oscillations of the OHP system are caused by the evaporation and condensation of the working fluid as it moves from the hot center of the spacecraft outward to the colder regions of the radiator surface [16]. Through the fluid oscillations at high temperatures, heat is transferred over the entire radiator surface area using the tubing, which increases the

effective surface area of the radiator and thus the radiation heat transfer [16]. Figure 22 below shows the OHP system of the VARES technology in its radiating and insulating states [16].

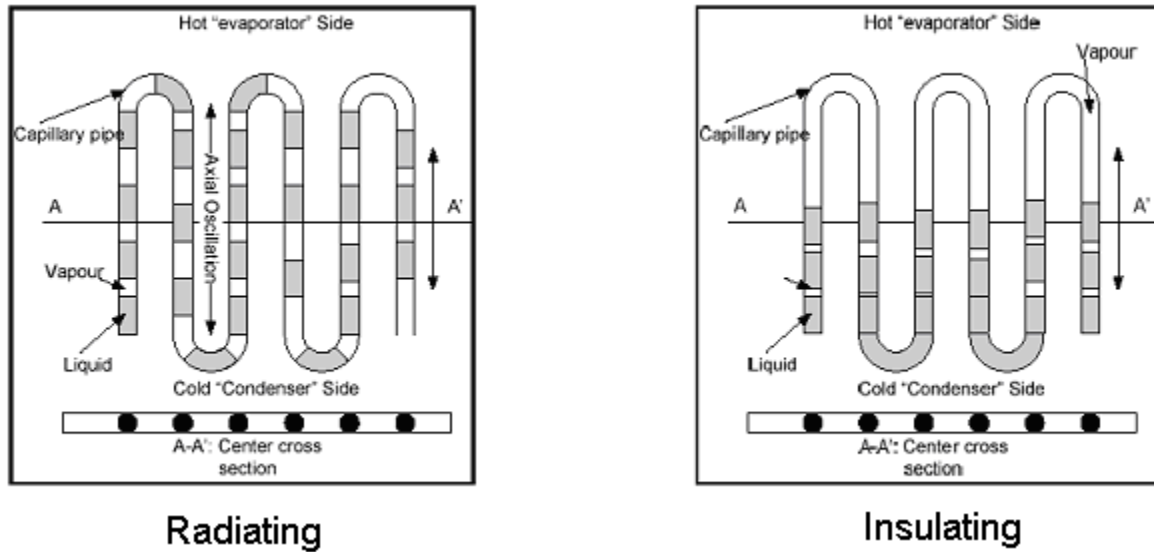


Figure 22: OHP System of the VARES Technology [16].

The switching mechanism of the VARES technology used to switch the system between radiating and insulating states is dependent on the feature of an OHP not oscillating below a certain temperature for different working fluids [16]. For colder temperatures below that switching temperature, the VARES system will operate in its insulating mode because the fluid oscillations in the OHP will not be able to transfer the heat of the electronics at the center of the spacecraft out over the radiator surface [16]. This will then decrease the effective surface area of the radiator and thus severely limit the radiation heat transfer of the system [16]. No power is needed in the VARES smart insulation system to keep the system in either of its two different states or to switch between the states [16]. Figure 23 shows the prototype model built by the National Aerospace Laboratory of the Netherlands to prove the VARES technology concept [16].

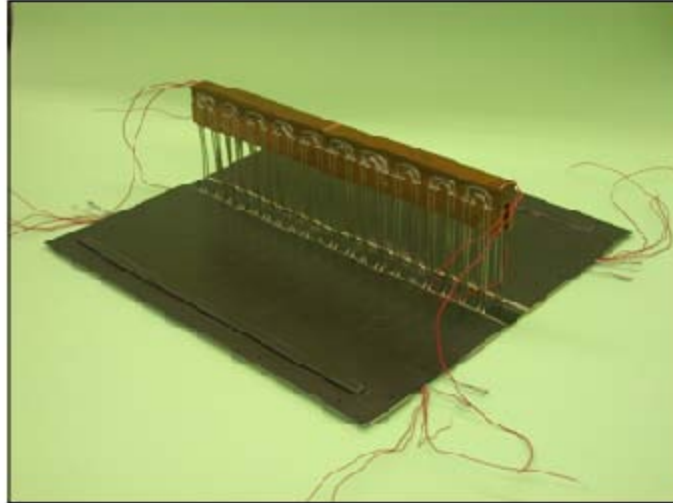


Figure 23: VARES Technology Demonstrator Model (TDM): VARES Radiator Connected to Copper Electronics Simulator [16].

Another very original concept for a variable radiation system is the smart greenhouse developed jointly by the Cleveland Botanical Garden and Kent State University's Liquid Crystal Institute [17-18]. Liquid crystal panels, consisting of liquid crystals dispersed as droplets in a polymer resin between two layers of glass, are used in the walls and ceiling of the greenhouse [17-18]. In addition, each panel is wired so that a very low current can pass through the liquid crystal matrix [17-18]. By varying the voltage applied to the panels, the transparency of the panels of the greenhouse can be varied because increasing the voltage causes the liquid crystal molecules to line up more and more in parallel, which allows light to pass through the panel without being scattered, increasing transparency [17-18]. Decreasing the applied voltage toward zero consequently causes the liquid crystal particles to become more randomly oriented, which causes light to be randomly reflected and scattered in the panel, resulting in a reduction in transparency [17-18]. Figure 24 shows how the basic concept of the smart greenhouse liquid crystal panels works [17-18].

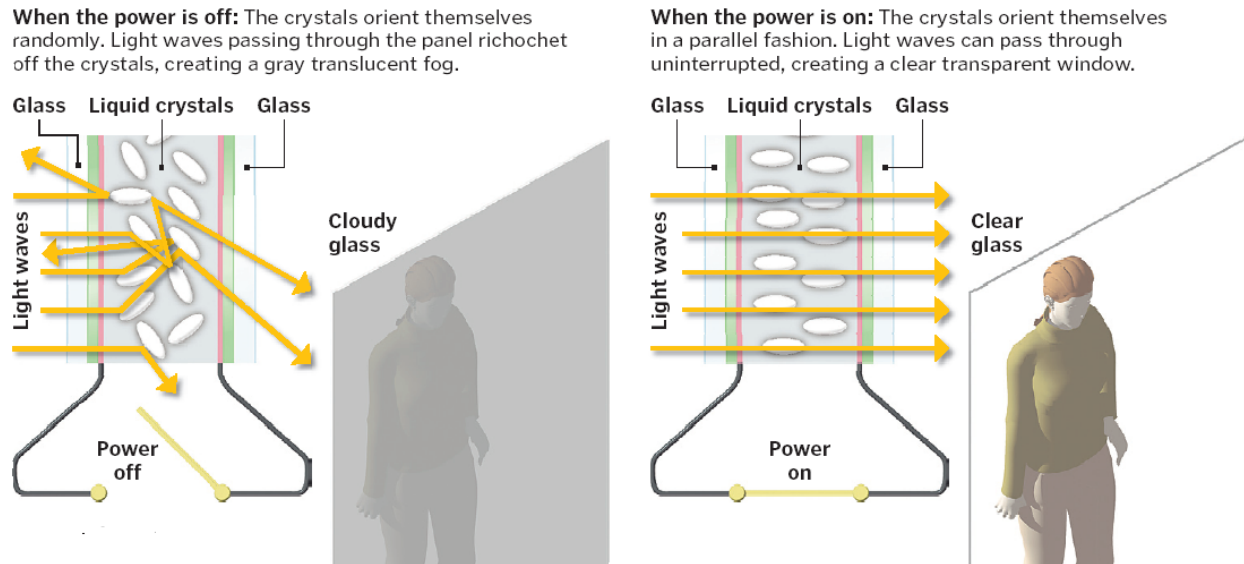


Figure 24: How Liquid Crystal Panels of Smart Greenhouse Work [17].

The main objective of the smart greenhouse research is to reduce the heating and cooling costs currently required to control the temperature of the greenhouse by controlling the thermal radiation passing through the panels [17-18]. By controlling the amount of light passing through the panels by changes in the voltage applied, the thermal radiation heat transfer from the exterior wall of the panels to the interior of the greenhouse can be controlled. Then, the smart greenhouse will be able to take advantage of cases such as the sunny winter day case by increasing the transparency of the panels to reduce heating costs, while still preventing overheating during times such as a sunny summer day by decreasing the transparency of the panels to reduce cooling costs [17-18].

1.3.3 Thermal Semiconductors

The final class of existing smart insulation devices deal with the third and final mode of heat transfer, convection. Only three examples of thermal semiconductors were found in the literature. The first type of variable convection insulation is a novel type of variable building insulation patented by Laing and Laing in 1974 [19]. The device consists of a building insulation panel containing two walls with fins to increase

the convective heat transfer with a chamber of air between them to stop any conduction from taking place over the panel and a moveable reflector sheet within the air space to decrease any radiation heat transfer through the panel [19]. The moveable reflector sheet in the device has many circular holes throughout the sheet for air to flow through for convection [19]. A diagram of the invention can be seen in Figure 25 shown below.

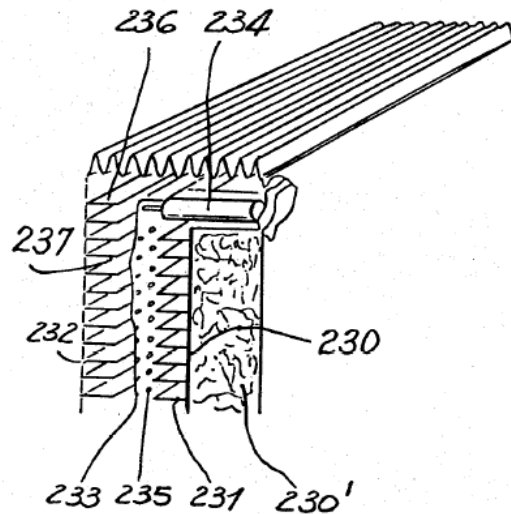


Figure 25: Invention Patented by Ingeborg and Nickolaus Laing for a Variable Convection Insulation [19].

Normally, the building insulation panel will be in its insulator state with very little convection heat transfer taking place [19]. When high heat transfer is needed across the panel, the moveable reflector sheet will be moved by electromagnetic vibrators energized by an alternating current of subsonic frequency, such that the holes in the sheet will act as nozzles, to cause eddy currents of air in the space between the walls of the panel [19]. The eddy currents will then cause high convection heat transfer through the building insulation panel when the temperature gradient across the panel is beneficial for high heat transfer [19]. The main problem of the invention is that power is needed the entire time to maintain

the device in its high heat transfer state, since the reflector sheet must be constantly vibrating for high convection heat transfer [19].

The second variable convection building insulation device patented by Davis and Strohlein in 1981 involved a series of inflatable tubes suspended under the roof of a structure in rows sides-by-side, stretching the length of a building [20]. The upper end of the tubes was tied shut, while the lower ends were split open at both ends to permit a pipe to pass through all of the tubes horizontally at their ends [20]. The remaining ends of the tubes are then wrapped and tied around the pipe [20]. A fan or blower is also attached to one end of the pipe to inflate or deflate the tubes using low pressure air through small holes in the pipe going through the tubes [20]. A schematic of the set-up for this smart convection building insulation system is given in Figure 26.

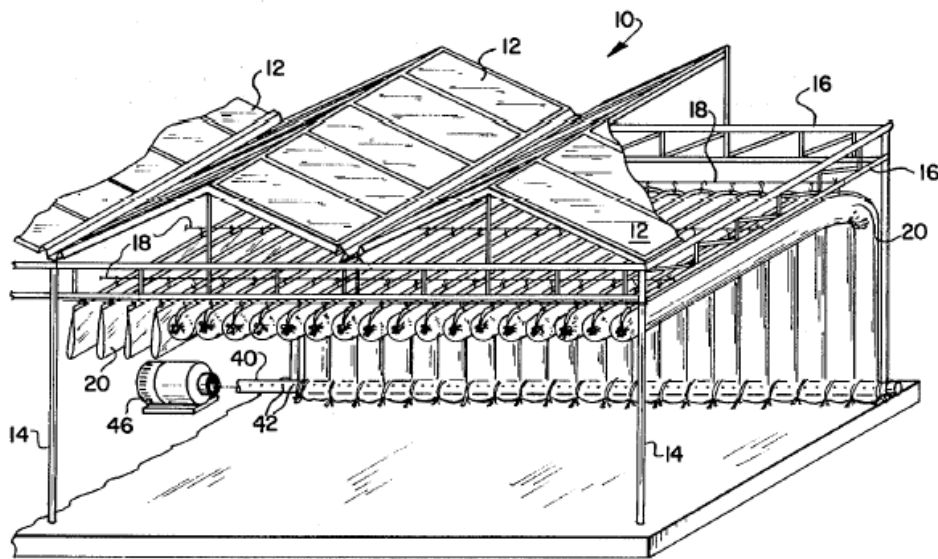


Figure 26: Invention Patented by Davis and Strohlein for an Inflatable Heat Barrier [20].

The smart insulation system was able to switch from a high convection heat transfer state when the tubes are deflated to a low convection heat transfer state when the tubes are inflated [20]. During times when the tubes are deflated, they will hang loosely from the ceiling with large amounts of space between

them for air to flow between the tubes upward from the building interior to the attic space and roof, causing high convection heat transfer between the rooms of the building and the outside environment [20]. To change the smart insulation back into a good insulator, the tubes would be inflated by the low pressure fan or blower until they are in contact with each other to form a barrier to the path of any air trying to flow from the building interior to the roof or attic space [20]. By impeding the flow of air, the tubes will greatly reduce convection heat transfer and instead act as a very good insulator [20].

The final type of smart building insulation that will be described is a bi-directional thermodiode system developed by Chun and Chen in several papers in recent years [21]. The bi-directional thermodiode examined in the paper consists of several vertically stacked closed loops that are filled with a fluid and rectangular in shape [21]. The horizontal segments of the plates are connected on each side to two plates with the outside-facing collector plate fixed and the inside-facing radiator plate able to move vertically to control the inclination angle of the tubing [21]. The two vertical plates are the hot and cold ends of the thermodiode and can be easily interchanged by pulling down or pushing up the movable plate [21]. A schematic of the thermodiode employed in the experimental study of the paper can be seen below in Figure 27.

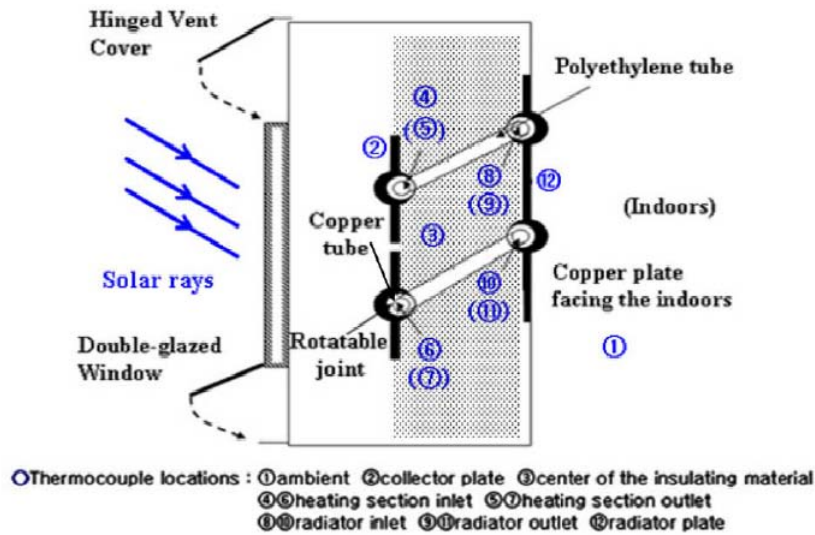


Figure 27: Diagram of the Thermodiode Employed in the Experimental Study [22].

Controlling the angle between the stacked closed loops and the horizontal is the key to the bi-directional thermodiode [21]. When the loops are at an angle and the lower ends of the loop is the hot side being heated, natural convection in the fluid inside of the loops will cause heat transfer to occur from one wall of the bi-directional thermodiode to the other [21]. In the paper, this is called the forward-biased operation mode where heat transfer is allowed to take place [21]. If the angle of the stacked closed loops and the horizontal is changed, however, so that the upper end of the stacked loops is being heated instead, no natural convection will take place in the fluid in the loops to transfer heat from the hot upper end to the cold lower end [21]. In the paper, this is called the reverse-biased operation mode where heat transfer is inhibited across the bi-directional thermodiode [21]. Figure 28 shown below illustrates how varying the inclination angle of the rectangular loops in the bi-directional thermodiode will change the favorable direction of heat flow [22].

The bi-directional thermodiode type of smart insulation could possibly be utilized to take advantage of solar heating in the winter in the United States and night or evening cooling in the summer. During the winter the inclination angle of the fluid loops could be set so that heat is allowed to transfer through convection from the outside wall of the building receiving thermal radiation to the building interior, while preventing any heat loss at other times occurring across the insulation module from the interior to the ambient environment. In the summer the inclination angle of the fluid loops could be reversed to allow convection heat transfer for cooling in the evening or at night from the building interior to the outside environment, while preventing heat from being able to transfer from the environment to the interior during the hot summer days.

The authors of the paper proposing the bi-directional thermodiode concept built and tested a prototype from the design given in the diagram of Figure 27. The results of their experimental testing of the prototype are shown below in Figures 29 and 30.

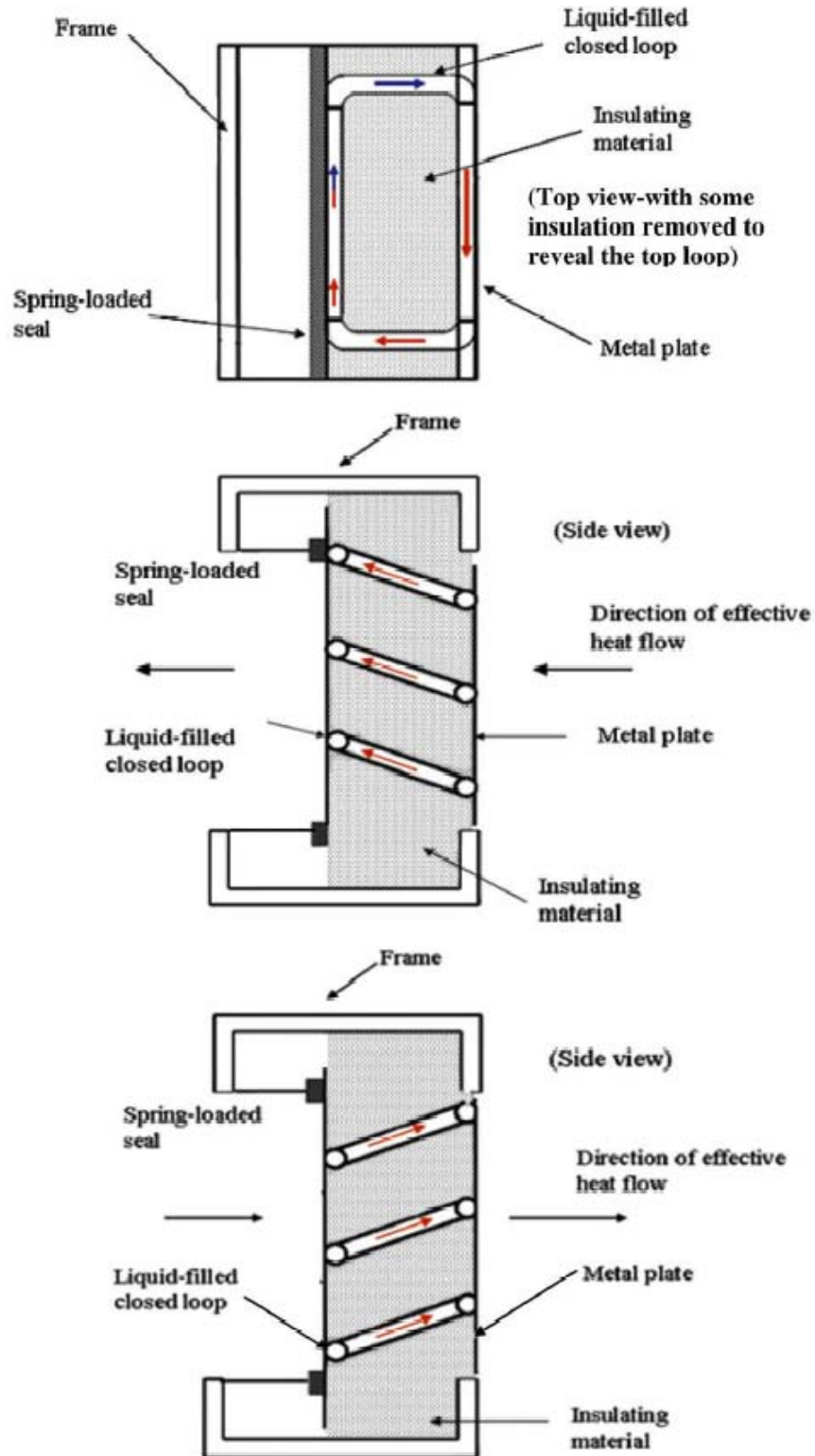


Figure 28: How Changing the Inclination Angle of the Fluid Loops Changes the Direction of Effective Heat Flow [22].

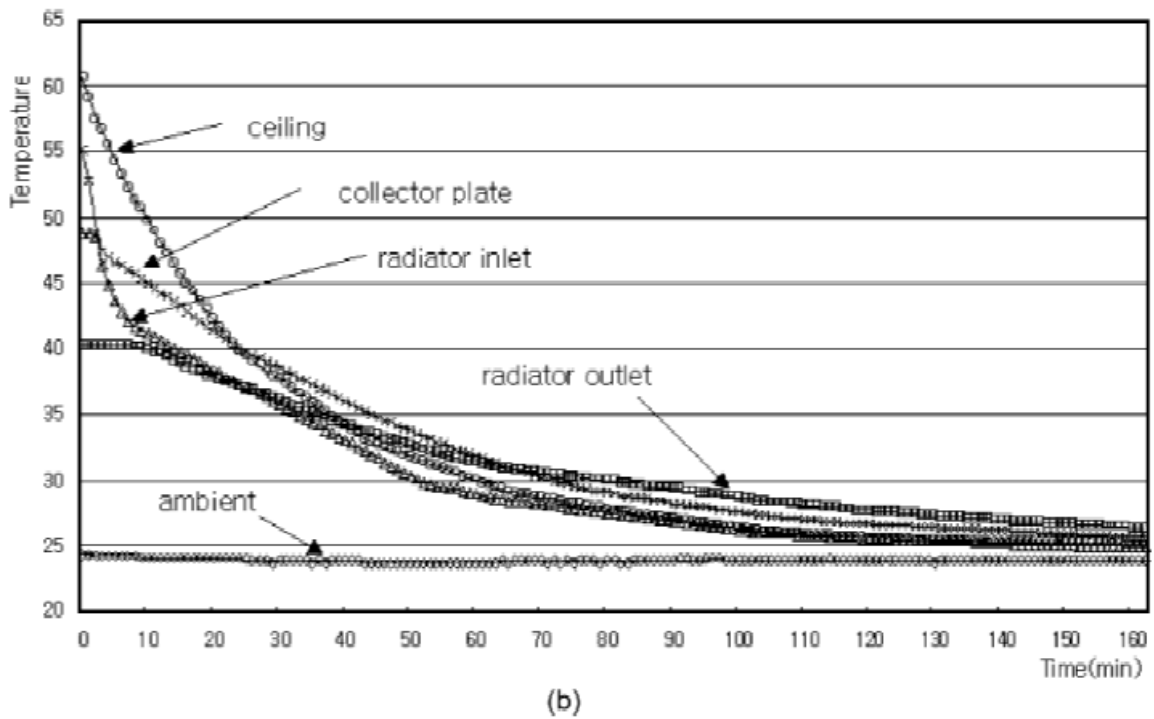
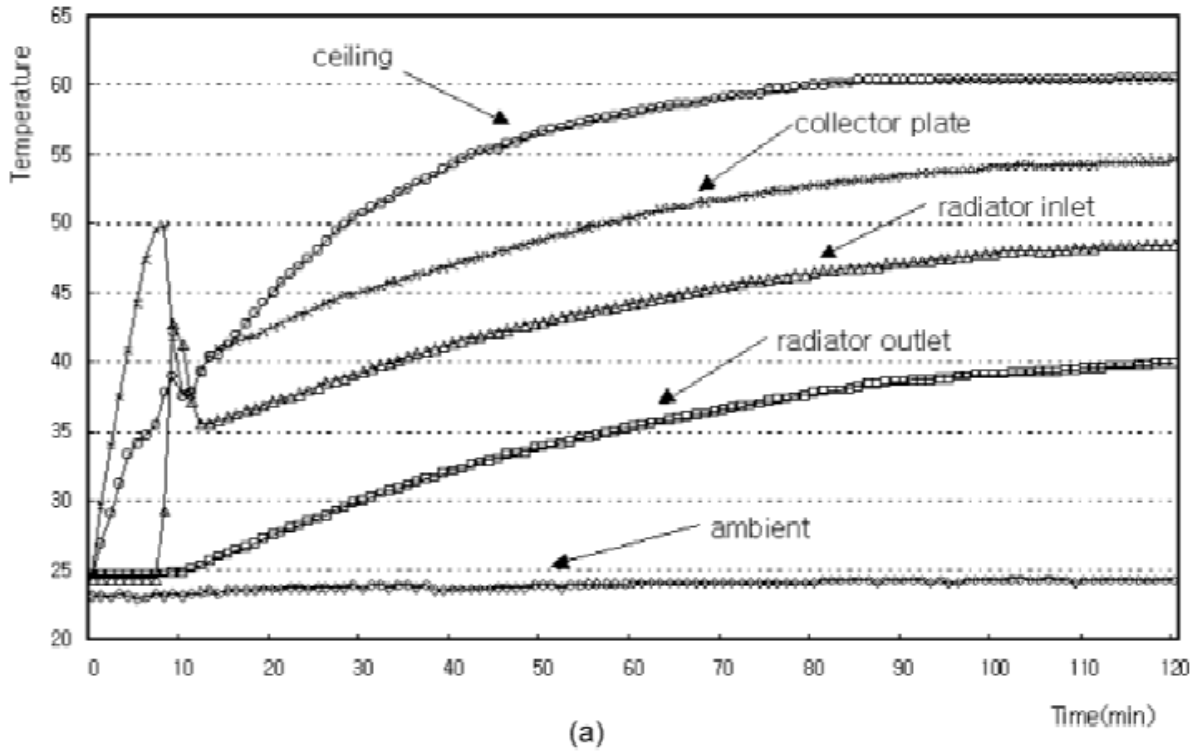


Figure 29: Indoor Test Results for a Radiation Flux of 800 W/m^2 :
 a) Heating Phase; (b) Cooling Phase [21].

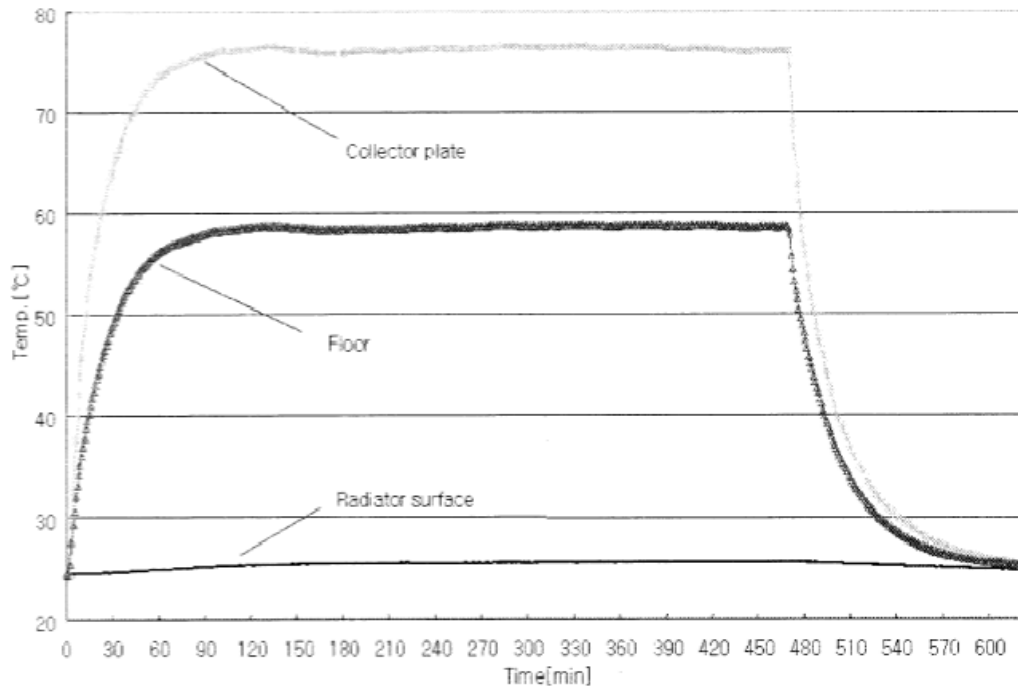


Figure 30: Temperature Variations of the Thermodiode Module under Reverse-Biased for a Radiation Flux of 800 W/m^2 [21].

Figure 29 shows the results of the experimental testing for heating and cooling when the inclination angle of the fluid tubing permits heat transfer to occur. For both of the plots, and especially for the cooling plot in b) of Figure 29, the temperatures of the two different walls of the bi-directional thermodiode, the collector plate facing the outside environment and the radiator plate facing the building interior, closely match each other. This shows that the heat transfer across the thermodiode is very high in the forward-biased configuration. In Figure 30, the inclination angle of the fluid tubing is altered to inhibit heat transfer. The resulting plot shows a significantly larger temperature difference between the collector plate and the radiator surface than before, over $50 \text{ }^\circ\text{C}$, showing that the heat transfer across the thermodiode tested is very low in the reverse-biased configuration.

Now that all of the existing variable insulation devices and concepts have been examined, the next step is to look into possible energy and cost savings of implementing smart insulation in buildings along with possible locations where smart insulation would be most beneficial.

1.4 POTENTIAL ENERGY CONSERVATION OF SMART INSULATION

A simulation study conducted by the Department of Energy of the potential for energy conservation of smart or active insulation systems will be described in the following section [23]. The results of the simulations in the study will be presented involving the possible yearly energy and costs savings of smart insulation implemented in buildings along with several problems that were found with the study and possible ways to further increase the benefits of smart insulation. Finally, several high-value building applications will be examined where smart insulation would have the maximum benefit to energy and cost savings.

1.4.1 Department of Energy Simulation of Smart or Active Insulation Systems

The study, "Assessment of the Energy Conservation Potential of Active (Variable Thermal Resistance and Switchable Absorptance) Building Thermal Insulation Systems," conducted by Fine and McElroy in 1990, focused on using simulations to calculate the potential energy conservation of smart or active insulation systems with variable thermal resistance values and variable surface properties [23]. Many different passive and active insulation systems were analyzed in the study, including active insulation systems with variable attic, wall, and/or floor thermal resistance, variable roof and/or wall absorptance, and variable window transmittance [23]. For all of the simulations of the study, annual heating-plus-cooling loads were calculated for a hypothetical 1600 ft² (148.64 m²) one-floor structure with a crawl space, a single heating/cooling room, and an attic or cathedral ceiling [23].

Predictions for the heating and cooling loads for the test structure with different passive insulation systems were made using the Electric Power Research Institute (EPRI) Simplified Program for Residential Energy (ESPRE) [23]. A simple-to-use tool for estimating seasonal, daily, and hourly average energy use, the ESPRE simulation program processes calculations at hourly increments based on thermal and moisture balances for average transfer rates for the increments (Quasi-Steady-State) [23]. Information

needed to be inputted into the program by the user consists of information about the structure, the structure's location, and Typical Meteorological Year (TMY) weather data for each hourly increment, which includes the dry-bulb temperature, wind velocity, humidity ratio, and the solar insolation rate [23]. Using the user inputs for each hour, the ESPRE program then calculates hourly heating and cooling loads for the structure [23]. Results of the ESPRE simulations for different passive insulation systems were analyzed with a database management program to determine the heating and cooling loads for the hypothetical structure implemented with active insulation systems [23]. Figure 31 shows a flow chart of the ESPRE simulation process for structures with passive and active insulation systems.

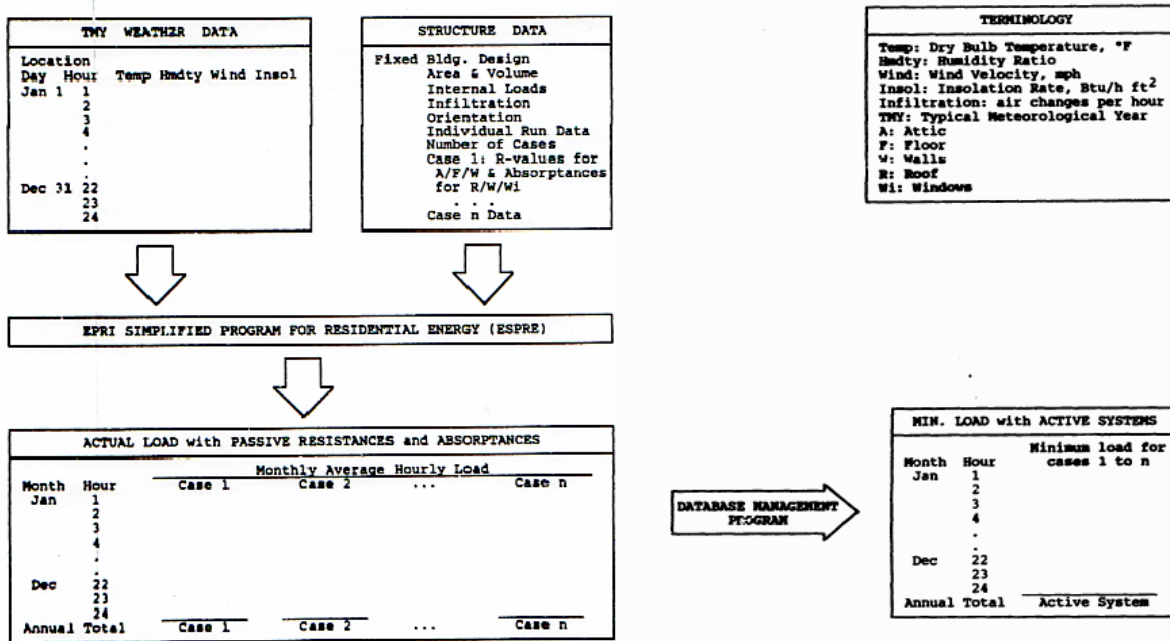


Figure 31: Flow Chart of Simulation Process for Passive and Active Insulation System Structures [23].

To analyze the potential for energy savings from active insulation in different climates, simulations were conducted using ESPRE for three actual locations of Minneapolis, MN, Lexington, KY, and Phoenix, AZ, representing a cold climate, a moderate climate, and a hot climate [23]. Different combinations of the three locations and the three different attic, floor, and wall insulation levels (R-value

= 38, 19, or 0.5 ft² F-hr/Btu (6.7, 3.4, or 0.1 m² K/W)) were examined for a total of 81 passive insulation cases [23]. For each of the 81 passive cases, hourly heating-plus-cooling loads were calculated using ESPRE for each hour of every day of the year [23]. To lessen the computational effort in the simulation, monthly average heating-plus-cooling loads were calculated for each of the 24 hours of the day using the hourly heating and cooling data calculated earlier [23]. Using the results of the passive simulations, the heating and cooling loads for the hypothetical structure with active systems were determined [23]. For hours 1-24 for each month of the year for the building, the thermal resistance was allowed to "switch" hourly to the levels for the passive system that achieved the lowest monthly average hourly heating-plus-cooling load for that hour [23]. Once the optimal insulation level was determined for each of the hours 1-24 in the month, the monthly average hourly heating-plus-cooling load for those insulation levels was also determined [23]. For the active system cases the R-values for the active elements of the building of the floor, walls, and attic were allowed to switch between either 38 or 19 ft² F-hr/Btu (6.7 or 3.4 m² K/W), 19 or 0.5 ft² F-hr/Btu (3.4 or 0.1 m² K/W), or 38 or 0.5 ft² F-hr/Btu (6.7 or 0.1 m² K/W) [23].

After analyzing the results of the simulations for the 81 passive insulation system cases, the authors of the study concluded that the passive case that gave the best results was the super-insulating case with R-values for the attic, floors, and walls of 38, 38, and 38 ft² F-hr/Btu (6.7, 6.7, and 6.7 m² K/W) [23]. When calculating the annual energy savings for the different passive and active insulation cases for all three locations, all of the cases were compared to a reference case with R-values of 38, 19, and 19 ft² F-hr/Btu (6.7, 3.4, and 3.4 m² K/W) for the attic, floors, and walls, representing the recommended insulation values for new construction in Lexington and Minneapolis as determined from the DOE Insulation Fact Sheet [23]. The results of the energy savings of the best passive insulation system for the three locations compared to the reference case is given in Table 1. It can be seen from the results that super-insulating the structure does offer significant energy savings over the normal insulation levels for the hypothetical structure.

Table 1: Energy Savings for Best Passive Insulation Case over Reference Case [23].

	Reference Case: R-values of 38/19/19 ft ² F-hr/Btu	Super-Insulated Case R-values of 38/38/38 ft ² F-hr/Btu	Savings for Super-Insulating
Location	Annual Heating-Plus-Cooling Load	Annual Heating-Plus-Cooling Load	Energy Savings
Lexington, KY	62.3 MBtu/yr (2.08 kW)	54.7 MBtu/yr (1.83 kW)	7.6 MBtu/yr (0.25 kW) (12.2%)
Minneapolis, MN	90.2 MBtu/yr (3.02 kW)	77.9 MBtu/yr (2.60 kW)	12.3 MBtu/yr (0.41 kW) (13.6%)
Phoenix, AZ	56.6 MBtu/yr (1.89 kW)	51.4 MBtu/yr (1.72 kW)	5.2 MBtu/yr (0.17 kW) (9.2%)

Once the 81 passive insulation case simulations were examined, the next step was to analyze the results of the active insulation simulations [23]. The study's simulations calculated that the variable thermal resistance system with the greatest potential for energy conservation was the active insulation system with active attic, floor, and wall insulations that can switch between high or low levels of 38 or 0.5 ft² F-hr/Btu (6.7 or 0.1 m² K/W) [23]. Table 2 gives the results for best-performing active insulation system when compared to the reference and super-insulating cases.

Table 2: Energy Savings for Best Active Insulation Case [23].

Location	Annual Heating-Plus-Cooling Load	Savings over Reference Case	Savings over Super-Insulated Case
Lexington, KY	51.2 MBtu/yr (1.71 kW)	11.2 MBtu/yr (0.37 kW) (18.0%)	3.6 MBtu/yr (0.12 kW) (6.58%)
Minneapolis, MN	75.4 MBtu/yr (2.52 kW)	14.8 MBtu/yr (0.49 kW) (16.4%)	2.5 MBtu/yr (0.08 kW) (3.20%)
Phoenix, AZ	50.5 MBtu/yr (1.69 kW)	6.1 MBtu/yr (0.20 kW) (10.8%)	0.9 MBtu/yr (0.03 kW) (1.75%)

When initially looking at the results of the best active insulation case the energy savings over the reference case are very large, up to nearly 20% for Lexington, KY [23]. After a closer examination, however, most of the energy savings for the active insulation system comes from using a high R-value of 38 ft² F-hr/Btu (6.7 m² K/W) for the walls and floor of the active insulation instead of a R-value of 19 ft²

F-hr/Btu ($3.4 \text{ m}^2 \text{ K/W}$) as with the reference case [23]. From Tables 1 and 2 it can be seen that the energy savings of super-insulating the structure with very high R-value insulation passively are much greater than the energy savings of using an active insulation system instead of the reference case [23].

After evaluating the energy savings of the optimal active insulation system, the next step in the DOE study was to calculate the annual monetary savings of using the best performing active insulation system over the typical reference case. Any monetary savings calculated for the best-case active insulation system in 1990 would be slightly lower today, since the average electricity cost in the United States has stayed about the same after adjustment for inflation, while the efficiency of heat pumps has improved greatly over the past 20 years. The yearly cost savings calculated in the 1990 study by making the attic, walls, and floor of the structure active between R-values of 0.5 and $38 \text{ ft}^2 \text{ F-hr/Btu}$ (0.1 and $6.7 \text{ m}^2 \text{ K/W}$) can be found in Table 3.

Table 3: Yearly Cost Savings in 1990 using Best-Case Active Insulation System in Structure (Yearly Cost Savings not adjusted for inflation) [23].

Location	Cost Savings over Reference Case	Cost Savings over Super-Insulated Case
Lexington, KY	\$123/yr	\$39/yr
Minneapolis, MN	\$163/yr	\$26/yr
Phoenix, AZ	\$67/yr	\$8.50/yr

After conducting their energy and cost savings analysis, the authors of the Department of Energy study made several final conclusions. As stated before, the examination of the passive and active insulation systems indicated that the majority of the savings resulted from simply increasing the level of insulation [23]. From that they also conclude that active insulation systems have a very small potential for energy conservation, but they do suggest that an analysis should be conducted in the future of variable thermal resistance systems which are more closely correlated to the climate with smaller increments for the high-low settings [23]. Although the conclusions by the authors in the Department of Energy study

showed marginal promise for variable thermal resistance insulation, the next section will show why smart insulation with varying thermal resistance should still be pursued further [23].

1.4.2 Why Further Study of Variable Thermal Resistance Insulation is Needed

Now that two decades have passed since the simulation study by the Department of Energy on active insulation systems was conducted, it is time to reassess the study to examine if a new simulation of smart insulation should be pursued and to see if smart insulation development can still possibly lead to significant energy and cost savings. In many ways the world has changed since 1990 in terms of buildings and computational abilities. For example, home sizes in the United States have increased greatly from the 1600 ft² (148.64 m²) hypothetical structure used in the study over the past twenty years, leading to increased energy usage for homeowners. If a typical home size today were used in the active insulation simulation, it would likely lead to increased annual energy and cost savings that might make smart insulation worth the investment for many homeowners. Also, even though the annual cost savings found from the study might seem small to the individual building occupants, the overall energy savings across the United States from implementation of smart insulation in many structures would be significant. This would make smart insulation development attractive in helping to solve the major problems today of trying to lower the country's energy consumption and carbon emissions. In addition, building energy simulation software has improved greatly since 1990. The ESPRE program was almost out of date in 1990, and much improved software, such as DOE-2 and EnergyPlus, have been developed by the Department of Energy since that time. A new study is clearly needed using newer more up-to-date building energy simulation software to analyze the benefits of smart insulation in buildings.

Furthermore, a new simulation study with several different features from the simulation by Fine and McElroy could result in much improved results for smart insulation systems as suggested by Potter and Tuluca's 1992 paper that also examined the Department of Energy study [2]. For example, in the 1990 study all of the different surfaces of the building, such as each of the walls, the floor, and the attic, had to have the same insulation R-value level of low or high at any given time. It is easy to see how this could

cause problems. In the sunny winter day case mentioned earlier significant thermal radiation might be impacting one wall of a building so that it would be beneficial for the insulation of that wall to be "turned off," while the opposing wall would also have to be "turned off" as well in the simulation even if it was in the shade. This would result in any heat gains to the building interior from the sunny wall being canceled out by heat losses through the now "turned off" insulation of the wall in the shade. A new simulation where only those surfaces with a beneficial temperature gradient for heating or cooling the building interior would have their insulation switched off at any time could show that smart insulation systems could have much larger energy and cost savings than found by the experimental study.

Several other possible changes to the 1990 study that could be incorporated in a new simulation study are given by Potter and Tuluca to further analyze active insulation systems [2]. One idea was to focus more on the area of roof cooling by conducting a cooling-load analysis of possible energy savings from radiative roof cooling [2]. Another change could be to target commercial buildings instead of the residential buildings of the Department of Energy study to see if they would more greatly benefit from the implementation of active insulation [2]. It was also suggested to use air exchange rates of 0.7 or less as a user input to the ESPRE simulation compared to the 1.0 used by Fine and McElroy [2].

Finally, the last major reason why a new simulation study is needed and why smart insulation development should still be pursued is the existence of a separate DOE study conducted by Caskey that suggests that large energy savings could indeed result from the implementation of smart insulation in buildings [29]. In the study, reflective aluminum foil was installed in the rafters of a pitched-roof single-family dwelling in Albuquerque, NM, in order to prevent high heat losses through the roof during the winter from high radiative heat transfer to the outside environment [29]. Experimental results in the study eventually showed a 25% decrease in roof heat losses during the winter nights, which were approximately 12 hours in length [29]. Unfortunately for the authors of the study, the reflective aluminum foil also caused a 40% decrease in roof heat gain from solar heating during the sunny winter day periods, which were approximately 8 hours in length, canceling out the decrease in heat losses during the winter nights

[29]. This led to the reflective aluminum foil having a zero net total effect on the heat losses through the roof of the building during the winter [29].

Although the reflective aluminum foil did not produce good results for the study by Caskey, it shows that if smart insulation were implemented in the roof of the building tested instead of the aluminum foil, large energy savings could result. During the winter nights the smart insulation could serve as a good insulator, as with the reflective aluminum foil, to prevent high heat losses through the roof. Later, during the winter days, unlike the aluminum foil, the smart insulation could change to a high heat transfer state to take advantage of the roof heat gain from solar heating. Thus, the smart insulation would be able to have the large decrease in roof heat losses during the winter nights and also still maintain the roof heat gain from solar heating during the winter days, resulting in a large net decrease in heating loads needed for the building over the winter and large heating cost savings.

1.4.3 High-Value Smart Insulation Building Applications

The final component of the review of the literature involving smart insulation systems is the identification of five building types where active insulation would be very beneficial: light manufacturing, strip shopping, shopping centers, and office buildings [2]. First, for structures for light manufacturing, machines involved in the manufacturing process give off large amounts of heat when in operation during the day even during the winter, requiring cooling for the building [2]. At night when the machines are turned off during colder times of year, heating of the building is needed [2]. Especially in the winter, if the smart insulation could have a low R-value during the day, cooling loads could be greatly reduced, while keeping the smart insulation at a high R-value during the night [2]. Next, for strip shopping centers containing a mix of retail stores, similar problems are encountered with cooling of the structures needed during operation during the day over much of the year due to process heat loads and excess heat resulting from the use of incandescent lamps for display lighting [2]. If smart insulation were implemented, it could switch from a low R-value during times when the temperature gradient between the store's interior and the outside environment is beneficial for cooling to a high R-value at other times [2].

Another high-value smart insulation building application would be shopping centers, where the cooling load on the upper floors can be high for much of the year due to multistory open spaces that allow significant convection heat transfer through air flowing upward from the lower floors [2]. In addition, if the roof insulation of the shopping centers could be "turned off" at times, it would allow some of that excess heat to be able to transfer from the upper floors to the ambient environment [2]. Smart insulation could be implemented in the roofs of shopping centers that would have a low R-value when outside air temperatures are lower than the building upper floors' interior temperature in temperate climates, while switching to a high R-value in times when the outside environment is either too hot for cooling or during the winter when heating of the building is required [2]. Finally, the overheating caused by heat generated by lighting and office equipment that often occurs in office buildings would make the use of smart insulation attractive to lower cooling loads and improve temperature comfort to increase worker productivity [2]. Smart insulation in office buildings could be switched from a low R-value when the outside ambient temperature is cooler than the interior office temperature, while switching to a high R-value when necessary [2]. Office applications where smart insulation would be most beneficial would be for locations in mild climates, such as Southern California and coastal locations, where cooling from the outside environment could be best taken advantage of, or for office buildings in any type of climate with especially high internal loads, such as desktop publishing or data processing [2].

2.0 SMART INSULATION CONCEPT DEVELOPMENT AND FABRICATION

Following the review of the previous literature on existing variable insulation concepts and devices, several new concepts and ideas for smart insulation devices were developed. The new concepts developed were compared against one another in terms of their feasibility, effectiveness, cost, and their potential for implementation in buildings in the near-term so that one or two basic concepts could be chosen for further fabrication and testing. After careful consideration, two main concepts were determined to be the most promising. The first concept involved the breaking and connecting of a thermal conduction path in the insulation through the use of aluminum metal fins that could be actuated to shift from a position in which they are in contact with one another to a non-contacting position. The second major concept used an inflatable honeycomb-like structure with small chambers of air that could go from a deflated conductor state to an inflated insulator state, which inhibited conduction through the use of air and convection by trapping air in the small volumes.

2.1 SMART INSULATION PROTOTYPE COMMON FEATURES

When designing the prototypes for the different smart insulation concepts to be tested, many of the same dimensions were used for all of the different prototypes in order to maintain consistency during testing and to allow for easy comparison between the different smart insulation devices to evaluate which had the best performance. First, it was determined that a roughly one square foot (0.3 m) size piece of smart insulation would be the optimal size for the area of all of the smart insulation concepts to be tested. One square foot (0.3 m) was chosen for the area of the devices because it would be large enough to

sufficiently provide "proof-of-concept" for thermal semiconductors; it could easily be scaled up for application in an actual building; and it was largest size that we would be able to experimentally test in our laboratories using the space and resources available. Eventually, as the design process continued for the smart insulation devices, dimensions of one of the smart insulation prototypes, the shifting fins device, required that the length and width of its design had to be enlarged slightly from 12 in. (0.3 m) to final length and width values of 13.25 in. (0.337 m). To again maintain consistency for all of the smart insulation devices, each of the smart insulation prototypes developed was given common length and width dimensions of 13.25 in. (0.337 m). Finally, the thickness of insulating state of the smart insulation prototypes was chosen to be 2.25 in. (5.715 cm) for easy implementation of the smart insulation in the walls and/or roof of existing or new buildings in place of or even on top of conventional insulation. Once the smart insulation devices were actuated into their conducting configuration, some of them would maintain the same thickness of 2.25 in. (5.715 cm), such as the shifting fins thermal semiconductor, while others, such as the inflatable thermal semiconductor, would have significantly decreased thickness in their conducting state.

2.2 SHIFTING ALUMINUM FINS THERMAL SEMICONDUCTOR DEVELOPMENT

2.2.1 Shifting Aluminum Fins Thermal Semiconductor Concept

One of the simplest ideas in the literature for smart insulation involved the connecting and breaking of a thermal conduction path to regulate the heat transfer over a device. Two patents mentioned previously by Riordan and Potter utilize this principle through the use of bimetallic switch elements that will bend or buckle following a change in temperature. Unlike the bimetallic switch patent designs, the first smart insulation concept developed for this thesis is a novel system consisting of aluminum metal fins that can be shifted by using a motor so that they are in either a contacting or non-contacting state. When the aluminum fins are in a contacting state, a thermal conduction path will exist between the fins so that high

heat transfer by conduction will be able to take place. Later on, once the fins have been actuated to a new position where they are not contacting, the thermal conduction path will be eliminated, vastly reducing the conduction heat transfer of the device. Figure 32 illustrates the shifting aluminum fins thermal semiconductor concept in both its low and high thermal conductivity states.

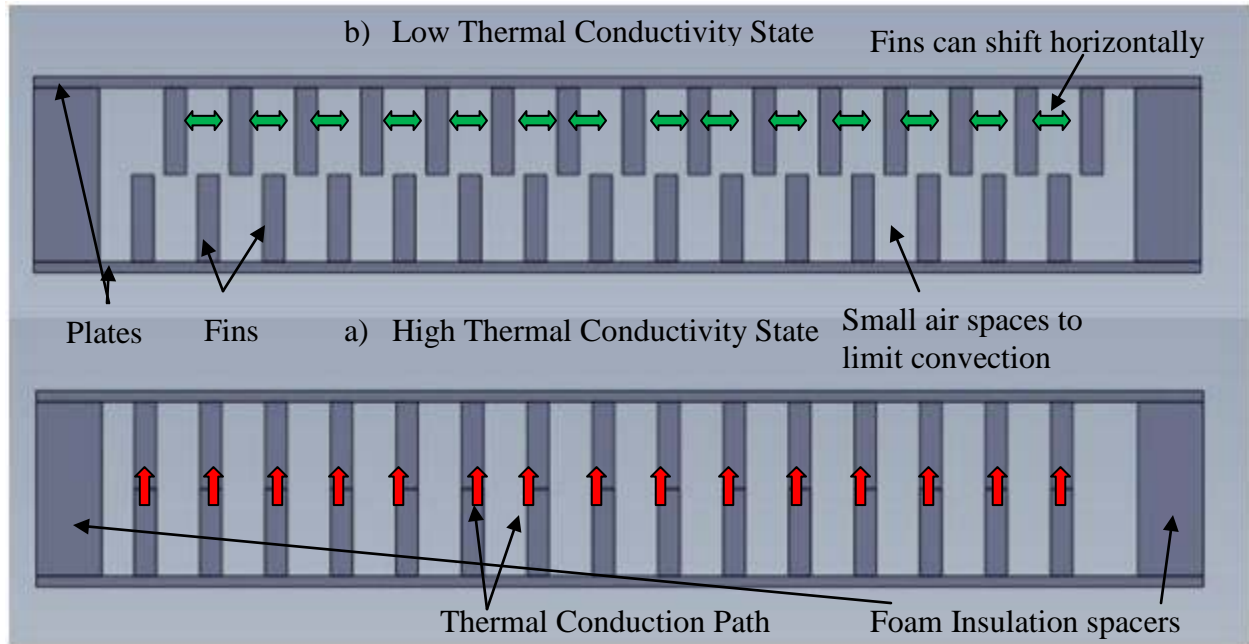


Figure 32: Contacting/Non-contacting Aluminum Fins Thermal Semiconductor Concept.

The basic design of the aluminum fin thermal semiconductor concept consists of many aluminum fins facing each other mounted to two thin aluminum plates. When high heat transfer between the two metal plates is desired, the fins on the top plate can be shifted horizontally so that they are in good thermal contact with the fins mounted to the bottom aluminum plate to create a thermal conduction path. Later on, if low heat transfer between the two plates is needed, the fins can be shifted to the low thermal conductivity state position as shown in Figure 32 where the top and bottom fins are offset from one another to eliminate the thermal conduction path. In order to keep the two plates separated when the system is in its low thermal conductivity state, spacers are added on either end of the device, which are

made of very low thermal conductivity foam insulation to prevent heat transfer between the plates through the spacers. Air is used in the spaces between the fins in the thermal semiconductor because of its very low thermal conductivity. To eliminate the effects of natural convection heat transfer of the air, in the final design the air spaces between the fins were kept very small in volume, since natural convection can be significantly limited by reducing the volume where the gas can flow. In addition, for the low conductivity state of the device, the volumes of air between the fins are divided in half vertically when the fins are shifted to the insulating state, which will help to reduce convection heat transfer in the device's insulating configuration compared to its conducting configuration. The next section describes the features and specifications of the actual smart insulation device that was designed for this concept.

2.2.2 Shifting Aluminum Fins Thermal Semiconductor Design

In order to turn the conceptual ideas for the shifting fins thermal semiconductor into an actual smart insulation device, several design decisions had to be made, such as what material to use, how to mount the fins to the plates of the device, how to actuate the fins between conducting and non-conducting configurations, and what dimensions were necessary for the first prototype device. An early decision that was made in the design process was to postpone the design and fabrication of the actual actuation mechanism that would change the smart insulation device between low and high conduction states for all of the smart insulation concepts developed until a later stage of the project. Instead, for all prototypes of the shifting fins thermal semiconductor, two devices would be built: one device with the fins shown in their conducting configuration in Figure 32 and a second device with the fins shown in their insulating configuration in Figure 32. The contacting/non-contacting aluminum fins concept could then be experimentally tested and modeled in its low and high heat transfer states to examine the amount of change in thermal conductivity the device can attain if implemented in an actual building setting. This will also allow for a comparison of the performance of the different smart insulation devices developed by examining the amount of change in thermal conductivity for different devices from their insulating state to their conducting state.

Pure aluminum was initially chosen for the metal fins and plates of the device because of its high thermal conductivity and relatively low cost when compared to other high thermal conductivity metals, such as copper and silver, which are prohibitively expensive for use as smart insulation materials. To obtain the 2.25 in. (5.715 cm) thickness of the overall design, the height of the fins mounted to the plates was selected to be 1 in. (2.54 cm), while the thickness of the aluminum plates themselves was chosen to be 1/8 inch (0.3175 cm) thick. Making the plates very thin was beneficial because in cases such as when the bottom plate is being heated, the bottom plate can heat up more quickly due to its smaller mass to transfer heat to the bottom fins when high heat transfer is needed, and the heat can spread out more evenly over thinner plates for a more even heat distribution.

Another important design consideration for the shifting aluminum fins device was how the fins were going to be mounted to the top and bottom aluminum plates. Screws were chosen as the best way to fasten the fins to the plates because of their simplicity, low-cost, and the ability to easily change fin configurations by removing some or all of the fins by unscrewing the fins from the plates. Figure 33 shows how screws were utilized to fasten the fins to the plates of the thermal semiconductor device by using threaded screw holes drilled into the fins and plates.

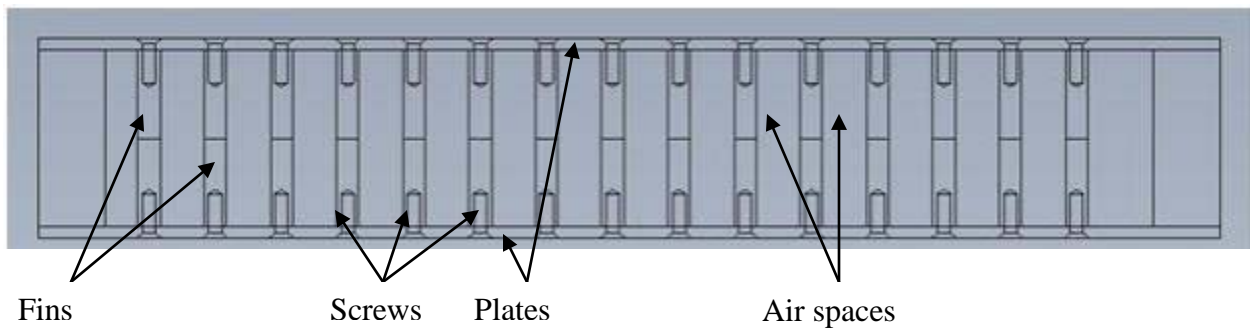


Figure 33: Schematic Showing How Screws are Used to Join Aluminum Fins and Plates.

Once the overall dimensions of the shifting fins thermal semiconductor design were chosen, the dimensions of the individual fins needed to be calculated along with the spacing between the fins. The goal was to pack as many fins into the smart insulation prototype as possible for two main reasons. First, the more fins were contained in the 13.25 x 13.25 in. (0.337 x 0.337 m) area of the device, the more contact area would exist between fins for higher conduction heat transfer. Second, by increasing the number of fins in the device, the distances between fins will be decreased, resulting in smaller volumes of air between the fins and lower natural convection heat transfer. In the final design, thirty fins were utilized with fifteen fins attached to both the bottom and top aluminum plates with all of the fins going the entire length of the device. The width of the fins was chosen to be 1/4 in. (0.635 cm), because that was the smallest possible fin dimension that we could use and still be able to drill the threaded screw holes into the aluminum fins to fasten them to the plates. Also, a center-to-center distance between the fins of 3/4 in. (1.905 cm) was chosen to separate the fins so that when the top fins were shifted and offset into their non-contacting arrangement similar to what is shown in the insulating state of Figure 32, a horizontal gap of 1/8 in. (0.318 cm) is still present between the top and bottom fins. After determining all of the dimensions of the shifting fins design, a 3-D mechanical CAD (computer-aided design) program was used to develop a 3-D model of the first prototype design to ensure that everything would fit together correctly when assembled during actual fabrication. Two multi-view drawings of the shifting fins device in its insulating and conducting states can be seen in Figures 34 and 35 with the final dimensions used in the actual fabrication of the device.

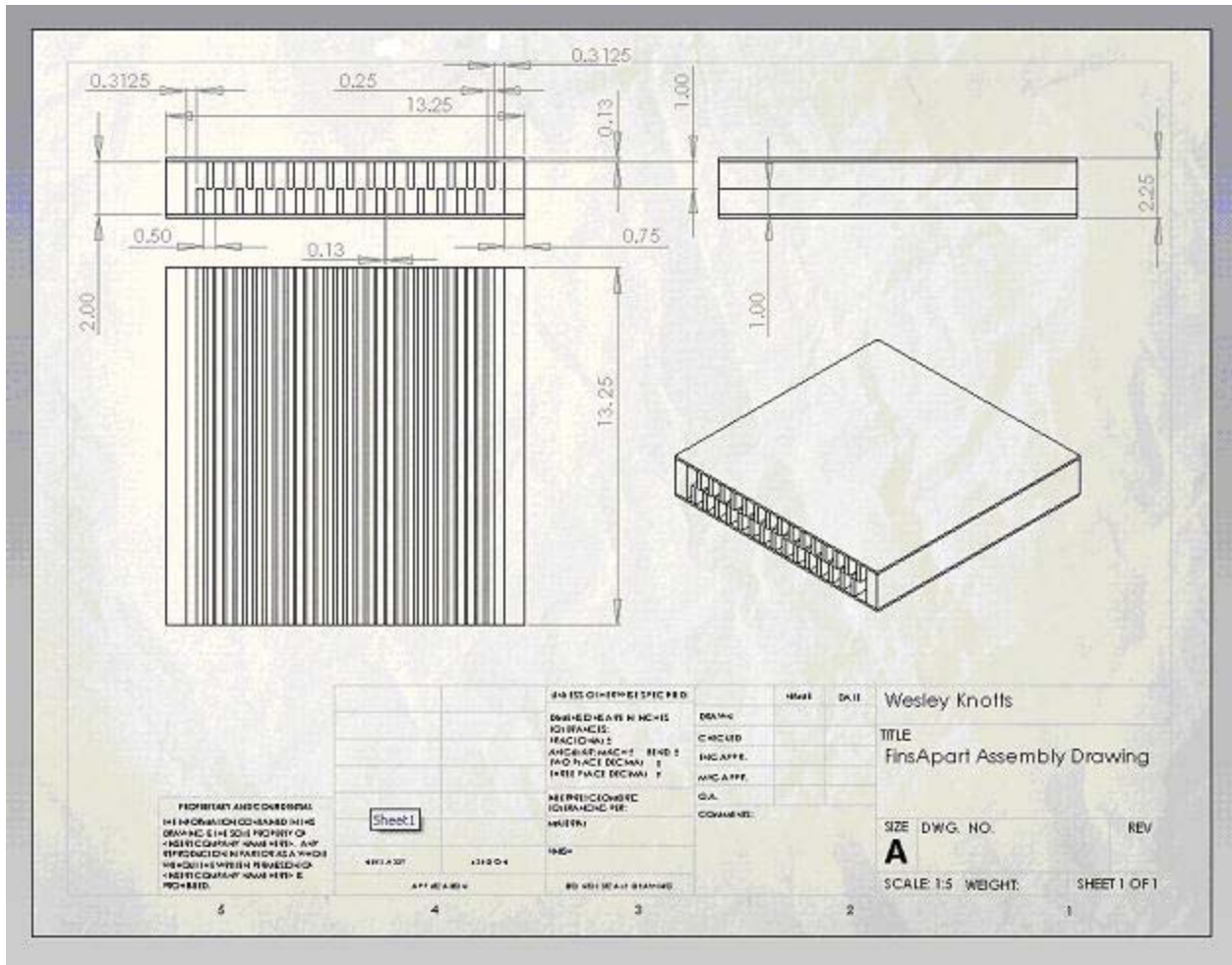


Figure 34: CAD Drawing of Shifting Fins Thermal Semiconductor Prototype in its Insulating Configuration.

One major benefit of the final design of the shifting fins prototype is that it actually only requires one prototype instead of the two mentioned previously to experimentally test both the conducting and insulating states of the device (while still leaving out the device's fin actuating mechanism for the time being). The final design gets around this problem by positioning the first and last fins specific distances from the left and right edges of the plate (19/16 in. and 25/16 in. (3.02 cm and 3.97 cm), respectively), as shown in Figure 34 when the device is in its conducting configuration. By using these exact fin positions on the bottom and top plates and rotating the top plate 180° while leaving the bottom plate stationary, the

resulting arrangement of the fins of the bottom and top plates exactly matches the insulating configuration of the shifting fins thermal semiconductor device.

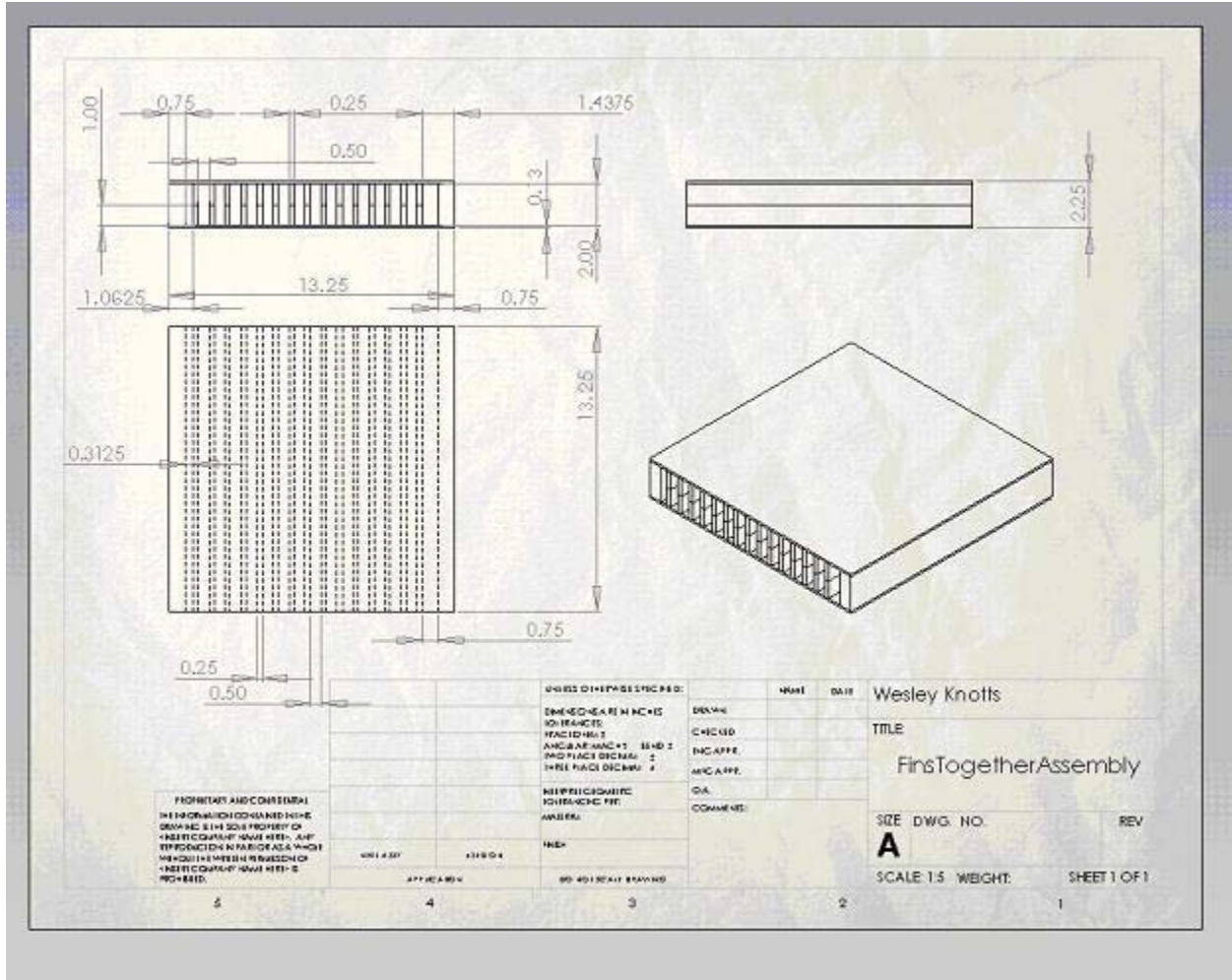


Figure 35: CAD Drawing of Shifting Fins Thermal Semiconductor Prototype in its Conducting Configuration.

2.2.3 Shifting Aluminum Fins Thermal Semiconductor Fabrication

During the fabrication of the shifting fins prototype, nearly all of the fabrication of the device was done by the author in the University of Pittsburgh's student machine shop. The first major decision in the fabrication process, which was made early on, was to use an aluminum alloy, Al 6061, instead of pure

aluminum as the material for the aluminum fins and plates. Although pure aluminum has a higher thermal conductivity of 222 W/m K when compared to the thermal conductivity of Al 6061 of 167 W/m K, pure aluminum is much softer and weaker than Al 6061, making it impractical for the machining needed for fabrication of the prototype [24-25]. Aluminum alloy 6061 was chosen over other aluminum alloys because it is the easiest to machine, while still being relatively inexpensive.

Using the bandsaw and the milling machine of the machine shop, the thirty aluminum fins and two aluminum plates were fabricated first. A very important consideration during the machining of the fins was for all thirty of them to be extremely close to the same height. If only one or two fins were off by even a small amount from the other fins, it could have caused a problem when the device was in its conducting configuration. Since the fins connected to the top plate essentially lay on top of the fins connected to the bottom plate, if even one fin is a different height by a small amount from the other fins, it will cause small air gaps where the other fins contact one another. This will result in a much greater thermal contact resistance between the fins and consequently, lower thermal conductivity and conduction heat transfer when the device is in its conducting configuration. Figure 36 shows how having fins with slightly different heights can result in air gaps and poor thermal contact between some of the fins. To avoid this problem, the fins were milled down in several batches together slowly and very carefully to ensure that the fins' height values were all within a few thousandths of an inch of each other, which is the maximum accuracy possible given the equipment of the student machine shop.

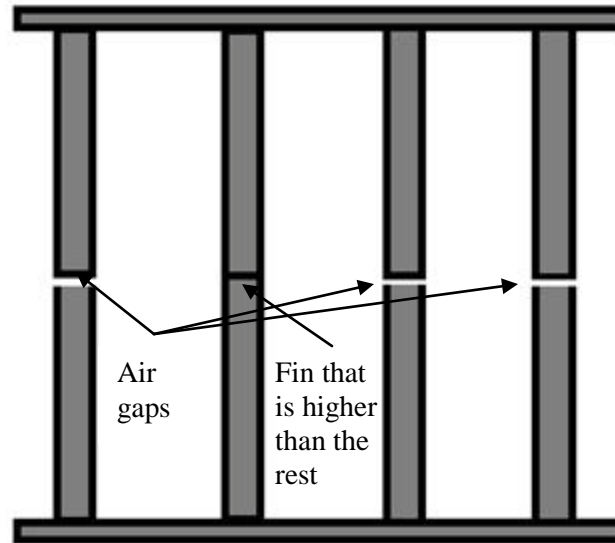


Figure 36: Schematic that Illustrates How Small Air Gaps can Result from Different Fin Heights during Fabrication.

After the aluminum fins and plates had been fabricated, the next step was to drill and tap holes into the plates and fins for the screws that would be used to fasten the fins to the plates. The screws were 6/32 x 1/2 in. (0.476 x 1.27 cm) long, Philips-head, countersunk, brass machine screws. Even though ideally the screws would have been made of the same aluminum alloy 6061 as the fins and plates for consistency, brass was chosen as the screw material because aluminum alloy 6061 machine screws were not available due to the lack of strength of aluminum. 2024 aluminum alloy screws were available, but they did not match the screw dimensions needed for the prototype's design, and they would have had almost exactly the same thermal conductivity as the brass screws. Brass's thermal conductivity of 109 W/m K is close to the thermal conductivity of aluminum alloy 6061 of 167 W/m K, which should result in a uniform thermal conduction distribution throughout the entire shifting fins prototype including the screws [24]. Three screws were used to mount each fin to the plates with one screw at the fin center and the other two screws one inch from the ends of the fin. Figure 37 gives the final CAD model of the shifting fins smart

insulation device prototype design with the location of the screw holes clearly visible for the top plate and fins.

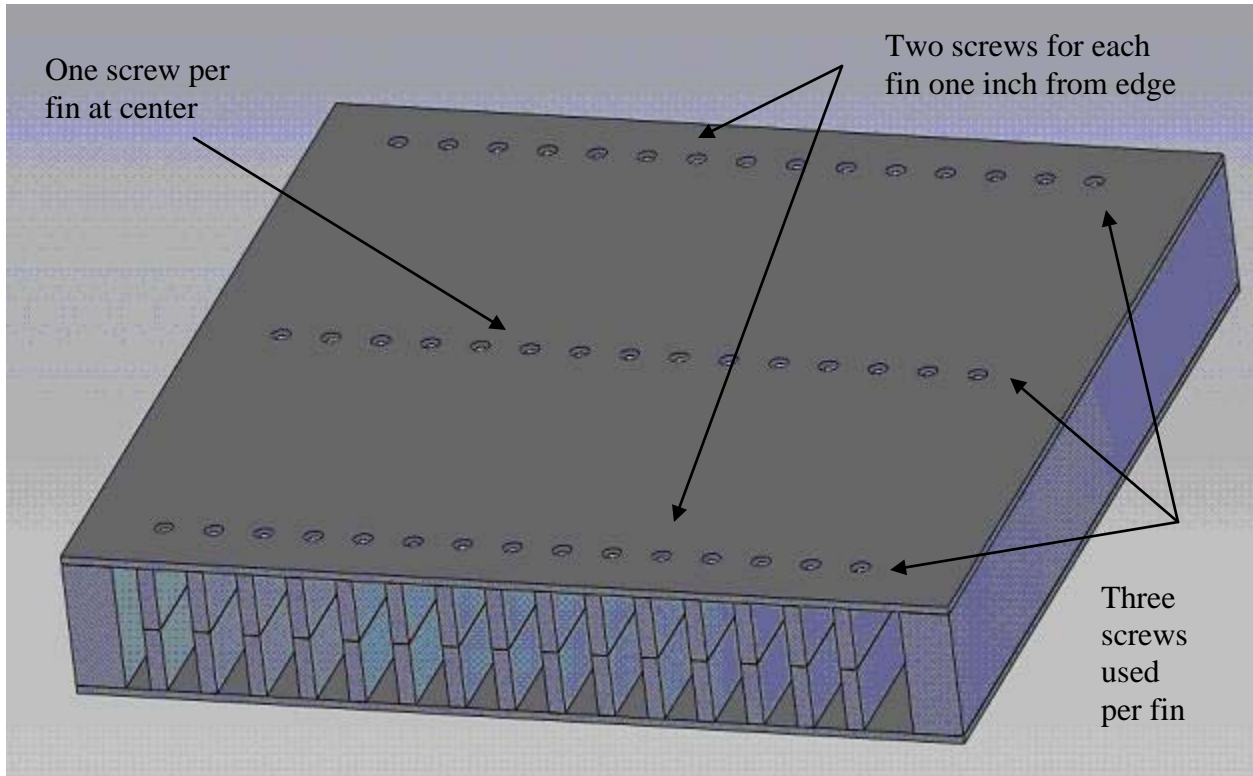


Figure 37: CAD Model of Shifting Fins Prototype with Screw Holes Added.

A photograph of the final fabricated bottom piece of the prototype consisting of the bottom fins mounted to the bottom plate can be seen in Figure 38. The top piece made up of the top fins mounted to the top plate is an exact replica of the bottom piece. Figures 39-40 show give the pieces of the shifting fins thermal semiconductor device prototype assembled in their conducting and non-conducting states

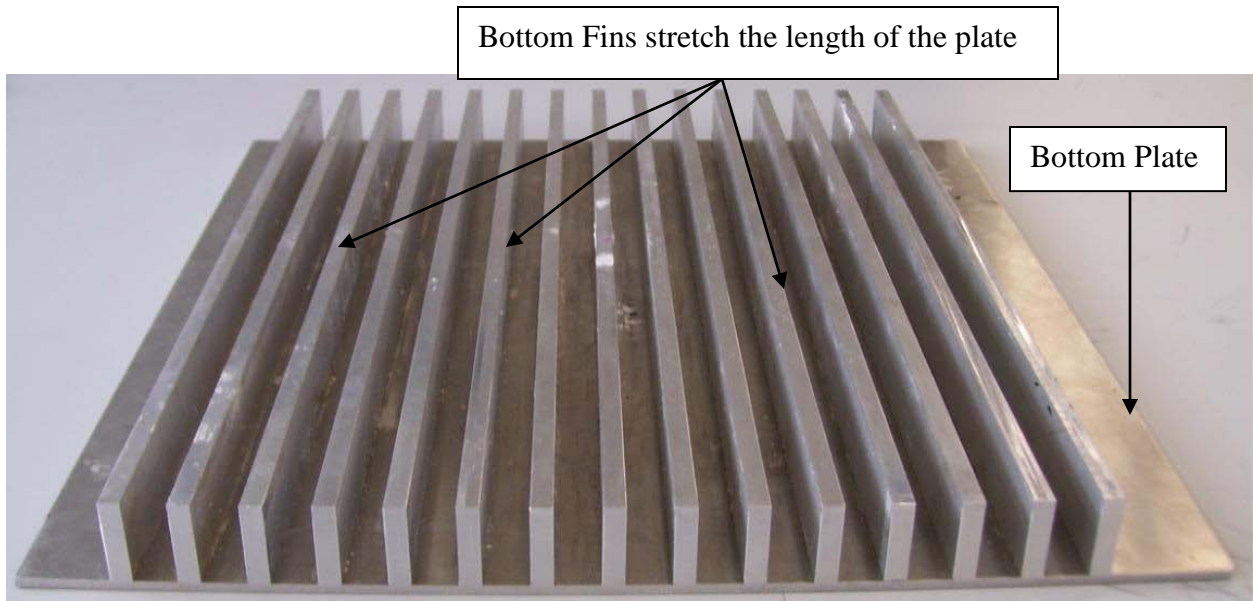


Figure 38: Bottom Piece of Shifting Fins Smart Insulation Device Prototype.

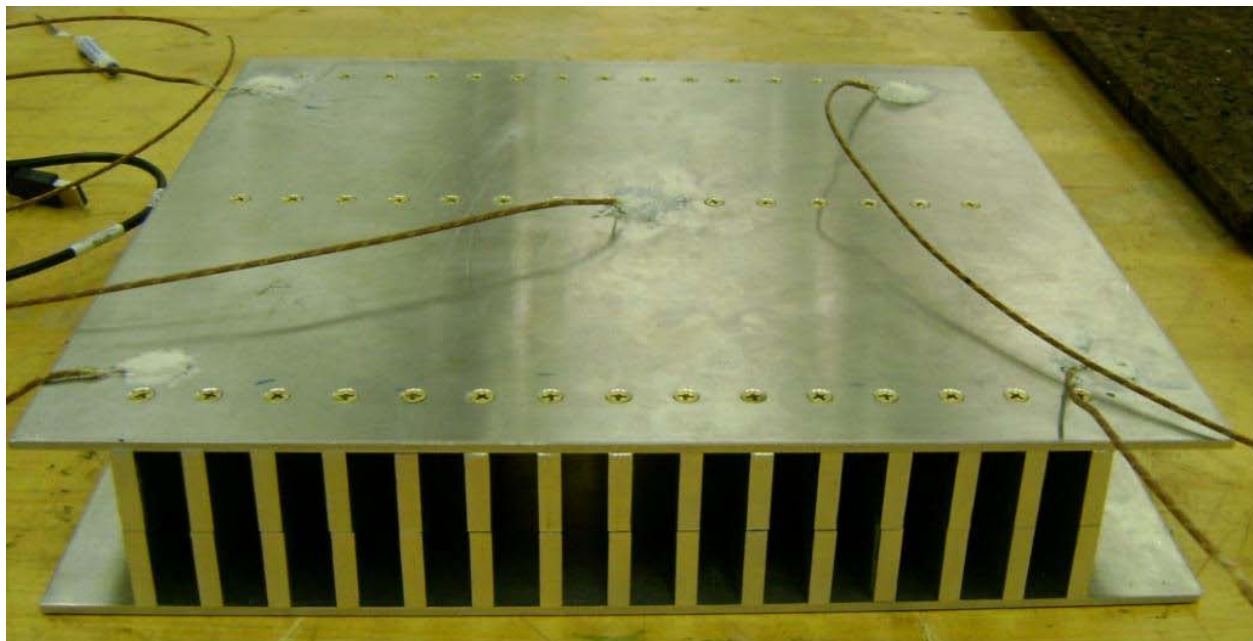


Figure 39: Shifting Fins Thermal Semiconductor Prototype Conducting Configuration.



Figure 40: Shifting Fins Thermal Semiconductor Prototype Insulating Configuration.

2.3 VARIATIONS OF THE SHIFTING FINS THERMAL SEMICONDUCTOR

After testing the original conducting and insulating configurations of the shifting fins thermal semiconductor prototype, several modifications were made to the prototype to test other cases slightly different from the original shifting fins concept. Some of the variations of the shifting fins device involved using foam insulation instead of air between the fins, using silver-and silicone-based thermal greases between the fins where they contact, and placing the aluminum plates back-to-back with the fins facing outward for several tests. Additionally, during the modeling phase of the project, several other concept with the fins were also examined that differed greatly from the shifting fins prototype to evaluate if different arrangements of the fins could offer improved performance over the shifting fins devices. Designs where the fins fold out to make contact with each other instead of shifting horizontally and shift horizontally making thermal contact at their sides instead of at the top/bottom interface were modeled using ANSYS finite element analysis software. The different variations of the shifting fins thermal semiconductor concept will be discussed in the following sections.

2.3.1 Using Foam Insulation in Spaces between the Fins instead of Air

Although most of the convection heat transfer of the air in the spaces between the fins of the shifting fins thermal semiconductor prototype was eliminated by having very tight spacing between the fins, some

convection heat transfer occurred, causing higher overall heat transfer than desired when the shifting fins prototype was in its insulating state. To eliminate all of the natural convection of the air between the fins, the spaces between the fins in the top and bottom pieces of the prototype were filled with pieces of polyisocyanurate foam building insulation, which can be easily cut into small rectangular pieces. The polyisocyanurate foam insulation also has a very low thermal conductivity of only 0.02163 W/m K, which is approximately that of air, resulting in very little conduction through the foam insulation between the plates. Even once the foam insulation was placed between the fins, the fins were still able to shift horizontally to change from a contacting, conducting state to a non-contacting, insulating state because the foam insulation will shift left and right in conjunction with the fins. Figure 41 shows how the polyisocyanurate foam insulation was used in the air spaces between the fins in the bottom plate piece, while Figure 42 shows the shifting fins prototype in its insulating state once the foam insulation has been placed between the fins.

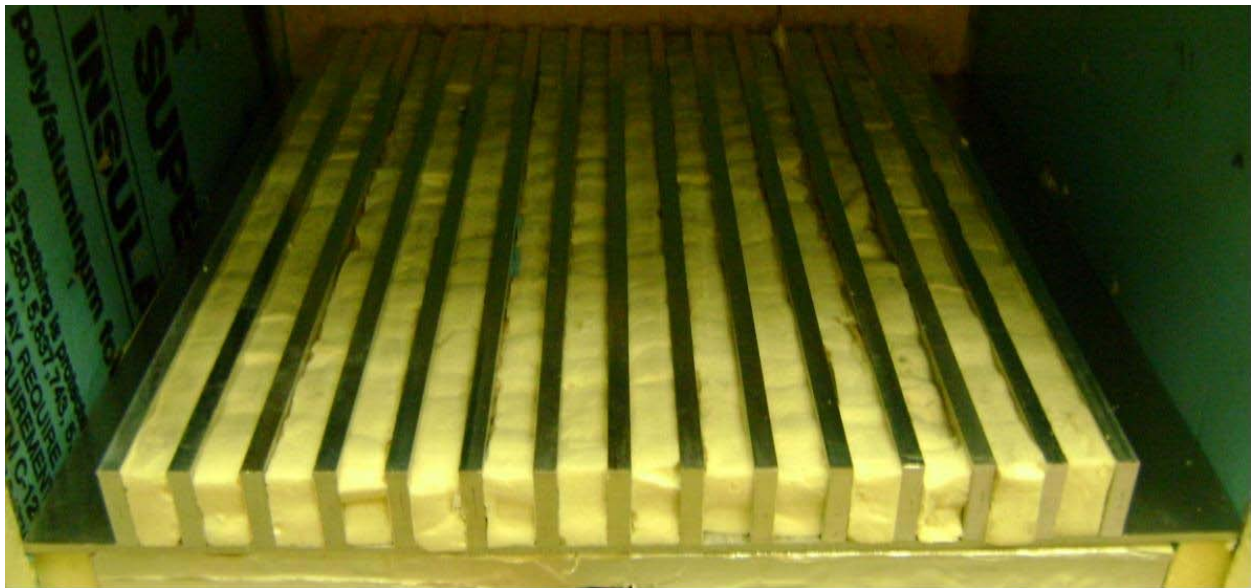


Figure 41: Bottom Piece of Shifting Fins Thermal Semiconductor Prototype with Foam Insulation between Fins.



Figure 42: Shifting Fins Thermal Semiconductor Prototype with Foam Insulation between Fins in its Insulating State.

2.3.2 Using Silver-and Silicone-based Thermal Grease to Improve Thermal Conduction

While adding foam building insulation to the air spaces between the fins helped to improve the insulating state of the shifting fins device by reducing natural convection, silver- and silicone-based thermal greases were utilized to improve the conducting state of the thermal semiconductor by reducing the thermal contact resistance where the fins touch each other. The problem of thermal contact resistance arises from the fact that no surface is perfectly smooth but has some level of surface roughness [26]. Due to surface roughness of two surfaces that are in contact, some areas of the two surfaces do not contact each other directly because of air that is trapped in tiny pockets in the surface roughness between the two materials [26]. A schematic that illustrates the effect of a small air gaps in the interface between two materials on thermal conduction is given in Figure 44, where the thermal contact resistance is given by R_C and the thermal contact conductance is given by h_C [27]. The thermal contact conductance is a property used to describe the amount of conduction between two material surfaces in contact and is dependent on the surface type, surface roughness, surface temperatures, and the amount of pressure between the two surfaces in contact [26]. If two surfaces had a perfect thermal contact with each other, both surfaces would have the same temperature, but as Figure 43 shows for real surfaces a temperature drop will occur in the direction of heat flow over the interface between the surfaces due to thermal contact resistance [27].

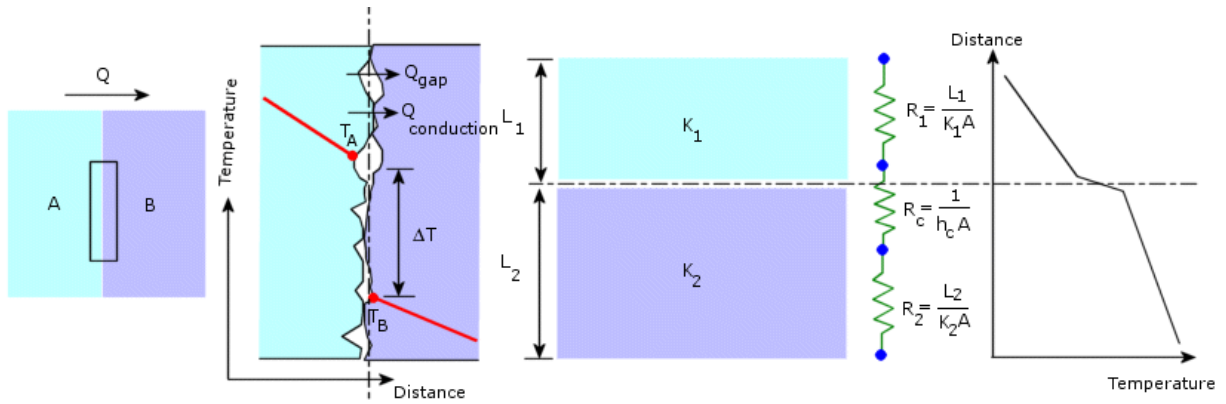


Figure 43: Schematic Diagram of the Effects of Thermal Contact Resistance at the Interface between Two Surfaces [27].

The largest amount of thermal contact resistance in the shifting fins prototype takes place at the interface where the top fins come into contact with the bottom fins to form a thermal conduction path. This location has the highest thermal contact resistance because the fins are not joined together and because very little pressure is applied at the point of contact, only the weight of the top plate and fins pushing down on the bottom fins. Some thermal contact resistance is also present at the interfaces where the bottom fins are mounted to the bottom plate and the top fins are mounted to the top plate due to surface roughness of the plates and fins. The amount of thermal contact resistance between the plates and fins is lower; however, than between the top and bottom fins, since the plates and fins are actually physically joined by screws instead of the top fins only lying on top of the bottom fins. To lessen the problem of thermal contact resistance at the interface between the top and bottom fins for some of the tests, two types of thermal greases were applied to the top and bottom fins in a very thin layer to enhance the conduction heat transfer at the interface between the fins. Since thermal contact resistance posed less of a problem at the interfaces between the fins and the two plates, thermal greases were not utilized at those two locations. A photo of the silver-based thermal grease being applied to the bottom fins is shown in Figure 44.

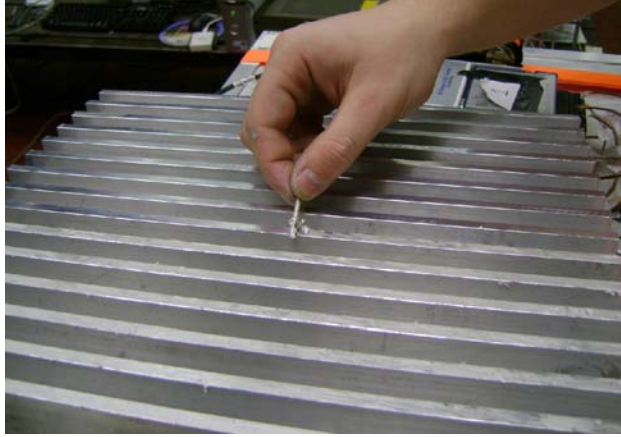


Figure 44: Application of Silver-Based Thermal Grease to the Bottom Fins of the Shifting Fins Prototype.

Thermal greases essentially work by spreading out to fill up the small, low conductivity air pockets with a much more highly conductive material at the interface between the fins. First, silver-based thermal grease was applied to the fins, which consists of silver particles suspended in a liquid and has a thermal conductivity of 8.652 W/m K , which is much lower than the thermal conductivity of the aluminum alloy 6061 being used for the fins, but still much higher than that of the air causing the thermal contact resistance. After conducting a few tests and discovering that the silver grease was extremely thick and difficult to apply in a very thin layer, silicone-based thermal grease was also tried. Typically, silicone-based greases consist of beryllium oxide, aluminum oxide, or aluminum nitride particles suspended in a liquid with an overall thermal conductivity between 0.7 and 3 W/m K . Although the silicone-based thermal grease had a lower thermal conductivity than the silver-based thermal grease, it ended up being much easier to apply in a thin layer during testing.

2.3.3 Back-to-Back Aluminum Plates with Fins Concept

Another variation on the shifting fins smart insulation concept involved flipping the bottom and top pieces over so that the aluminum plates were back-to-back, and the fins were sticking outward, as shown in Figure 45. The rationale behind this design was to use the fins' large amount of surface area to capture

heat to quicken the heating of the bottom plate for cases such as the sunny winter day case. The top plate was then placed directly on top of the bottom plate so that the two plates were in direct thermal contact for the conducting configuration. Finally, the top fins were positioned sticking upward to act as a heat sink with a large amount of surface area to dissipate heat quickly when the device is in conducting mode to the area on the other side of the smart insulation device.

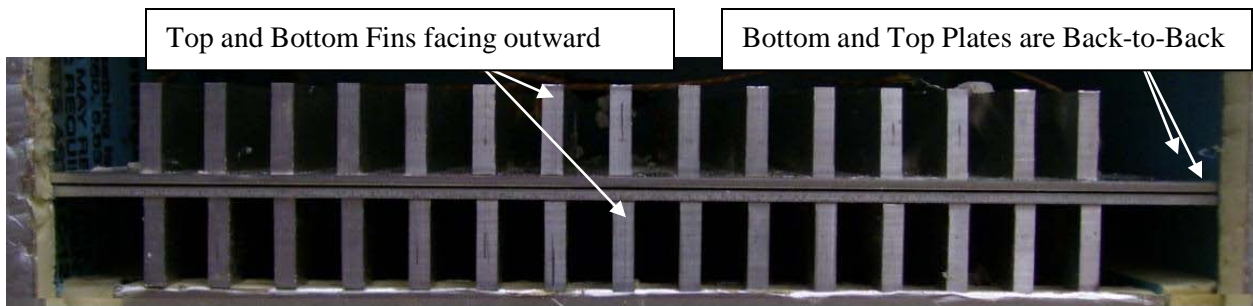


Figure 45: Back-to-Back Aluminum Plates with Fins Device in its Conducting Configuration.

For the back-to-back plate device the previous method of actuation between conducting and insulating states of horizontally shifting the fins was no longer feasible so a different type of actuation was necessary. To change the back-to-back plates concept to an insulator state, it was decided that the two plates would move vertically apart until a two inch (5.08 cm) air gap was present between the plates. Although natural convection heat transfer now played a much larger role when the device was in its insulating state due to the much larger air space than before, conductive heat transfer was now nearly eliminated. Figure 46 gives an image of the back-to-back plates device when it has been changed to its insulator state, where two low conductivity pieces of polyisocyanurate foam insulation spacers have been placed between the plates so that heat transfer by conduction is still prevented through the spacers.

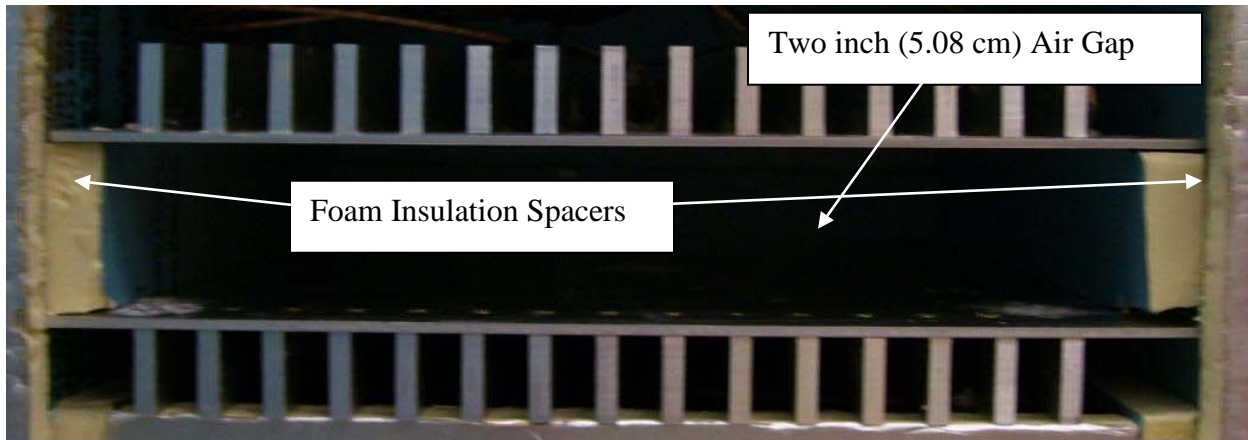


Figure 46: Back-to-Back Aluminum Plates with Fins Device in its Insulating Configuration.

2.3.4 Variations of Shifting Aluminum Fins Thermal Semiconductor Modeled in ANSYS

In addition to testing several different types of related thermal semiconductor systems using the original shifting aluminum fins smart insulation concept, three other related ideas were also modeled and analyzed in ANSYS without ever being built or tested. After the original shifting fins thermal semiconductor device was experimentally tested, a mathematical model of the heat transfer through the original device was constructed for the design's conducting and insulating configurations using ANSYS finite element analysis software and some of the experimental data. Once a model was obtained for the original shifting fins smart insulation concept, it could then be extended and applied to other similar concepts. The first of the three concepts modeled in ANSYS also used the idea of shifting fins between contacting and non-contacting positions to connect or break a thermal conduction path as in the previous device, but now the bottom and top fins contact at the sides instead of vertically. As a result, the fins had to be lengthened as shown in Figure 47 which shows schematics of the system modeled in ANSYS in both its insulating and conducting states. Besides changing the length of the fins and slightly changing the fin positioning, the device has the same basic design and dimensions as the original shifting fins thermal semiconductor.

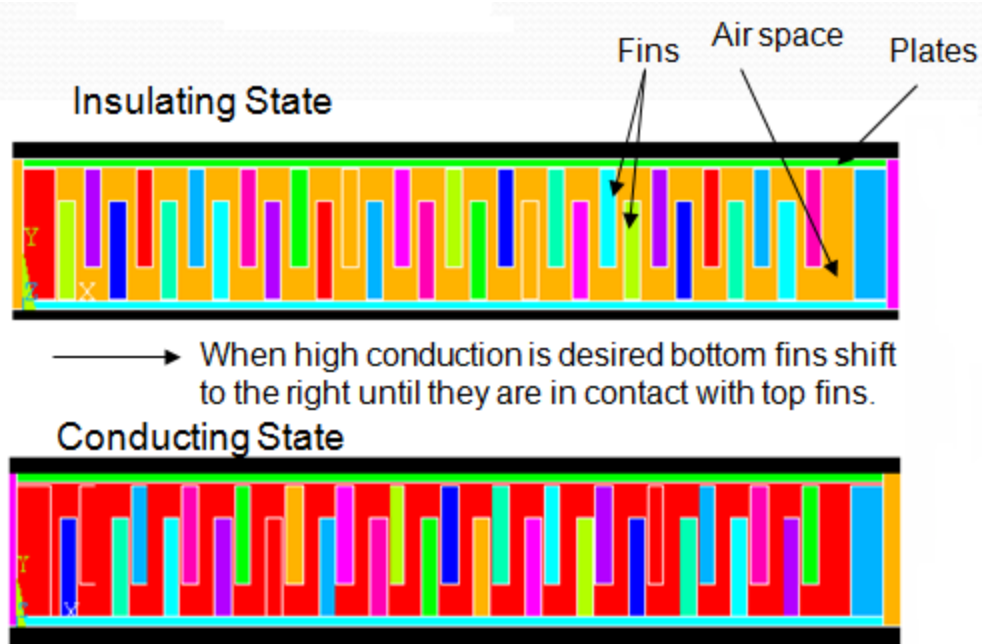


Figure 47: Insulating and Conducting States of Fins Shifting with Side Contact ANSYS Model.

Next, the second invention modeled using ANSYS also used fins that would contact vertically when the device was in its conducting state, but the second device had the fins fold in from a horizontal position to a vertical position to vertically contact the fins on the opposite plate by rotating 90° from their original positions. In this design a $1\frac{1}{2}$ in. (3.81 cm) air gap is present between the fins on opposite plates when the fins are in their folded down position, which eliminates almost all conduction between the top and bottom plates, but also allows for more natural convection heat transfer of the air. This device had almost all of the same specifications as the original shifting fins thermal semiconductor, except that it had only twenty-two fins instead of thirty fins with different positioning of the fins. Due to the feature of the fins folding out to a horizontal position, greater spacing was needed between the fins in the new design requiring the number of fins to be reduced. Schematics of the ANSYS model of the folding fin device, in both its insulating and conducting states is shown in Figure 48.

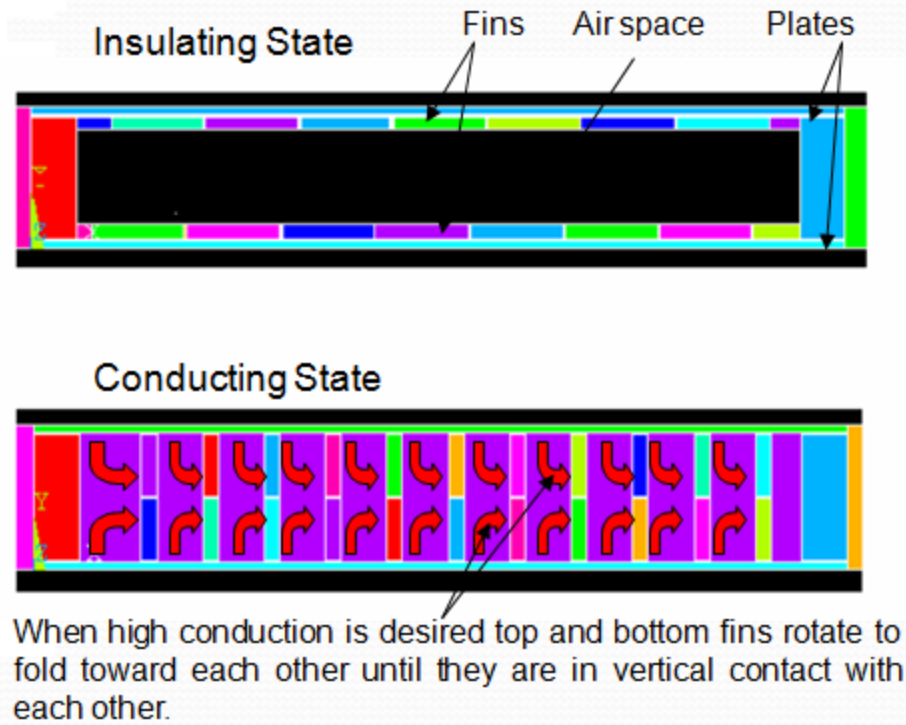


Figure 48: Insulating and Conducting States of Fins Fold in with Vertical Contact ANSYS Model.

Finally, the last variation of the shifting fins thermal semiconductor modeled in ANSYS combined the two previous ideas by having the fins fold in and make side contact. As with the earlier folding fins model, the number of fins had to be reduced because of the space needed between the fins when they are in their horizontal, stowed position. To accommodate for the additional fin length needed for side contact; however, the space between the fins in the design must be even larger. Thus, the amount of fin reduction needed for the fins fold in with side contact device is much larger than before with the number of overall fins reduced from thirty originally to only fourteen. The insulating state of the folding fins with side contact device looks almost exactly the same as the fins fold in with vertical contact device's insulating configuration as shown in Figure 48. The conducting configuration of this device modeled, as modeled in ANSYS, is illustrated in Figure 49.

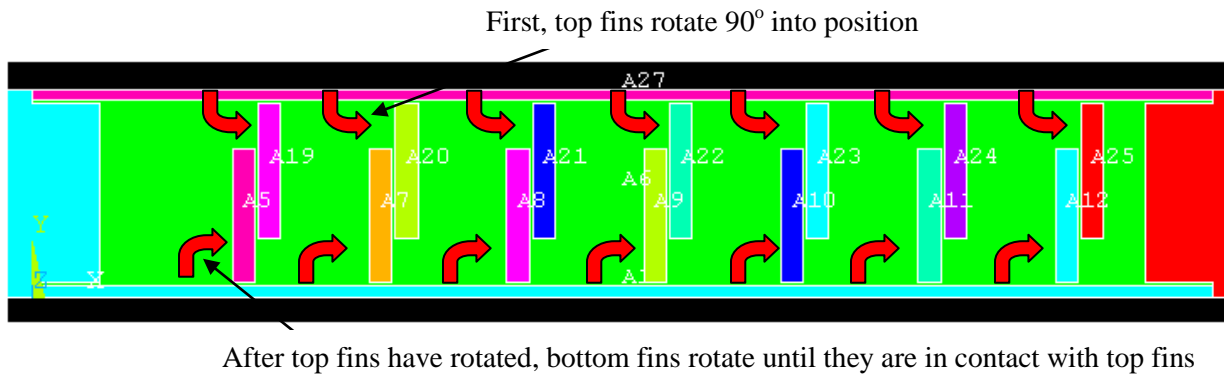


Figure 49: Conducting State of Fins Fold in with Side Contact ANSYS Model.

2.4 INFLATABLE HONEYCOMB-LIKE STRUCTURE THERMAL SEMICONDUCTOR DEVELOPMENT

2.4.1 Inflatable Honeycomb-like Structure Thermal Semiconductor Concept

The second major smart insulation concept chosen for fabrication and testing was an inflatable honeycomb-like structure. The basic principles for the inflatable honeycomb-like smart insulation idea are similar to those of Laing [12]. The general concept for the second thermal semiconductor device called for an inflatable structure made of up a very thin material, such as plastic, filled with a low conductivity gas, such as air, that can be inflated and deflated with an air pump to change the device between its conducting and insulating states. When the smart insulation device needs to have low thermal conductivity, the inflatable structure will be deflated by suctioning the air outside of the structure. Without the air expanding the inflatable device, the deflated thermal semiconductor will become extremely thin, since it will consist of only a very thin layer of the material used to contain the air. From Equation 2.1 for the thermal resistance to conduction for a plane wall material with a specified thermal conductivity, thickness, and cross-sectional area, the thermal conduction resistance will decrease when either the thermal conductivity, k , is increased or the thickness of the material, Δx , is decreased [26].

$$R_{th,conduction} = \frac{\Delta x}{kA} \quad (2.1)$$

In the deflated case, the thickness of the device is decreased greatly, while the thermal conductivity of the device had also been increased, since the device is now only made up of a very thin solid material instead of primarily air, resulting in much less thermal conduction resistance and a conducting state for the honeycomb-like structure.

In order to switch the inflatable thermal semiconductor to its insulating state, an air pump would be used as the actuation mechanism, which would require some amount of energy, but no energy will be needed to keep the device in its insulating or conducting states. By inflating the honeycomb-like structure with air, the thickness of the structure will then increase, while the thermal conductivity of the structure will decrease significantly. This will result in much higher thermal conduction resistance, giving it an insulating state. Figure 50 illustrates the inflatable honeycomb-like thermal semiconductor concept in both its conducting and insulating states.

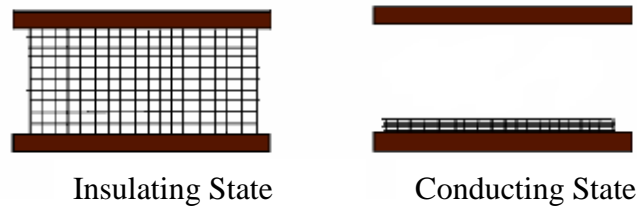


Figure 50: Inflatable honeycomb-like Structure Thermal Semiconductor Concept.

Even though simply inflating and deflating the structure would allow the smart insulation device to function as a thermal semiconductor by allowing and inhibiting the conduction of heat, the problem of natural convection of the air within the structure during its insulating state posed a problem. To solve the problem of natural convection, the inflatable thermal semiconductor structure is arranged in a honeycomb pattern. Since high levels of natural convection will occur in larger volumes of air, the interior space of the device was divided into many small chambers of air similar to honeycombs in a beehive. By breaking the air up into many tiny volumes, the air will not be able to circulate through the total volume of the

device for natural convection, resulting in much less convective heat transfer across the inflatable thermal semiconductor. One additional feature that the inflatable honeycomb-like device had that differs from a honeycomb is the need for small holes in the small air chamber to allow air to flow from chamber to chamber during the inflation and deflation of the thermal semiconductor. The holes must be designed so that they are large enough to allow for easy inflation and deflation of the entire structure, while still being small enough to keep the levels of natural convection in the air chambers very low.

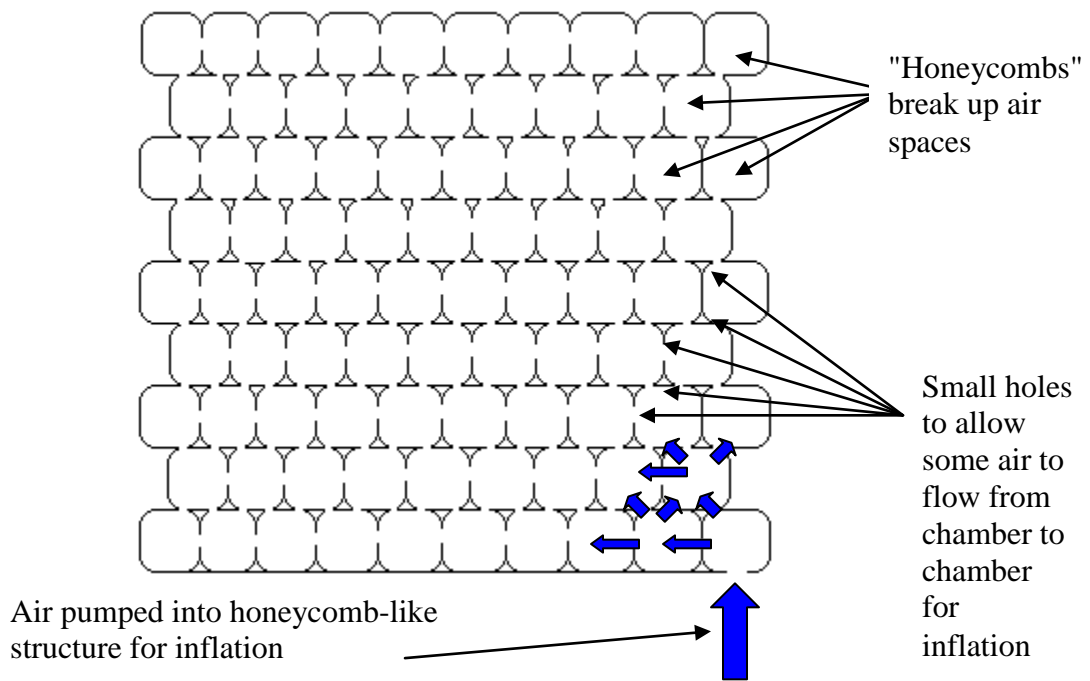


Figure 51: 2-D Side-View Schematic of Inflatable Honeycomb-like Structure for Thermal Semiconductor Concept.

A two-dimensional diagram of the inflatable honeycomb-like structure given in Figure 51 shows how the structure is arranged with small "honeycombs" of air with small holes in the air chambers to allow air to flow throughout the device for inflation and deflation.

Although the inflatable honeycomb-like thermal semiconductor device may have been based on the same general concepts from a previous patent, our inflatable honeycomb-like smart insulation device is

the first ever actually fabricated and tested from the those general concepts. Moreover, the actual design, materials, and fabrication of our invention discussed in the following sections were very different from previous devices proposed, resulting in a novel smart insulation device. In the next section the general design of the inflatable smart insulation devices built and tested in our laboratories will be described.

2.4.2 Inflatable Honeycomb-like Structure Thermal Semiconductor Design

As with the shifting fins thermal semiconductor device discussed earlier, the first major design decision was to postpone the design and fabrication of the actual actuation mechanism that would be used to switch the inflatable honeycomb device between its insulating and conducting states. Instead, the main focus of the design would be to develop an inflatable honeycomb-like device that could be tested in its insulating and conducting states separately to evaluate the device's performance in terms of its change in thermal conductivity between the two states. Each of the different designs for the inflatable honeycomb-like thermal semiconductor concept would eventually have two prototypes separately built to represent the design's deflated, conducting state and inflated, insulating state. For consistency in testing many of the dimensions of the inflatable honeycomb-like structure were set to match those of the first concept, the shifting fins thermal semiconductor.

One of the major difficulties encountered during the design of the inflatable honeycomb-like thermal semiconductor was trying to either find a honeycomb-like material available commercially that could be modified to be inflated or deflated or to construct a honeycomb-like device that could be inflated or deflated in our own laboratories. After determining that it was not feasible to develop this type of material in the laboratory at this time, much effort was placed into obtaining a suitable material from an outside company. All of the materials found to be available for use in the inflatable honeycomb smart insulation design were very thin, much thinner than the 2.25 in. (5.715 cm) desired, but the materials did serve the main purposes of the design of trapping air into small chambers and being able to be tested in both inflated and deflated states. In order to reach the total thickness needed for the inflated state of the thermal semiconductor, thin pieces of Bubble Wrap-like material were layered on top on each other.

Although layering thin pieces of honeycomb-like material together does not truly produce an inflatable thermal semiconductor device that could actually be used at this time, it does allow for "proof-of-concept" testing of an inflatable honeycomb-like smart insulation device that could significantly change its thermal conductivity when actuated. In addition, the performance of the conducting state of the inflated thermal semiconductor could also be determined by deflating all of the layers collectively and testing to see whether or not high thermal conduction can be achieved through the now deflated, extremely thin structure. After completing the basic design, two very similar types of inflated honeycomb-like thermal semiconductors using two different types of materials were fabricated for testing.

2.4.3 Reflectix Inflatable Thermal Semiconductor

Two materials were found commercially that were utilized to fabricate two inflated honeycomb-like thermal semiconductor devices. Both of the materials were very similar in construction and appearance to Bubble Wrap, which is a clear plastic material often used in packaging. The first type of inflated smart insulation device was constructed using Reflectix bubble wrap building insulation. The primary application of Reflectix is as a radiant barrier in an attic space to greatly reduce the radiation heat transfer between the attic space and the outside roof or exterior environment. The insulation has also been designed for a secondary application as thermal insulation to stop conduction and convection heat transfer that can be used in many areas of the home on top of conventional building insulation with R-values ranging from 3.0 to 18 ft²F-hr/Btu (0.5 to 3.2 m² K/W) depending on the application. Reflectix insulation is composed of two layers of 96% reflective metalized aluminum foil separated by two horizontal rows containing many small, ellipsoid-shaped air spaces. The honeycomb-like air spaces in Reflectix building insulation are about 1/4 in. (0.635 cm) in thickness with a diameter of about 3/8 in. (0.953 cm). A side-view of one layer of the Reflectix building insulation composition is given in Figure 52, while a top view is given in Figure 53.

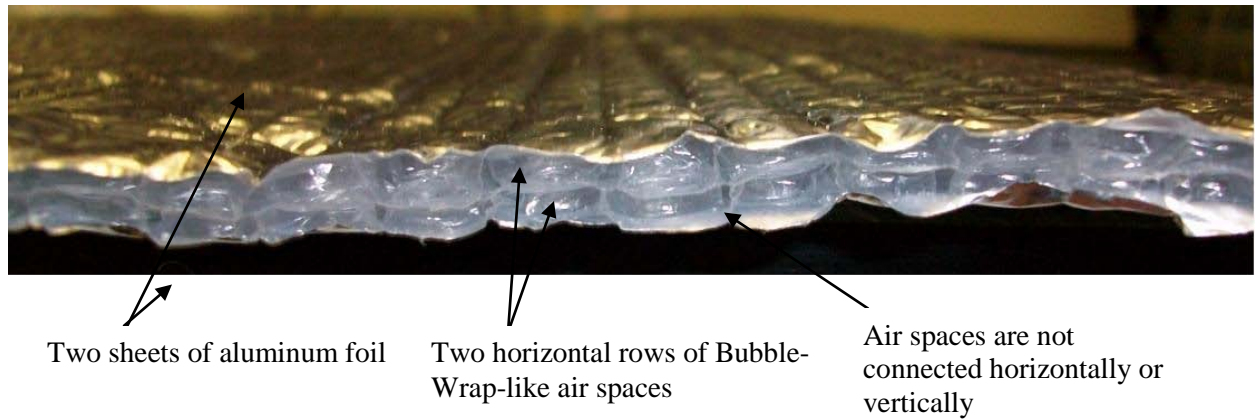


Figure 52: Side-View of One Layer of Reflectix Building Insulation.



Figure 53: Top-View of One Layer of Reflectix Building Insulation.

By trapping air into tiny chambers between the two aluminum foil sheets, the Reflectix insulation is able to provide the honeycomb-like structure needed for the inflatable thermal semiconductor design.

When purchased Reflectix building insulation is sold as a coil containing a very long continuous sheet of insulation. Since the air spaces in the insulation were not joined at any points vertically or horizontally to each other, the Reflectix insulation could be cut into 13.25 x 13.25 in. (0.337 x 0.337 m) pieces to be layered as shown in Figure 53 earlier. Nine pieces of Reflectix insulation were layered on top of one other to obtain approximately the 2.25 in. (5.715 cm) total thickness for the inflatable honeycomb-like thermal

semiconductor design. Some very thin air spaces between the Reflectix building insulation pieces did occur in the final prototype after layering, but they did not pose a problem because they were only a very small fraction of the thickness of than the actual layers of Reflectix insulation. A photo of the completed Reflectix inflatable honeycomb-like thermal semiconductor in its inflated, insulating configuration can be seen below in Figure 54. A close-up side-view of the completed Reflectix inflatable thermal semiconductor is also given in Figure 55 to show how the nine pieces were layered together.

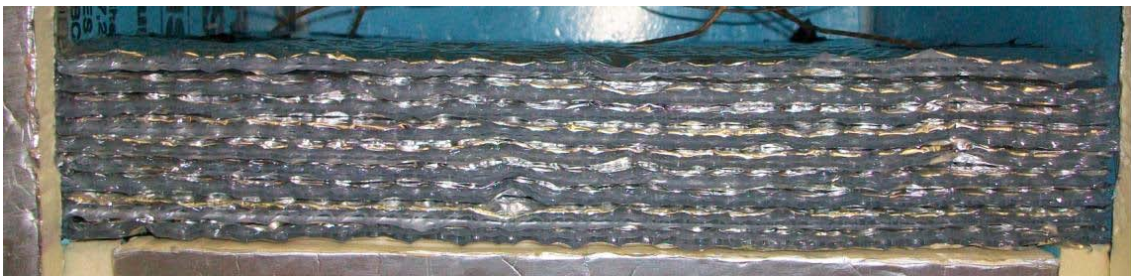


Figure 54: Reflectix Inflatable Thermal Semiconductor Prototype in its Insulating Configuration.



Figure 55: Close-Up View of Reflectix Inflatable Thermal Semiconductor in its Insulating State.

In order to develop a second Reflectix inflatable thermal semiconductor prototype in a deflated, conducting state, nine additional pieces of Reflectix building insulation were cut to the same dimensions specified beforehand. Then, each of the nine layers of insulation was deflated by popping the Bubble-Wrap-like air spaces in each individual layer to allow the air to escape. Figure 56 gives an image of the fabricated Reflectix inflatable thermal semiconductor prototype in its deflated, conducting state, while a close-up side-view of the Reflectix thermal semiconductor in its conducting state is also given in Figure 57. Although as much air as possible was removed from the deflated layers of Reflectix insulation as possible, some air did remain trapped due to the difficulty in removing the air from the many small individual air spaces between the two aluminum sheets. The final deflated Reflectix smart insulation prototype completed had a total thickness of 1.125 in. (2.858 cm), which was half of the original thickness of the inflated Reflectix smart insulation device. The reduction in thickness from deflating the Reflectix thermal semiconductor was not as large as expected due to the thickness of the sheets of aluminum foil, the amount of plastic left over after deflating the air spaces, and some leftover air that could not be removed from the insulation layers. If the Reflectix smart insulation prototype was actually implemented in the walls and/or roof of a building, a vacuum pump would likely be utilized to inflate and deflate the insulation when needed instead of manually deflating the honeycomb-like spaces in each layer to produce a deflated prototype. With a vacuum pump, the air inside of the Reflectix smart insulation would be much more effectively suctioned out of the insulation, leaving little leftover air in the device and producing a greater reduction in thickness of the Reflectix thermal semiconductor. In Figure 58, the inflated and deflated Reflectix thermal semiconductor prototypes are shown side-by-side for comparison to demonstrate the change in thickness that could be obtained if the honeycomb-like structure of the Reflectix building insulation could be inflated and deflated to switch between conducting and insulating states.

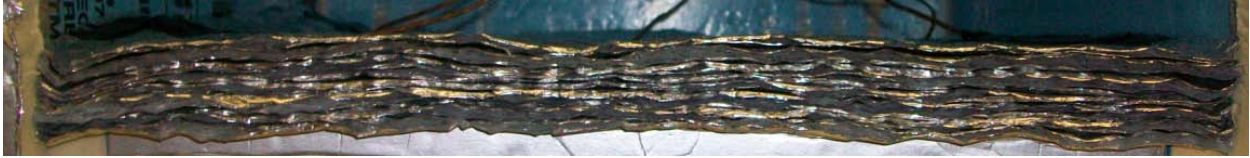


Figure 56: Reflectix Inflatable Thermal Semiconductor Prototype in its Conducting Configuration.



Figure 57: Close-Up View of Reflectix Inflatable Thermal Semiconductor in its Conducting State.



Figure 58: Side-by-Side Comparison of Reflectix Inflatable Thermal Semiconductor Inflated and Deflated Prototypes.

2.4.4 NOVUS Inflatable Thermal Semiconductor

One of the main problems of the Reflectix inflatable thermal semiconductor device was the lack of change in thickness when the device is deflated. Ideally, an inflatable smart insulation device would be able to be deflated from the 2.25 in. (5.715 cm) thickness to an extremely small thickness. The main focus then in the fabrication of the second inflatable honeycomb-like thermal semiconductor was to find a material that functioned in a similar manner to the Reflectix insulation material, while being able to demonstrate a much larger change in thickness between states and thus, a much larger change in thermal conductivity between states. Eventually, a suitable material was found in the NOVUS inflatable bubble-wrap-like packaging material.

From the several different types of NOVUS inflatable packaging systems available, the type named “quilt, air-smooth” was chosen because it had the smallest air spaces needed for the honeycomb-like structure of the thermal semiconductor. The NOVUS inflatable packaging system utilizes a machine that prints out bubble packaging material in thin sheets by inserting a very thin polyethylene film material with a thermal conductivity of 0.33 W/m-K into the machine and inflating rows of circular air spaces in one direction connected by small passageways. In the opposite direction, the circular air spaces are not joined together at any point. Also, unlike the Reflectix building insulation used earlier, only one row of Bubble-Wrap-like air spaces make up the material instead of two rows stacked on top of one another. After inflating small pieces of packaging that were slightly larger in dimension than the 13.25 x 13.25 in. (0.337 x 0.337 m) size used in the prototypes beforehand, the machine would seal the air spaces at the end of the piece of packaging and start inflating the air spaces of the next piece. This resulted in a very long continuous coil of packing that was about 13.25 in. (0.337 m) wide, consisting of many smaller pieces with long rows of circular air spaces that were each slightly larger than 13.25 in. (0.337 m) in length. Depending on how much packaging is needed for shipping a certain good, the smaller pieces of the packaging could be easily torn from the long continuous coil. Many companies purchase NOVUS inflatable packaging machines so they can produce their packaging on-site when needed. The only

packaging material that needs to be continually purchased with the NOVUS system is the thin polyethylene film, which is much easier to store and transport when deflated than other types of packaging that has already been inflated with air. Whenever a company needs packaging, their NOVUS packaging system can inflate whatever amount is needed, and the packaging will be at maximum effectiveness, since it was just inflated.

Several individual pieces of the NOVUS packaging material were torn from the thirty-foot long coil and were cut to the desired dimensions of 13.25 x 13.25 in. (0.337 x 0.337 m). The individual circular air spaces of the pieces, which had the appearance of large Bubble-Wrap, were ½ in. (1.27 cm) in diameter and 0.45 in. (1.143 cm) in thickness. The total thickness of the 13.25 x 13.25 in. (0.337 x 0.337 m) pieces overall was taken to be 0.45 in. (1.143 cm) because the thickness of the thin plastic material of the packaging was negligible when compared to the thickness of the air spaces. A top-view of one layer of the NOVUS packaging thermal semiconductor in its inflated state is given in Figure 59.

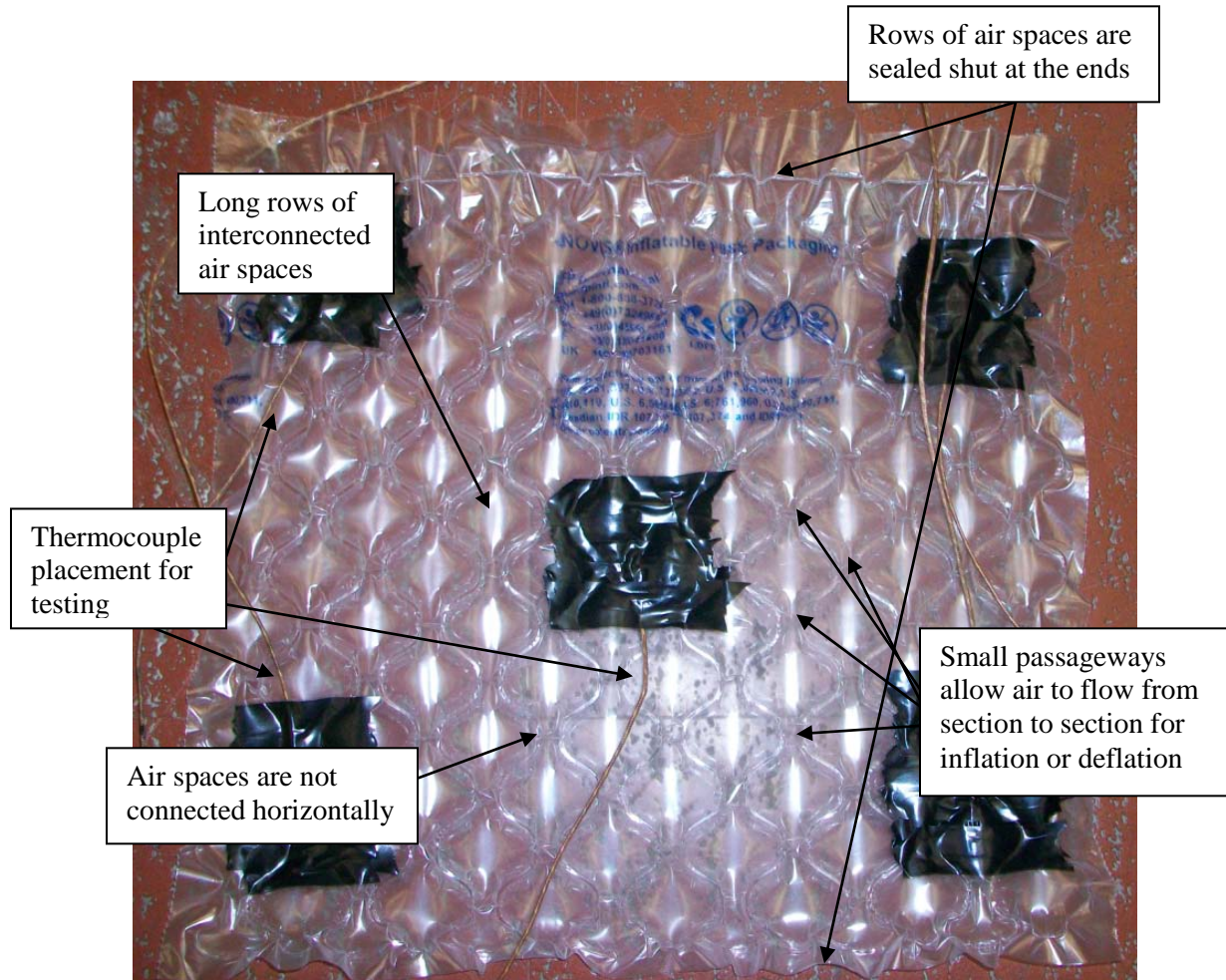


Figure 59: Top-View of One Layer of NOVUS Packaging Material.

As seen in Figure 59, the NOVUS packaging material is closer than the Reflectix building insulation material to the inflatable honeycomb-like structure eventually desired for an inflatable thermal semiconductor in that it does feature the small holes between air spaces to allow air to flow from space to space for inflation or deflation, albeit in only one of the eventually three desired dimensions.

To produce an inflated NOVUS thermal semiconductor prototype with the consistent overall thickness of 2.25 in. (5.715 cm) used for all of the previous prototypes, layering of the NOVUS packaging material was utilized again. Fewer layers were required; however, than for the Reflectix building insulation, since the inflated NOVUS packaging material is much thicker than the Reflectix material. Eventually, five layers of NOVUS packaging material were used. A photo of the completed

NOVUS inflatable honeycomb-like thermal semiconductor in its inflated, insulating configuration can be seen below in Figure 60. A close-up side-view of the completed NOVUS inflatable thermal semiconductor is also given in Figure 61 to show how the five pieces were layered together.



Figure 60: NOVUS Inflatable Thermal Semiconductor Prototype in its Insulating Configuration.



Figure 61: Close-Up View of NOVUS Inflatable Thermal Semiconductor in its Insulating State.

After the first prototype of the NOVUS smart insulation device was fabricated in its inflated configuration, a second prototype was also built for the deflated configuration. Again for fabrication, five layers of NOVUS packaging material of the same dimensions were cut and layered on top of one another. Before layering the five layers were deflated by inserting a needle into each row of air bubbles to make one tiny hole in one of the bubbles. Once a tiny hole was made in one of the bubbles, the entire row of air

spaces was able to be deflated, since all of the bubbles were interconnected. Figure 62 gives an image of the fabricated NOVUS inflatable thermal semiconductor prototype in its deflated, conducting state, while a close-up side-view of the NOVUS thermal semiconductor in its conducting state is also given in Figure 63. Unlike the Reflectix smart insulation the NOVUS thermal semiconductor did exhibit a very large change in thickness once deflated, with a final deflated thickness of between 1/4-3/8 in. (0.635-0.953 cm) compared to the initial thickness of 2.25 in. (5.715 cm) depending on how amount of air was present between the layers of packaging.

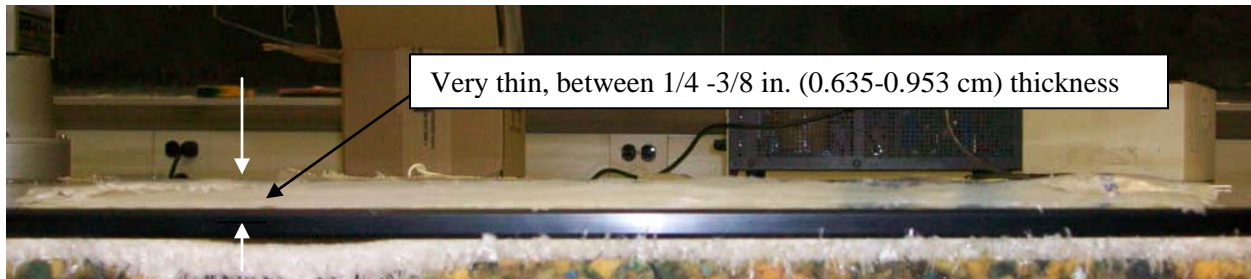


Figure 62: NOVUS Inflatable Thermal Semiconductor Prototype in its Conducting Configuration.

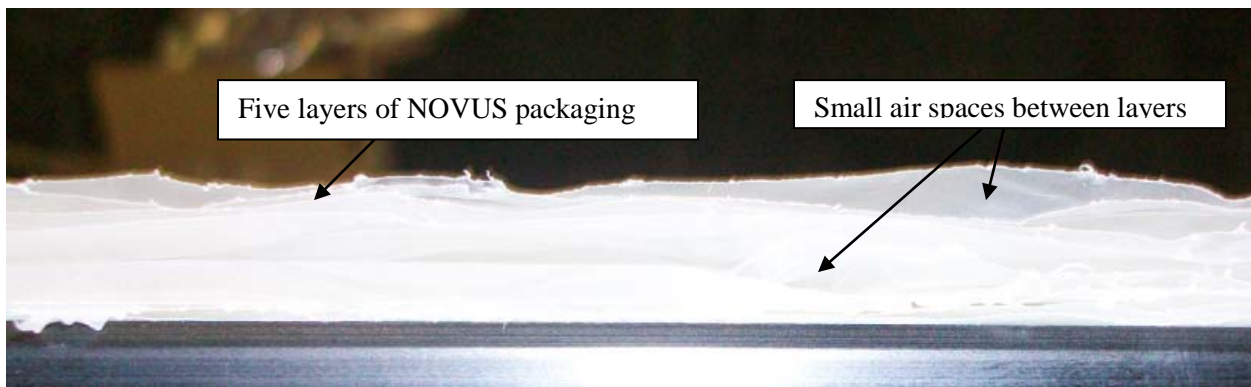


Figure 63: Close-Up View of NOVUS Inflatable Thermal Semiconductor in its Conducting State.

In Figure 64 the inflated and deflated NOVUS thermal semiconductor prototypes are shown side-by-side for comparison to demonstrate the change in thickness that could be obtained if the honeycomb-like

structure of the NOVUS smart insulation could be inflated and deflated to switch between conducting and insulating states.

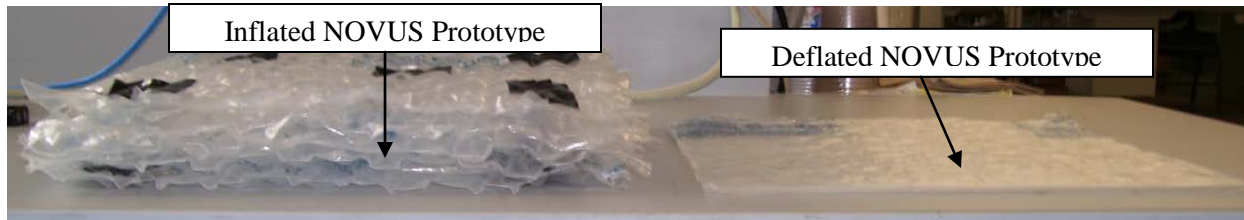


Figure 64: Side-by-Side Comparison of NOVUS Inflatable Thermal Semiconductor Inflated and Deflated Prototypes.

While the NOVUS inflatable thermal semiconductor had a major advantage over the Reflectix inflatable thermal semiconductor because of its ability to drastically change its thickness and thus, thermal conductivity between its conducting and insulating states, it does also have a major drawback. The honeycomb-like air spaces of the NOVUS smart insulation device are much larger than those of the Reflectix inflated prototype, which will result in much greater natural convection within the air spaces and a higher heat transfer overall for the NOVUS inflated prototype. This means that the even though the NOVUS thermal semiconductor will have a much higher thermal conductivity in its conducting state since it is much thinner than the Reflectix thermal semiconductor, it will also not function as well as an insulator due to the higher levels of natural convection.

2.4.5 Variations of the Inflatable Thermal Semiconductor

During the experimental testing of the NOVUS inflatable thermal semiconductor prototypes, the thermal conductivities for the device in its deflated, conducting state were found to be lower than expected. The reason behind this result was determined to be the small air spaces that were present between the layers of the thermal semiconductor prototypes. The air spaces in the NOVUS deflated

prototype in particular proved to be a problem because the air spaces between the layers were larger than the actual layers of deflated NOVUS packaging. To solve the problem of the small air spaces between layers in a real-world building setting, a vacuum pump would be used to more effectively suction the air out of the NOVUS smart insulation device during deflation, which would also result in the layers of plastic containing the air spaces in the NOVUS packaging to be compressed together. In order to easily compress the NOVUS packaging layers in the laboratory setting of the experimental testing, pressure was applied using two 1/8 in. (0.318 cm) aluminum alloy 6061 plates fabricated with the same thickness as the top and bottom plates of the shifting fins thermal semiconductor prototype. The two plates were then placed above and below the layers of NOVUS smart insulation to compress them to reduce the air spaces between layers. Figures 65 and 66 give images of the NOVUS inflatable thermal semiconductor with aluminum plates in both its insulating and conducting configurations.



Figure 65: NOVUS Inflatable Thermal Semiconductor Prototype with Aluminum Plates for Compression in its Insulating State.



Figure 66: NOVUS Inflatable Thermal Semiconductor Prototype with Aluminum Plates for Compression in its Conducting State.

3.0 INSULATION TEST CHAMBER FABRICATION AND EXPERIMENTAL SET-UP

To evaluate the performance of the smart insulation prototypes, many experiments were conducted to analyze the heat transfer and thermal conductivity across the devices in both their conducting and insulating configurations. The main focus used in the design of the experimental testing set-up was to design a set-up that would reproduce the conditions the smart insulation devices would be under if implemented in a real-world building setting. During the course of the development of the smart insulation prototype testing procedure, it was also determined that the experimental test set-up should focus primarily on representing the roof area of buildings, while in the experiments themselves both constant temperature and constant heat flux conditions would be applied to the smart insulation prototypes to simulate real-world temperature gradients across the insulation.

The first step in developing the experimental testing set-up for the smart insulation prototypes was to design an insulation test chamber that could produce the desired testing conditions for the thermal semiconductor devices on the inside, while isolating the thermal semiconductor prototypes from the outside ambient conditions of the laboratory. Next, equipment and computer software was chosen and obtained for the collection of the experimental data measured during the testing to complete the basic experimental set-up. In order to prove that the insulation test chamber sufficiently isolated the interior smart insulation devices from the exterior environment, several tests were conducted with a heat source placed inside an empty test chamber to measure the amount of heat that was escaping from the chamber over a long period of time. Once it was shown that the performance of the insulation test chamber was satisfactory, each of the different smart insulation prototypes was tested in both its conducting and insulating states for both constant temperature and constant heat flux conditions. To allow the smart

insulation prototypes to be compared more easily to conventional insulation and to each other, an additional test piece composed of a conventional type of building insulation was also constructed and tested.

3.1 SMART INSULATION TEST CHAMBER DEVELOPMENT

3.1.1 Insulation Test Chamber Interior Design

The first step of the design of the smart insulation test chamber was to decide on the dimensions required for the inner chamber and the overall configuration of the inner chamber needed to reproduce the conditions the smart insulation prototype would be under if implemented in an actual building setting. Two dimensions of the inner chamber, the length and the width, were already constrained to closely match the dimensions of the smart insulation prototypes for a tight fit between the devices and the inner chamber walls. To achieve a tight fit, a value of 13 1/2 in. (0.343 m) was utilized for the length and width of the inner chamber to give a small spacing of 1/8 in. (0.318 cm) between the 13.25 x 13.25 in. (0.337 x 0.337 m) smart insulation prototypes and the insulation chamber walls. The location of actual buildings that the smart insulation test chamber would most closely recreate for testing was chosen to be the attic, since it was the easiest to test and was determined to be the building location where smart insulation would likely be easiest to implement with the greatest short-term payback. In order to test cases mentioned before where smart insulation would be very beneficial, such as the sunny winter day and cool summer evening cases, two air spaces would be included in the inner test chamber design above and below the smart insulation prototypes. The bottom air space would represent the hot side of the smart insulation devices and contain a heat source, while the top air space would represent the cold side of the devices.

The bottom air space of the smart insulation test chamber consisted of a heat source, a thin layer of cork, and a 1.5 in. (3.81 cm) air gap between the heat source and the bottom of the thermal semiconductor

device being tested. The main purpose of the bottom air space and heat source was to reproduce the hot side of the device for all possible cases. For example, in the sunny winter day case, the bottom air space would reproduce the heating caused by thermal radiation on the roof of a building by having the heat source provide a constant heat flux to the hot side of the smart insulation prototype. For the cloudy winter day case, however, the bottom air space would switch roles to instead represent the warm building interior compared to the cold exterior roof by having the heat source maintain a constant warm temperature for the hot side of the smart insulation prototype. Similarly, the conditions of the hot side of the two summer cases of a cool summer evening and hot summer day could also be reproduced by the bottom air space. In the cool summer evening case the bottom air space would represent the hot interior building environment by maintaining a constant hot temperature compared to the cool outside environment, and in the hot summer day case the bottom air space would switch roles again to mimic the hot outside environment compared to the much cooler, likely air-conditioned, rooms of the building. The heat source chosen for the insulation test chamber was a Kapton (Polyimide film) Insulated Flexible Heater, consisting of an etched foil element of 0.0005 or 0.0001 in. (0.0127 or 0.00254 mm) thickness that is sealed between two layers of 0.002 in. (0.0528 cm) polyimide film and 0.001 in. (0.0254 cm) FEP adhesive. Among the different Kapton heaters available, the specific model of Kapton heater chosen was the 1212, which is a rectangular heater with a resistance of 9.2 Ω and a power density of 10 W/in², which results in a maximum power output of 1440 W for an input voltage and current of 115 V AC and 12.52 A respectively. The 1212 Kapton Insulated Flexible Heater was chosen as the heat source because it would be able to provide the amount of heating necessary for the testing, it was extremely thin since it was only 0.010 in. (0.254 cm) thick, it was relatively low cost, and it was the largest size heater available. Below the heat source a 12 x 12 in. (0.3 x 0.3 m) cross-sectional area, thin (1/2 in. (1.27 cm)) layer of semi-rigid cork insulation was used for safety purposes to help prevent the material of the insulation test chamber itself underneath the heater from melting or overheating if something caused the Kapton heater to overheat. Cork was chosen as the material to place underneath the heating element because of its remarkably high tolerance to heat [28]. To enable high heat transfer between the Kapton heat source and

the hot side of the smart insulation prototype, the bottom air space thickness had a small height of 1 1/2 in. (3.81 cm) thick. Adding in the 1/2 in. (1.27 cm) thickness of the cork insulation layer to the bottom air space thickness resulted in a final height of two inches (5.08 cm) needed below the smart insulation prototype. In order to elevate the thermal semiconductor prototypes above the Kapton heater, a shelf composed of a very low thermal conductivity polyisocyanurate foam building insulation was constructed by cutting large sheets of the foam insulation. A low thermal conductivity material was necessary for the shelf to prevent conduction heat transfer from occurring between the heat source and the high temperature side of the smart insulation devices, since only convection heating would be utilized. The thickness of the polyisocyanurate building insulation was 0.75 in. (1.91 cm), which allowed the shelf to fit exactly around the 12 x 12 in. (0.3 x 0.3 m) Kapton heater in the 13.5 x 13.5 in. (0.343 x 0.343 m) test chamber interior. Figure 67 gives an image of the bottom air space in the final fabrication of the insulation test chamber.

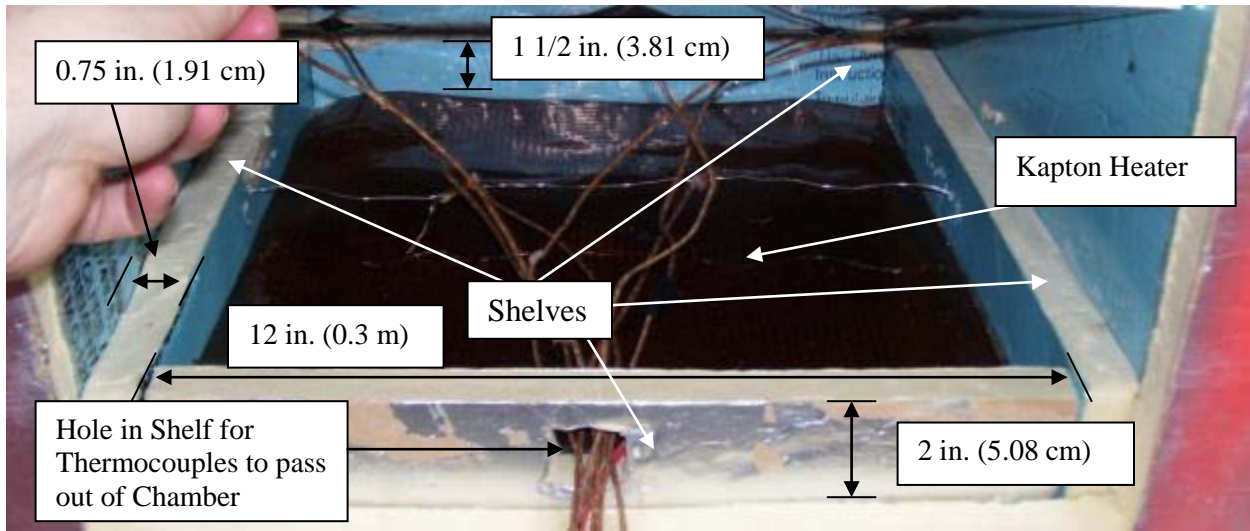


Figure 67: Bottom Air Space of the Smart Insulation Test Chamber with Kapton Heater Heat Source.

While the hot side of the thermal semiconductor devices will be sitting on top of the shelf facing the bottom air space below, the top cold side of the devices will be facing another much larger top air space. The major reason the bottom air space had to be kept very small was to expedite the heating of the

bottom, hot side of the smart insulation devices by the heat source, but no such requirement existed for the top air space, since it represented the cold side of the smart insulation prototypes. The height of the top air space was set to a value of 6 in. (15.24 cm), giving a total height of the test chamber interior of 10.25 in. (26.04 cm) once the heights of the shelf, smart insulation prototype devices, and top air space have been added. During the course of the experimental testing, however, the top air space height sometimes had to be increased or decreased in accordance with changes in the thickness of the thermal semiconductor devices. For example, when the NOVUS inflatable thermal semiconductor device was deflated the thickness was decreased to much less than the 2.25 in. (5.715 cm) thickness of its inflated configuration, which meant that the top air space height increased due to the decrease in the thickness of the smart insulation prototype. As with the rest of the test chamber interior, the top air space had a square cross-sectional area of 13.5 x 13.5 in. (0.343 x 0.343 m). An image of the entire smart insulation test chamber interior with a thermal semiconductor prototype inserted can be seen below in Figure 68.

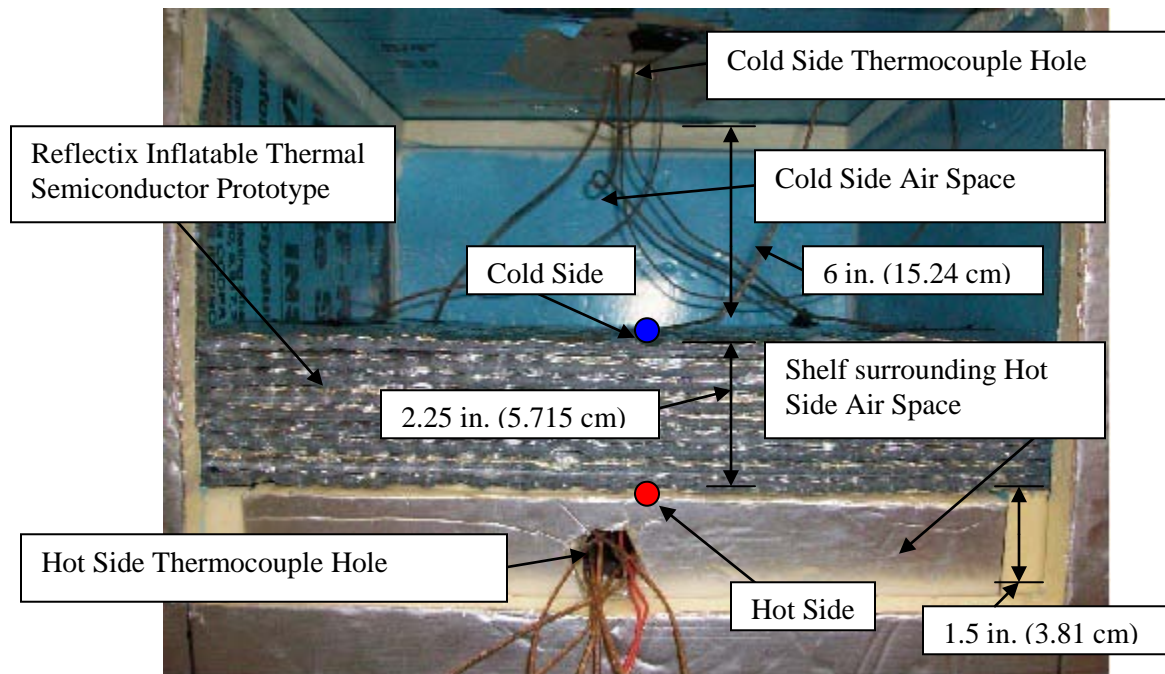


Figure 68: Insulation Test Chamber Interior with Smart Insulation Prototype Inserted.

The basic goal of all of the experimental tests that were run using the various smart insulation devices developed was to measure the level of heat transfer across the devices from the hot side to the cold side in order to compare between the prototypes' conducting and insulating states and between the prototypes themselves.

3.1.2 Insulation Test Chamber Overall Design and Fabrication

After the interior of the insulation test chamber had been designed and dimensioned, the next step was to design and fabricate the outer pieces of the insulation test chamber. The test chamber would be composed of many pieces of a very high R-value foam building insulation adhered together to form the structure. The first major decision of the design was to make the conventional foam building insulation around the interior test chamber at least five inches (12.70 cm) thick in all directions with a total R-value of at least 20 ft² F-hr/Btu (3.52 m² K/W) . This was estimated to be enough insulation to sufficiently prevent any of the heat emitting from the heat source from leaking out of the test chamber to the laboratory environment instead of heating up the bottom air space and hot side of the smart insulation devices as desired. Eventually, a suitable foam building insulation was found in Dow Building Solutions Super TUFF-R polyisocyanurate foam insulation, which consists of a closed-cell polyisocyanurate foam core sandwiched between an aluminum foil spacer and a Super Tri-Plex facer, which is a three-ply laminate of durable polyester, kraft, and reinforced aluminum foil. The main reasons why the Super TUFF-R building insulation was chosen over other types of foam insulation are its low cost and a very high R-value of 5 ft² F-hr/Btu (0.9 m² K/W) for each 0.75 in. (1.27 cm) layer. Fiberglass insulation was also considered as a building material for the insulation test chamber, but it was determined that it would be much more difficult to work with than the foam types of building insulation.

Similarly to the Bubble-Wrap-like smart insulation devices fabricated earlier that were layered to achieve the desired thickness, the Super TUFF-R building insulation was also layered to achieve the desired insulation thickness of the test chamber of at least five inches. To join the layers of the Super TUFF-R foam building insulation together, Loctite PowerGrab Foamboard Construction Adhesive was

utilized because it is designed specifically as an adhesive for materials such as foam building insulation, giving a very solid attachment between layers without destroying the foam insulation as with other types of adhesives. Before layering was done each of the different layers were cut with a utility knife to the necessary dimensions from very large sheets of polyisocyanurate building insulation. Since each of the polyisocyanurate foam insulation layers was 0.75 in. (1.91 cm) thick, seven layers were required to obtain the minimum five inch (12.70 cm) overall thickness. After adding together the individual layers' R-values of 5 ft² F-hr/Btu (0.9 m² K/W) , a total R-value of 35 ft² F-hr/Btu (6.2 m² K/W) for a final layered foam insulation thickness of 5.25 in. (13.34 cm) was calculated; this was nearly double the original desired R-value of 20 ft² F-hr/Btu (3.52 m² K/W) , showing that the polyisocyanurate foam insulation allows the test chamber design to greatly exceed expectations. Figure 69 shown illustrates how seven layers were used to fabricate the front piece of the insulation test chamber.

To fabricate the final insulation test chamber six layered components were utilized: the bottom wall, the front wall, the back wall, the top wall, and two side walls. Each of the six walls was constructed by cutting out sections of the polyisocyanurate foam insulation to the necessary dimensions and layering them together. Much care was taken to achieve as close to the correct dimensions as possible to ensure that the six walls would fit tightly together in the final fabrication of the test chamber without gaps. In order to be able to open and close the insulation test chamber to allow the different smart insulation



Figure 69: Front Wall of Insulation Test Chamber showing Seven Layers Bonded Together.

prototypes to be switched in and out, the front wall of the chamber was designed to be removable. In addition, the top wall of the chamber was also designed to be removable as well so that the smart insulation devices could be examined from a top-view during testing if the test chamber was left open. The other four wall of the final insulation test chamber constructed would be adhered to each other permanently using the Loctite PowerGrab Foamboard Construction Adhesive that was also used to layer together the polyisocyanurate foam to build the six walls. Figures 70 and 71 give a side-view and a front-view of the final insulation test chamber to show how the six walls of the final test chamber design fit together.

Whenever the insulation test chamber needed to be sealed shut, four ratcheting straps were utilized that would compress the front and top removable walls so that the two walls were joined together very tightly with the rest of the test chamber. In addition, front and top polyisocyanurate foam frames were cut out and glued with the construction adhesive to the other four walls of the insulation test chamber already constructed. The main purpose of the two frames was to provide a very smooth surface for the front and top removable walls to be compressed with, which would result in a very airtight seal between the walls when the chamber is closed, reducing heat losses from the test chamber to the environment. Although the top removable wall of the insulation test chamber would just lie on top of the top frame, the front removable wall also had an additional small foam section added to it that would fit very tightly in

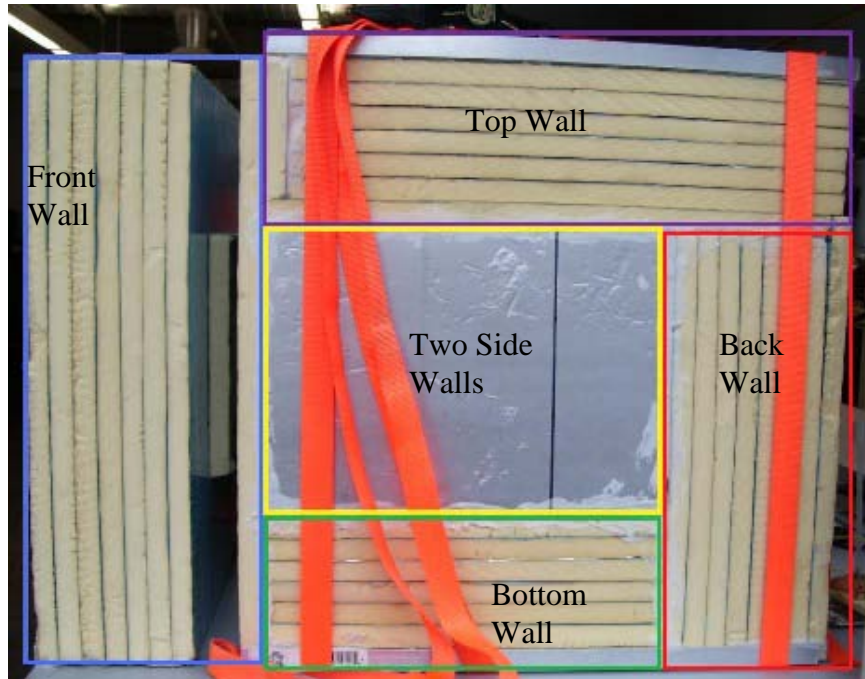


Figure 70: Side-View of Final Insulation Test Chamber Fabricated showing How Individual Walls Fit Together.

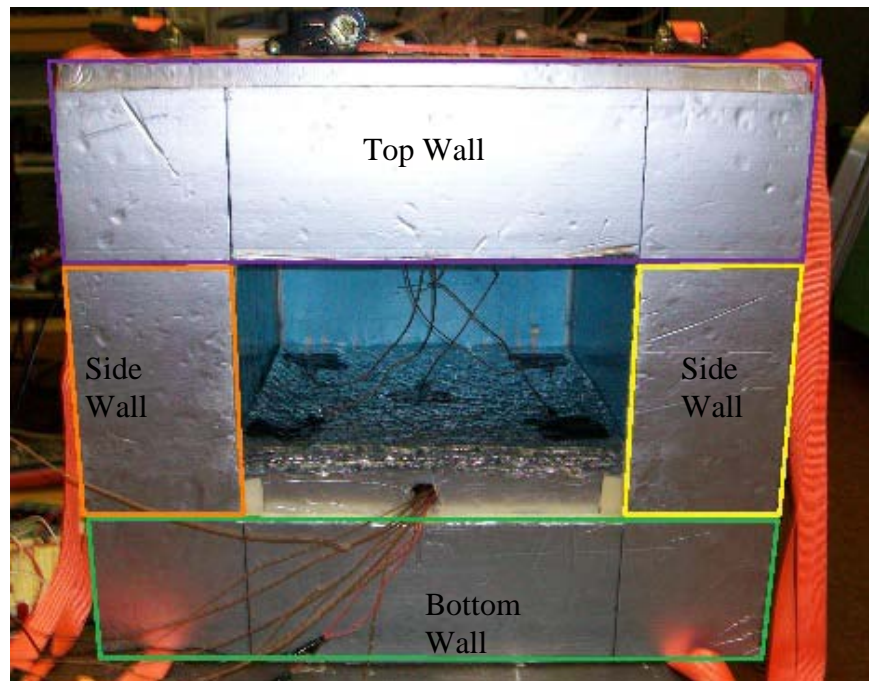


Figure 71: Front-View of Final Insulation Test Chamber Fabricated showing How Individual Walls Fit Together.

the front frame opening to provide an even better seal when the test chamber was closed. One problem that did arise with the ratcheting straps early on was their compressing of the corners of the foam chamber, which was causing damage to the foam layers of the chamber. To solve this problem L-shaped angle brackets were used at the corners of the test chamber where the ratcheting straps were compressing the structure to keep the foam itself from being damaged. Figure 72 shows how the L-shaped angle brackets were glued with the construction adhesive to the corners of the foam of the insulation test chamber. An image is also given in Figure 73 that shows how the front removable wall fits together with the front frame of the test chamber, while another image shown in Figure 74 illustrates how the top removable wall fits together with the top frame of the chamber.



Figure 72: L-shaped Metal Angle Bracket Applied to Corner of Front Removable Wall.

One final feature of the insulation test chamber was the addition of two one inch (2.54 cm) diameter holes in the front and top removable walls. The two purposes of these two holes was to allow the many thermocouples used during the testing for acquiring temperature data to pass outside of the chamber to the data acquisition equipment and to allow the power cables for the Kapton heater to pass outside of the

chamber to the power supply. To lower the amount of heat leaking out of the two holes from the chamber interior, two small 1/2 in. (1.27 cm) diameter foam plugs were constructed by layering small circular pieces of polyisocyanurate foam with construction adhesive to fill up any empty air space present in the front and top holes in the chamber. Figure 75 shows both the front and top thermocouple holes cut out of the front and top removable walls, and the final fabricated insulation test chamber with the front and top walls closed shut is also given in Figure 76. The final dimensions of the entire insulation test chamber when it was sealed shut were 2.125 x 2 x 1.75 ft. (0.648 x 0.610 x 0.533 m).

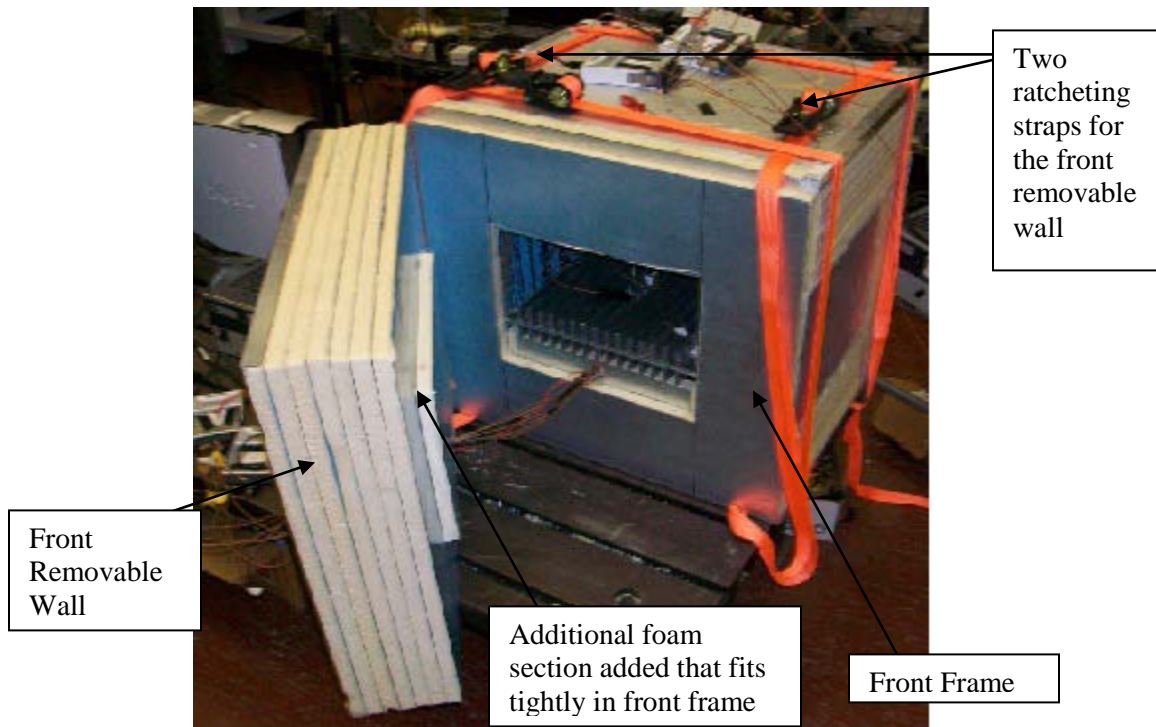


Figure 73: Process of How Front Removable Wall is used to Open and Close Test Chamber.

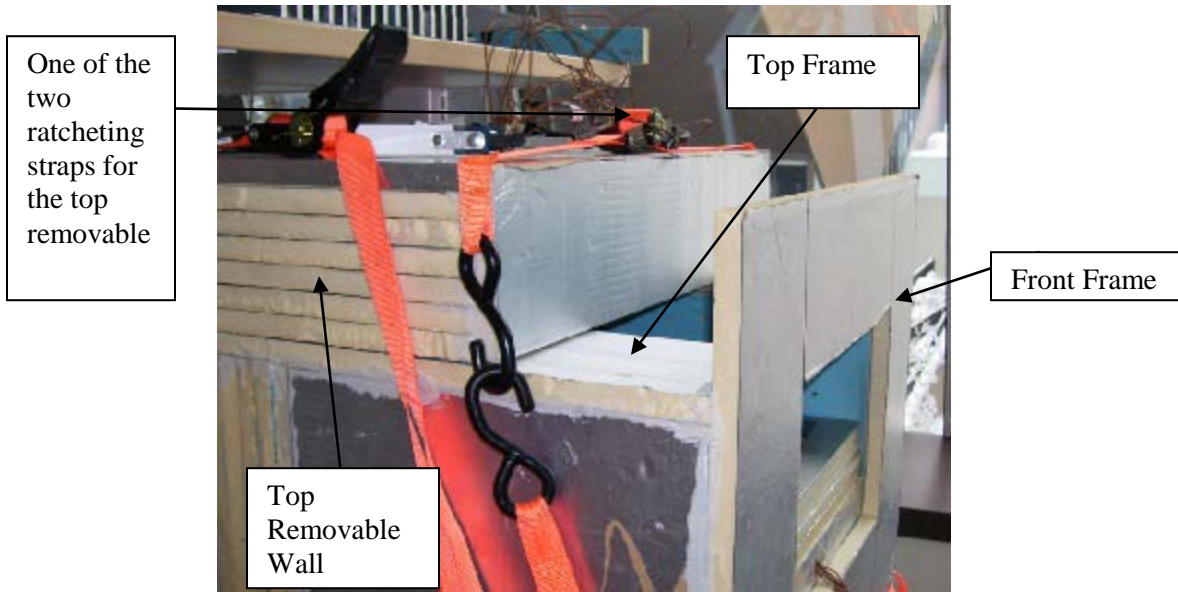


Figure 74: Process of How Top Removable Wall is used to Open and Close Test Chamber.

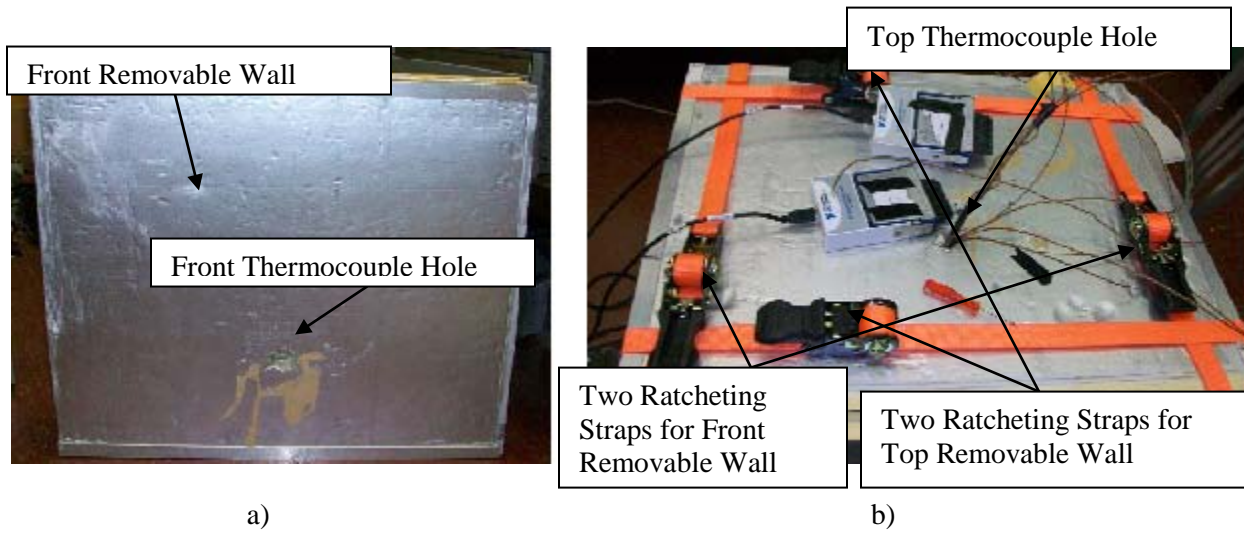


Figure 75: Locations of Thermocouple Holes: a) Front Thermocouple Hole; b) Top Thermocouple Hole.

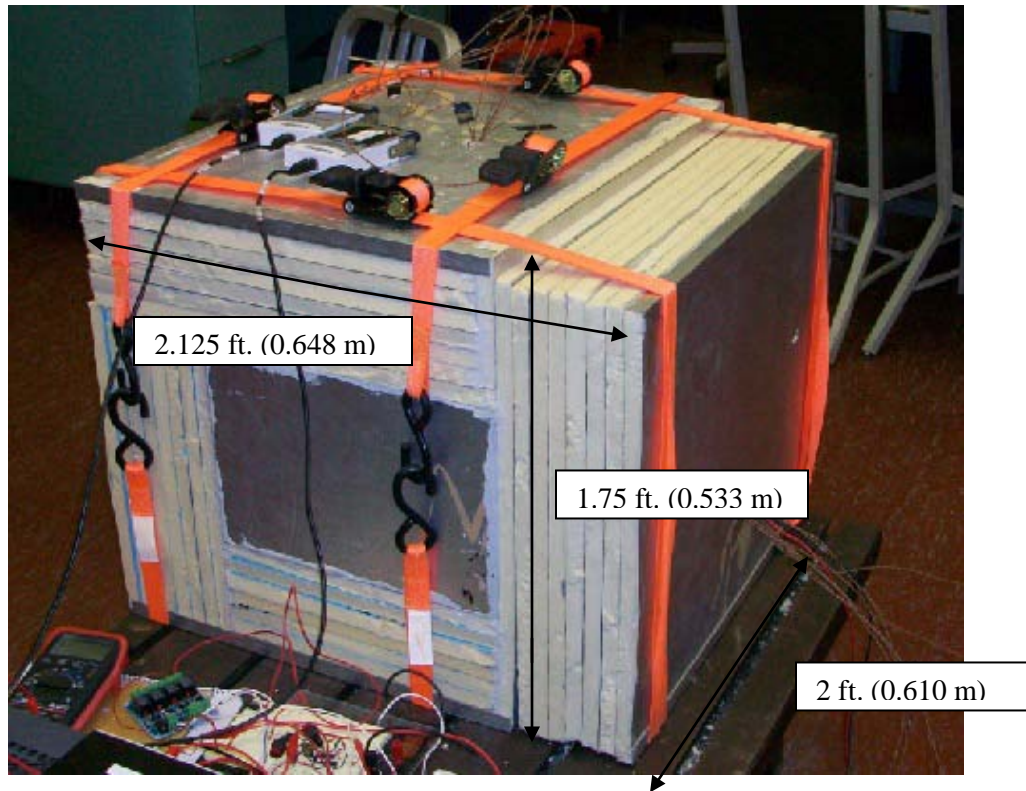


Figure 76: Final Fabricated Insulation Test Chamber with Front and Top Removable Walls Closed.

3.2 EXPERIMENTAL DATA ACQUISITION AND TESTING SET-UP

3.2.1 Temperature Measurement

The main goal of the testing of the smart insulation prototypes was to measure the temperatures of the hot and cold sides of the devices, as shown in Figure 68, so that the temperature difference, ΔT , over the smart insulation devices could be calculated. Once the temperature differences over the thermal semiconductor devices was calculated for the devices' insulating and conducting configurations, the changes in thermal conductivity of the different devices would be analyzed and compared with one another to determine which smart insulation concepts had the best performance. In order to measure the temperature differences across the thermal semiconductor devices, the temperatures of the devices' hot and cold sides would need to be measured. 24 gauge Type K chromel/alumel thermocouples with

fiberglass insulation were chosen as the temperature measurement sensor because they are considered the most general purpose type of thermocouple and because of their low cost. The range of type K thermocouples is from -200 °C to +1200 °C, which makes them very suitable for the smart insulation testing, since the experiments will only involve temperatures in the much narrower range from roughly 20 °C to 50 °C. The Type K thermocouples used in the thermal semiconductor experiments were constructed in the laboratory from Type K thermocouple wire using a thermocouple arc-welder. A total of sixteen thermocouples were fabricated for use in the experimental testing.

3.2.2 Thermocouple Placement

All of the smart insulation experimental tests utilized the same general locations for the Type K thermocouples for the temperature measurements. Within the 1 1/2 in. (3.81 cm) hot side air space below the smart insulation devices, two thermocouples would be used with one of the thermocouples placed as close as possible to the Kapton Insulated Flexible Heater surface without touching it in order to measure the heater temperature during the testing. For the second thermocouple a 13.5 in. (0.343 m) piece of wire was placed at the center of the hot side air space both horizontally and vertically by inserting each end of the wire into the corresponding shelf on each side for support. The shelf was then able to support wire in mid-air, allowing the second thermocouple to be wrapped around the wire and suspended in mid-air at the midpoint of the hot side air space horizontally and vertically as well. The main purpose of the second thermocouple was to measure the air temperature of the hot side air space, which would also be used as the temperature to be kept constant for all of the constant temperature testing. A picture of the hot side air space with the locations of its two thermocouples can be seen below in Figure 77.

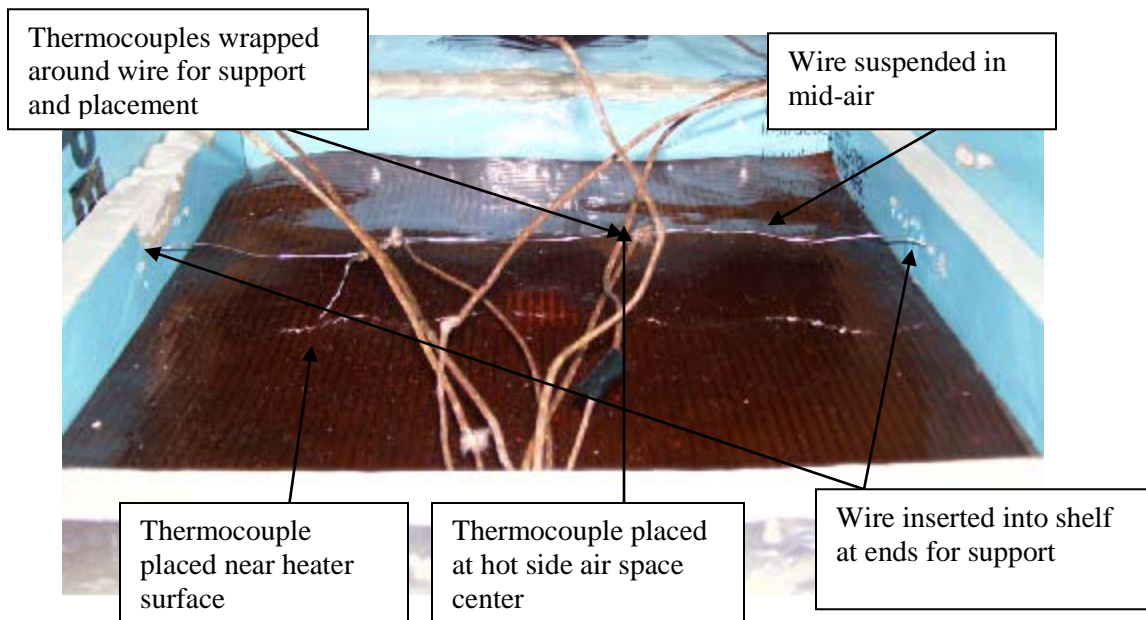


Figure 77: Hot Side Air Space Thermocouple Placement.

In a similar manner to the hot side air space, the cold side air space above the thermal semiconductor prototypes in the insulation test chamber would also utilize two thermocouples for temperature measurement. One of the thermocouples was always placed at the center of the cold side air space halfway between the top of the chamber interior and the cold side of the smart insulation prototypes to measure the cold side air space temperature during the testing. The thermocouple at the center of the cold side air space did not need to actually be mounted. Since the thermocouple was inserted through the top thermocouple hole downward into the chamber and the wire was fairly rigid, the thermocouple was able to stay hanging in place during the test once it was positioned where needed. The other thermocouple was mounted using a small piece of electrical tape onto the bottom of the top removable wall facing the chamber interior near the center of the chamber to measure the temperature at that location. Figure 78 shown provides an image of locations of the two thermocouples in the cold side air space of the test chamber.

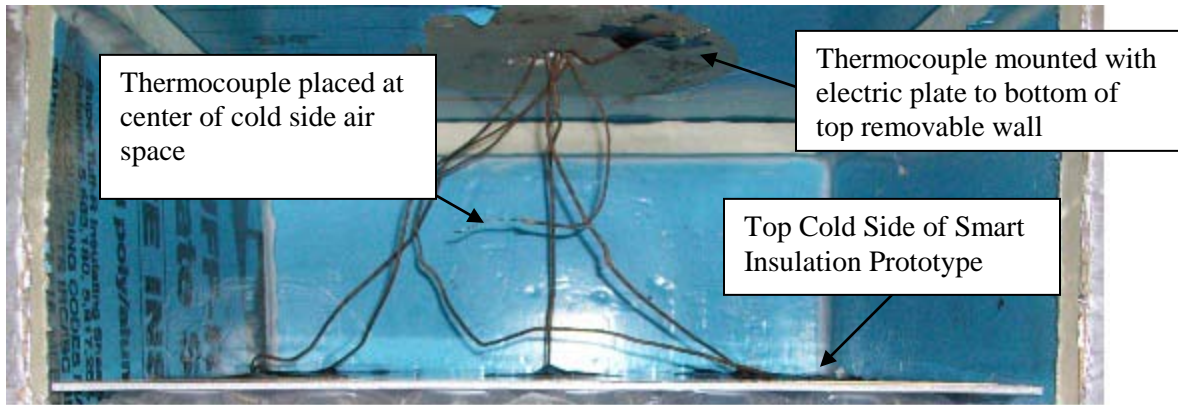


Figure 78: Cold Side Air Space Thermocouple Placement.

The majority of the thermocouples used during the experimental testing of the smart insulation prototypes were mounted to the hot and cold sides of the prototypes so that the temperature difference across the smart insulation devices could be quantified. Generally, for all of the different smart insulation prototypes, five thermocouples were mounted to each of the two sides of the devices with one thermocouple mounted near the center and the other four thermocouples mounted near the four corners. The exact placement of the thermocouples on each side of the smart insulation devices for each of the different prototypes will be discussed in later sections of this thesis. In order to mount the thermocouples to the plates of the shifting fins thermal semiconductor devices, Omega CC high temperature cement was used by applying high temperatures to bond the thermocouples with the cement to the plates of the devices. Later, for the inflatable thermal semiconductor prototypes, the Omega CC high temperature cement would prove to not be feasible for mounting the thermocouples to the hot and cold sides of the prototypes because the high temperatures needed to mount the thermocouples using the cement would have melted the plastic Bubble-Wrap material the prototypes. Instead, electrical tape was utilized to bond the thermocouples to the inflatable smart insulation devices. Additional testing of the shifting fins thermal semiconductor prototypes using electrical tape mounted thermocouples instead of cement mounting thermocouples showed no differences in the temperatures that were measured during testing. Thus, it was assumed that electrical tape was a sufficient method of mounting thermocouples to the smart insulation

devices and it was utilized for all subsequent testing. The general placement of the thermocouples on the hot and cold sides of the thermal semiconductor devices can be seen using the Reflectix inflatable thermal semiconductor prototype shown in Figure 79.

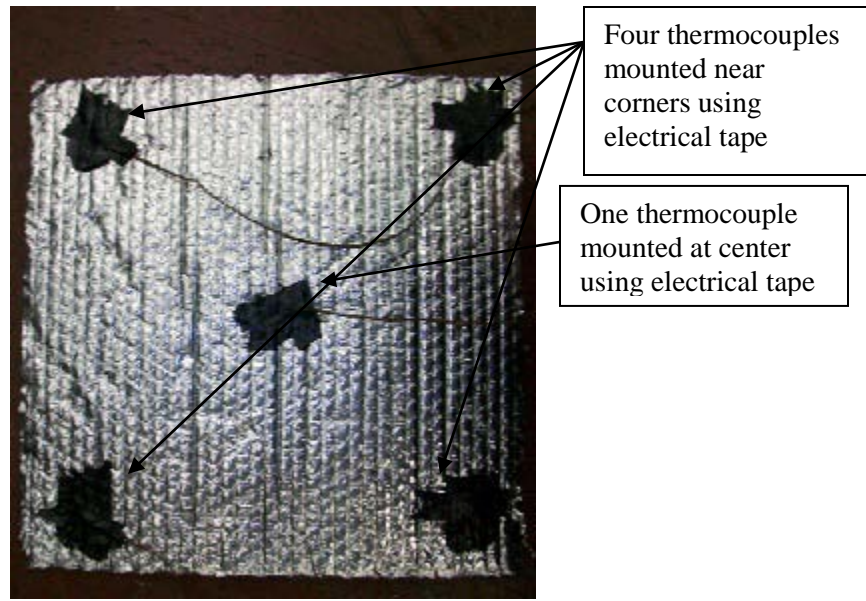


Figure 79: Reflectix Inflatable Smart Insulation Prototype Showing the General Thermocouple Placement on the Hot and Cold Sides of the Smart Insulation Devices.

The two final Type K thermocouples made were mounted using electrical tape on the exterior of the insulation test chamber near the front and top thermocouple holes during all of the experimental tests conducted to help measure any heat escaping from the chamber through the two small openings.

3.2.3 Temperature Measurement Data Acquisition

Once the sixteen thermocouples for the experimental testing were made and mounted in the chosen locations of the insulation test chamber, four National Instruments 9211A data acquisition modules were utilized in conjunction with the National Instruments (NI) Labview 8.0 software to collect the thermocouple data being measured and convert it from the actual voltage values being measured to the

corresponding temperature values. Each NI 9211A module was designed specifically for thermocouple data acquisition with USB connectivity and featured four channels for thermocouples, so the four NI 9211A modules together were able to collect data for the sixteen thermocouples mounted at various locations in the testing set-up. In addition, sensors are also included in the NI 9211A for internal cold-junction compensation, eliminating the need for any type of outside cold-junction measurements, such as an ice water bath. After the thermocouple data was read into the device through the four channels, a signal conditioning circuit and analog-to-digital converter (ADC) were used to convert the analog voltages being measured directly by the thermocouples into digital voltage values that could be used by the Labview 8.0 software.

Within the Labview program written for the insulation test chamber thermocouple measurement collection, the sample rate of the NI 9211A data acquisition was set to 0.1 minutes or 0.6 Hz. At first glance this seems to be a very slow sample rate, but for the up to six hour length of the smart insulation tests, the 0.6 Hz sample rate was sufficient. Sample rates higher than 0.6 Hz also resulted in overwhelming large data files being saved when the tests were completed, which was another reason why the sample rate was kept fairly low. Once the Labview smart insulation program was finished, the main features of the front panel were numerical displays for the instantaneous temperature values being measured for the insulation test chamber rig and graphical displays so that the change in the temperature values of the thermocouples over the entire length of the test being run could be examined. After each of the smart insulation tests, the temperature data collected from the thermocouples was outputted to a data file for later examination.

3.2.4 Kapton Heater Equipment and Temperature Control of Bottom Air Space

Several pieces of equipment were needed in the experimental test set-up to provide the correct levels of heating and power to the Kapton Insulated Flexible heater. First, a Kepco JQE 55-10 M DC power supply capable of providing up to 55 V and 10 A of current was acquired for powering the heater. Initially, the dials on the power supply for setting the voltage and current levels were used to record the voltage and

current running through the heater during the testing, but the voltage and current levels given on the power supply itself proved to not be very accurate. Thus, two multimeters were added to the test set-up to provide more accurate heater current and voltage measurements: a TENMA True RMS 72-410A digital multimeter for measuring the output voltage of the power supply and a Triplet 9010 handheld ammeter for measuring the current outputted by the power supply. Using the two multimeters, the voltage and power levels for each of the different smart insulation prototype tests was closely monitored and recorded by hand at several different times during the testing.

The last major concern involving the experimental testing set-up was how to control the hot side air temperature for the constant temperature tests that would be run. Many of the real-world cases mentioned before to be tested in the insulation test chamber involved the bottom air space on the hot side of the smart insulation prototypes having a constant temperature value during the testing. For example, in the clear summer evening case the warm building interior would be represented by the bottom, hot side air space at a constant hot temperature, while the outside cool night environment would be represented by the top, cold side air space of the test chamber. For the constant temperature tests the thermocouple placed at the center of the hot side air space suspended in mid-air on a wire was chosen as the temperature to be controlled. During all of the constant temperature thermal semiconductor tests, the hot side air space thermocouple would be controlled to be a constant temperature value of 100 °F (37.78 °C) using bang-band control with the Labview 8.0 software and a MaxxTronic MXA017 four-channel relay card. Within the Labview software the temperature measured by the hot side air space thermocouple would constantly be compared to the required constant temperature value of 100 °F (37.78 °C) to keep the thermocouple at that temperature once it was reached after the initially heating up of the test chamber. If the hot side air space temperature was below 100 °F (37.78 °C), Labview would produce a “true” digital output via a NI 6008 DAQ device to be sent to the MaxxTronic MXA017 relay card to open the relay and allow the current from the DC power supply to pass through the relay into the Kapton heater so the hot side air space could continue to be heated to 100 °F (37.78 °C). Eventually, once the hot side air space thermocouple was heated to a value greater than 100 °F (37.78 °C), Labview would then produce a

“false” digital output via the NI 6008 DAQ device to be sent to the relay card to close the relay and stop the current from the power supply from passing through the relay into the Kapton heater to cool down the bottom air space. This process would then continue during the entire length of the constant temperature test being run to maintain the hot side air space temperature at 100 °F (37.78 °C). One final piece of equipment that had to be added to the experimental test set-up was a small 15 V variable DC power supply that was set to a value of twelve volts needed to power the MaxxTronic MXA017 four-channel relay card.

3.2.5 Final Experimental Set-up

A top view of the electronic equipment used in the smart insulation prototype testing is given in Figure 80. In addition, in Figure 81 an image of the entire overall insulation test chamber experimental set-up is shown. Finally, Table 4 lists all of the different electronic equipment used in the final insulation test chamber experimental set-up.

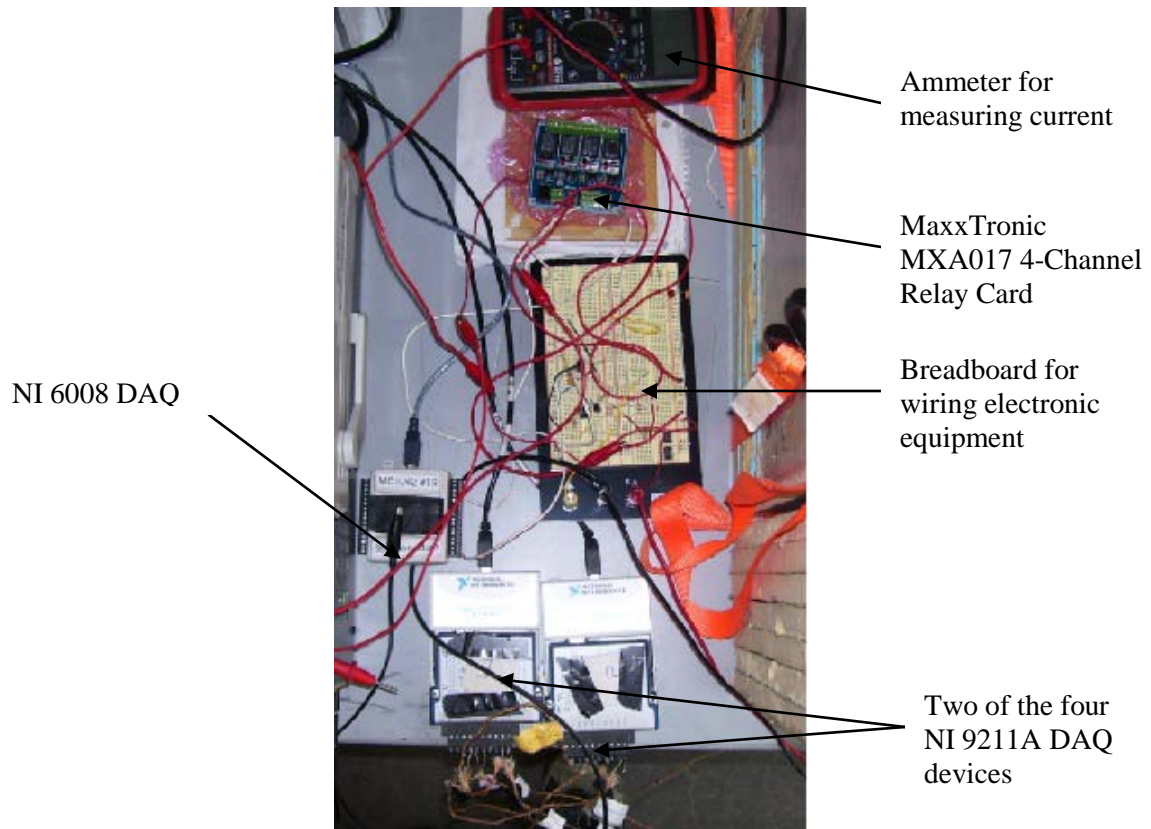


Figure 80: Top View of the Experimental Set-up Electronic Equipment.

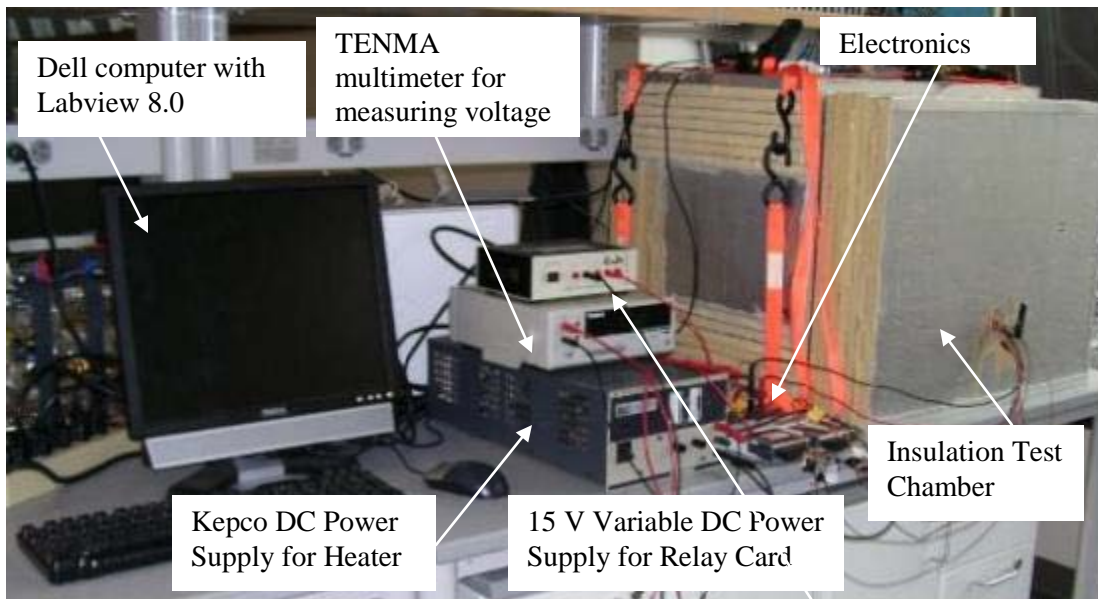


Figure 81: View of the Overall Experimental Set-up for the Insulation Test Chamber.

Table 4: Smart Insulation Prototype Testing Experimental Set-up Electronic Equipment.

Smart Insulation Prototype Testing Experimental Set-up Electronic Equipment			
Item	Quantity	Vendor	Model Number
Thermocouple Data Acquisition Module	4	NI	9211A
Multifunction Data Acquisition Device	1	NI	6008
DC Power Supply	1	Keeco	JQE 55-10 M
Digital Multimeter	1	TENMA	72-410A
Handheld Multimeter	1	Triplett	9010
4-Channel Relay Card	1	MaxxTronic	MXA017
DC Power Supply	1	-	-
Breadboard	1	-	-

3.3 INSULATION TEST CHAMBER PERFORMANCE TEST

Before experiments could begin on the different thermal semiconductor prototypes discussed earlier in the insulation test chamber, an insulation test chamber thermal efficiency test was conducted to examine whether or not the level of insulation used in the test chamber was large enough to sufficiently stop heat losses between the chamber interior and the ambient laboratory environment. To prepare for the chamber thermal efficiency test, first, eight thermocouples were placed at various locations throughout the inside of the test chamber from very near the Kapton heater surface at the bottom to the top of the chamber interior. One of the eight thermocouples, which was placed as close to the heater surface as possible, was chosen to be the thermocouple whose temperature would be controlled at a constant temperature of 48 °C for the duration of the test. The reason 48 °C was chosen as the constant temperature for the thermal efficiency test was that any higher temperatures could have caused the heater to overheat and melt the foam insulation building material of the test chamber itself. By placing the controlled thermocouple as close to the heater as possible, its temperature will be very close to that of the Kapton heater, so the Kapton heater's temperature will also be controlled to values not much greater than 48 °C. In addition, an effort was also made to heat the chamber interior to the highest temperatures possible for the test chamber thermal efficiency test, since the highest temperatures will result in the greatest heat escaping through the

insulation of the chamber or through small cracks or gaps between the pieces of insulation to the ambient environment.

After eight of the thermocouples were placed inside of the test chamber, the remaining eight thermocouples were placed at different locations on the outside of the foam insulation test chamber to measure the amount of heat escaping from the inside of the chamber to the laboratory environment. First, two of the thermocouples were placed near the front and top thermocouple holes, since these appeared to be areas where the greatest heat could likely leak out of the chamber. Next, the rest of the six thermocouples were placed at locations where the front and top removable walls made contact with the rest of the test chamber when it was closed. Since the top and front walls of the chamber are not adhered to the rest of the test chamber with construction adhesive, such as the other foam chamber walls, and are simply closed using the ratcheting straps, one of the most likely locations for heat losses from the test chamber is through the small air gaps at the interfaces between the two removable walls and the rest of the chamber. The largest air gap at the two interfaces occurred between the front removable wall and the front frame of the test chamber. Since this gap appeared to be larger than the rest, three thermocouples were placed at various locations in the gap to quantify any heat escaping through it. An image of this gap is shown in Figure 82. The final three thermocouples were placed at the interfaces between the two removable walls and the two frames. Two of them were placed on the outside of the chamber where the top removable wall lies on top of the top frame with one of the two at the interface on the left side of the insulation test chamber and the other one at the interface on the back side of the test chamber. The final thermocouple was placed at the interface between the front removable wall and the front frame near the top of the insulation test chamber.

During the insulation test chamber thermal efficiency test approximately 10 W of power (1 A at 10V) was supplied for the duration of the test to the heat source. The lab ambient temperature at the beginning of the test was measured to be 23.5 °C. The thermocouple temperatures measured in the test appeared to reach near steady-state conditions after about thirty minutes, but the thermal efficiency test was continued

for a total duration of two hours to ensure that steady-state conditions were reached. Figure 83 gives a plot of the thermocouple temperatures measured for the thermal efficiency test.

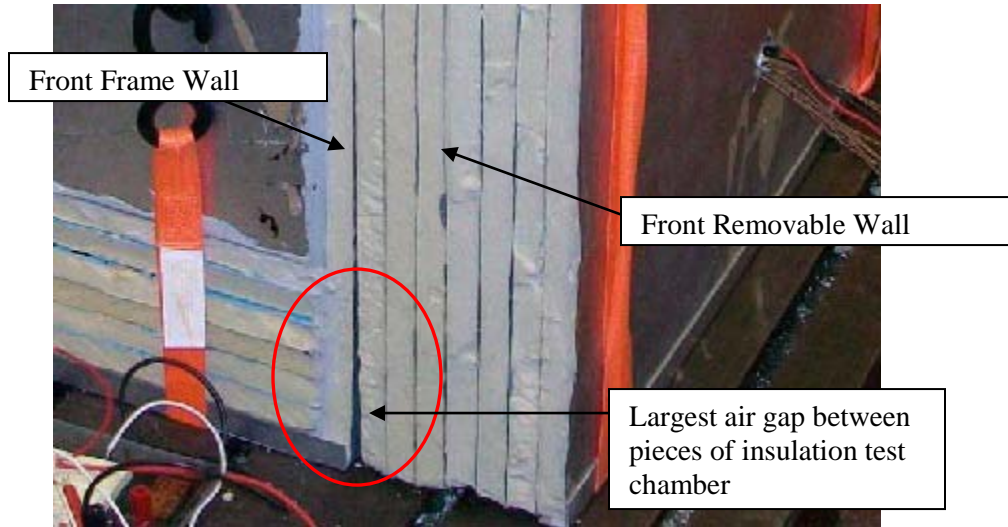


Figure 82: Largest Gap in Insulation Test Chamber between Front Removable Wall and Front Frame for Potential Greatest Heat Losses.

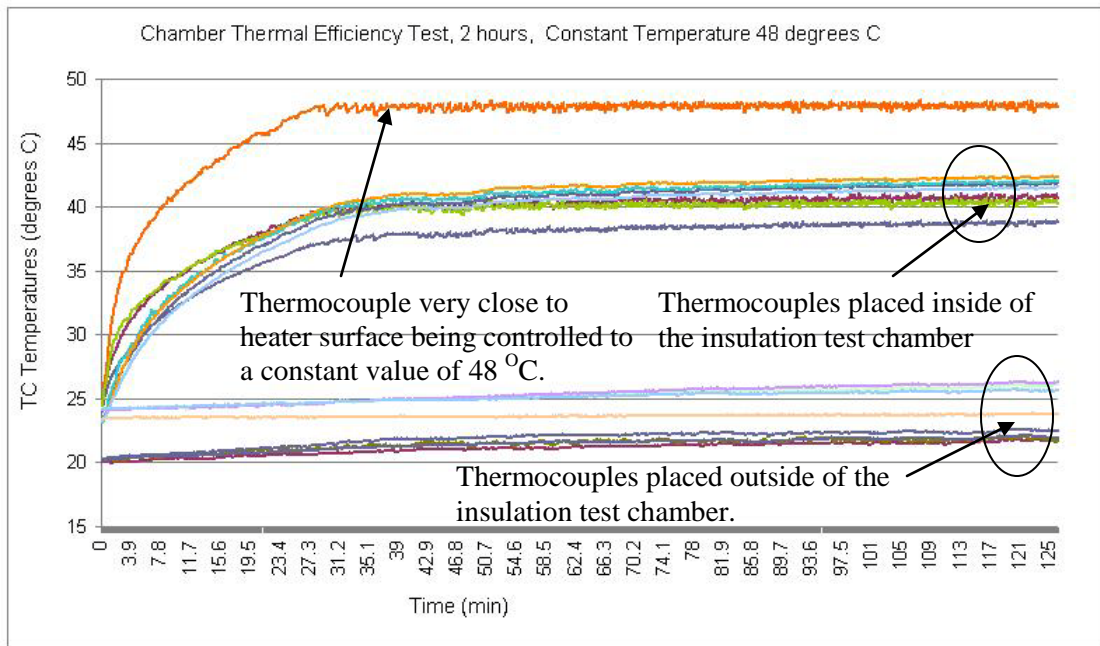


Figure 83: Chamber Thermal Efficiency Test Results.

From the review of the results of the chamber thermal efficiency test, the least heat was found to have escaped from the chamber through the front thermocouple hole, since its temperature only increased by 0.358 °C over the course of the test. The rest of the thermocouples placed at locations on the exterior of the insulation test chamber increased by between 1.42 to 2.16 °C over the two hour long test, which did prove that a small amount of the heat inside of the chamber did escape during the test. Overall, however, the chamber thermal efficiency test proved that the insulation test chamber has satisfactory performance in that it was able to retain the vast majority of the heat provided by the Kapton heater during the test. The final temperatures of the thermocouples inside of the test chamber were in the range of 39-42 °C, which was much higher than the final temperatures on the outside of the test chamber, which were all less than 26.3 °C even at the end of the test.

3.4 EXPERIMENTAL TESTING PARAMETERS

Before testing of the fabricated smart insulation prototypes could begin, several testing parameters, such as the type of tests to be run, the level of voltage and current to be supplied to the heater, and the time duration of the tests had to be determined. As mentioned earlier both constant temperature and constant heat flux boundary conditions would be tested for the hot side of the thermal semiconductor devices with a temperature of 100 °F (37.78 °C) being used for the constant temperature cases. For both the conducting and insulating states for each of the different smart insulation devices both a constant temperature test and a constant heat flux test was run. During the constant temperature testing approximately 20 V at 2 A for a total power of 40 W was initially supplied to the Kapton heater to enable the hot side air space to quickly reach the desired constant temperature of 100 °F (37.78 °C) (in 5-10 minutes). Once the hot side air space thermocouple reached 100 °F (37.78 °C), the amount of power supplied to the Kapton heater was decreased to approximately 10 W at 10 V and 1 A for rest of the constant temperature test. Later during the testing, the level of power was determined to actually be 13.28

W at 11.35 V and 1.17 A once a multimeter was utilized to measure the voltage outputted by the power supply instead of simply trusting the dials on the DC power supply to be correct.

The main reason the power was decreased from 40 W to 10 W after a temperature of 100 °F (37.78 °C) was obtained was to lessen the fairly large oscillations that were occurring in all of the thermocouples placed in the hot side air space, due to the relatively slow sample rate of the bang-bang control method. After the temperature level of 100 °F (37.78 °C) was reached for the hot side air space the heater was repeatedly turned on and off as the temperature of the hot side air space fell below and exceeded the desired temperature of 100 °F (37.78 °C) to maintain a hot side air space temperature of approximately 100 °F (37.78 °C) at all times. Each time the heater was turned back on, the high level of power at 40 W would cause a large overshoot of the desired 100 °F (37.78 °C) temperature to occur before the heater was turned back off again to decrease the temperature back to 100 °F (37.78 °C) causing the appearance of oscillations. The simplest solution found to solve this problem was to decrease the heater power level to 10 W once the constant temperature level was initially reached, which proved to greatly mitigate the temperature overshoot and oscillations to the point where they were negligible during the testing.

During the constant heat flux testing a constant power level was applied to the heat source in the hot side air space for the entire duration of the tests. As shown in Equation 3.1 the heat flux emanating from the heat source was simply the heater thermal efficiency times the electrical power supplied to the heater divided by the cross-sectional area.

$$q = \eta_{heater} \frac{Q_{electrical}}{A} \quad (3.1)$$

Since the electrical power supplied to the heater was constant for the constant heat flux tests and the cross-sectional area of both the heater and the bottom air space was constant, from Equation 3.1 the insulation test chamber experimental set-up was able to provide the constant heat flux boundary condition for the hot side of the smart insulation prototypes. The constant power level used for the heater in the constant heat flux tests was designed to be approximately 5.85 W (0.78 A at 7.5 V), although later when a

multimeter was used to measure the voltage and current outputs of the power supply, they were determined to be actually set at 7.61 V and 0.78 A. Since a constant power level was being provided for the constant heat flux tests over the entire length of the tests, the temperatures of the heater and hot side air space kept increasing during the test to levels greater than 100 °F (37.78 °C). In order to keep the heater temperature from reaching dangerous levels that could have melted or damaged the foam insulation of the test chamber itself, the power level supplied to the heater was decreased from the constant temperature tests. In addition, if the hot side air space temperature ever exceeded a level of 110 °F (43.33 °C) during the constant heat flux tests, the hot side air space temperature would be controlled for the rest of that test to be a constant value of 110 °F (43.33 °C) to both prevent overheating and temperatures of the hot side air space in a similar range as the constant temperature tests.

Finally, the last major testing parameter to be determined was the overall length of the tests. A time duration of 6 hours was utilized for all of the constant temperature tests for the thermal semiconductor prototypes, while a time duration of 3.5 hours was utilized for all of the constant heat flux tests. A problem that arose early on with the constant temperature tests was that the temperature values measured during the test were taking a very long time to reach steady-state conditions. In the end a testing duration of six hours was settled upon because after that time the insulation test chamber temperatures were beginning to approach steady-state values, and six hours was still a short enough time period to keep the test length from becoming prohibitively long for the larger number of experimental tests to be run. Since steady-state conditions did not need to be reached for the constant heat flux tests, a shorter time duration of 3.5 hours was chosen. In addition, during the course of the testing it was found that within the test length of 3.5 hours some of the tests did reach the maximum temperature of 110 °F (43.33 °C), so any longer testing duration would likely not have been beneficial for the constant heat flux tests.

3.5 POLYISOCYANURATE FOAM INSULATION TEST PIECE

Although the performance of the different smart insulation concepts could partly be evaluated simply by comparing the experimental results of the smart insulation prototypes to each other, it was decided that another insulation test piece needed to be constructed to serve as a benchmark case for the different smart insulation device results. The benchmark insulation test piece would basically represent conventional building insulation already implemented in buildings, and it would be tested in the same manner as the smart insulation prototypes to quantify the temperature difference, ΔT , across the insulation from the hot side to the cold side. Ideally, when the smart insulation devices are tested in their insulating state they will have a ΔT value measured that is very close to that of the benchmark conventional insulation test piece to show that the smart insulation prototypes can have very low thermal conductivities and be good insulators. Conversely, when the smart insulation devices are tested in their conducting state, the goal would be for them to have a ΔT value that is much lower than the benchmark insulation test piece to show that the smart insulation prototypes can have very high thermal conductivities and be good conductors.

In order to fabricate a benchmark insulation test piece, the polyisocyanurate foam building insulation material used to build the insulation test chamber was utilized again. Three layers of the polyisocyanurate foam were cut into pieces and layered together with the Loctite FoamBoard PowerGrab construction adhesive to form a conventional insulation test piece with dimensions that matched the thermal semiconductor prototypes constructed earlier with a 13.25 x 13.25 in. (0.337 x 0.337 m) size top surface area and a thickness of 2.25 in. (5.715 cm). The total R-value of the foam test piece ended up being 15 ft² F-hr/Btu (2.6 m² K/W), which is close to the R- value of typical building wall insulation of 19 ft² F-hr/Btu (3.3 m² K/W), so the final benchmark insulation test piece was able to closely represent conventional building insulation. Figure 84 provides an image of the final fabrication of the benchmark insulation test piece.

During the testing of the benchmark smart insulation test piece, only a constant temperature test was run with a time duration of six hours to match all of the smart insulation prototype constant temperature



Figure 84: Final Fabricated Benchmark Insulation Test Piece.

tests. A constant heat flux test was not done for the conventional insulation test piece because the hot side air space underneath of the test piece in the insulation test chamber would have overheated very early into the test due to very little heat being transferred out of the hot side air space through the insulation test piece into the cold side air space. In addition, the same power values to be supplied to the heater for the constant temperature smart insulation prototype tests were also applied during the benchmark insulation test. On both the hot and cold sides of the insulation test piece five thermocouples were mounted with electrical tape. Two were placed at the center location of each side, while the other eight were placed two inches in both directions inward from the four outer corners on both sides. A plot that shows the results of the benchmark insulation test piece constant temperature test can be seen in Figure 85.

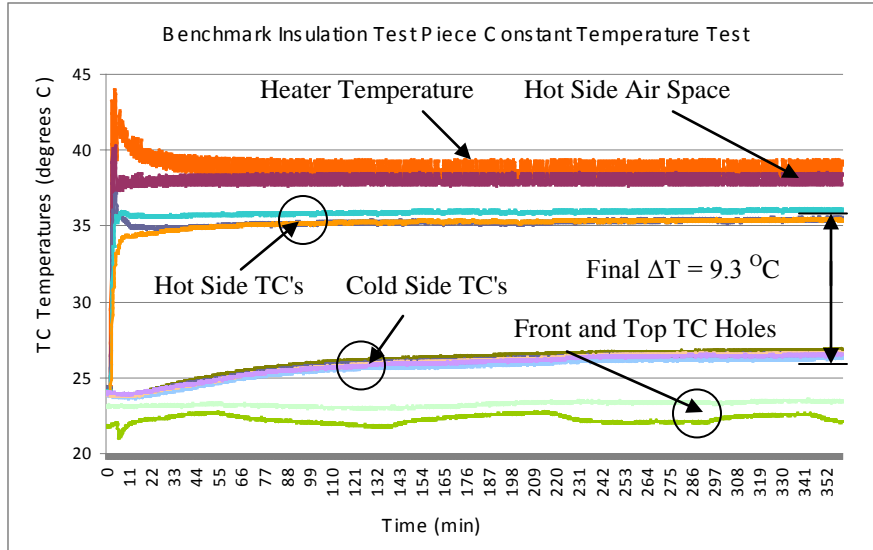


Figure 85: Plot of Benchmark Insulation Test Piece Constant Temperature Test.

From the plot of the benchmark insulation test piece test, the thermocouples mounted on the hot side of the insulation test piece reach steady-state values of around 36 °C by the one-hour point of the six-hour test. It takes a little longer time period of about three hours for thermocouples mounted on the cold side of the insulation test piece to reach steady-state because of the delay that occurs as some of the heat that builds up on the hot side of the test piece dissipates through the foam insulation to the cold side. The final ΔT value measured across the conventional insulation test piece was 9.3 °C at the conclusion of the six-hour test, and it can also be assumed to be the steady-state ΔT value for this test, since all of the temperatures being measured appear to have reached steady-state by the end of the test from the plot.

4.0 SMART INSULATION EXPERIMENTAL RESULTS AND DISCUSSION

During the smart insulation experiments, both constant temperature and constant heat flux tests were run for each of the different prototypes in the devices' insulating and conducting configurations. First, the experiments were conducted for the different variations of the shifting fins thermal semiconductor, including the basic shifting fins smart insulation device, the shifting fins prototype with insulation between the fins, the shifting fins prototype using thermal greases, and the back-to-back aluminum plates with fins thermal semiconductor. Once those tests were completed, experiments were next conducted for the two types of inflatable thermal semiconductors constructed: the Reflectix Bubble-Wrap-like building insulation and the NOVUS Bubble-Wrap-like packaging. The final experimental results for the smart insulation testing were then compared to one another and the benchmark foam insulation test piece results to examine which smart insulation prototypes had the best overall performance by demonstrating the greatest change in ΔT measured from the hot side to the cold side of the devices between the prototypes' insulating and conducting states. The thermal semiconductor prototypes with the greatest changes in ΔT would then consequently have the greatest changes in thermal conductivity and R-value between the devices' low and high heat transfer states and thus the best performance. The experimental results of the different smart insulation prototypes will now be presented.

4.1 SHIFTING FINS THERMAL SEMICONDUCTOR EXPERIMENTAL RESULTS

4.1.1 Basic Shifting Fins Thermal Semiconductor Testing Results

The first thermal semiconductor to be tested was the basic shifting aluminum fins smart insulation prototype with air between the fins. First, a 6 hour constant temperature test was conducted with a constant temperature boundary condition of 100 °F (37.78 °C) being applied to the bottom air space of the insulation test chamber facing the hot side of the basic shifting fins device for the entire duration of the test. Later on, a second 3.5 hour constant heat flux test was conducted with a constant power of 5.87 W applied to the heater in the test chamber for a constant heat flux boundary condition. Figure 86 shows the basic shifting fins prototype placed in the insulation test chamber in both its insulating and conducting configurations.

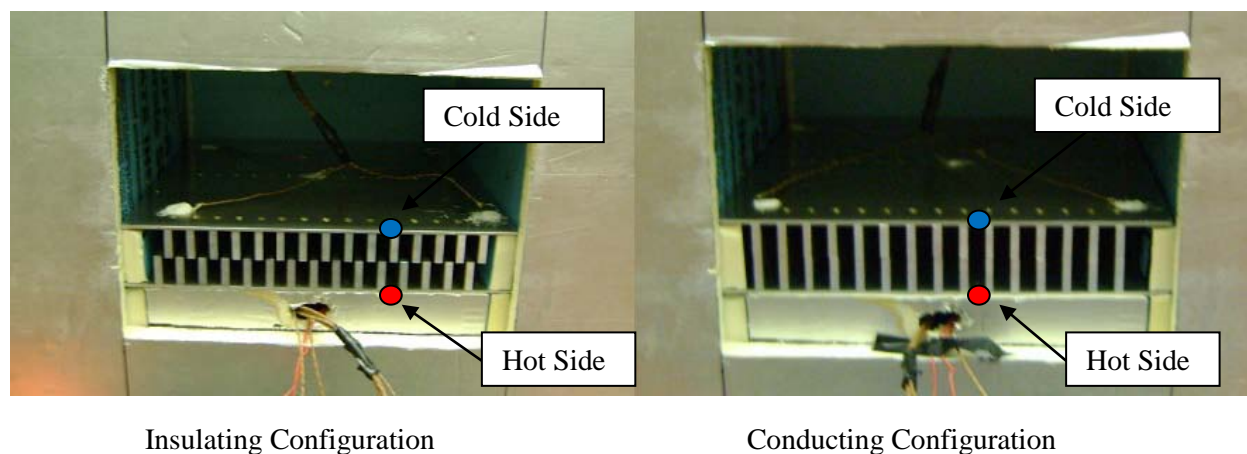


Figure 86: Basic Shifting Fins Smart Insulation Prototype in Test Chamber.

Sixteen thermocouples were used to collect temperature data during the tests with the thermocouple placement matching the locations mentioned earlier during the discussion of the experimental set-up. Also, in the placement of the eight corner thermocouples on the hot and cold sides of the shifting fins

device, two thermocouples on the cold side were mounted to the plate directly above the outer most fins of the device, while two additional thermocouples were mounted to the plate on the hot side directly below those same two fins. The other four corner thermocouples were mounted to the top and bottom plates at locations where the fins were not screwed into the plates. This was done in order to examine whether or not the heat transfer through the contacting fins of the shifting fins prototype in its conducting configuration would cause the cold side plate temperatures to be higher at the locations where the fins were in contact with the plates. The last two center thermocouples mounted on the top and bottom plates of the device were placed at the center of the plates at locations between where two of fins were mounted. Figure 87 gives the thermocouple placement on the top and bottom plates of the shifting fins device.

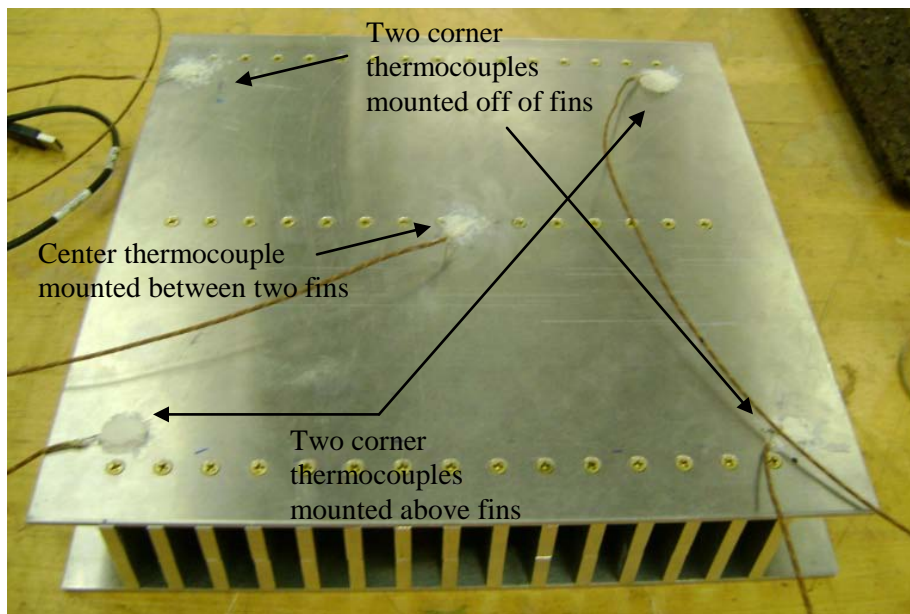


Figure 87: Shifting Fins Smart Insulation Prototype Plates' Thermocouple Placement.

The thermocouple measurement results of the constant temperature basic shifting fins prototype tests are given in the plots of Figures 88 and 89, where Figure 88 shows the results of the prototype in its conducting configuration and Figure 89 shows the results of the prototype in its insulating configuration. Then, the constant heat flux test results for the basic shifting fins thermal semiconductor are next

displayed in Figures 90 and 91 for the device's conducting and insulating states respectively. Finally, the average hot and cold plate temperatures and the ΔT values for the basic shifting fins prototype at the quarter-point, halfway-point and end of the tests can be seen in Table 5. In addition, in Table 5 the final ΔT values at the end of the device's constant temperature tests are expressed as a percentage of the benchmark foam insulation test piece's ΔT value measured during its constant temperature test for comparison. Since the benchmark foam insulation test piece was standard foam building insulation and not a smart insulation device, it serves as the ideal insulator for the different smart insulation devices to be compared against. Both the conducting and insulating states' ΔT values were compared to the ΔT values from the benchmark insulation test piece. Ideally, the ΔT value for the conducting states of the smart insulation devices would be 0% of the benchmark insulation test piece value, while the ΔT value for the insulating states of the smart insulation device would be $\geq 100\%$ of the benchmark insulation test piece value. Equation 4.1 shows how the percentage of the benchmark insulation test piece's ΔT value is calculated.

$$\% \text{ of Benchmark Insulation Test Piece } \Delta T \text{ Value} = \frac{\Delta T_{\text{Smart Insulation}}}{\Delta T_{\text{Benchmark Insulation Test Piece}}} \times 100\% \quad (4.1)$$

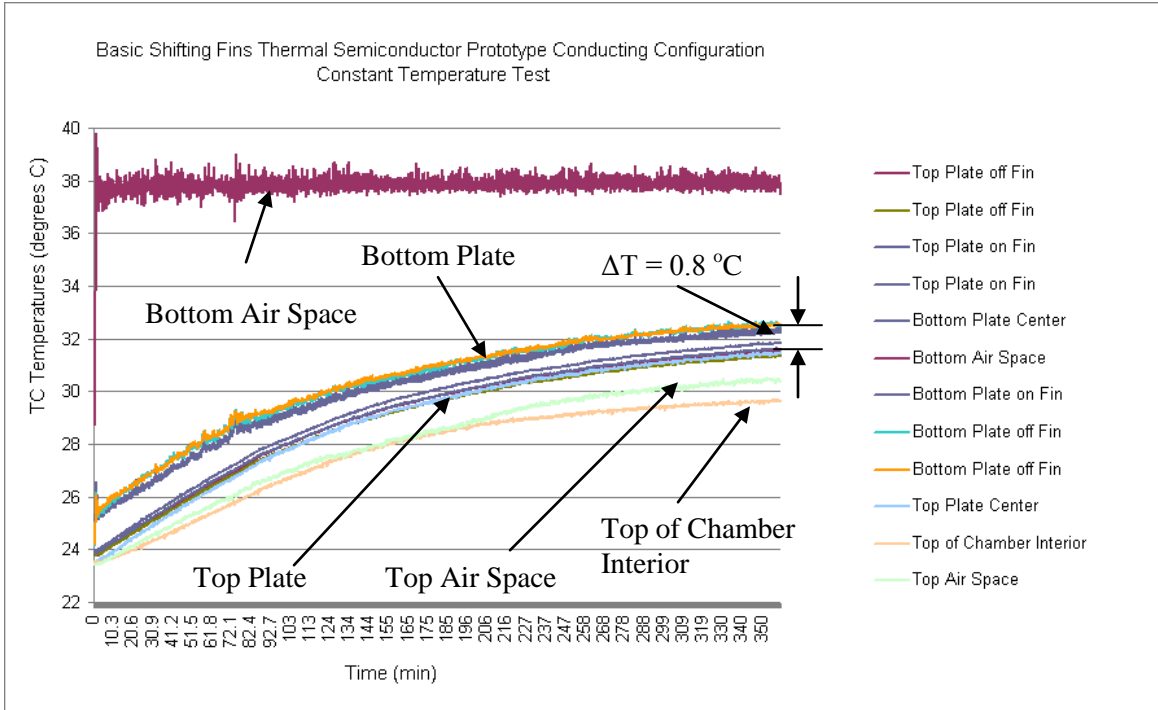


Figure 88: Basic Shifting Fins Thermal Semiconductor Prototype Conducting State, Constant Temperature Test.

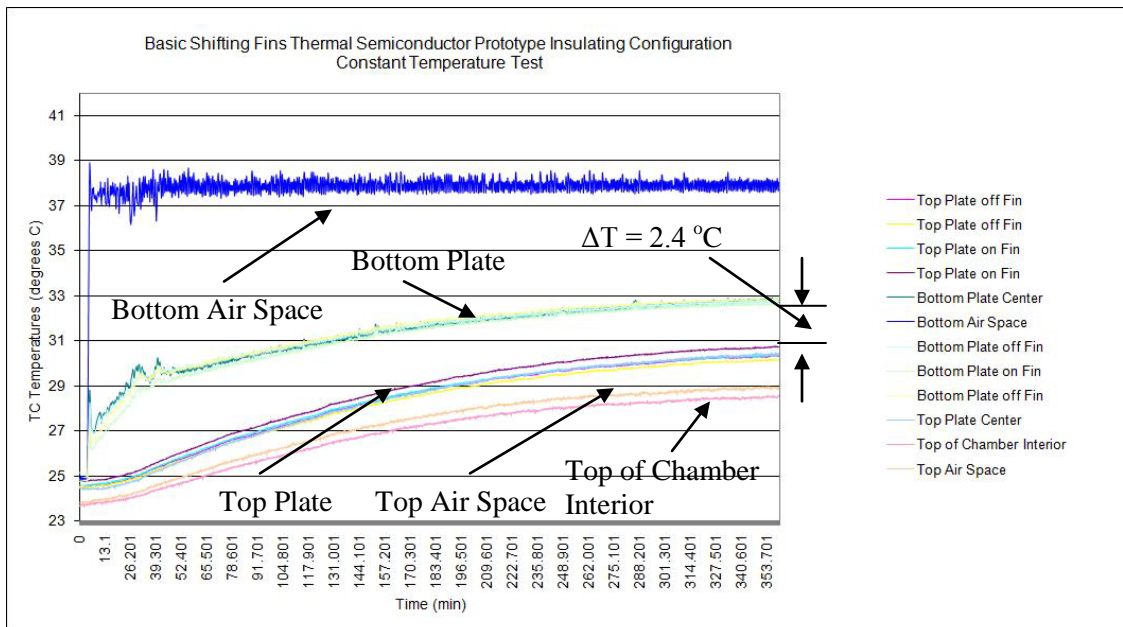


Figure 89: Basic Shifting Fins Thermal Semiconductor Prototype Insulating State, Constant Temperature Test.

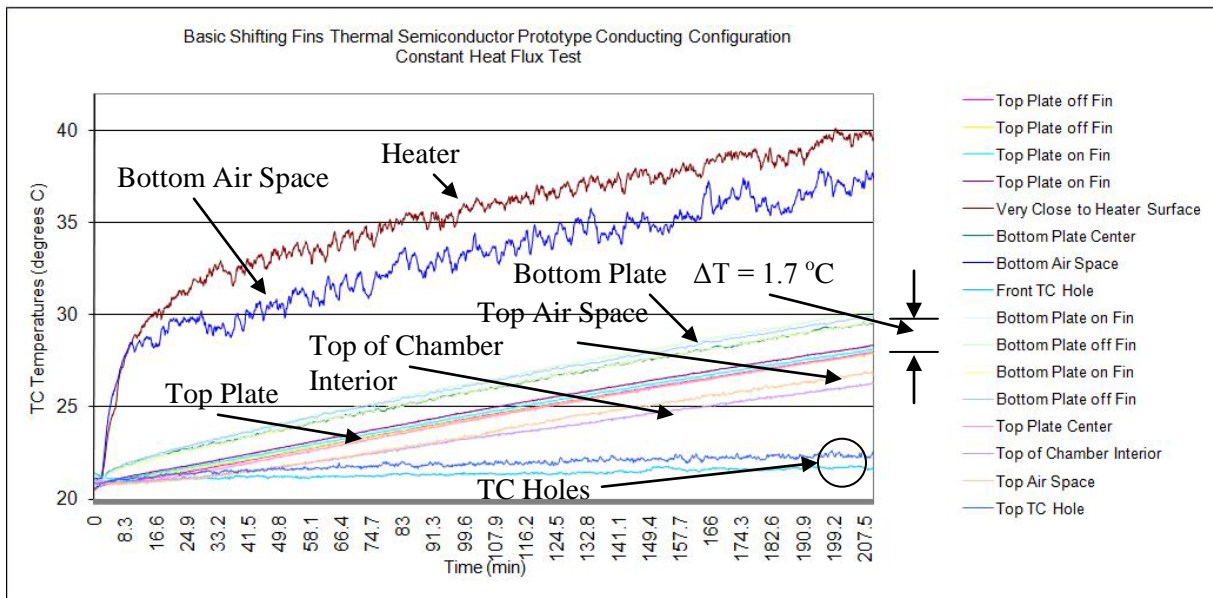


Figure 90: Basic Shifting Fins Thermal Semiconductor Prototype Conducting State, Constant Heat Flux Test.

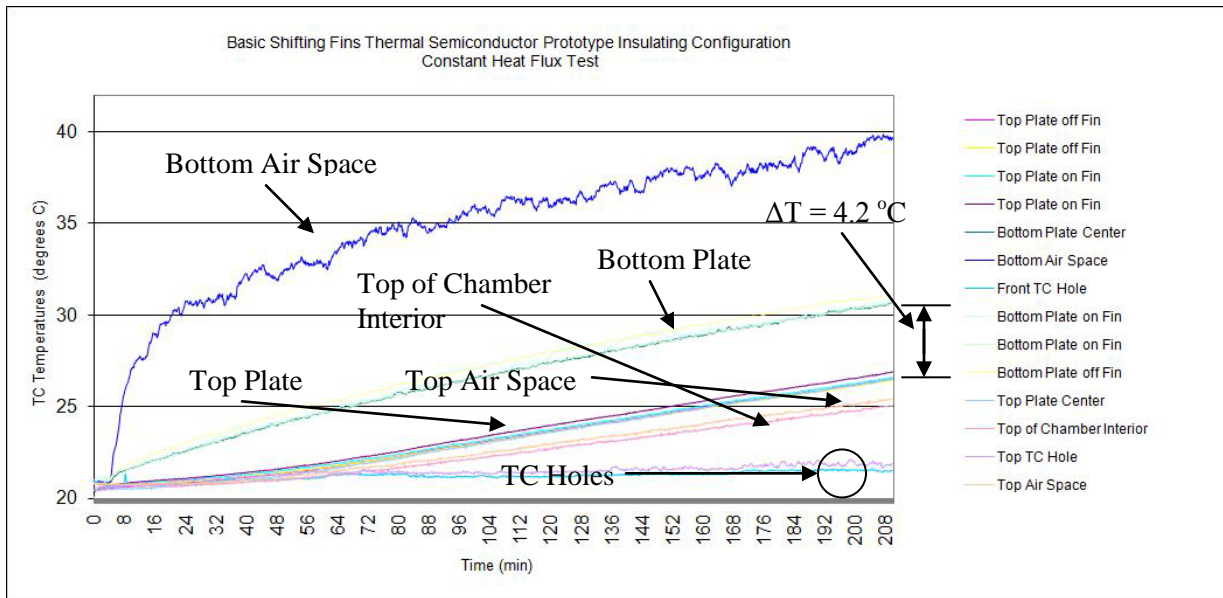


Figure 91: Basic Shifting Fins Thermal Semiconductor Prototype Insulating State, Constant Heat Flux Test.

Table 5: Basic Shifting Fins Thermal Semiconductor Prototype Experimental Results.

Constant Temperature Tests (Standard Deviations of All Measurements < 0.21 °C)					
Conducting Configuration			Insulating Configuration		
1.5 hours into the test			1.5 hours into the test		
Measurement	T (°C)	% of Benchmark	Measurement	T (°C)	% of Benchmark
Bottom Plate Average	29.0		Bottom Plate Average	30.5	
Top Plate Average	27.6		Top Plate Average	26.9	
ΔT	1.3	14.1	ΔT	3.6	37.3
3 hours into the test			3 hours into the test		
Measurement	T (°C)	% of Benchmark	Measurement	T (°C)	% of Benchmark
Bottom Plate Average	30.8		Bottom Plate Average	31.7	
Top Plate Average	29.8		Top Plate Average	28.9	
ΔT	1.0	11.1	ΔT	2.9	31.5
At the end of the 6 hour test			At the end of the 6 hour test		
Measurement	T (°C)	% of Benchmark	Measurement	T (°C)	% of Benchmark
Bottom Plate Average	32.4		Bottom Plate Average	32.8	
Top Plate Average	31.6		Top Plate Average	30.4	
Bottom Air Space	37.8		Bottom Air Space	37.8	
Top Air Space	30.4		Top Air Space	28.9	
ΔT	0.8	9.4	ΔT	2.4	27.2
Constant Heat Flux Tests (Standard Deviations of All Measurements < 0.34 °C)					
Conducting Configuration			Insulating Configuration		
1.75 hours into the test			1.75 hours into the test		
Measurement	T (°C)		Measurement	T (°C)	
Bottom Plate Average	26.1		Bottom Plate Average	27.1	
Top Plate Average	24.6		Top Plate Average	23.2	
ΔT	1.5		ΔT	3.8	
At the end of the 3.5 hour test			At the end of the 3.5 hour test		
Measurement	T (°C)		Measurement	T (°C)	
Bottom Plate Average	29.7		Bottom Plate Average	30.8	
Top Plate Average	28.1		Top Plate Average	26.6	
Bottom Air Space	37.4		Bottom Air Space	39.6	
Top Air Space	26.8		Top Air Space	25.4	
ΔT	1.7		ΔT	4.2	

A direct comparison between the insulating and conducting configurations' average hot side temperature, average cold side temperature, and ΔT for the constant temperature tests for the basic shifting fins prototype is illustrated in the plot of Figure 92. Moreover, a similar comparison between the prototype's insulating and conducting states for the constant heat flux tests is found in Figure 93.

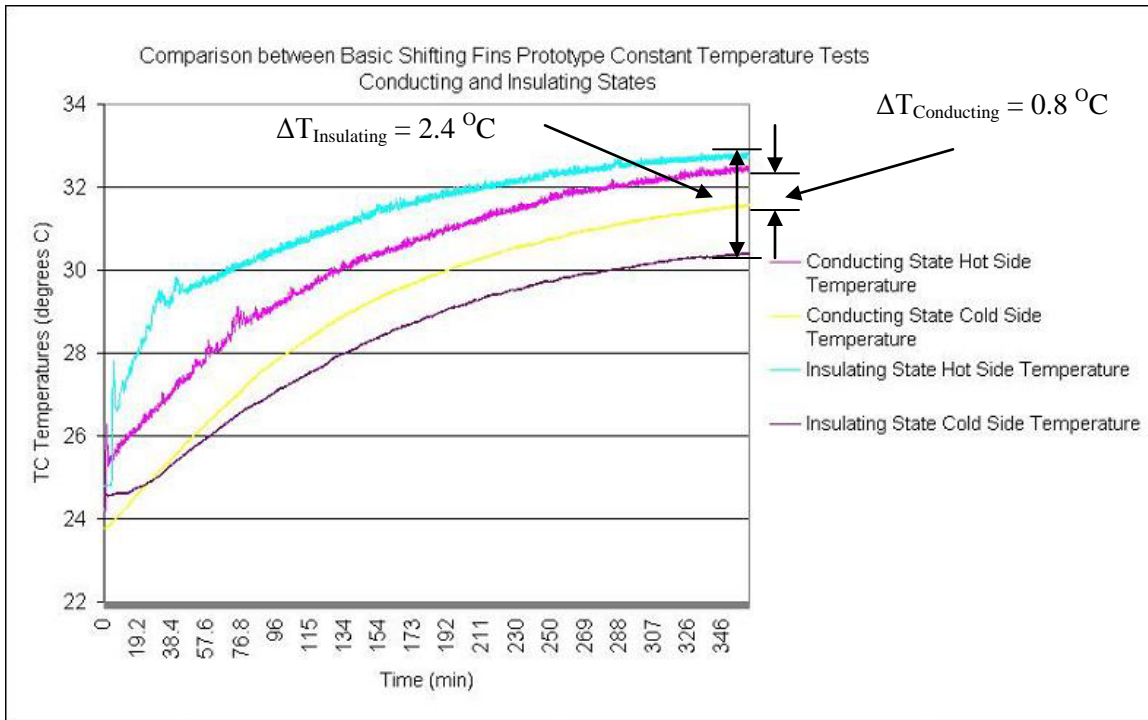


Figure 92: Comparison between Basic Shifting Fins Prototype Conducting and Insulating States for Constant Temperature Tests.

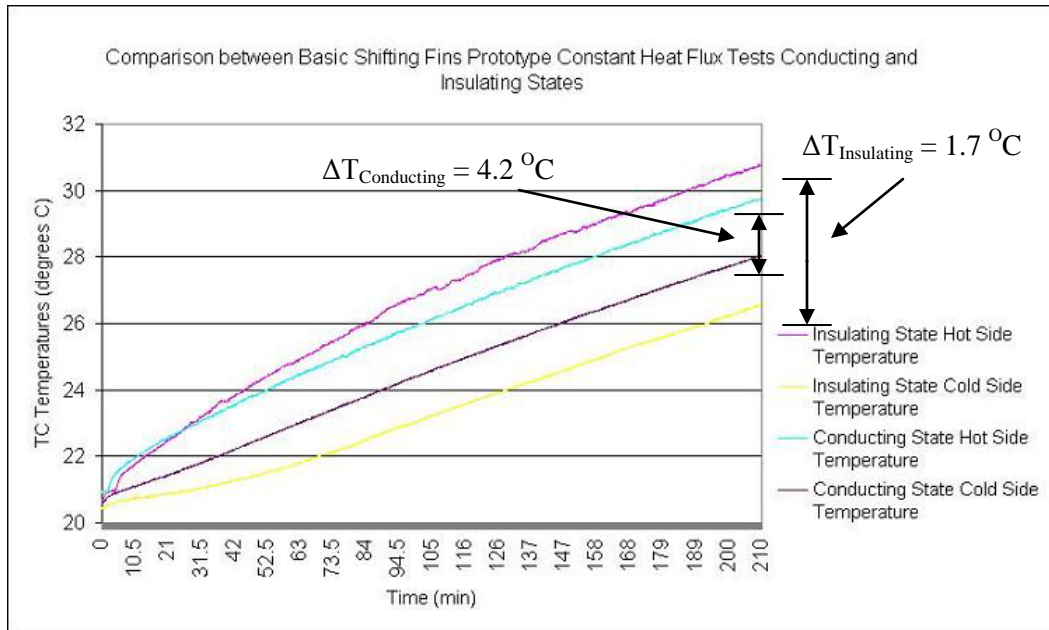


Figure 93: Comparison between Basic Shifting Fins Prototype Conducting and Insulating States for Constant Heat Flux Tests.

From the constant temperature experimental results of Table 5, a significant change in ΔT across the basic shifting fins device from 0.8 to 2.4 °C can be seen as the device switches states from its conducting configuration to its insulating configuration. This sufficiently provides proof-of-concept for smart insulation devices by showing that shifting the fins in the prototype to break the heat conduction path will cause the device to change its thermal conductivity. In addition, an even larger change in ΔT was measured when the device switched between its conducting and insulating states for the constant heat flux tests, showing that greater variation in thermal conductivity is possible for the basic shifting fins prototype when a constant heat flux boundary condition is applied compared to a constant temperature boundary condition.

In terms of the temperature distribution on the top and bottom plates of the prototype, the five bottom plate thermocouples all had approximately the same temperature values at the conclusion of the tests regardless of location, so it can be assumed that the temperature distribution on the bottom plate was uniform for all of the shifting fins prototype tests. The five top plate thermocouples did, however, have

some slight variation dependent on their location on the top plate with the thermocouples mounted directly on top of fins being roughly 0.3 °C warmer than the thermocouples not mounted above fins. This shows that when the top and bottom fins of the device are in thermal contact, the heat flowing from the bottom fins to the top fins caused the areas of the top plate where fins were mounted to be slightly warmer than other areas of the top plate. In addition, the temperature of the center thermocouple of the top plate, which was not mounted above a fin, was always slightly higher than the temperatures of the top plate corner thermocouples not mounted directly above a fin in the amount of less than 0.1 °C, while still being slightly cooler than the corner thermocouples that were mounted above a fin.

When comparing the basic shifting fins prototype to the benchmark insulation test piece, the shifting fins thermal semiconductor performed well in its conducting state, as the final ΔT value measured across the prototype was only 9.4% of the final ΔT value measured across the benchmark insulation test piece. This essentially means that the basic shifting fins prototype had only 9.4% of the insulating capability of the foam building insulation test piece of the same dimensions, which shows that it can function as a good conductor. Unfortunately, the basic shifting fins device did not function as a very good insulator in its insulating configuration. The final ΔT value measured across the device in its insulating state was only 27.2% of the final ΔT value measured across the benchmark insulation test piece. Consequently, the basic shifting prototype was only one-quarter as effective an insulator as the benchmark polyisocyanurate foam building insulation test piece. To try and improve the insulating state of the shifting fins device, foam polyisocyanurate insulation was placed in between of the fins in the device to inhibit convection heat transfer of the air between the fins. The results of the shifting fins thermal semiconductor with insulation between the fins will be presented in the next section.

4.1.2 Shifting Fins Thermal Semiconductor with Insulation between Fins Testing Results

Once polyisocyanurate foam insulation pieces were inserted between the fins of the shifting aluminum fins device, two constant temperature boundary condition tests and two constant heat flux boundary

condition tests were conducted for the new thermal semiconductor set-up's insulating and conducting states. The same testing procedures that were used for the basic shifting fins thermal semiconductor were also utilized for the shifting fins device with insulation between the fins, including the same amount of power supplied to the heater in the test chamber. Likewise, the same thermocouple placement used for the original shifting fins thermal semiconductor's top and bottom aluminum plates was also utilized for the new shifting fins prototype with insulation between the fins. An image of the new shifting fins device with foam insulation between the fins placed in the insulation test chamber for experimentation is shown in Figure 94.

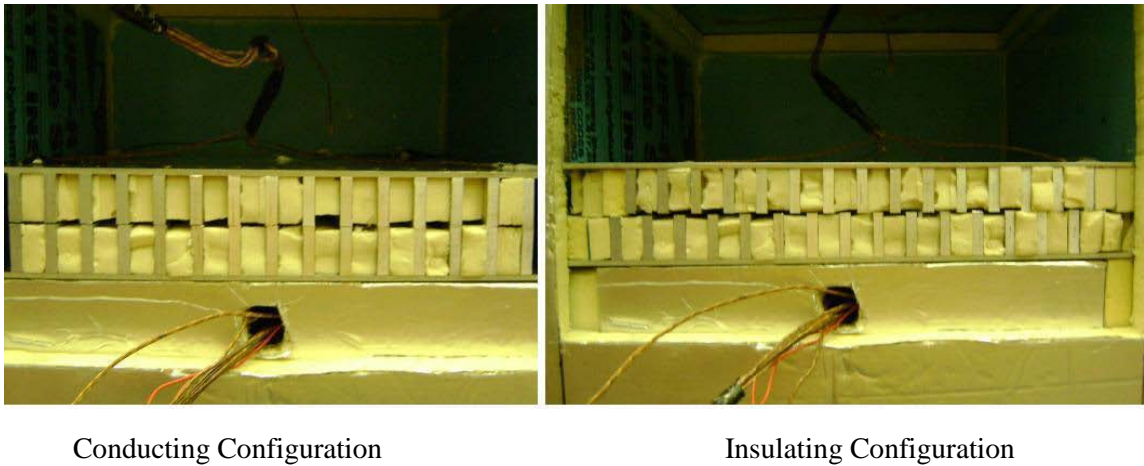


Figure 94: Shifting Fins Smart Insulation Prototype with Foam Insulation between Fins in Test Chamber.

Plots for the constant temperature tests of the shifting fins prototype with insulation between the fins are given in Figure 95 for the prototype's conducting state and Figure 96 for the prototype's insulating state. Additionally, for the second shifting fins prototype's constant heat flux tests, plot of the temperature measurements for the prototype's conducting and insulating arrangements can be found in Figures 97 and 98 respectively. Finally, the average hot and cold plate temperatures and the ΔT values for the shifting fins prototype with foam insulation between the fins at the quarter-point, halfway-point and end of the tests can be seen in Table 6.

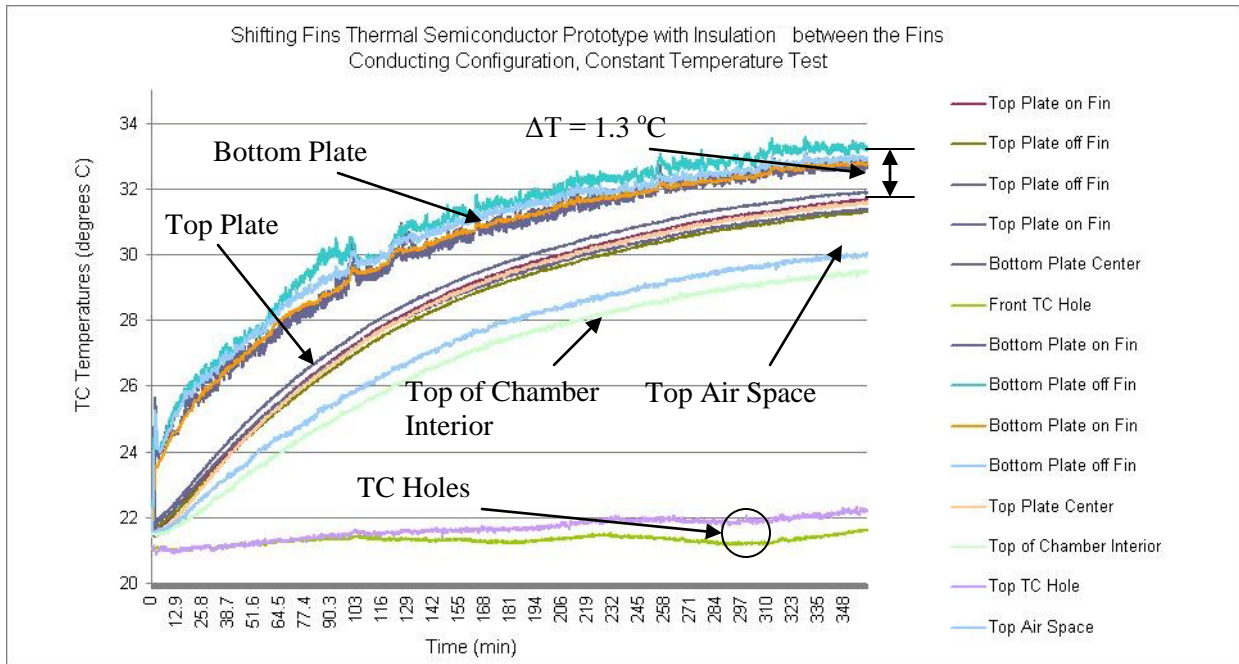


Figure 95: Shifting Fins Thermal Semiconductor Prototype with Insulation between the Fins Conducting State, Constant Temperature Test.

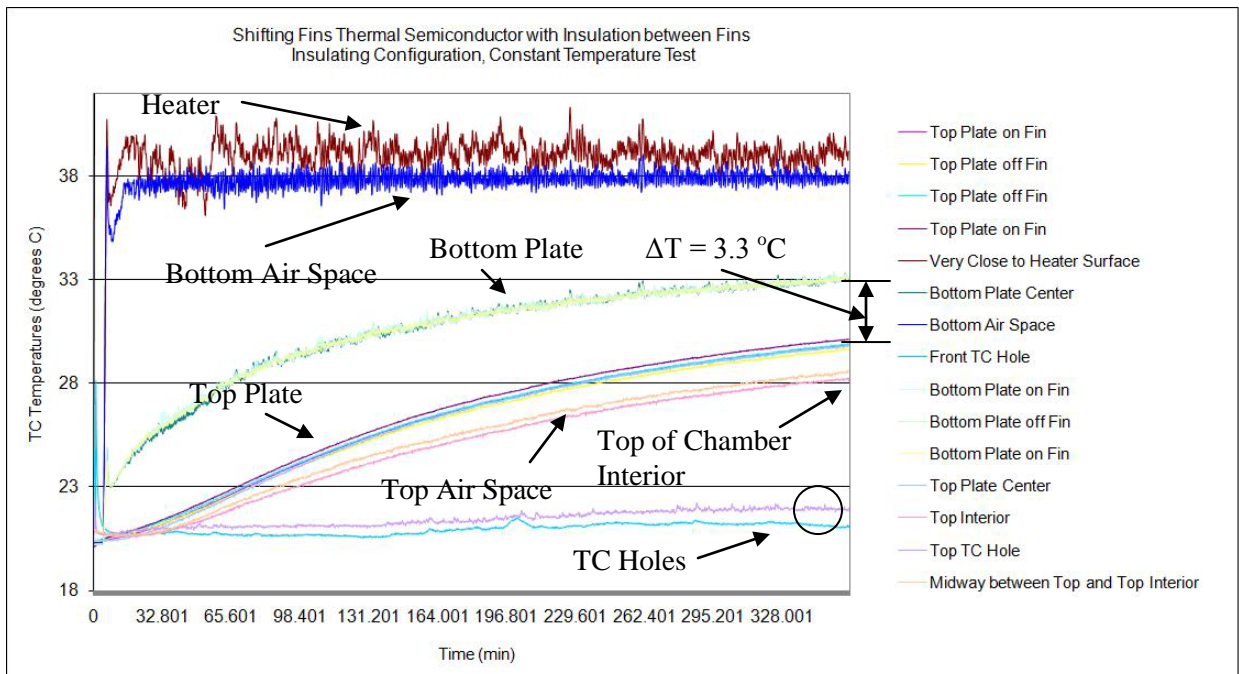


Figure 96: Shifting Fins Thermal Semiconductor Prototype with Insulation between the Fins Insulating State, Constant Temperature Test.

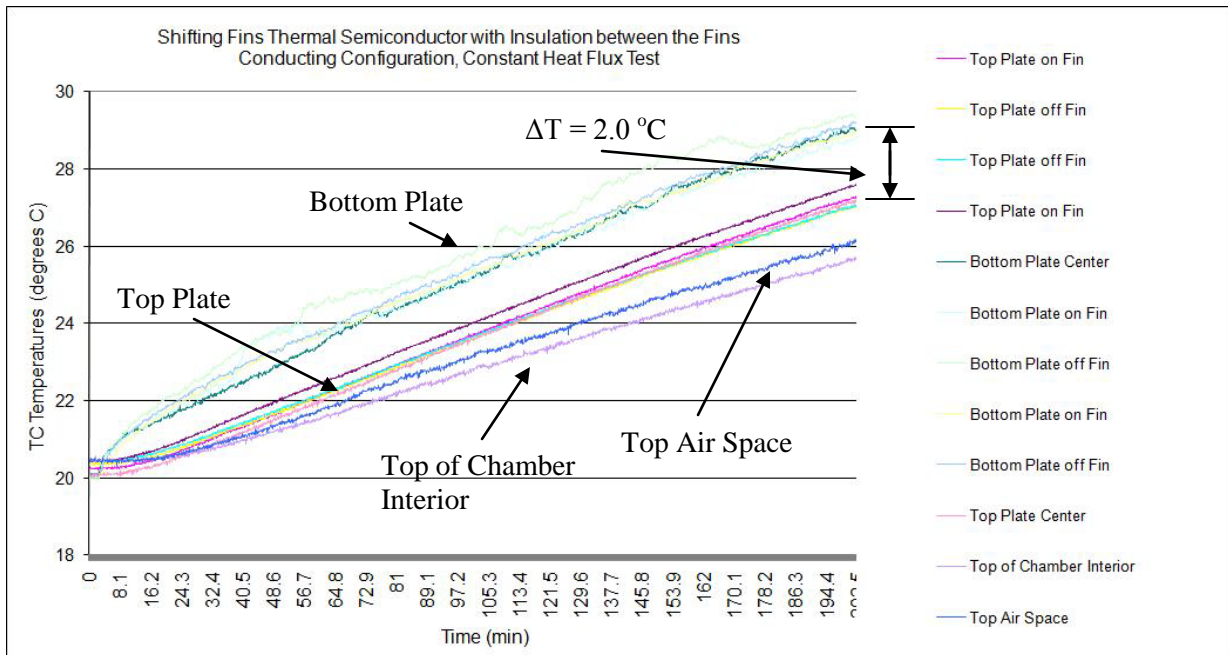


Figure 97: Shifting Fins Thermal Semiconductor Prototype with Insulation between the Fins Conducting State, Constant Heat Flux Test

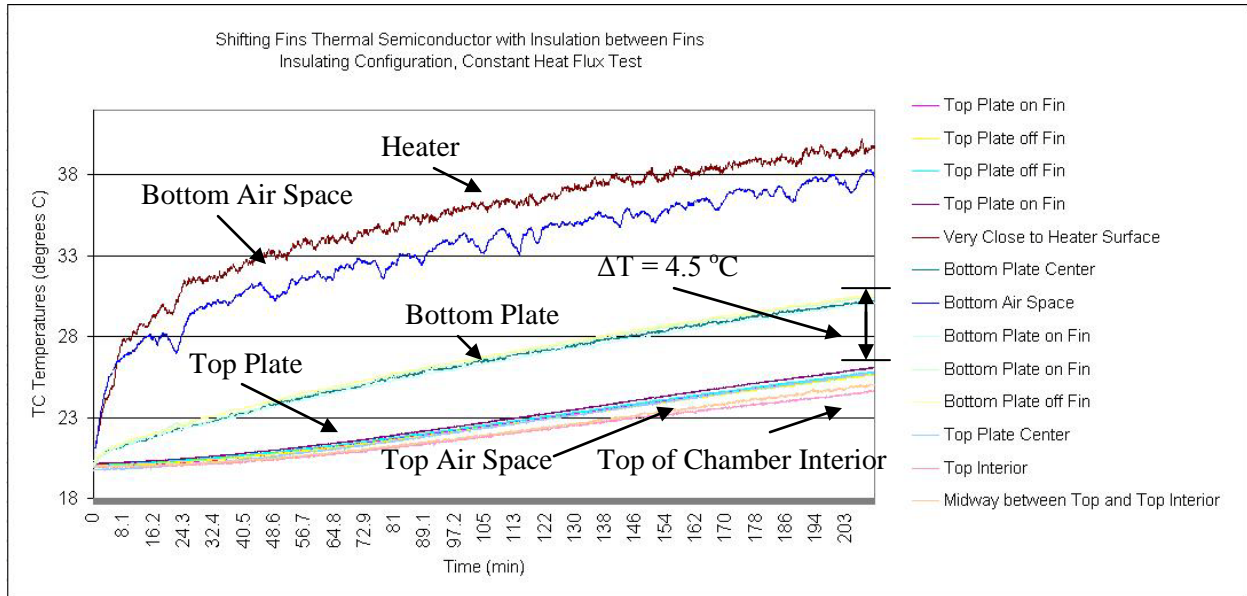


Figure 98: Shifting Fins Thermal Semiconductor Prototype with Insulation between the Fins Insulating State, Constant Heat Flux Test.

Table 6: Shifting Fins Prototype with Insulation between the Fins Experimental Results.

Constant Temperature Tests (Standard Deviations of All Measurements < 0.29 °C)					
Conducting Configuration			Insulating Configuration		
1.5 hours into the test			1.5 hours into the test		
Measurement	T (°C)	% of Benchmark	Measurement	T (°C)	% of Benchmark
Bottom Plate Average	29.2		Bottom Plate Average	29.0	
Top Plate Average	26.7		Top Plate Average	23.8	
ΔT	2.5	25.7	ΔT	5.2	54.6
3 hours into the test			3 hours into the test		
Measurement	T (°C)	% of Benchmark	Measurement	T (°C)	% of Benchmark
Bottom Plate Average	31.1		Bottom Plate Average	31.3	
Top Plate Average	29.5		Top Plate Average	26.9	
ΔT	1.7	18.2	ΔT	4.5	49.1
At the end of the 6 hour test			At the end of the 6 hour test		
Measurement	T (°C)	% of Benchmark	Measurement	T (°C)	% of Benchmark
Bottom Plate Average	32.8		Bottom Plate Average	33.1	
Top Plate Average	31.6		Top Plate Average	29.9	
Bottom Air Space	37.8		Bottom Air Space	37.8	
Top Air Space	30.1		Top Air Space	28.6	
ΔT	1.3	14.2	ΔT	3.3	36.7
Constant Heat Flux Tests (Standard Deviations of All Measurements < 0.28 °C)					
Conducting Configuration			Insulating Configuration		
1.75 hours into the test			1.75 hours into the test		
Measurement	T (°C)		Measurement	T (°C)	
Bottom Plate Average	25.5		Bottom Plate Average	26.6	
Top Plate Average	23.9		Top Plate Average	22.5	
ΔT	1.7		ΔT	4.1	
At the end of the 3.5 hour test			At the end of the 3.5 hour test		
Measurement	T (°C)		Measurement	T (°C)	
Bottom Plate Average	29.4		Bottom Plate Average	30.3	
Top Plate Average	27.5		Top Plate Average	25.8	
Bottom Air Space	37.3		Bottom Air Space	39.6	
Top Air Space	26.4		Top Air Space	25.0	
ΔT	2.0		ΔT	4.5	

In order to more easily compare changes in the hot side temperature, cold side temperature, and ΔT for the shifting fins prototype with insulation between the fins as it changed from its conducting state to its insulating state, two plots were produced. Figure 99 displays a plot of the average hot and cold side temperatures for the insulating and conducting states of the shifting fins prototype with foam insulation

between the fins constant temperatures tests, while Figure 100 provides a plot for the corresponding two constant heat flux tests.

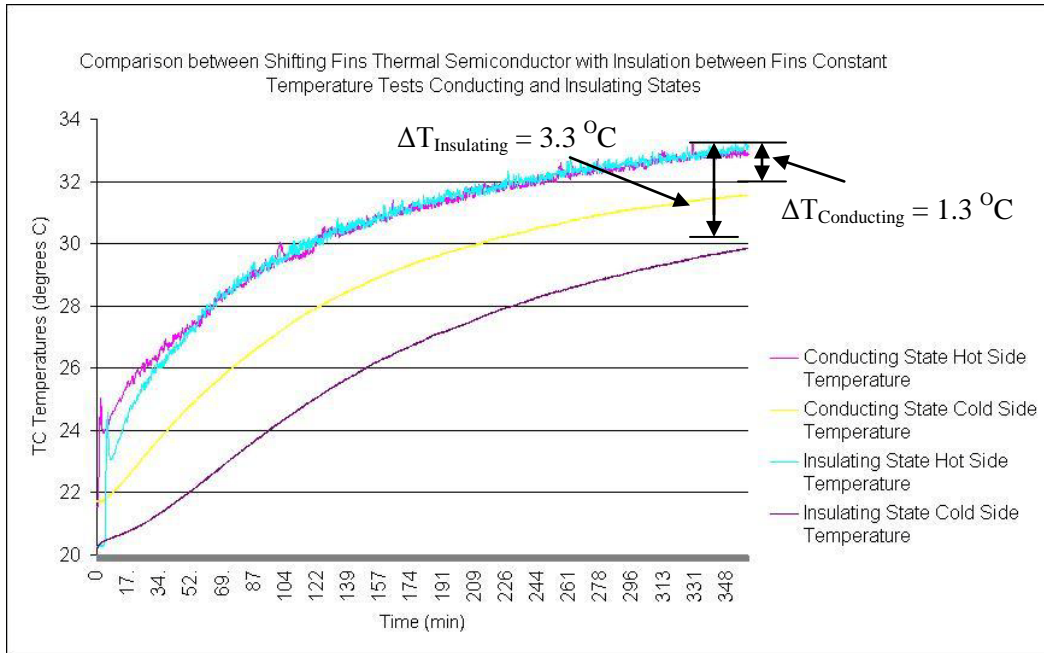


Figure 99: Comparison between Shifting Fins Thermal Semiconductor with Insulation between the Fins Conducting and Insulating States for Constant Temperature Tests.

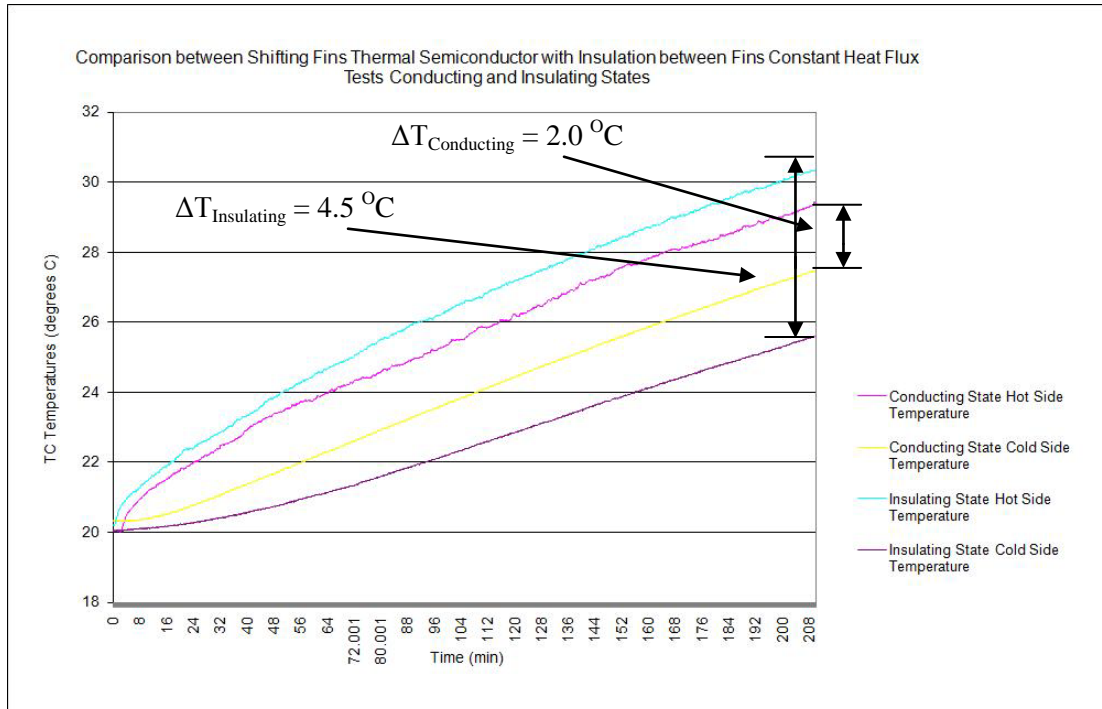


Figure 100: Comparison between Shifting Fins Thermal Semiconductor with Insulation between the Fins Conducting and Insulating States for Constant Heat Flux Tests.

By inserting pieces of foam polyisocyanurate insulation into the air spaces between the fins of the shifting fins thermal semiconductor prototype, the performance of the insulator state of the device was significantly improved for both the constant temperature and constant heat flux tests as shown in Table 6. At the end of the constant temperature test for the insulating configuration of the prototype with insulation between the fins, the ΔT value measured across the device had increased by 34.8% from the original basic shifting device's ΔT value of $2.4\text{ }^{\circ}\text{C}$ to a value of $3.3\text{ }^{\circ}\text{C}$. This shows that for the basic shifting fins prototype convection of the air between the fins was causing high convective heat transfer between the hot and cold side plates even when the prototype was in its insulating configuration. Once foam insulation was added to fill up the air spaces between the fins, convective heat transfer in the shifting fins thermal semiconductor was essentially eliminated, causing the increase in the ΔT value.

Unfortunately, although the insulator state of the modified thermal semiconductor was improved by adding insulation between the fins, the performance of the high heat transfer state of the thermal

semiconductor was also decreased. For the shifting fins device with insulation between the fins, the conducting state's ΔT value measured at the end of the constant temperature test also increased by 51.4% from the original basic shifting fins device's ΔT value of $0.8\text{ }^{\circ}\text{C}$ to a value of $1.3\text{ }^{\circ}\text{C}$. Similar changes occurred in the ΔT values for the constant heat flux tests for the modified shifting fins prototype, resulting in the shifting fins device with insulation between the fins having about the same level of performance as a smart insulation device as the basic shifting fins prototype with air between the fins. Two plots comparing the average hot side temperatures, average cold side temperatures, and ΔT values of the basic shifting fins device and the shifting fins device with insulation between the fins are shown in Figures 101 and 102 for the constant temperature tests' conducting and insulating configurations. Using the final ΔT values measured for the constant temperature tests for the shifting fins prototype with insulation between the fins, the ΔT values were able to change from 14.2% to 36.7% of the ΔT values of the benchmark insulation test piece when the prototype was switched between its conducting and insulating state, which was similar to the range of change in ΔT for the basic shifting fins prototype.

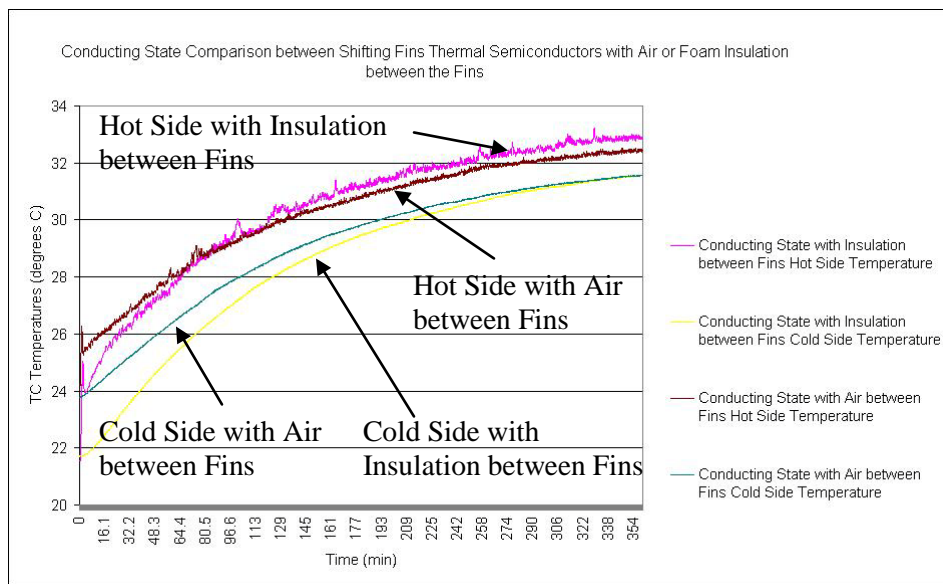


Figure 101: Conducting State Comparison between Shifting Fins Thermal Semiconductors with Air or Foam Insulation between the Fins.

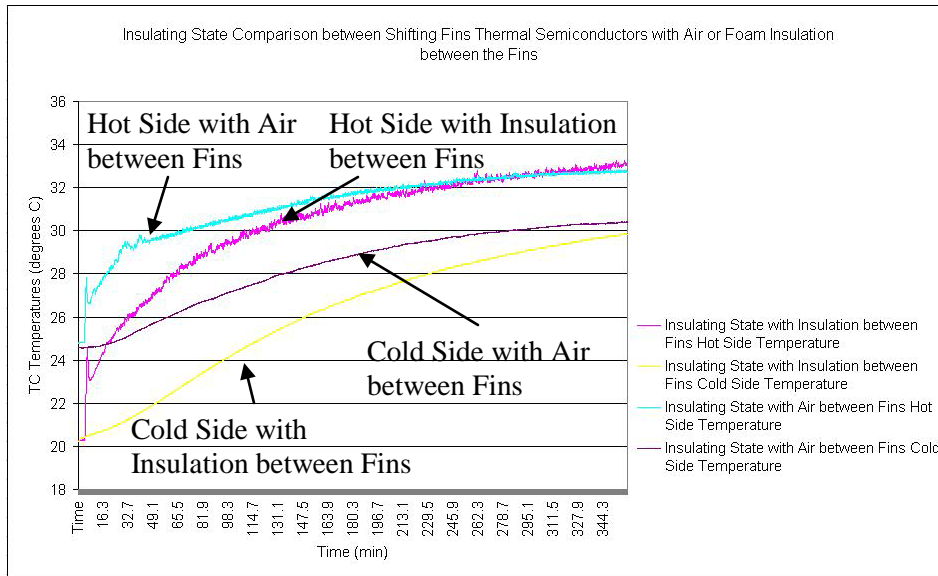


Figure 102: Insulating State Comparison between Shifting Fins Thermal Semiconductors with Air or Foam Insulation between the Fins.

4.1.3 Shifting Fins Thermal Semiconductor with Thermal Greases Testing Results

In order to improve the thermal conduction path between the lower and upper aluminum fins of the basic shifting fins thermal semiconductor when the device was in its conducting configuration, two types of thermal greases were applied to the lower and upper fins to reduce the thermal contact resistance. First, silver-based thermal grease was applied to the fins, and later on, silicone-based thermal grease was also tried. Both constant temperature and constant heat flux tests were run for each type of thermal grease with the same testing parameters and thermocouple placement as for the tests of the basic shifting fins device and the shifting fins prototype with insulation between the fins. For the testing of the shifting fins thermal semiconductor with thermal greases, air was used in the spaces between the fins of the device instead of the foam polyisocyanurate insulation pieces.

Once the results of the shifting fins device with thermal greases were reviewed, it was clear any improvements the thermal greases provided to the conducting state of the prototype were negligible. In fact, the silver-based thermal grease actually caused the ΔT values measured across the shifting fins

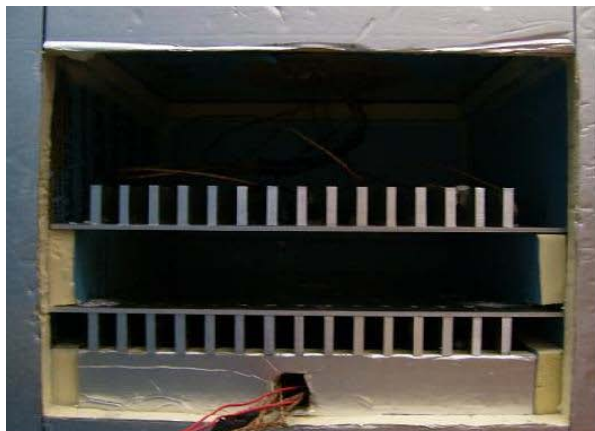
device's conducting configuration to increase slightly by $0.0245\text{ }^{\circ}\text{C}$ at the end of the 6 hour constant temperature test over the ΔT value measured for the basic shifting fins prototype without thermal grease. At first this increase in ΔT for the shifting fins prototype was attributed to the silver-based thermal grease being extremely thick and hence, very difficult to spread out evenly over the surface of the fins to effectively reduce contact resistance. After the testing of a much thinner and easy-to-spread silicone-based thermal grease also produced only very slight changes in the ΔT value measured across the prototype,, it was determined that neither of the thermal greases had improved the original shifting fins thermal semiconductor.

Although thermal greases typically significantly improve the conduction heat transfer between two surfaces in contact, several possible reasons exist for why no improvement occurred for the shifting fins thermal semiconductor prototype. First, as a result of the aluminum fins of the devices being very accurately milled in the machine shop to nearly the same dimensions within several thousandths of an inch, the top and bottom fins of the thermal semiconductor prototype had a very good contact with one another with minimal contact resistance caused by the small air gaps at the interface between the surfaces. By applying thermal greases in a thin layer to the fins of the device, the grease would have served to fill any small air gaps from thermal contact resistance at the interface between the two surfaces, helping to improve the conduction heat transfer at those locations. At locations where the top and bottom fins were already in direct contact with one another, however, the thin layer of thermal grease would have actually increased the thermal resistance due to the thermal greases having a much lower thermal conductivity between $0.7\text{ -}8.65\text{ W/m-K}$ compared to the thermal conductivity of the 6061 aluminum alloy fins of 167 W/m- K [24]. If the thermal greases improved the thermal conduction at some locations where the fins were not in good contact, while decreasing the thermal conduction at other locations where the fins were in very good thermal contact with one another, the effects of the thermal greases at the different locations could have canceled each other out. This would have resulted in roughly the same ΔT value measured across the device's conducting configuration during the testing whether or not the thermal greases were applied to the fins.

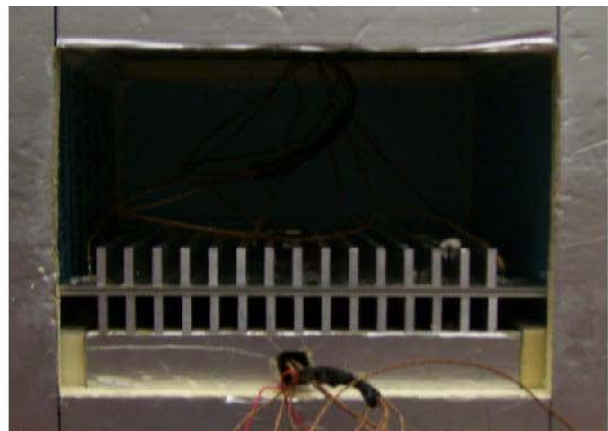
In addition, the ΔT value measured across the original basic shifting fins prototype's conducting state was only a very low value $0.8\text{ }^{\circ}\text{C}$, which showed that good conduction heat transfer was already taking place through the contacting fins across the smart insulation device. Even with thermal greases applied to the surfaces of the contacting fins, it might be very difficult to achieve a lower ΔT value measured between the hot and cold sides of the thermal semiconductor prototype due to some thermal contact resistance always being present. In a different situation such as the case of a device that needs to transfer a large amount of heat via conduction from a very hot component on the order of hundreds of degrees Celsius to a heat sink and the ambient environment, thermal greases can significantly improve the conductive heat transfer, but in the case of the shifting fins thermal semiconductor, the ΔT is already small enough that the thermal greases do not have much effect.

4.1.4 Back-to-Back Aluminum Plates Thermal Semiconductor Testing Results

The next type of smart insulation device tested was the back-to-back plates with outward facing fins prototype. Figure 103 provides an image of the back-to-back plates with fins prototype inserted into the insulation test chamber in both its insulating and conducting configurations.



Insulating Configuration



Conducting Configuration

Figure 103: Back-to-Back Plates with Fins Smart Insulation Prototype in Test Chamber.

Since the back-to-back plates with fins thermal semiconductor operated much differently than the first few shifting fins prototypes, a new arrangement for the thermocouple placement was necessary. In the back-to-back plates with fins prototype, the top and bottom fins in addition to the top and bottom plates make up the hot and cold sides of the device facing the bottom and top air spaces in the chamber respectively. Before, with the shifting fins thermal semiconductor, the hot and cold sides of the device only consisted of the two plates, so the five thermocouples mounted to the hot and cold sides of the device were all mounted directly to the plates. For the back-to-back plates with fins prototype, however, some of the thermocouples used to calculate the ΔT across the device would need to be mounted on the top and bottom fins themselves, since they make up a significant portion of the hot and cold sides of the device.

As with the shifting fins devices earlier, four thermocouples were placed in the corners of both the top and bottom pieces of the device facing the top and bottom air spaces. In two of the corners the thermocouples were mounted to the plates, while in the other two corners the thermocouples were mounted on top of the fins. In addition, two more thermocouples were also placed in the center of both the top and bottom pieces with again one thermocouple mounted to the plate and a second thermocouple mounted to the center-most fin. Eventually, twelve thermocouples were mounted to the hot and cold sides of the back-to-back plates with fins device, which was two more than for the shifting fins devices. The data acquisition equipment used in the experimental set-up to acquire the temperature measurement data from the thermocouples could only handle up to sixteen thermocouples, so the two thermocouples placed near the insulation test chamber's two thermocouple holes used to monitor any heat leakage were instead moved to the hot and cold sides of the prototype. Figure 104 gives an image of the thermocouple placement on the top and bottom pieces of the back-to-back plates with fins device.

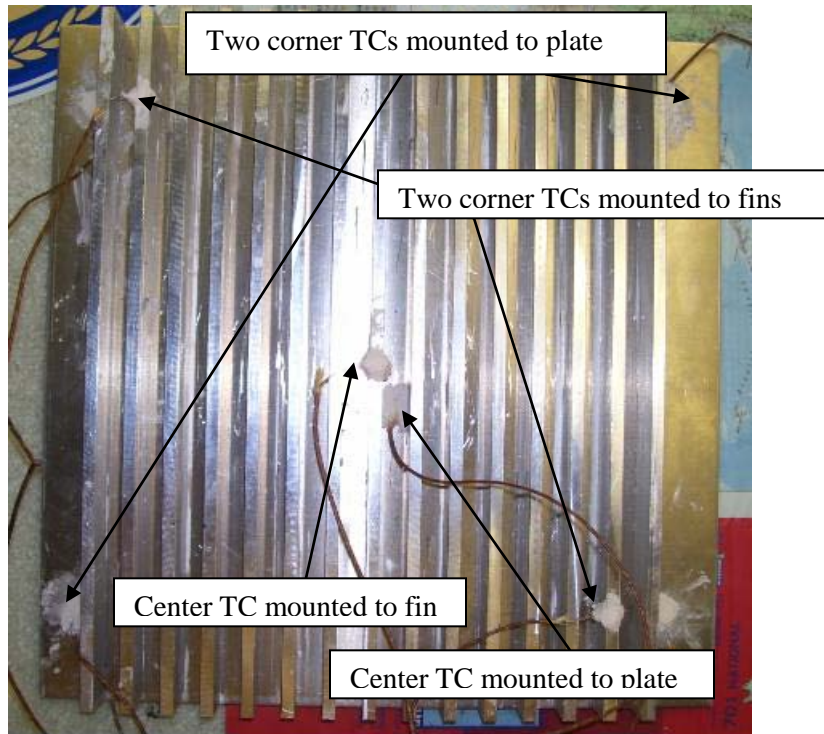


Figure 104: Back-to-Back Plates with Fins Smart Insulation Prototype Plates' Thermocouple Placement.

The major reason for mounting some of the thermocouples directly to the top and bottom fins was to examine whether or not the outward facing fins were assisting in smart insulation device's capture of heat from the hot air space and dissipation of heat to the cold air space. The thermocouples mounted to the bottom facing fins of the device should, in theory, heat up quicker than the thermocouples mounted to the bottom plate, since they are closer to the heat source and more heat is transferred across the fin's large surface area. Likewise, the thermocouples mounted to the top facing fins should be cooler than the ones mounted to the top plate, since the top fins' large surface area will be much more effective at dissipating heat to the top air space than the top plate. Plots of the constant temperature tests for the back-to-back plates with fins device can be seen in Figures 105 and 106 for the device's conducting and insulating arrangements respectively. The results of the device's constant heat flux tests are also given for its conducting configuration in Figure 107 and for its insulating configuration in Figure 108. In addition, important temperature measurement data and the ΔT values calculated for the back-to-back plates with

fins prototype is shown in Table 7. Finally, to easily analyze the changes in the average hot side temperature, average cold side temperature, and ΔT as the device changes from its conducting state to its insulating state, an additional plot was produced that is shown in Figure 109 for the constant temperature tests.

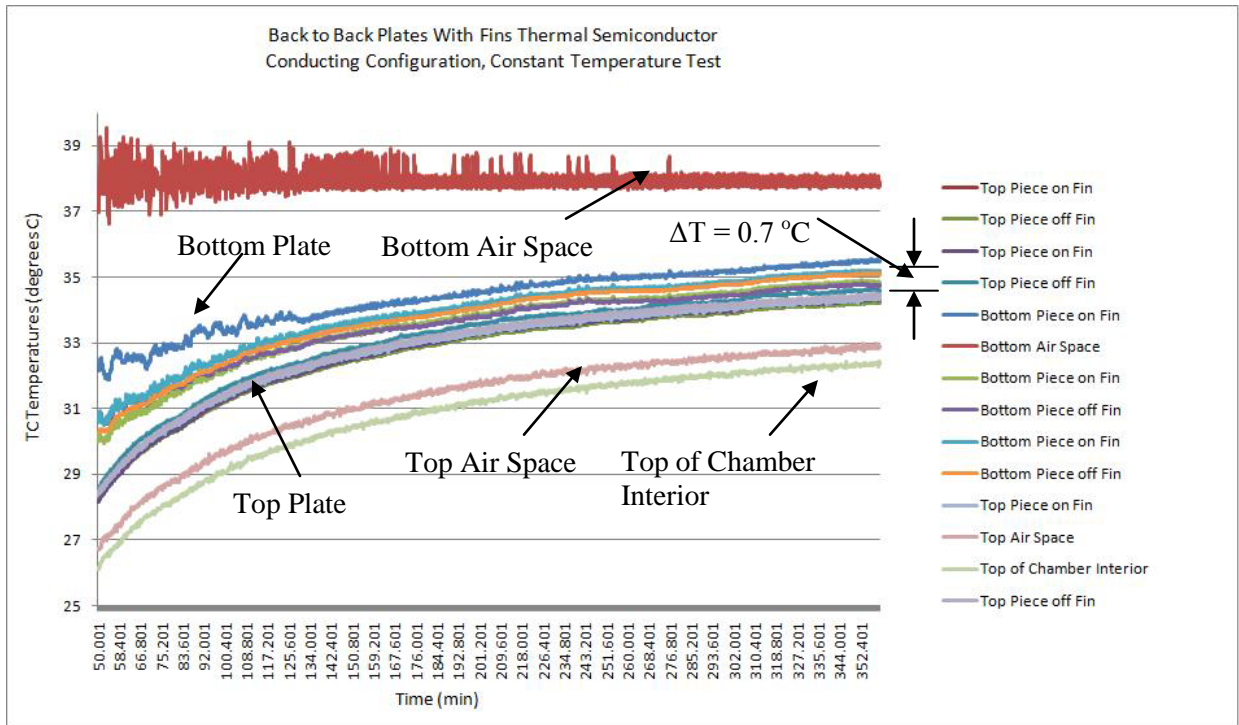


Figure 105: Back-to-Back Plates with Fins Thermal Semiconductor Prototype Conducting State, Constant Temperature Test.

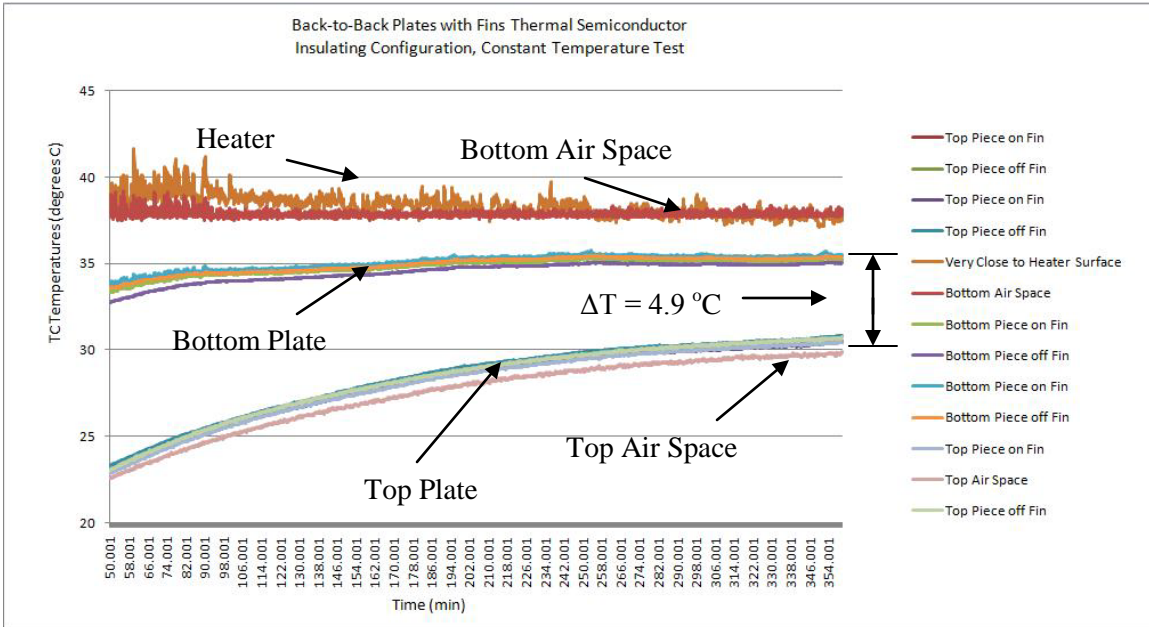


Figure 106: Back-to-Back Plates with Fins Thermal Semiconductor Prototype Insulating State, Constant Temperature Test.

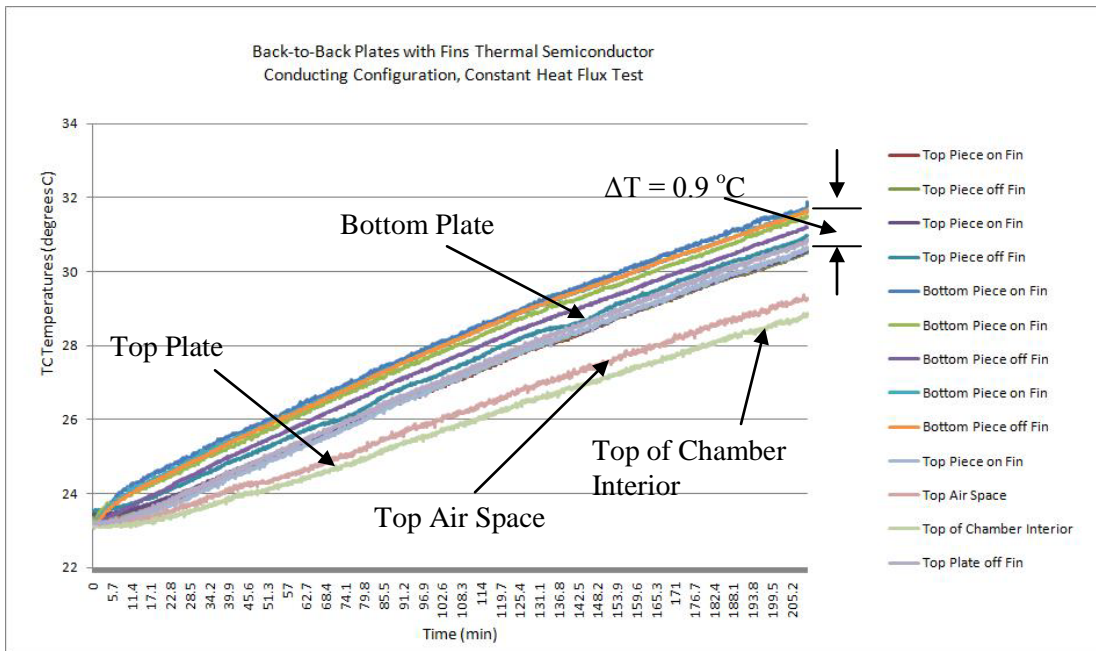


Figure 107: Back-to-Back Plates with Fins Thermal Semiconductor Prototype Conducting State, Constant Heat Flux Test.

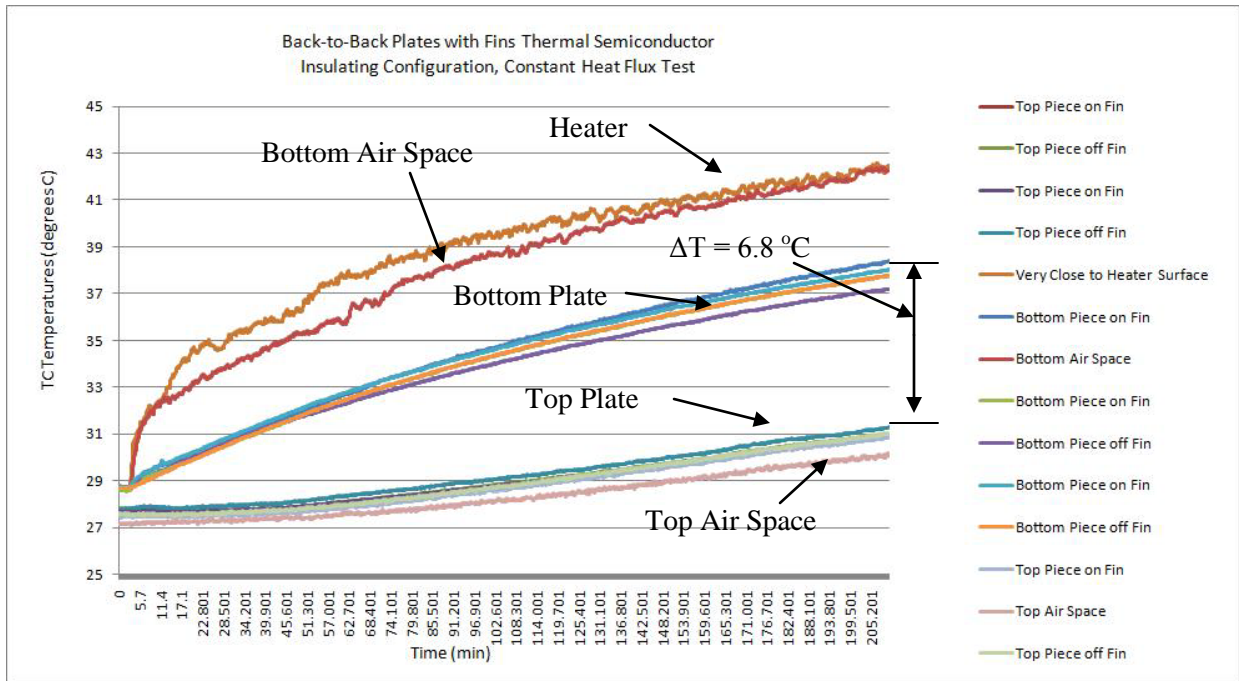


Figure 108: Back-to-Back Plates with Fins Thermal Semiconductor Prototype Insulating State, Constant Heat Flux Test.

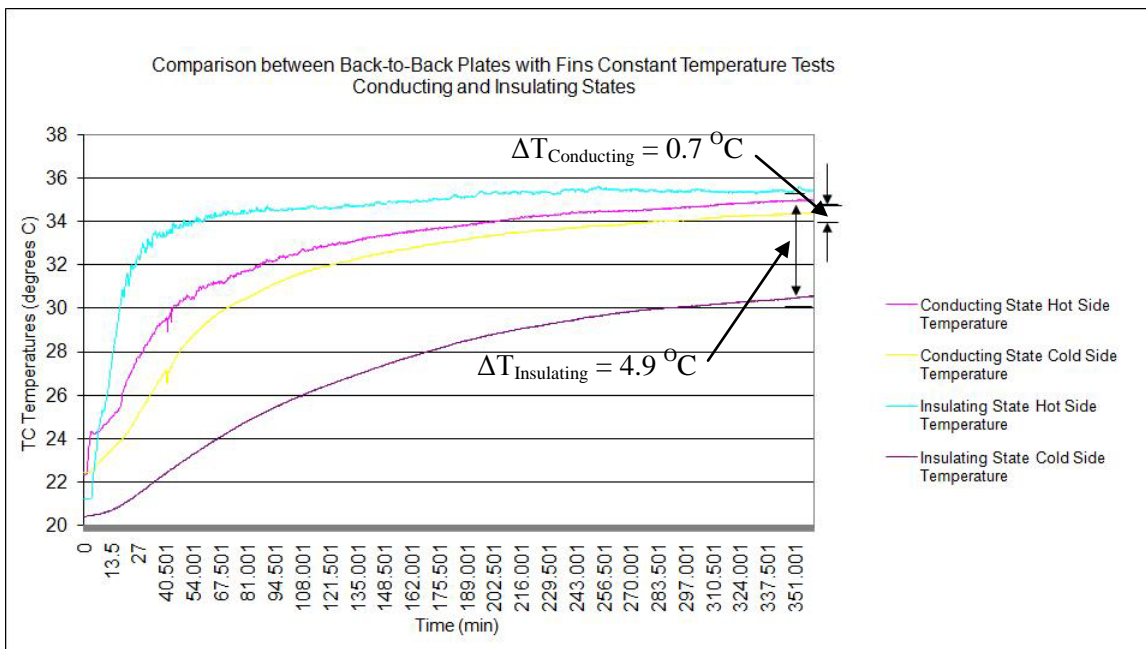


Figure 109: Comparison between Back-to-Back Plates with Fins Conducting and Insulating States for Constant Temperature Tests.

Table 7: Back-to-Back Plates with Outward Facing Fins Thermal Semiconductor Experimental Results.

Constant Temperature Tests (Standard Deviations of All Measurements < 0.34 °C)					
Conducting Configuration			Insulating Configuration		
1.5 hours into the test			1.5 hours into the test		
Measurement	T (°C)	% of Benchmark	Measurement	T (°C)	% of Benchmark
Bottom Piece Average	32.4		Bottom Piece Average	34.6	
Top Piece Average	30.9		Top Piece Average	26.8	
ΔT	1.5	15.5	ΔT	9.3	98.0
3 hours into the test			3 hours into the test		
Measurement	T (°C)	% of Benchmark	Measurement	T (°C)	% of Benchmark
Bottom Piece Average	33.8		Bottom Piece Average	35.0	
Top Piece Average	33.1		Top Piece Average	29.4	
ΔT	0.8	8.3	ΔT	6.7	73.6
At the end of the 6 hour test			At the end of the 6 hour test		
Measurement	T (°C)	% of Benchmark	Measurement	T (°C)	% of Benchmark
Bottom Piece Average	35.1		Bottom Piece Average	35.4	
Top Piece Average	34.4		Top Piece Average	31.3	
Bottom Air Space	37.8		Bottom Air Space	37.8	
Top Air Space	32.9		Top Air Space	29.9	
ΔT	0.7	7.8	ΔT	4.9	54.6
Constant Heat Flux Tests (Standard Deviations of All Measurements < 0.45 °C)					
Conducting Configuration			Insulating Configuration		
1.75 hours into the test			1.75 hours into the test		
Measurement	T (°C)		Measurement	T (°C)	
Bottom Piece Average	28.0		Bottom Piece Average	34.5	
Top Piece Average	27.1		Top Plate Average	28.8	
ΔT	0.9		ΔT	5.7	
At the end of the 3.5 hour test			At the end of the 3.5 hour test		
Measurement	T (°C)		Measurement	T (°C)	
Bottom Piece Average	31.6		Bottom Piece Average	37.8	
Top Piece Average	30.7		Top Piece Average	31.0	
Bottom Air Space	37.8		Bottom Air Space	42.2	
Top Air Space	29.3		Top Air Space	30.1	
ΔT	0.9		ΔT	6.8	

From the experimental results of Table 7, the back-to-back plates with outward facing fins prototype had much better performance than the earlier shifting fins devices in that a much greater change in ΔT was obtained as the device was changed from its conducting configuration to its insulating configuration. For example, at the end of the back-to-back plates with fins constant temperature tests, ΔT had a range

from 0.7 °C for the device's conducting configuration to 4.9 °C for the device's insulating configuration, which was much better than the basic shifting fins thermal semiconductor's ΔT range from 0.8 to 2.4 °C. Compared to the basic shifting fins device, the back-to-back plates with outward facing fins prototype had slightly better performance in its conducting state and much better performance in its insulating state. In addition, when the % of the benchmark foam insulation test piece's ΔT value is used to evaluate the device's performance, the back-to-back fins with plates device continues to exhibit a large range of thermal conductivity. The ΔT value of the back-to-back plates with fins device was able to vary at the end of the constant temperature tests from 7.8% to 54.6% of the benchmark foam insulation test piece, proving that the device is a very good conductor when necessary since its ΔT value is less than 1/10 of the insulation test piece, while also being a decent insulator when necessary but still not near as good an insulator as standard foam building insulation.

One possible way to improve the insulating configuration of the back-to-back plates with fins concept would be to have the outward facing fins of the device fold inward to a horizontal, stowed position when the device is actuated from its conducting state to its insulating state. Since the main purpose of the fins in the back-to-back plates concept was to use the large surface area of the fins to speed up the heat transfer through the device in only its conducting state, the fins are not needed in the device for its insulating state. In fact, the fins actually decreased the performance of the device in its insulating state by increasing the heat transfer of the device in that state as well. By folding the fins to a horizontal, stowed position in the device's insulating state, the surface area of the hot and cold sides of the device will be greatly decreased, lowering the level of heat transfer through the device in its insulating state.

The results of the constant heat flux tests in Table 7 also show that the back-to-back plates with fins prototype continues has increased performance over the shifting fins devices. At the end of the constant heat flux tests, the ΔT value measured is able to vary over the range from 0.9 °C for the device's conducting state to 6.8 °C for the device's insulating state. As with the constant temperature testing the range of ΔT and thus thermal conductivity obtained for the constant heat flux tests of the back-to-back plates with outward facing fins device was much larger than that of the basic shifting fins prototype for

which ΔT varied over a range of 1.7 - 4.2 °C as the device was actuated from its conducting state to its insulating state.

The final consideration in the back-to-back plates with fins testing was whether there were any differences between the temperatures measured for thermocouples mounted on the fins compared to the thermocouples mounted directly on the plates on the hot and cold sides of the device. On the cold side of the device the thermocouples mounted on top of the fins were found to be 0.1-0.2 °C cooler than the thermocouples mounted directly to the top plate during the testing. Meanwhile, on the hot side of the device, the thermocouples mounted directly to the bottom plate were found to be between 0.3-0.7 °C warmer than the thermocouples mounted on top of the fins during the testing. This shows that using outward facing fins instead of only the plates is more effective for both capturing the heat of the bottom air space and dissipating heat to the top air space.

4.1.5 Folding Fins with Vertical Contact Testing Results

Although a folding fins with vertical contact thermal semiconductor prototype was never actually constructed in the laboratory, a few tests were run in order to get a good idea of the possible performance of such a device. Since in the folding fins concept the conducting state of the device had essentially the same features as the basic shifting fins prototype except for greater spacing between the fins and twenty-two fins overall instead of thirty, it was assumed that for the folding fin device's conducting configuration the ΔT values would be very close to the ΔT values experimentally measured for the basic shifting fins prototype. In order to calculate some evaluation of the overall performance of a possible folding fins device, a ΔT value for the insulating state of the device also had to be obtained; however, additional experimental tests had to be run because the insulating configuration of the folding fins concept was much different than any of the tests already conducted.

To measure the ΔT value for the insulating, stowed fins position of the device, a simple smart insulation device consisting of two aluminum plates of the same dimensions of the plates of the original basic shifting fins prototype separated by a two inch (5.08 cm) air space and two foam insulation spacers

was constructed. Even though the set-up for this device does not completely represent the actual folding fins device later modeled in ANSYS, since it does not have any fins in their stowed position, it does provide an adequate representation to give a good idea of a possible range of ΔT values for a folding fins with vertical contact device. In addition, the experimental results obtained from the folding fins device's insulating configuration tests can also later on be used to calculate the natural convection coefficient as a function of temperature for the convective heat transfer across the air gap from the hot side to the cold side of the device for the ANSYS modeling of the folding fins with vertical contact device. The folding fins insulating state device developed can be seen in the insulation test chamber in Figure 110.

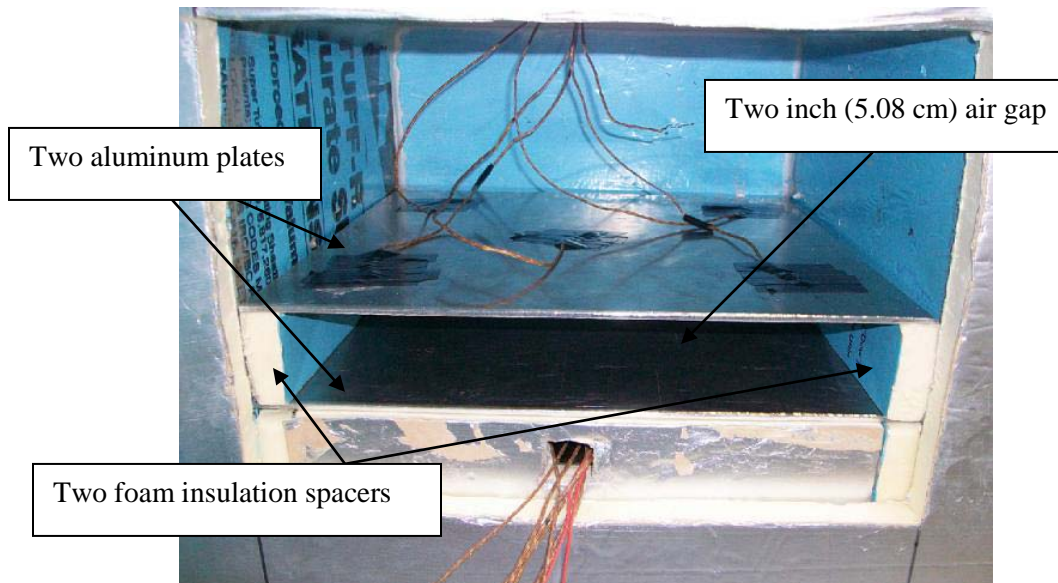


Figure 110: Folding Fins with Vertical Contact Insulating State Device in Insulation Test Chamber.

Both a constant temperature test and a constant heat flux test were conducted for the prototype fabricated for the insulating state of the folding fins device. The thermocouple placement on the hot and cold sides of the device consisted of one thermocouple mounted at the center each of the two plates and four thermocouples mounted at the corners of each plate at locations two inches (5.08 cm) inward in both directions from the plate corners. Plots of the results over time of the two tests ran for the device are given

in Figure 111 for the constant temperature test and Figure 112 for the constant heat flux test, while important temperature data for the two tests along with the ΔT values calculated are also given in Table 8. Finally, Figure 113 gives a plot that shows a comparison between the insulating and conducting states of a possible folding fins prototype using the basic shifting fins device's conducting configuration test results to represent the conducting state of the folding fins prototype. In Figure 113 the insulating and conducting states of the constant temperature tests for the folding fins device are compared by plotting the average hot side temperatures and average cold side temperatures for both heat transfer states.

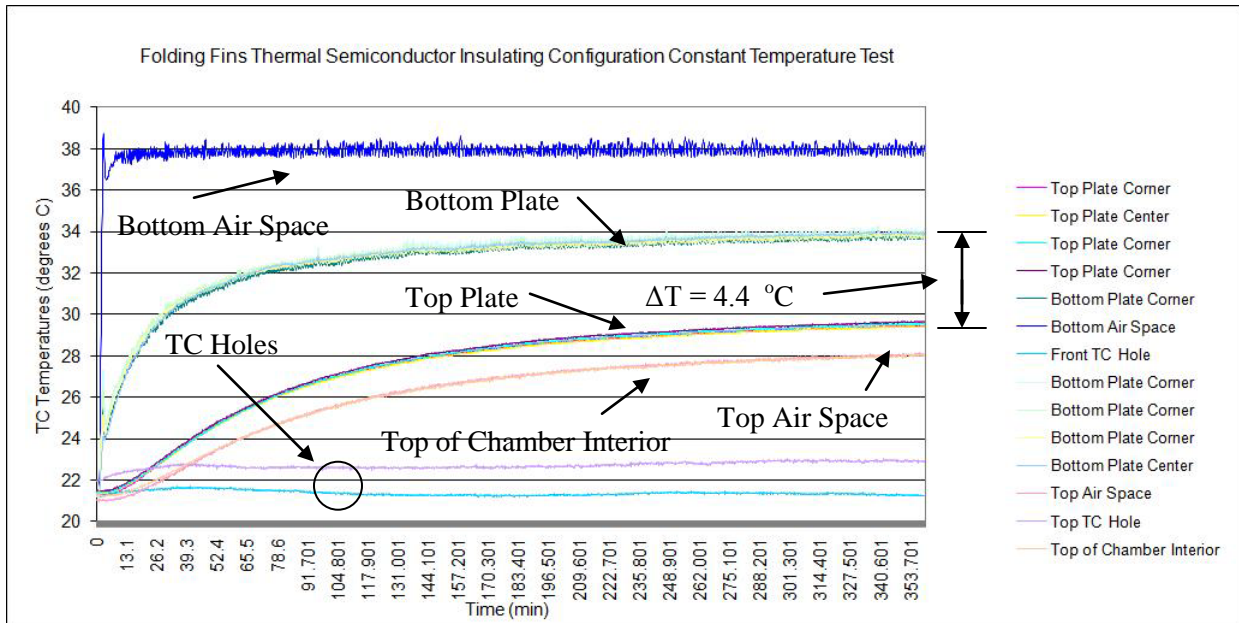


Figure 111: Folding Fins Thermal Semiconductor Insulating Configuration, Constant Temperature Test.

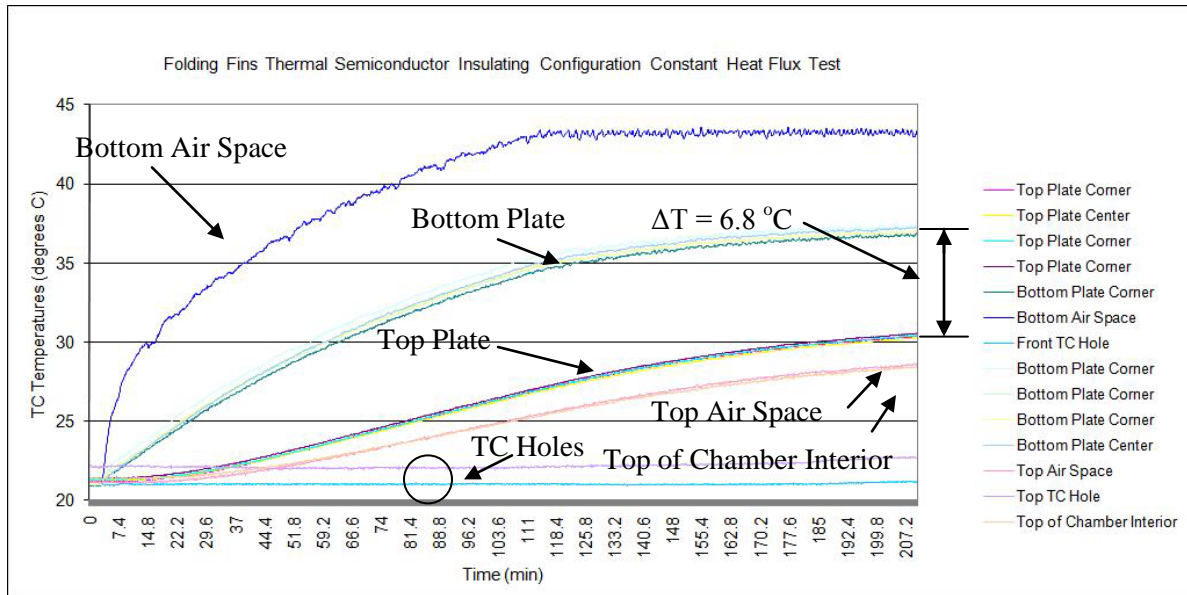


Figure 112: Folding Fins Thermal Semiconductor Insulating Configuration, Constant Heat Flux Test.

Table 8: Folding Fins Thermal Semiconductor Experimental Results.

Insulating Configuration				
Constant Temperature Test (Standard Deviations of All Measurements < 0.14 °C)			Constant Heat Flux Test (Standard Deviations of All Measurements < 0.36 °C)	
1.5 hours into the test			1.75 hours into the test	
Measurement	T (°C)	% of Benchmark	Measurement	T (°C)
Bottom Piece Average	32.4		Bottom Piece Average	34.2
Top Piece Average	26.6		Top Piece Average	26.4
ΔT	5.9	61.7	ΔT	7.8
3 hours into the test			At the end of the 3.75 hour test	
Measurement	T (°C)	% of Benchmark	Measurement	T (°C)
Bottom Piece Average	33.5		Bottom Plate Average	37.2
Top Piece Average	28.5		Top Plate Average	30.4
ΔT	5.0	54.8	Bottom Air Space	43.2
At the end of the 6 hour test			Top Air Space	30.2
Measurement	T (°C)	% of Benchmark	ΔT	6.8
Bottom Plate Average	33.9			
Top Plate Average	29.5			
Bottom Air Space	37.8			
Top Air Space	28.0			
ΔT	4.4	48.4		

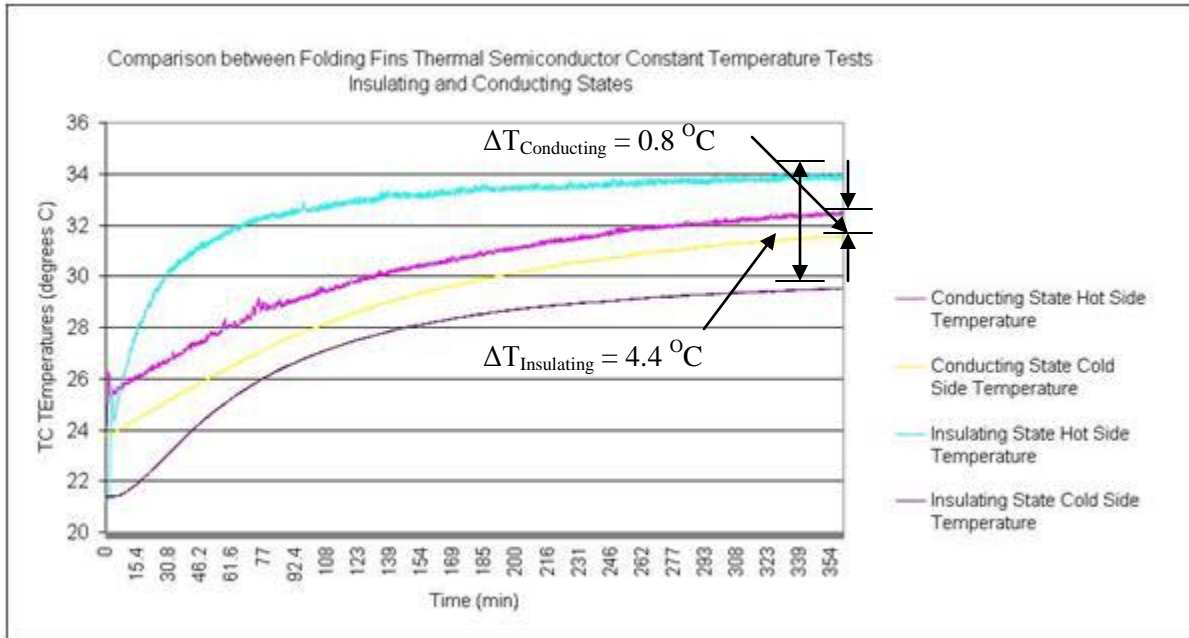


Figure 113: Comparison between the Conducting and Insulating States of the Folding Fins Thermal Semiconductor for the Constant Temperature Tests.

The experimental results of the insulating configuration of the folding fins with vertical contact device measured a ΔT value across the device of $4.4\text{ }^{\circ}\text{C}$ at the end of the constant temperature test, which was 48.5% of the benchmark foam insulation test piece's ΔT value. This shows that the insulator state of the folding fins prototype functioned about half as good an insulator as conventional building insulation and that the device functioned as a slightly better insulator than the back-to-back-plates with fins device, which had a final ΔT value for its constant temperature test that was 45.7% of the benchmark insulation test piece. In addition, the insulating configuration of the folding fins device performed much better than the insulating configuration of the original basic shifting fins thermal semiconductor, which had a final ΔT value for its constant temperature test that was 27.2% of the ΔT value of the benchmark insulation test piece.

In order to evaluate the overall performance of the folding fins with vertical contact device as a thermal semiconductor, the experimental test results obtained from the conducting state of the earlier

basic shifting fins device were used again for the folding fins device's conducting state, which was not actually constructed, since the conducting configurations of the two thermal semiconductor devices were very similar to one another. Although this will not give the exact same results as the actual conducting configuration of the folding fins with vertical contact device, the conducting states of the two devices are similar enough that the experimental results of the basic shifting fins prototype should at least give a good idea of the possible performance of the folding fins thermal semiconductor. For the constant temperature tests the folding fins device was able to vary between ΔT values at the end of the test of $4.4\text{ }^{\circ}\text{C}$ for the device's insulating state to $0.8\text{ }^{\circ}\text{C}$ for the device's conducting state. This means that the ΔT value at the end of the constant temperature tests for the folding fins with vertical contact device was able to vary from 9.4% of the benchmark insulation test piece in its conducting state to 48.5% of the benchmark insulation test piece in its insulating state. Consequently, the folding fins with vertical contact device was able to have much larger variations in thermal conductivity when actuated between conducting and insulating states than the basic shifting fins thermal semiconductor, which itself only varied between 9.4 - 27.2% of the benchmark foam insulation test piece when actuated between its conducting and insulating states. When comparing the performance of the back-to-back plates with fins thermal semiconductor and the folding fins with vertical contact thermal semiconductor, both devices had about the same range of thermal conductivity between their low and high heat transfer states with the back-to-back plates with outward facing fins device functioning as a slightly better conductor when needed and the folding fins device functioning as a slightly better insulator when needed.

4.2 EMPTY CHAMBER CONSTANT TEMPERATURE TEST

As the different shifting fins thermal semiconductors were tested to evaluate their performance, most of the temperatures measured were taking very long to reach steady-state values during the constant temperature tests and did not ever reach steady-state values during the test. In order to better understand the transient effects of the insulation test chamber experimental set-up, one additional test was run with

the test chamber empty without any smart insulation devices to determine the amount of time it took for the entire test chamber to reach a uniform temperature of 100 °F (37.78 °C). In a similar manner to the previous experiments conducted, a thermocouple mounted in the same location as the bottom air space thermocouple, 0.75 in. (1.91 cm) above the heat source, was controlled to be a constant temperature of 100 °F (37.78 °C) during the test. In addition, the same voltage and current levels were applied to the heater for the empty chamber test as for the smart insulation prototype constant temperature tests to maintain consistency between the results. Finally, the same test length of six hours was utilized for the empty chamber constant temperature test. Two additional thermocouples were again also utilized to monitor the temperatures of the front and top thermocouple holes to monitor any heat leaking out of the test chamber to the ambient laboratory environment. The rest of the sixteen thermocouples were mounted at various locations throughout the test chamber interior in order to accurately determine the time required for the entire empty chamber to reach steady-state temperature values. A plot of the results of the empty chamber test was produced and is shown in Figure 114.

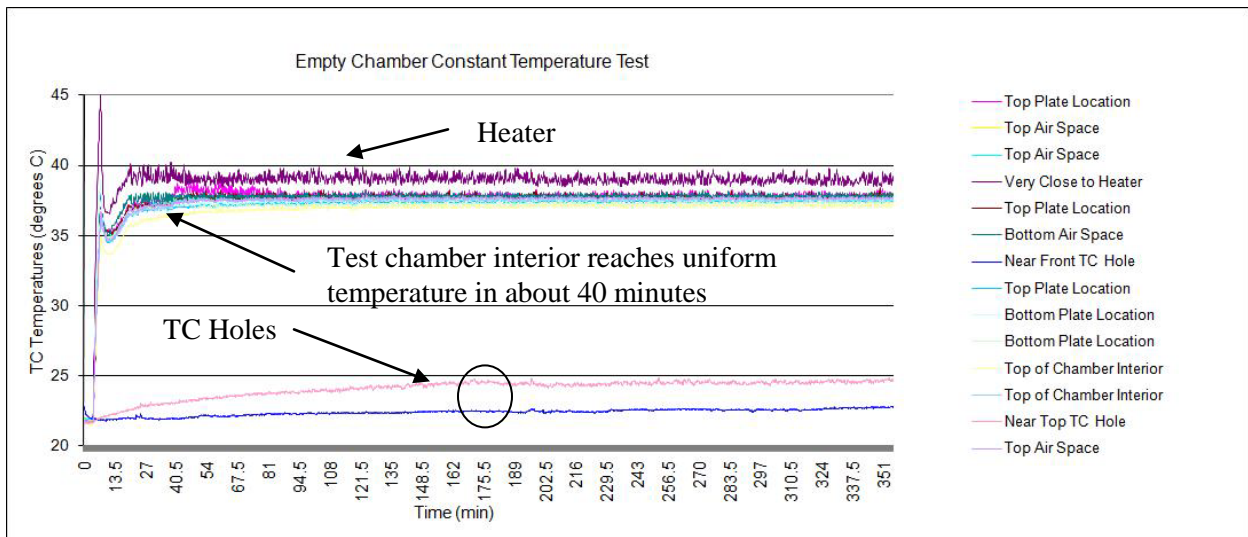


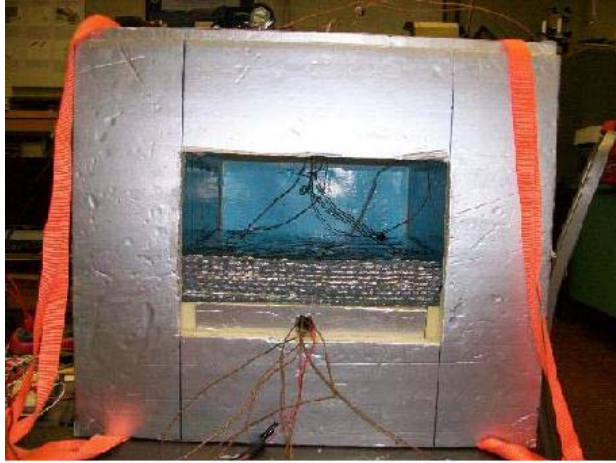
Figure 114: Empty Insulation Test Chamber Constant Temperature Test.

From the results of Figure 114 the interior of the empty insulation test chamber reaches a steady-state, uniform temperature of 100 °F (37.78 °C) very quickly, in about forty minutes, with all of the thermocouples mounted at various locations in the test chamber having a temperature of approximately 100 °F (37.78 °C) after that time. The only thermocouple to not have a value of 100 °F (37.78 °C) was a thermocouple placed very close to the heater surface in order to monitor to heater's temperature. Its temperature was roughly 1 °C warmer than the uniform 100 °F (37.78 °C) temperature of the rest of the test chamber because it was much closer to the heat source than the bottom air space thermocouple, which was controlled to be 100 °F (37.78 °C). The heater thermocouple also reaches a steady-state value of 102 °F (38.89 °C) about forty minutes into the test. The results of the empty test chamber constant temperature test show that steady-state conditions can be reached very quickly when the test chamber is filled with only air compared to the smart insulation tests where steady-state temperature measurements are not obtained even after a testing duration of six hours.

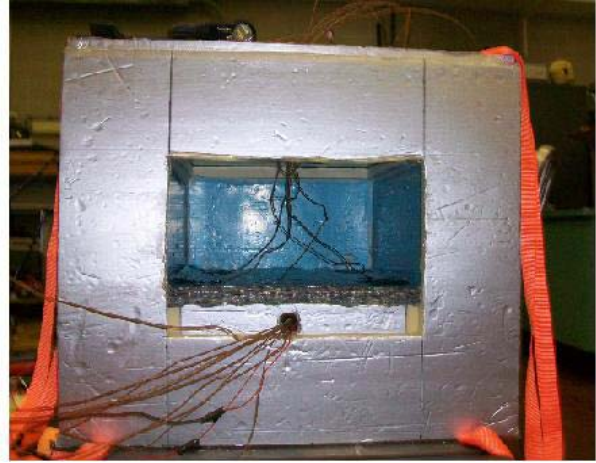
4.3 INFLATABLE THERMAL SEMICONDUCTOR EXPERIMENTAL RESULTS

4.3.1 Reflectix Inflatable Thermal Semiconductor Testing Results

The first inflatable device that was tested was the Reflectix inflatable thermal semiconductor prototype. During the testing of the Reflectix device, the same general thermocouple placement was used on the hot and cold sides of the device with four thermocouples mounted in the corners of the device and one thermocouple placed at the center of the device on each side. The exact placement of the four corner thermocouples was 1.5 in. (3.81 cm) from the outer edges of the device in either direction. Figure 115 gives an image of the Reflectix inflatable thermal semiconductor inserted in the insulation test chamber in both its conducting and insulating arrangements.



Insulating Configuration



Conducting Configuration

Figure 115: Reflectix Inflation Smart Insulation Prototype in Chamber.

Plots of the thermocouple measurement data for the Reflectix device's constant temperature tests are shown in Figures 116 and 117 for the device's conducting and insulating states respectively, while two corresponding plots are given in Figures 118 and 119 for the constant heat flux tests of the Reflectix device. In addition to the plots, the average hot and cold side temperatures, the calculated ΔT values across the device, and the device's ΔT values computed as a percentage of the benchmark foam insulation test piece's ΔT value at several different points during the tests are given in Table 8. Finally, a direct comparison between the insulating and conducting configurations' average hot side temperature, average cold side temperature, and ΔT for the constant temperature tests for the Reflectix inflatable prototype is illustrated in the plot of Figure 120. A similar comparison between the prototype's insulating and conducting states for the constant heat flux tests is also given in Figure 121.

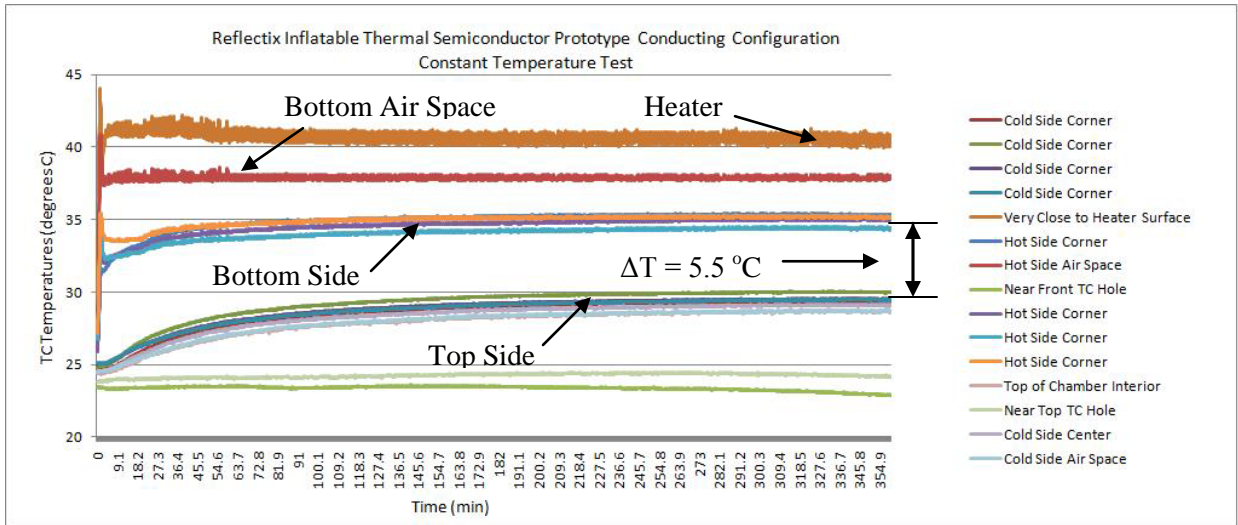


Figure 116: Reflectix Inflatable Thermal Semiconductor Prototype Conducting State, Constant Temperature Test.

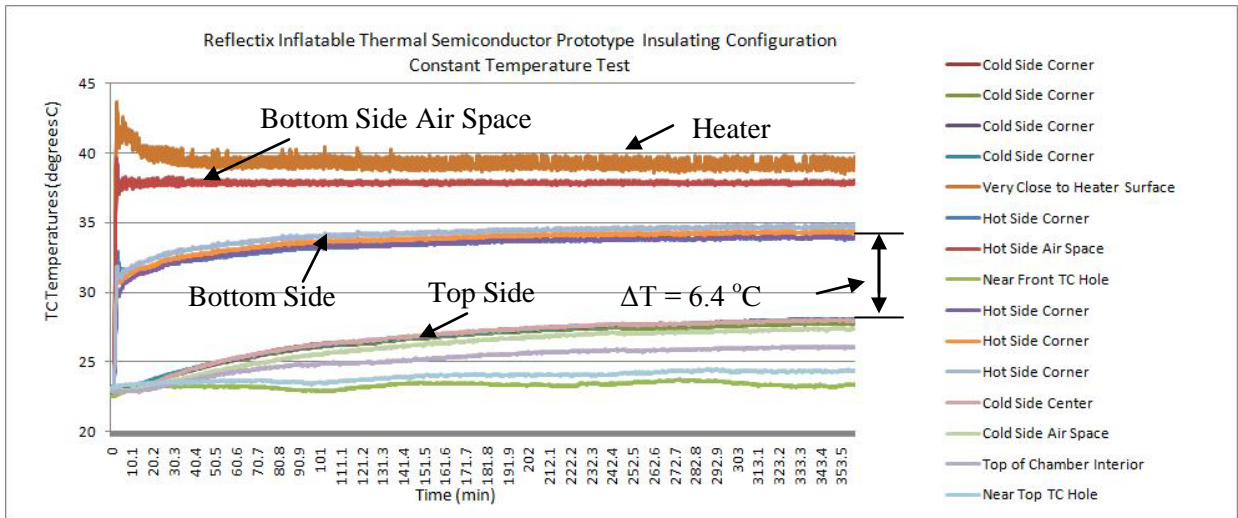


Figure 117: Reflectix Inflatable Thermal Semiconductor Prototype Insulating State, Constant Temperature Test.

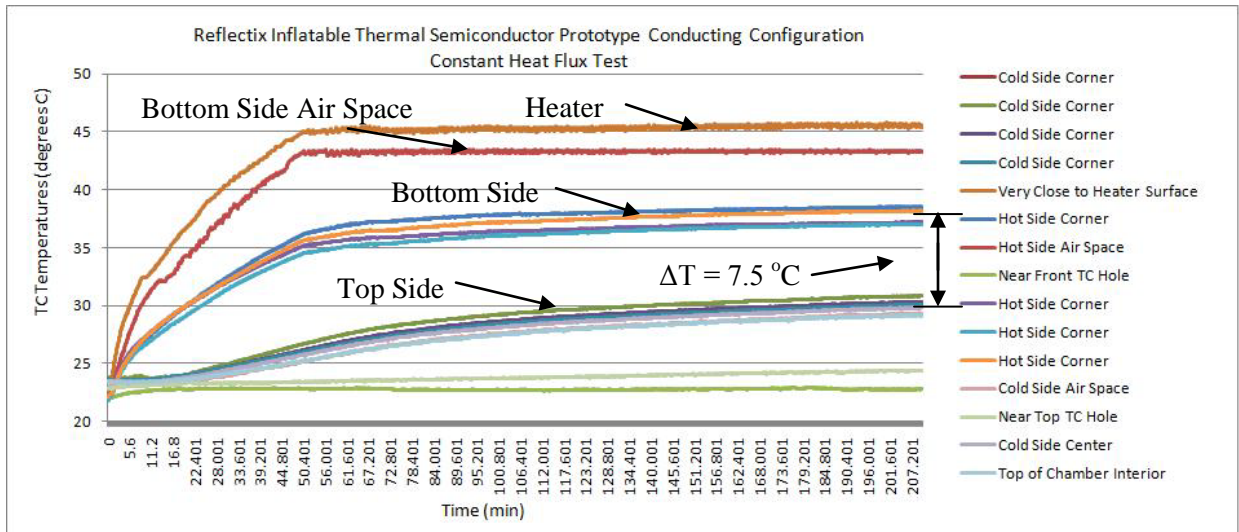


Figure 118: Reflectix Inflatable Thermal Semiconductor Prototype Conducting State, Constant Heat Flux Test.

Table 9: Reflectix Inflatable Thermal Semiconductor Experimental Results.

Constant Temperature Tests (Standard Deviations of All Measurements < 0.50 °C)					
Conducting Configuration			Insulating Configuration		
1.5 hours into the test			1.5 hours into the test		
Measurement	T (°C)	% of Benchmark	Measurement	T (°C)	% of Benchmark
Bottom Side Average	34.5		Bottom Side Average	33.6	
Top Side Average	28.4		Top Side Average	26.0	
ΔT	6.1	63.4	ΔT	7.6	79.8
3 hours into the test			3 hours into the test		
Measurement	T (°C)	% of Benchmark	Measurement	T (°C)	% of Benchmark
Bottom Side Average	34.8		Bottom Side Average	33.9	
Top Side Average	29.1		Top Side Average	27.1	
ΔT	5.6	61.9	ΔT	6.8	74.7
At the end of the 6 hour test			At the end of the 6 hour test		
Measurement	T (°C)	% of Benchmark	Measurement	T (°C)	% of Benchmark
Bottom Side Average	35.0		Bottom Side Average	34.3	
Top Side Average	29.5		Top Side Average	27.9	
Bottom Side Air Space	37.8		Bottom Side Air Space	37.8	
Top Side Air Space	28.7		Top Side Air Space	27.4	
ΔT	5.5	62.1	ΔT	6.4	72.0
Constant Heat Flux Tests (Standard Deviations of All Measurements < 0.80 °C)					
Conducting Configuration			Insulating Configuration		
1.75 hours into the test			1.75 hours into the test		
Measurement	T (°C)		Measurement	T (°C)	
Bottom Side Average	36.9		Bottom Side Average	37.1	
Top Side Average	28.7		Top Side Average	26.8	
ΔT	8.2		ΔT	10.3	
At the end of the 3.5 hour test			At the end of the 3.5 hour test		
Measurement	T (°C)		Measurement	T (°C)	
Bottom Side Average	37.7		Bottom Side Average	37.9	
Top Side Average	30.2		Top Side Average	28.7	
Bottom Side Air Space	43.3		Bottom Side Air Space	43.4	
Top Side Air Space	29.3		Top Side Air Space	28.0	
ΔT	7.5		ΔT	9.2	

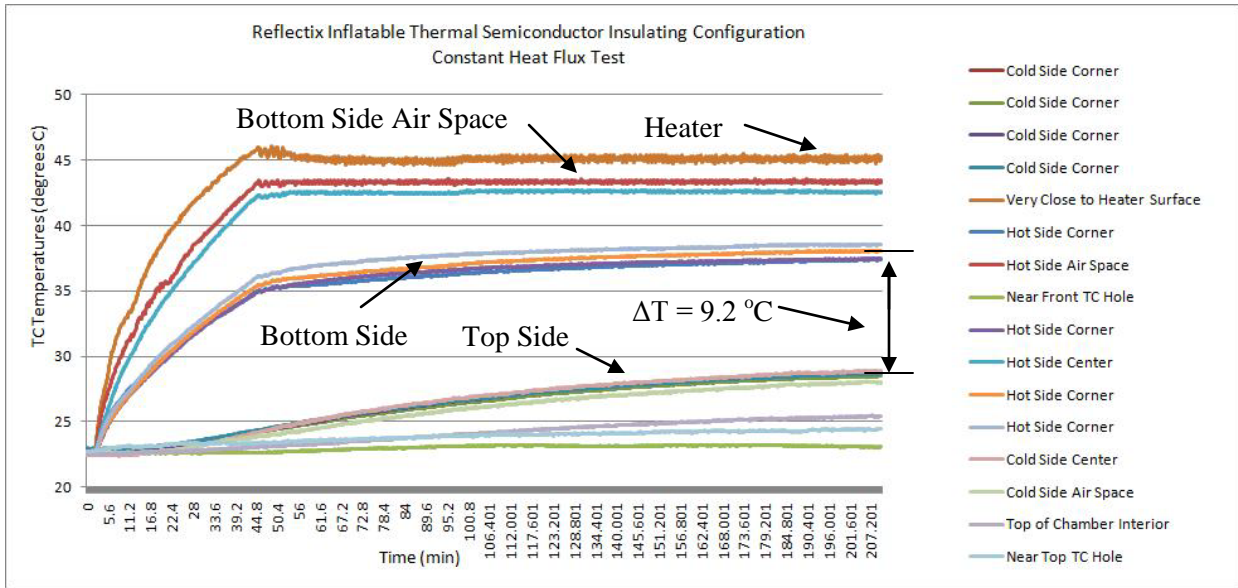


Figure 119: Reflectix Inflatable Thermal Semiconductor Prototype Insulating State, Constant Heat Flux Test.

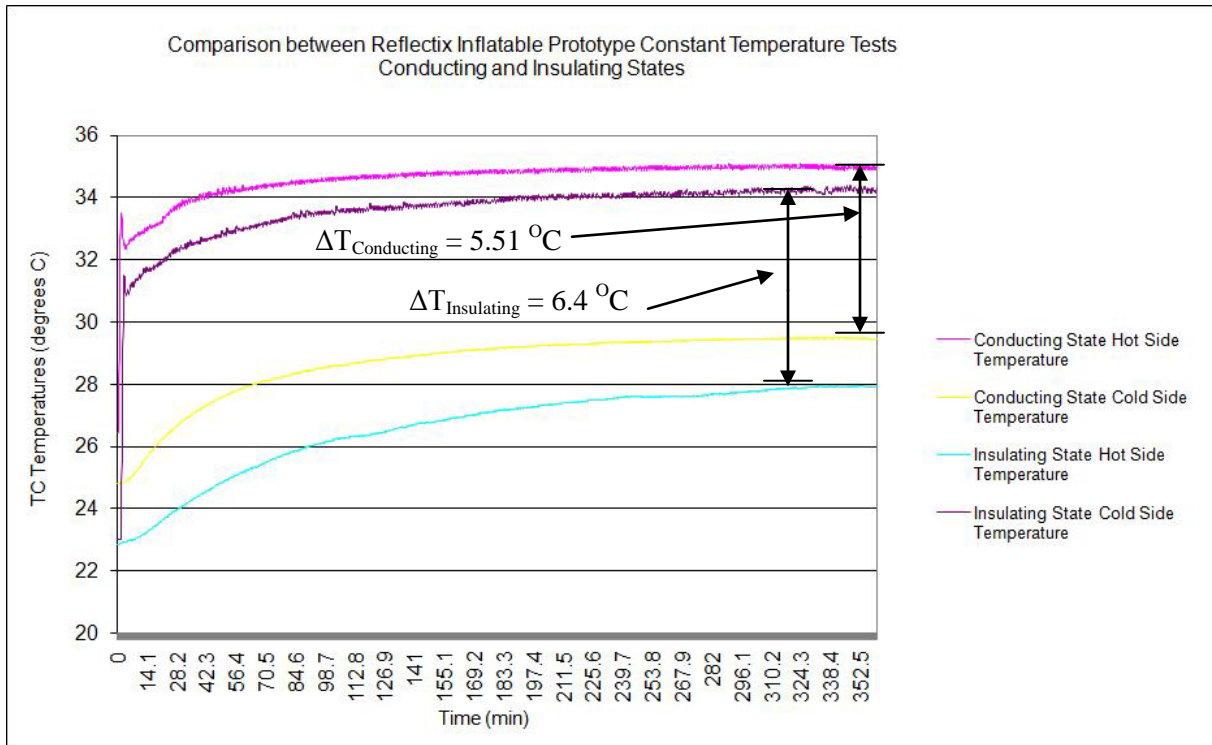


Figure 120: Comparison between Reflectix Inflatable Prototype Conducting and Insulating States for Constant Temperature Tests.

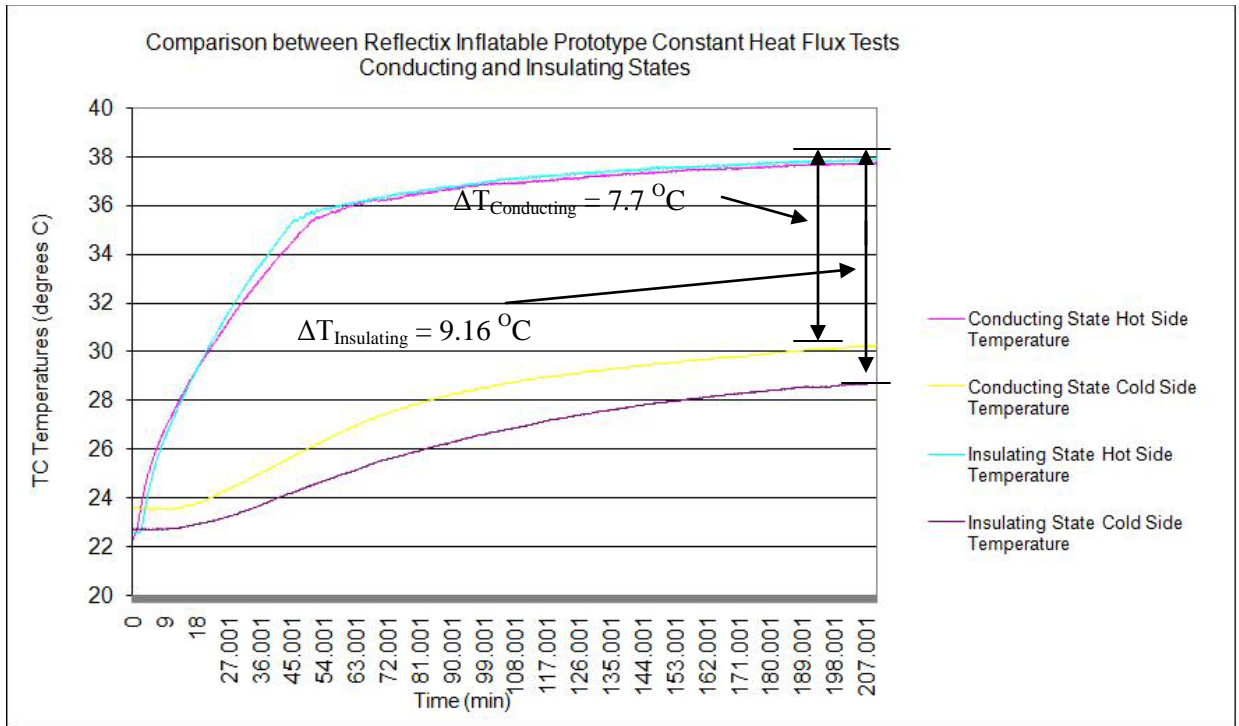


Figure 121: Comparison between Reflectix Inflatable Prototype Conducting and Insulating States for Constant Heat Flux Tests.

From the experimental results of both the constant temperature and constant heat flux tests, the Reflectix inflatable thermal semiconductor prototype performed poorly as a smart insulation device with little variation in ΔT when the device changed between insulating and conducting states, and thus little variation was observed in the device's thermal conductivity. For example in the constant temperature tests, the measured ΔT only changed from $5.5\text{ }^{\circ}\text{C}$ in the conducting state to $6.4\text{ }^{\circ}\text{C}$ in the insulating state, which is a change in ΔT of less than $1\text{ }^{\circ}\text{C}$. When examining the prototype's performance with respect to the benchmark insulation test piece, the ΔT value at the end of the constant temperature tests is able to only change from 62.1% of the benchmark foam insulation test piece's ΔT value when the device is in its conducting state to 72.0% after inflating the device into its insulating state. Consequently, the device never functions as a very good insulator or a very good conductor but instead always functions somewhere between the two desired heat transfer states. The major reason behind the poor performance

of the Reflectix smart insulation device was the still significant thickness of the inflatable device after it had been deflated into its conducting state. Ideally, the Reflectix device would be extremely thin in its deflated, conducting state compared to its inflated, insulating state, but the first Reflectix prototype had a deflated thickness that was still about half of the thickness of the device during its inflated state. To eliminate this problem for future Reflectix prototypes and testing, a vacuum pump could be added to the Reflectix inflatable thermal semiconductor to much more effectively deflate the small air chambers of the Reflectix device.

During the constant heat flux tests for the Reflectix prototype, the hot side air space did quickly reach the maximum allowable temperature of 110 °F (43.33 °C) very early during the test with the maximum temperature being reached in about 50 minutes when the device was in its conducting state and about 45 minutes when the device was in its insulating state. After that temperature was reached, for the duration of the test the hot side air space was maintained at a constant temperature of 110 °F (43.33 °C). The main reason the maximum hot side air space temperature was reached during the 3.5 hour constant heat flux test for the Reflectix device and but not for any of the shifting fins prototypes is the much smaller thermal mass of the Reflectix inflatable prototype compared to the shifting fins devices. In order to determine how quickly a thermal system will increase in temperature due to convective heat transfer, the important parameter to calculate is the thermal time constant, τ , which is dependent on four properties of the system: the device's density, the device's specific heat capacity, the convection coefficient of the system, and the device's surface area. Equation 4.2 gives the expression used for calculating the thermal time constant [26].

$$\tau = \frac{c_p \rho V}{h A_s} \quad (4.2)$$

From Equation 4.2 the only variables that change when the inflatable thermal semiconductors are heated in the test chamber instead of the shifting fins thermal semiconductors are the specific heat capacity and density of the material of the smart insulation prototype. The convection coefficient, volume,

and surface area in the insulation test chamber set-up did not change for the different prototypes because all of the prototypes were designed with the same dimensions and heating set-up in the insulation test chamber. In the design of the shifting fins thermal semiconductors, the prototypes were constructed out of 6061 aluminum alloy, which has a specific heat capacity of 896 J/kg-K and a density of 2713 kg/m³ [30]. Conversely, in the design of the inflatable thermal semiconductors, the vast majority of the material of the prototypes was simply the air within the chambers of the honeycomb structure, so it can be assumed that the overall specific heat capacity and density of the inflatable semiconductors were approximately that of air, which has a specific heat capacity of 1005 J/kg-K and a density of 1.166 kg/m³ [31]. Since the density of the shifting fins devices was significantly higher than the density of the inflatable smart insulation devices, a much longer time constant resulted from Equation 4.2 for the convective heating of the shifting fins devices compared to the inflatable prototypes. The much shorter time constant during the constant heat flux tests for the inflatable devices caused the devices to be heated to their maximum possible temperatures in a much lower time period than the shifting fins prototypes for the same level of heat flux applied to both types of thermal semiconductors.

4.3.2 NOVUS Inflatable Thermal Semiconductor Testing Results

The second inflatable smart insulation device that was tested in the insulation test chamber was the NOVUS Bubble-Wrap-like packaging inflatable thermal semiconductor. To maintain consistency with the other inflatable smart insulation devices, the same thermocouple placement on the hot and cold sides of the devices used to calculate the ΔT values for the Reflectix inflatable prototype was also used for the NOVUS inflatable thermal semiconductor. Two photos that show the NOVUS inflatable prototype in its insulating and conducting states inserted into the insulation test chamber are given in Figure 122.



Insulating Configuration

Conducting Configuration

Figure 122: NOVUS Inflation Smart Insulation Prototype in Chamber.

Plots of the NOVUS device's constant temperature tests are given in Figures 123 and 124 for the conducting and insulating states, while two additional plots are given in Figures 125 and 126 for the device's constant heat flux tests. In addition to the plots, the average hot and cold side temperatures, the calculated ΔT values across the device, and the device's ΔT values expressed as a percentage of the benchmark insulation test piece's ΔT value at several points during the tests are given in Table 10. Finally, a direct comparison between the insulating and conducting states of the NOVUS prototype is provided in Figure 127 for the device's constant temperature test.

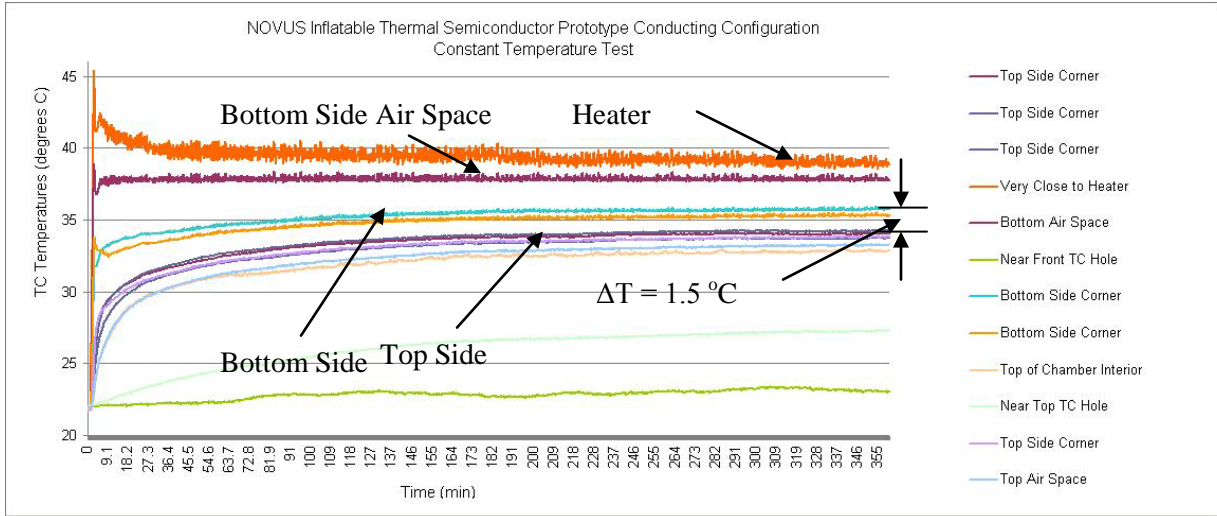


Figure 123: NOVUS Inflatable Thermal Semiconductor Prototype Conducting State, Constant Temperature Test.

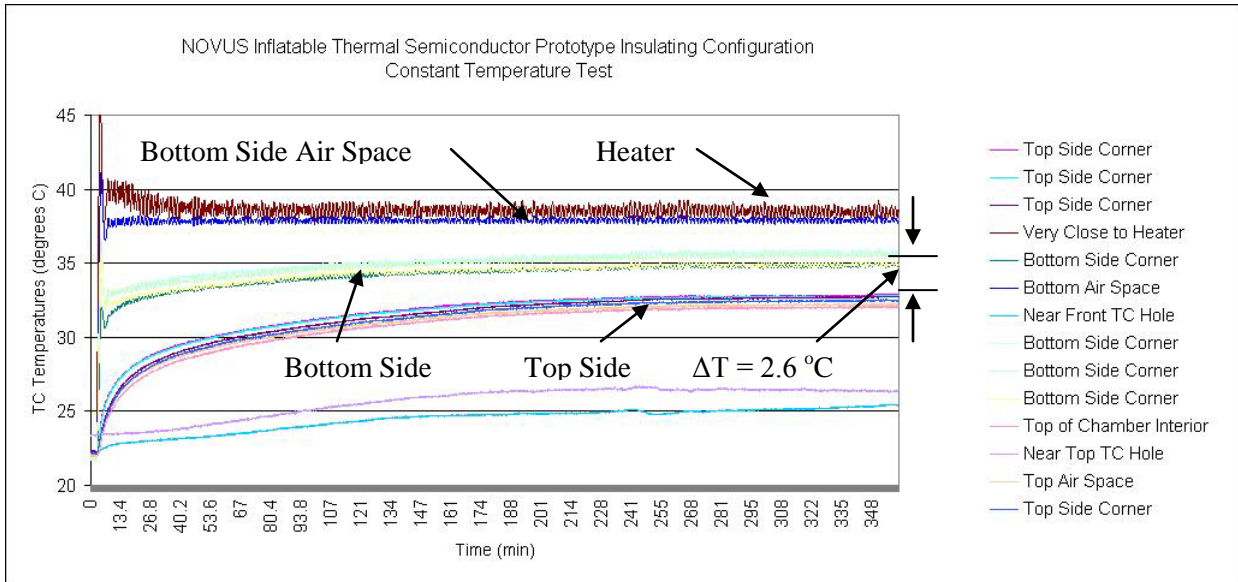


Figure 124: NOVUS Inflatable Thermal Semiconductor Prototype Insulating State, Constant Temperature Test.

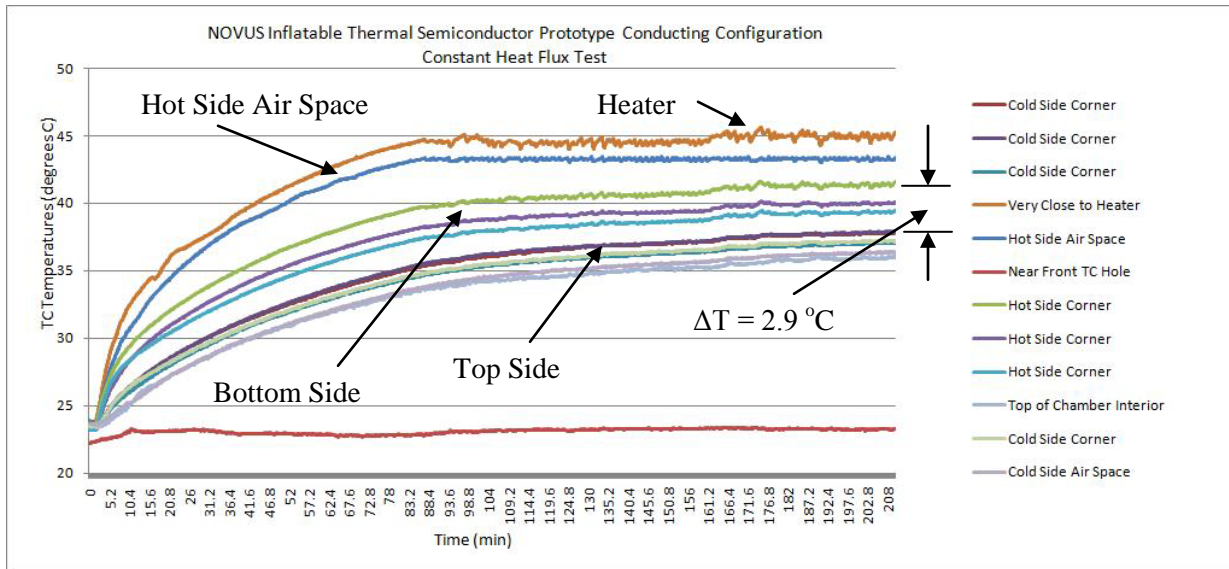


Figure 125: NOVUS Inflatable Thermal Semiconductor Prototype Conducting State, Constant Heat Flux Test.

Table 10: NOVUS Inflatable Thermal Semiconductor Experimental Results.

Constant Temperature Tests (Standard Deviations of All Measurements < 0.45 °C)					
Conducting Configuration			Insulating Configuration		
1.5 hours into the test			1.5 hours into the test		
Measurement	T (°C)	% of Benchmark	Measurement	T (°C)	% of Benchmark
Bottom Side Average	34.7		Bottom Side Average	34.3	
Top Side Average	32.8		Top Side Average	30.7	
ΔT	1.9	19.8	ΔT	3.6	37.6
3 hours into the test			3 hours into the test		
Measurement	T (°C)	% of Benchmark	Measurement	T (°C)	% of Benchmark
Bottom Side Average	35.3		Bottom Side Average	34.9	
Top Side Average	33.6		Top Side Average	32.1	
ΔT	1.7	18.4	ΔT	2.8	30.8
At the end of the 6 hour test			At the end of the 6 hour test		
Measurement	T (°C)	% of Benchmark	Measurement	T (°C)	% of Benchmark
Bottom Side Average	35.5		Bottom Side Average	35.3	
Top Side Average	34.0		Top Side Average	32.7	
Bottom Side Air Space	37.8		Bottom Side Air Space	37.8	
Top Side Air Space	33.3		Top Side Air Space	32.2	
ΔT	1.5	17.2	ΔT	2.6	28.8
Constant Heat Flux Tests (Standard Deviations of All Measurements < 1.16 °C)					
Conducting Configuration			Insulating Configuration		
1.75 hours into the test			1.75 hours into the test		
Measurement	T (°C)		Measurement	T (°C)	
Bottom Side Average	39.0		Bottom Side Average	37.8	
Top Side Average	35.8		Top Side Average	32.5	
ΔT	3.2		ΔT	5.3	
At the end of the 3.5 hour test			At the end of the 3.5 hour test		
Measurement	T (°C)		Measurement	T (°C)	
Bottom Side Average	40.4		Bottom Side Average	38.7	
Top Side Average	37.5		Top Side Average	34.3	
Bottom Side Air Space	43.4		Bottom Side Air Space	43.3	
Top Side Air Space	36.4		Top Side Air Space	33.8	
ΔT	2.9		ΔT	4.4	

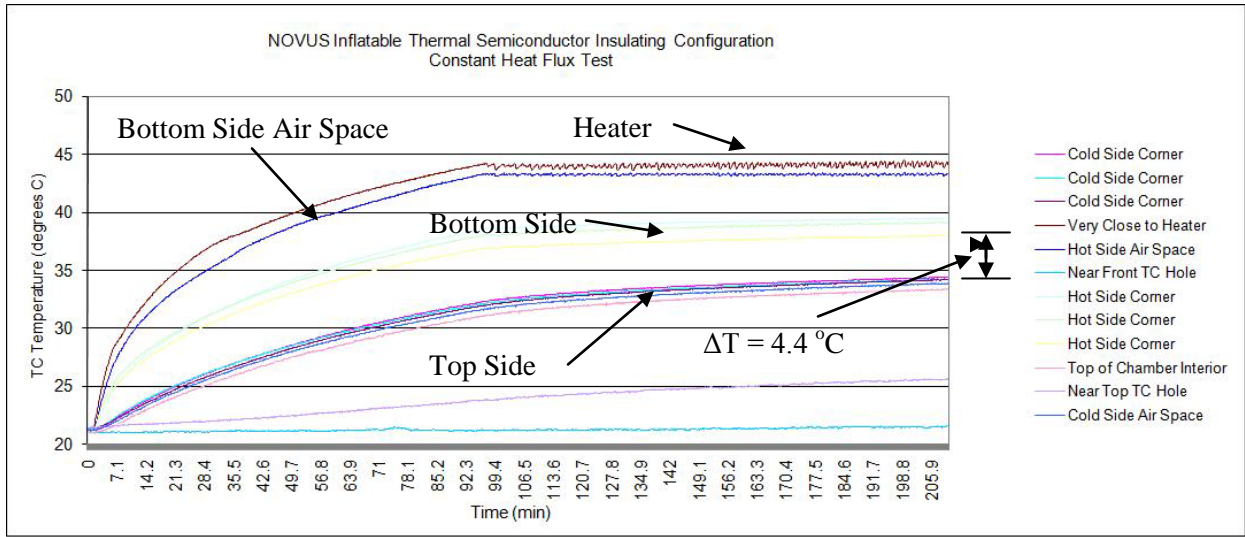


Figure 126: NOVUS Inflatable Thermal Semiconductor Prototype Insulating State, Constant Heat Flux Test.

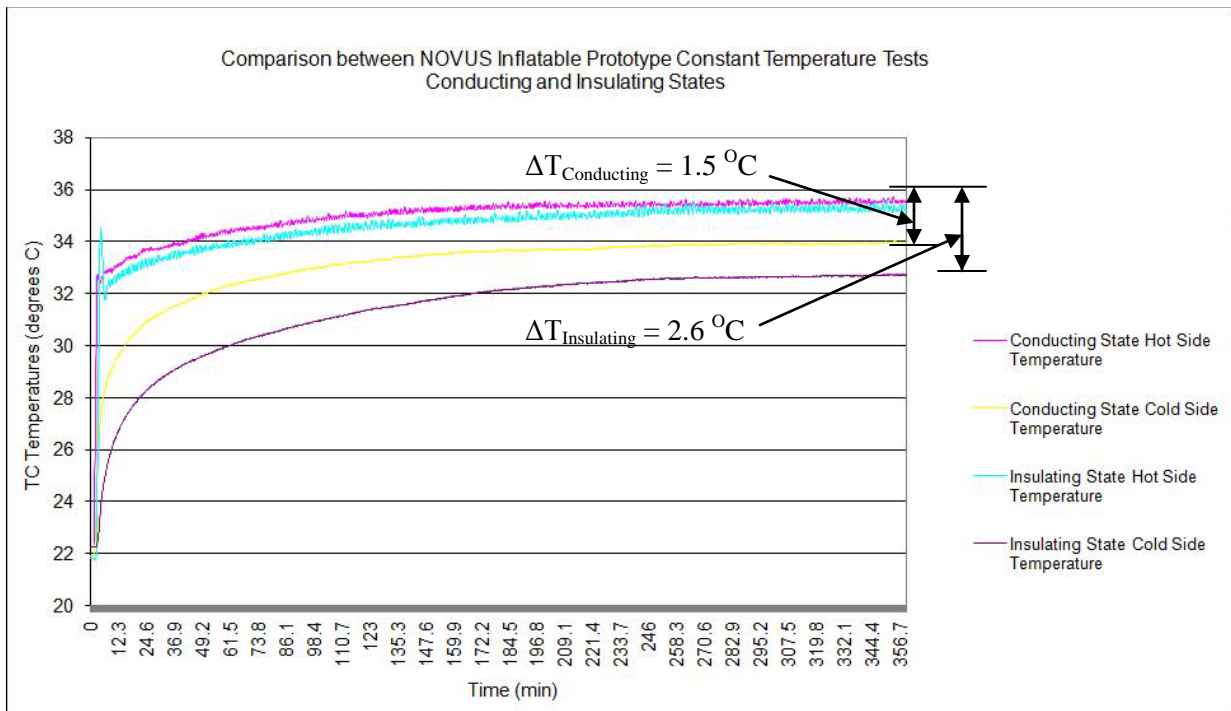


Figure 127: Comparison between NOVUS Inflatable Prototype Conducting and Insulating States for Constant Temperature Tests.

The performance of the device as smart insulation was slightly better than that of the Reflectix inflatable prototype, since it had a slightly larger range of ΔT values between its insulating and conducting configurations. At the end of its constant temperature tests, for example, the ΔT value measured across the NOVUS device was able to vary between a value of 1.5 °C for its conducting state to a value of 2.6 °C for its insulating state, which is a change in ΔT of slightly more than 1 °C compared to the change in ΔT of about 0.9 °C for the Reflectix prototype testing. Although the NOVUS and Reflectix inflatable prototypes had about the same level of overall performance, the NOVUS device functioned much better in its conducting state, while the Reflectix device functioned much better in its insulating state. When examining the NOVUS thermal semiconductor's ΔT value at the end of its constant temperature test as a percentage of the benchmark insulation test piece's ΔT value, the NOVUS device had less than 1/5 of the insulating capability of standard building insulation for its conducting state, which shows that the NOVUS device can serve as a good conductor when needed. For its insulating state, however, the NOVUS device performs very poorly with a measured ΔT value that was only 28.8% of the benchmark insulation test piece's ΔT value.

To improve the performance of the NOVUS inflatable thermal semiconductor in its insulating state, a new type of honeycomb-like material could be fabricated with much smaller chambers of air than the NOVUS packaging material, which has fairly large Bubble-Wrap-like air spaces. By using smaller chambers of air in the device's inflated state, natural convection of the air will significantly decrease, which will greatly improve the insulating state of the device. In addition, the performance of the device in its conducting state will not be affected because the device is essentially the same in its deflated configuration regardless of the size of the chambers of air in the device.

Similarly to the Reflectix inflatable prototype constant heat flux tests, the NOVUS inflatable thermal semiconductor also reached its maximum allowable temperature very quickly due to its small thermal mass and thermal time constant. The NOVUS device's conducting configuration reached the maximum

allowable hot side air space temperature in approximately 87 minutes, while the device's insulating configuration reached the maximum temperature of 110 °F (43.33 °C) in approximately 95 minutes.

4.3.3 NOVUS Inflatable Thermal Semiconductor with Aluminum Plates Testing Results

In order to further improve the conduction state of the NOVUS inflatable smart insulation device, two aluminum plates were added to the original prototype on its hot and cold sides to compress any remaining air out of the deflated NOVUS prototype. By eliminating any leftover air in the smart insulation prototype, the thickness of the deflated device will be reduced, giving a higher thermal conductivity than before through the very thin layers of plastic packaging material. In practice, a vacuum pump would actually be used to much more effectively inflate and deflate the NOVUS inflatable device, but for the purpose of testing the two heat transfer states of the device without an actual actuation mechanism, using the two aluminum plates to better deflate the NOVUS prototype was a very simple, but effective solution.

In Figure 128 an image is provided of the NOVUS inflatable prototype placed in the insulation test chamber in both its conducting and insulating state.



Insulating Configuration



Conducting Configuration

Figure 128: NOVUS Inflatable Prototype with Aluminum Plates in Chamber Experimental Set-up.

In Figures 129 and 130 constant temperature test plots are given for the conducting and insulating states of the NOVUS inflatable device with aluminum plates, while for the device's constant heat flux tests, two additional plots are given in Figures 131 and 132. In addition to the plots, the average hot and cold side temperatures, the calculated ΔT values across the device, and the device's ΔT values expressed as a percentage of the benchmark insulation test piece's ΔT value are given in Table 11. Finally, a direct comparison between the insulating and conducting states of the NOVUS prototype with two aluminum plates is provided in Figure 133 for the device's constant temperature test and Figure 134 for the device's constant heat flux test.

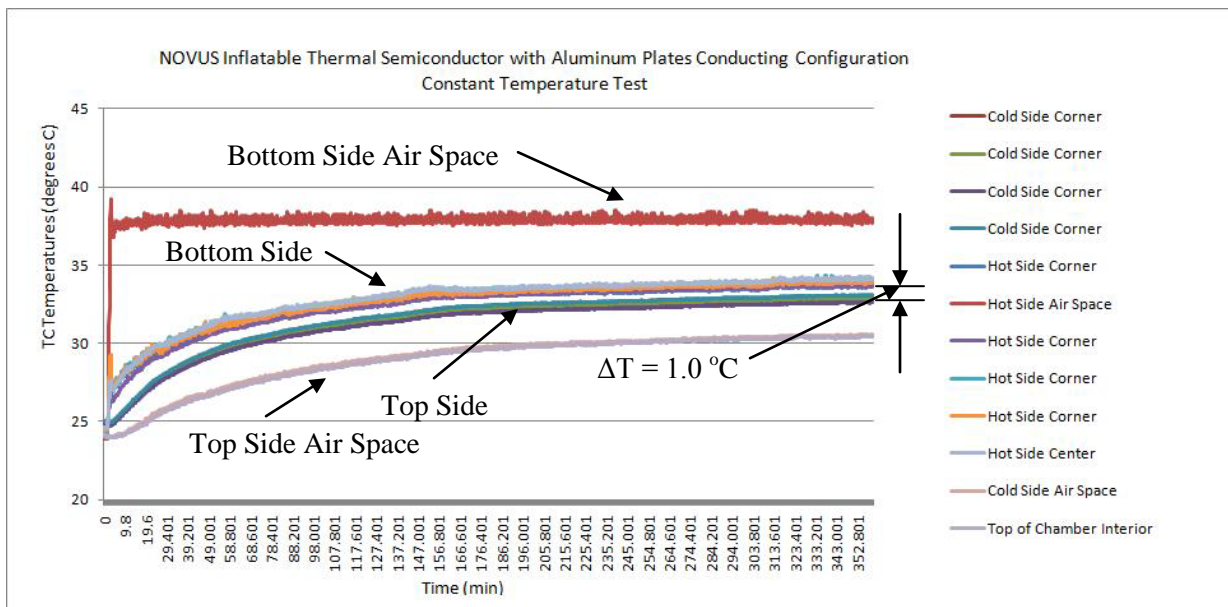


Figure 129: NOVUS Inflatable Thermal Semiconductor with Aluminum Plates Prototype Conducting State, Constant Temperature Test.

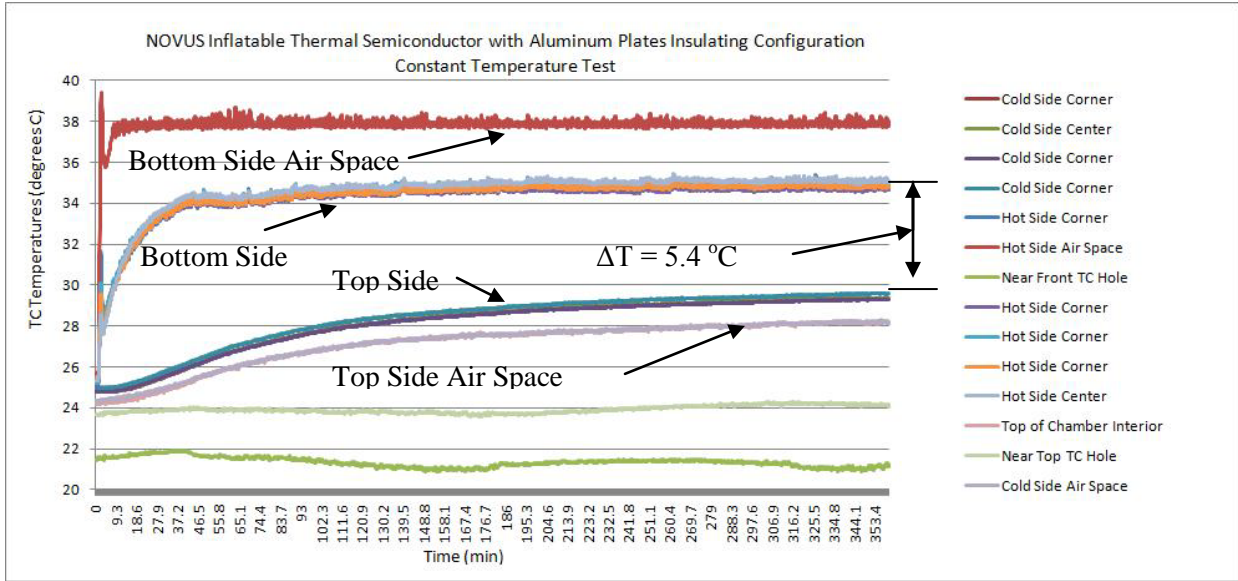


Figure 130: NOVUS Inflatable Thermal Semiconductor with Aluminum Plates Prototype Insulating State, Constant Temperature Test.

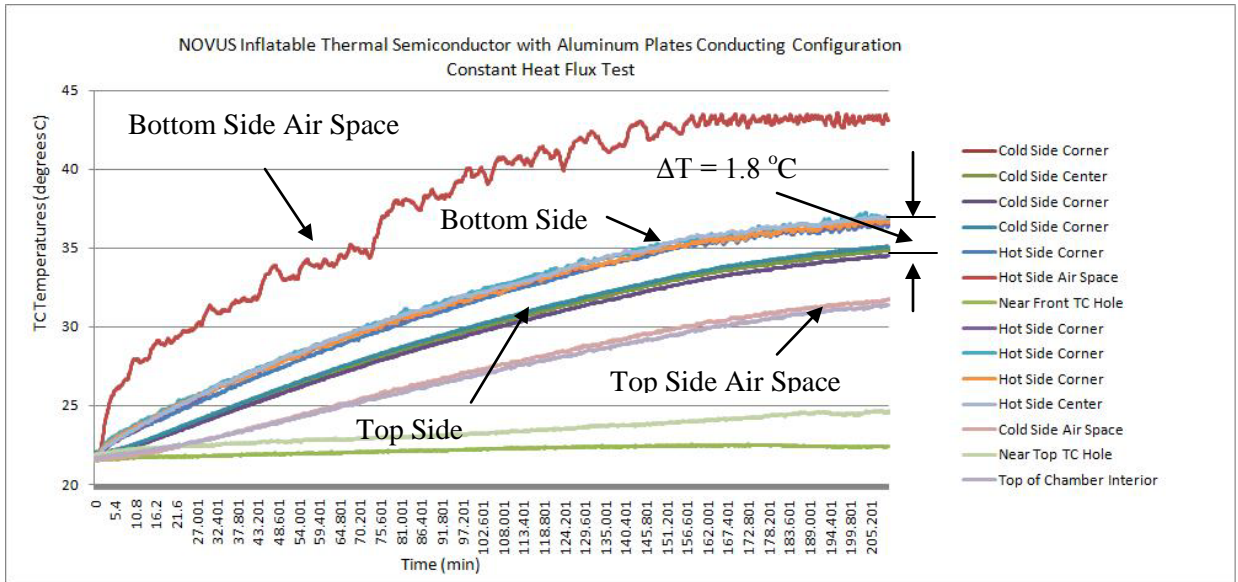


Figure 131: NOVUS Inflatable Thermal Semiconductor with Aluminum Plates Prototype Conducting State, Constant Heat Flux Test.

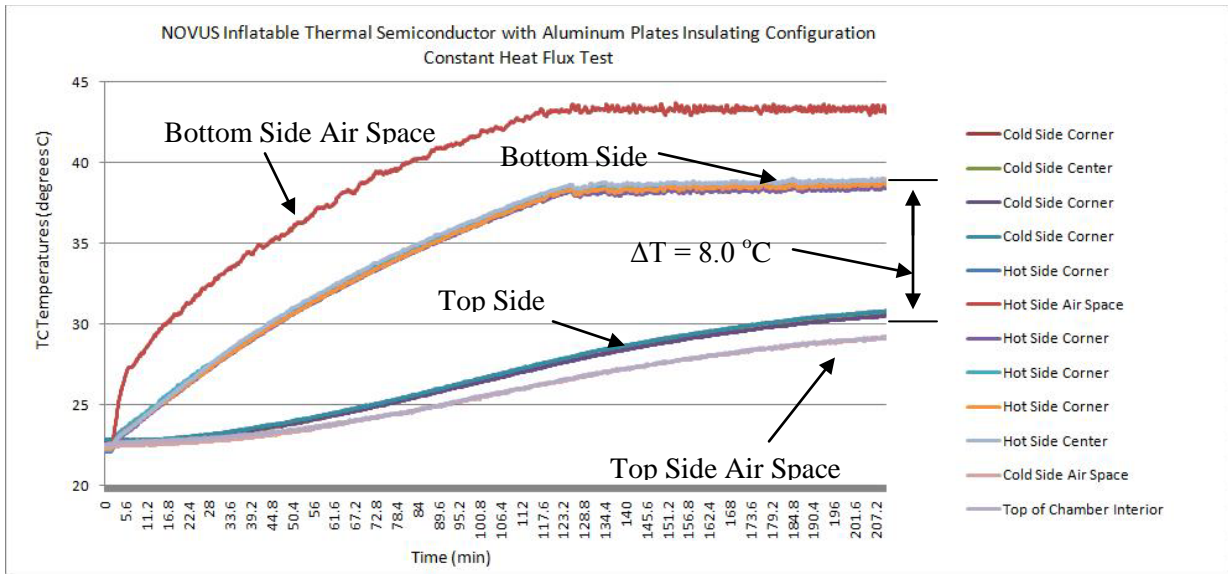


Figure 132: NOVUS Inflatable Thermal Semiconductor with Aluminum Plates Prototype Insulating State, Constant Heat Flux Test.

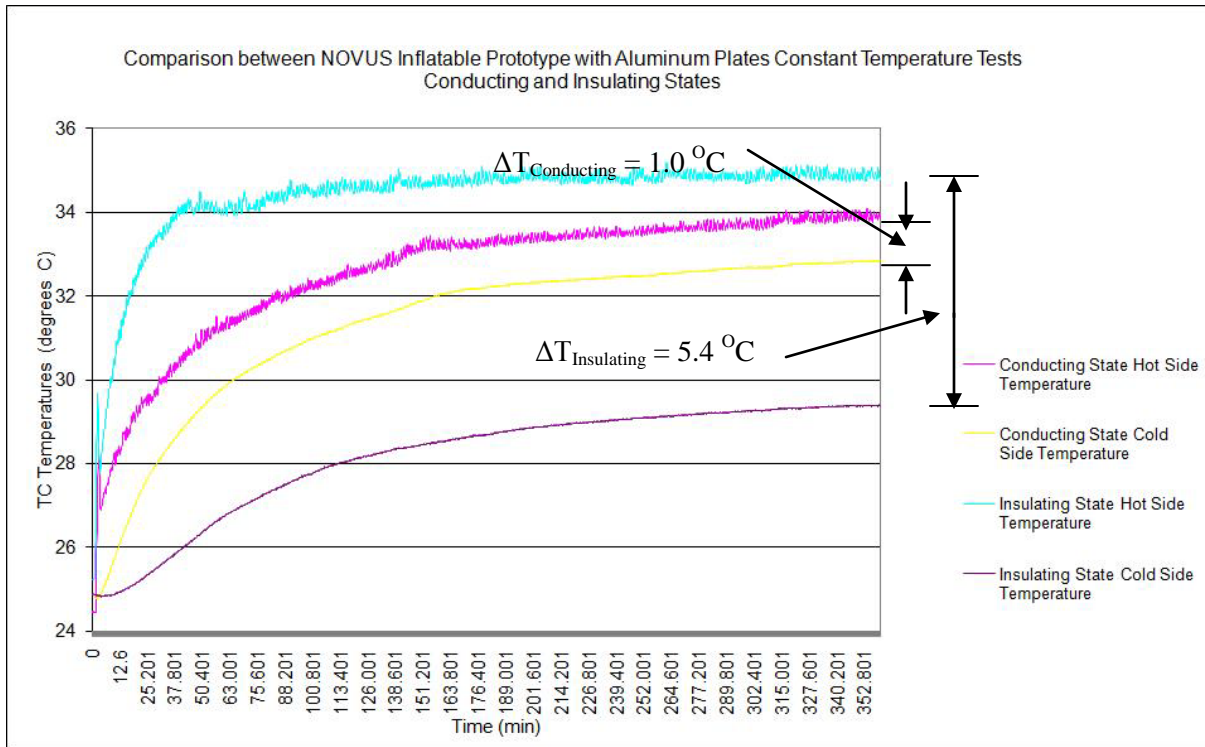


Figure 133: Comparison between NOVUS Inflatable Prototype with Aluminum Plates Conducting and Insulating States for Constant Temperature Tests.

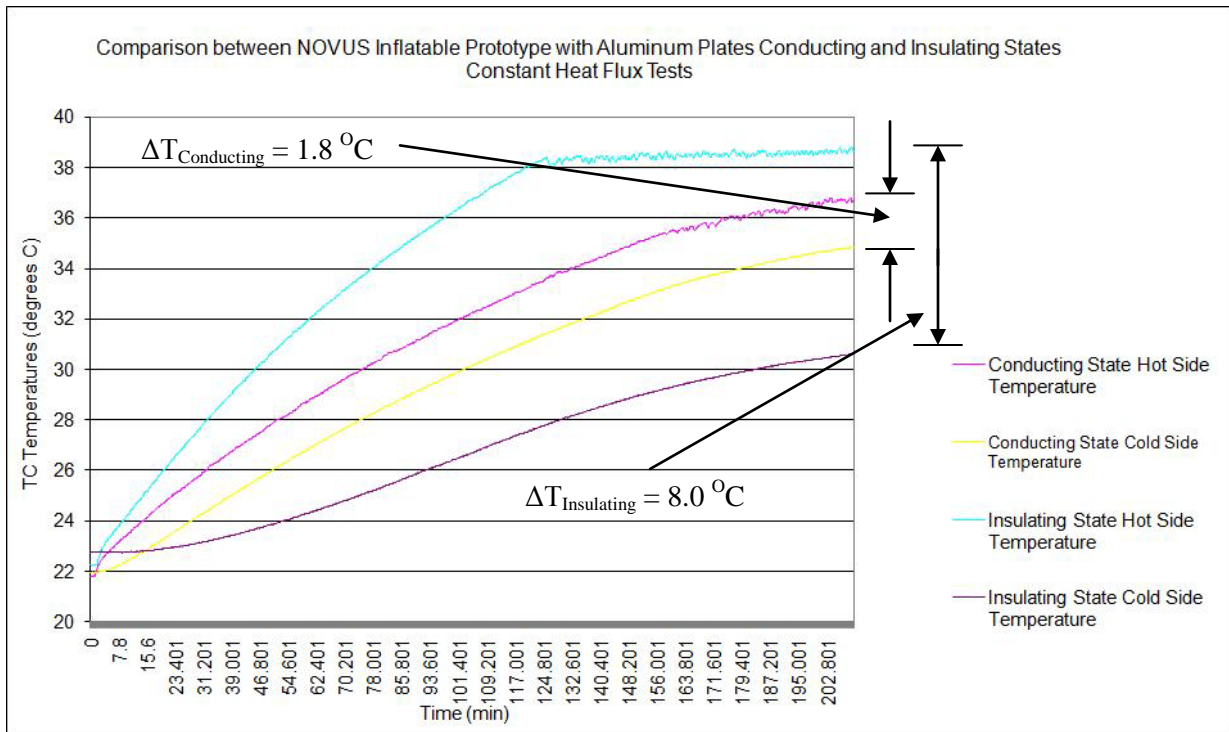


Figure 134: Comparison between NOVUS Inflatable Prototype with Aluminum Plates Conducting and Insulating States for Constant Heat Flux Tests.

Table 11: NOVUS Inflatable Thermal Semiconductor with Aluminum Plates Experimental Results.

Constant Temperature Tests (Standard Deviations of All Measurements < 0.21 °C)					
Conducting Configuration			Insulating Configuration		
1.5 hours into the test			1.5 hours into the test		
Measurement	T (°C)	% of Benchmark	Measurement	T (°C)	% of Benchmark
Bottom Side Average	32.0		Bottom Side Average	34.5	
Top Side Average	30.7		Top Side Average	27.5	
ΔT	1.2	12.8	ΔT	6.9	72.6
3 hours into the test			3 hours into the test		
Measurement	T (°C)	% of Benchmark	Measurement	T (°C)	% of Benchmark
Bottom Side Average	33.4		Bottom Side Average	35.0	
Top Side Average	32.2		Top Side Average	28.7	
ΔT	1.2	12.8	ΔT	6.3	68.8
At the end of the 6 hour test			At the end of the 6 hour test		
Measurement	T (°C)	% of Benchmark	Measurement	T (°C)	% of Benchmark
Bottom Side Average	33.8		Bottom Side Average	34.8	
Top Side Average	32.8		Top Side Average	29.4	
Bottom Side Air Space	37.8		Bottom Side Air Space	37.8	
Top Side Air Space	30.4		Top Side Air Space	28.2	
ΔT	1.0	11.3	ΔT	5.4	60.8
Constant Heat Flux Tests (Standard Deviations of All Measurements < 0.25 °C)					
Conducting Configuration			Insulating Configuration		
1.75 hours into the test			1.75 hours into the test		
Measurement	T (°C)		Measurement	T (°C)	
Bottom Side Average	32.3		Bottom Side Average	36.7	
Top Side Average	30.1		Top Side Average	26.7	
ΔT	2.1		ΔT	10.0	
At the end of the 3.5 hour test			At the end of the 3.5 hour test		
Measurement	T (°C)		Measurement	T (°C)	
Bottom Side Average	36.7		Bottom Side Average	38.6	
Top Side Average	34.8		Top Side Average	30.6	
Bottom Side Air Space	43.1		Bottom Side Air Space	43.1	
Top Side Air Space	31.7		Top Side Air Space	29.2	
ΔT	1.8		ΔT	8.0	

Adding the two aluminum plates to compress and deflate the original NOVUS thermal semiconductor greatly improved its performance as a thermal semiconductor from the experimental results. At the end of the device's constant temperature test for its conducting configuration, the ΔT value was reduced by

34.4% from a value of 1.53 °C for the original NOVUS prototype to a new value of 1.0 °C for the modified NOVUS device. This shows that applying the plates to the original device did help to much more effectively deflate the inflatable structure by removing any leftover air within the NOVUS packaging layers, which improved the smart insulation device's performance as a conductor when necessary. Also, unexpectedly, using the aluminum plates on the hot and cold sides of the NOVUS device significantly improved the new prototype's performance as an insulator compared to the original NOVUS thermal semiconductor by more than doubling the original NOVUS prototype's ΔT value at the end of its insulating state, constant temperature test from 2.6 °C to 5.4 °C. The modified NOVUS prototype's large improvement in its performance as an insulator most likely was caused by the added thermal mass of the two aluminum plates due to aluminum's very high density compared to the original NOVUS device.

When evaluating the NOVUS inflatable device with aluminum plates compared to the benchmark insulation test piece's constant temperature test ΔT values, the modified NOVUS device continued to show marked improvement over the original NOVUS prototype. The range of ΔT at the end of the constant temperature tests for the new NOVUS device varied from 11.3-60.8% of the benchmark insulation test piece's ΔT value, showing that the NOVUS device with aluminum plates could perform as both an excellent conductor and still reasonable insulator when necessary with possible variation in ΔT of over 49% from the device's conducting state to its insulating state. This is a much larger change in ΔT for the actuation of the device from its conducting configuration to its insulating configuration than was achieved for the original NOVUS inflatable device, which only had a change in ΔT from 17.2% to 28.8% of the benchmark insulation values. Similar improvements in the NOVUS device with aluminum plates' performance as both a conductor and an insulator were also found for the modified prototype's constant heat flux tests. Two plots comparing the hot side temperatures, cold side temperatures, and ΔT values of the original NOVUS inflatable device and the NOVUS inflatable device with aluminum plates are shown in Figures 135 and 136 for the constant temperature tests' conducting and insulating configurations.

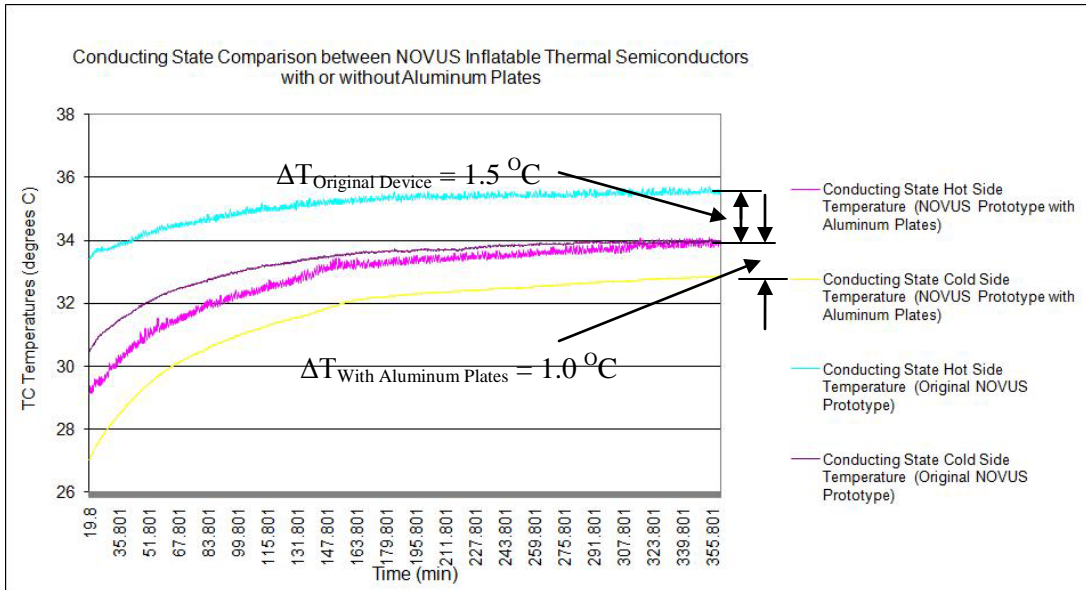


Figure 135: Conducting State Comparison between NOVUS Inflatable Thermal Semiconductors with or without Aluminum Plates.

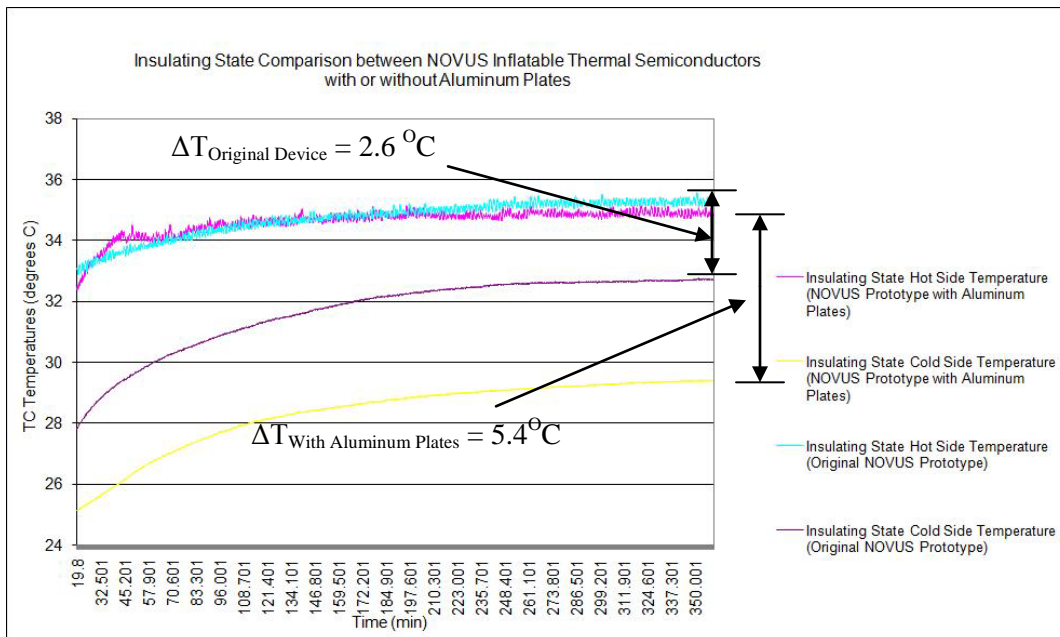


Figure 136: Conducting State Comparison between NOVUS Inflatable Thermal Semiconductors with or without Aluminum Plates.

Although utilizing the two aluminum plates to more effectively deflate the NOVUS prototype substantially improved the device's conducting state, it is speculated that even better conductor performance would be possible if the NOVUS prototype could be deflated and compressed very well by using a vacuum pump instead of the two plates. By adding the two plates to the original NOVUS device, the conduction heat transfer through the device is increased due to the decreased thickness of the original NOVUS insulation; however, the aluminum plates themselves also served to decrease the heat transfer simply by their added thickness. In the end the benefits the plates contributed by better deflating the smart insulation outweighed the costs of the additional thickness of the two plates, leading to improved performance overall for the NOVUS device.

To show how effectively deflating the NOVUS insulation without the use of the plates could lead to a reduced ΔT value for the device's conducting state, one final constant temperature test was conducted utilizing a device consisting of only two aluminum plates back-to-back with none of the NOVUS insulation between them. In theory, the ΔT value for a well-deflated NOVUS prototype without any plates would be equal to the difference between the ΔT value for the well-deflated NOVUS device with two added plates and the ΔT value for a device consisting of only two back-to-back aluminum plates. A plot of the constant temperature test of the two back-to-back aluminum plates is given in Figure 137.

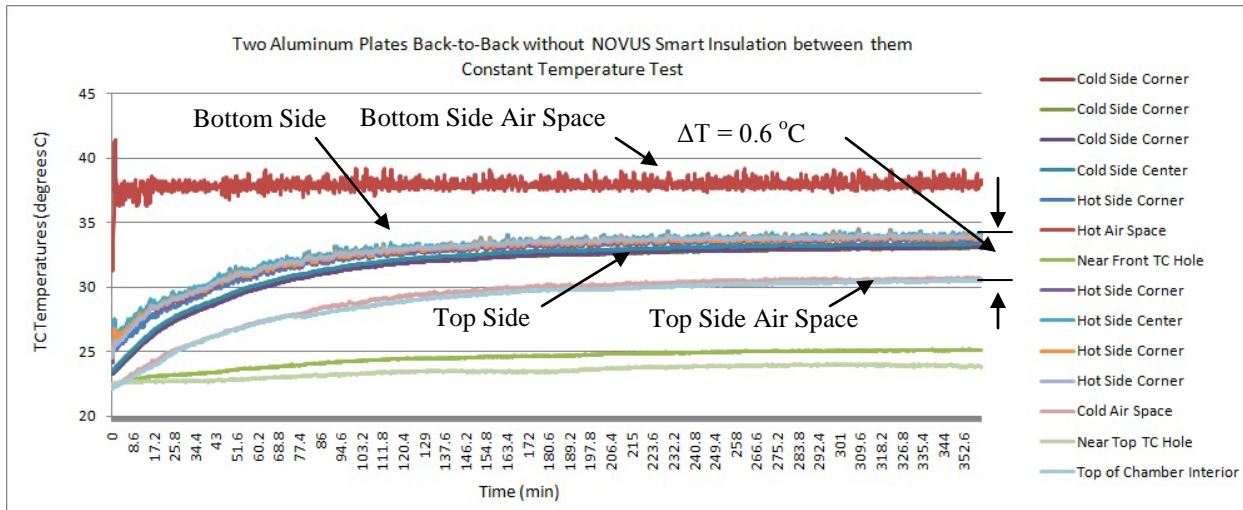


Figure 137: Back-to-Back Aluminum Plates Constant Temperature Test.

From the experimental results of Figure 137, the ΔT value at the conclusion of the back-to-back aluminum plates' constant temperature test was calculated to be $0.6\text{ }^{\circ}\text{C}$, which shows that once the NOVUS insulation is well-deflated through the use of the two aluminum plates in the earlier test, most of the remaining thermal resistance is from the two plates themselves. Using the results of both the NOVUS inflatable device with aluminum plates test and the back-to-back aluminum plates test, it was determined that in the former test the two aluminum plates contributed $0.6\text{ }^{\circ}\text{C}$ of the total $1.0\text{ }^{\circ}\text{C}$ overall ΔT value measured across the device, while the well-deflated NOVUS insulation contributed only $0.36\text{ }^{\circ}\text{C}$ of the total ΔT value. Consequently, if a vacuum pump were utilized to very effectively deflate the original NOVUS prototype, it is estimated that the ΔT value for the end of the device's constant temperature test for its conducting state would be only about $0.4\text{ }^{\circ}\text{C}$ compared to the original value of $1.5\text{ }^{\circ}\text{C}$, resulting in a much better conducting state for the original thermal semiconductor with a ΔT value decreased by 69.5%. This would result in much better performance for the conducting state of the original NOVUS inflatable device with possible variation in ΔT from 5.3% of the benchmark insulation test piece's ΔT value for the device's conducting state to 28.8% of the benchmark insulation test piece's ΔT value for the device's insulating state. By using a vacuum pump for effective deflation, however, the insulating

configuration of the original NOVUS device will not improve such as for the case with the added aluminum plates which provided additional thermal mass to the overall device.

4.4 DISCUSSION OF SMART INSULATION EXPERIMENTAL RESULTS

In order to compare the performance of the different fins-related smart insulation devices to the benchmark insulation test piece and to each other, a bar graph was created, which is shown in Figure 138. Within Figure 138, the ranges of the ΔT values' measured from the devices' conducting states to their insulating states as a percentage of the benchmark insulation test piece's ΔT values are given for each of the three main fins-related smart insulation prototypes. In addition, in Figure 138 the ideal smart insulation case with ΔT values ranging from 0 to 100% of the benchmark insulation test piece is also given for comparison

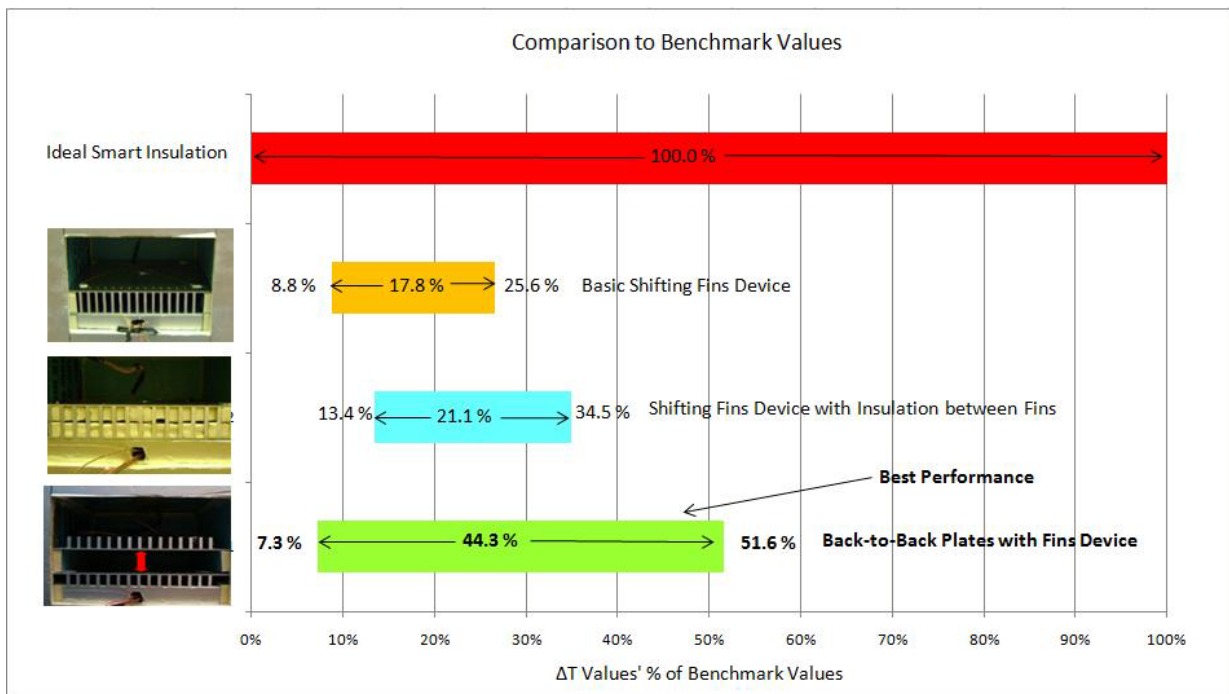


Figure 138: Comparison of Fins-Related Prototype ΔT Values to Ideal Smart Insulation Case.

As seen in Figure 138, the fins-related prototype that performed the best as smart insulation was the back-to-back plates with outward facing fins device. The back-to-back plates with fins thermal semiconductor's ΔT value was able to vary from 7.8% to 54.6% of the benchmark insulation test piece's ΔT value. On the basis of these experimental results, the back-to-back plates with outward facing fins concept should be pursued further over the other shifting fins concepts by possibly implementing and testing it in an actual building setting.

Next, in order to compare the performance of the different inflatable honeycomb-structure smart insulation devices to the benchmark insulation test piece and to each other, a second bar graph was also created, which is given in Figure 139. Within Figure 139, for each of the three main inflatable thermal semiconductor devices, the ranges of the ΔT values' measured from the devices' conducting states to their insulating states are given as a percentage of the benchmark insulation test piece's ΔT values. Similarly to Figure 138, the ideal smart insulation case is also given for comparison in Figure 139 with ΔT values ranging from 0 to 100% of the benchmark insulation test piece.

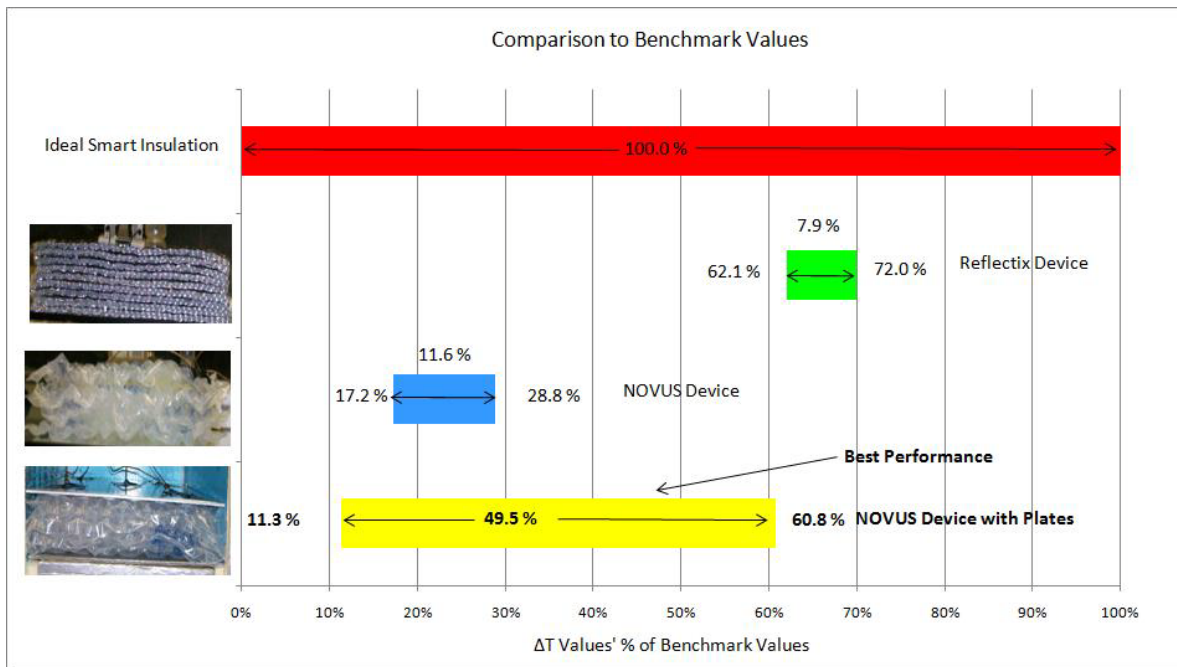


Figure 139: Comparison of Inflatable Prototype ΔT Values to Ideal Smart Insulation Case.

As illustrated in Figure 139, the inflatable thermal semiconductor device that had the best performance by far was the NOVUS inflatable device with two aluminum plates, which was able to vary its final constant temperature test ΔT value when changing heat transfer states from 11.29% to 60.76% of the benchmark insulation test piece's ΔT value. This large range of ΔT values reached by the NOVUS inflatable device with two plates was much larger than the range of ΔT values obtained by the Reflectix inflatable prototype or the original NOVUS inflatable prototype, which will also give it the largest possible change in thermal conductivity when it is actuated between its conducting and insulating states. In addition, when comparing the NOVUS device with two aluminum plates to the best fins-related prototype, it continues to have the best performance. This makes the NOVUS inflatable prototype with two plates the best smart insulation candidate to be pursued for further implementation and testing in real-world building settings among not only the inflatable thermal semiconductors but also among any of the different smart insulation devices experimentally tested.

Although all of the different smart insulation prototypes exhibited some change in their ΔT values and thermal conductivities when changed between their conducting and insulating states, many of the devices had poor performance in their insulator states, and none of the devices' ΔT values were able to attain the level of the benchmark conventional insulation test piece. For smart insulation to obtain energy and cost savings over conventional building insulation, any smart insulation prototypes developed will need their insulating states to have performance close to or even greater than conventional building insulation. One method that could be used to improve the insulating configurations of the smart insulation devices tested would be to add an additional layer of conventional building insulation to the original smart insulation devices to increase their ΔT values until their insulator performance attains that of the conventional building insulation. While this will also result in decreased performance for the conducting configurations of the smart insulation prototypes, overall, the amount of change in the ΔT values between the devices' insulating and conducting states should remain the same.

5.0 MODELING OF THE SHIFTING FINS THERMAL SEMICONDUCTOR WITH INSULATION BETWEEN THE FINS

In order to gain a deeper understanding of the experimental results of the smart insulation prototype testing, an analytical model was developed for one of the simplest prototypes, the shifting fins thermal semiconductor with insulation between the fins. A major decision in the modeling of the shifting fins prototype was to only model the constant temperature tests of the device and to postpone the modeling of the constant heat flux tests of the device. Once an analytical model of the constant temperature tests for the shifting fins device is produced that adequately helps to explain the experimental results, it should not be difficult to then extend and modify that model for the constant heat flux tests as well.

At first, a simple one-dimensional, steady-state model of both the insulating and conducting configurations of the shifting fins device in the test chamber set-up was constructed using the thermal resistor approach in Matlab to calculate the theoretical steady-state ΔT values across the device for its two heat transfer states. After comparing the Matlab model's calculated theoretical ΔT values for the shifting fins device to the ΔT values at the conclusion of the constant temperature tests for the experimental testing, a large discrepancy was present between the experimental and theoretical ΔT values. For the insulating state of the shifting fins prototype, the Matlab model's theoretical ΔT values were much larger than the ΔT values measured from the experimental testing. Conversely, for the conducting state of the shifting fins prototype, the Matlab model's theoretical ΔT values were much smaller than the ΔT values measured from the experimental testing. Thus, the Matlab 1-D, steady-state, thermal resistor model was determined to be insufficient to adequately describe the shifting fins prototype, requiring the development of a more in-depth model.

When developing the second and final model of the shifting fins device, several shortcomings of the original Matlab model were addressed. First, the new model would be two-dimensional instead of one-dimensional to allow heat to transfer both vertically and horizontally within the shifting fins prototype. Even though a more detailed 3-D model could have been developed for the shifting fins device, a 2-D model was determined to be sufficient, since the geometry and characteristics of the device and test chamber set-up did not change in the third direction. Next, the new model would be transient in nature instead of steady-state because during constant temperature tests being modeled, the temperature measurements did not reach their steady-state values, which could have caused the discrepancy in the ΔT values between the simple Matlab model results and the experimental results for the shifting fins prototype. To meet these requirements for the new model, ANSYS finite element software was utilized in the development of the second improved mathematical model because it allowed for both 2-D and transient thermal modeling. As a result of using FEA (Finite Element Analysis), the final model of the shifting fins prototype was primarily a numerical model instead of an analytical one. The formulation and results of the 2-D, transient finite element shifting fins device model are discussed in the following sections.

5.1 DEVELOPMENT OF THE SHIFTING FINS PROTOTYPE TRANSIENT FINITE ELEMENT MODEL

5.1.1 Modeling of Shifting Fins Prototype with Thermal Contact Resistance Added

The first step in building the thermal finite element model of the shifting fins device was to construct the insulating and conducting configurations of the 2-D shifting fins prototype in the software to match the geometry and dimensions of the actual fabricated device. Except for the differences in the fin arrangement of the insulating and conducting models of the shifting fins device, all other features of the numerical model were the same for both the insulating and conducting states of the device. Figures 140

and 141 show the conducting and insulating configurations of the shifting fins prototype constructed in the finite element model. One issue that was never accounted for in the original Matlab model of the shifting fins device was the problem of the thermal contact resistance at the interfaces where the fins and plates contact each other and where the lower and upper fins contact each other during the conduction case. Thermal contact resistance between two surfaces occurs from the roughness of the two surfaces causing small air gaps to be present at the interface between the surfaces. To incorporate thermal contact resistance into the 2-D model, small air spaces were added into the conducting configuration model at the locations where the fins contact each other and at the interfaces between the fins and the aluminum plates. From examining the actual shifting fins prototype in its conducting arrangement, the air gap thickness between contacting surfaces in the device was estimated to be roughly 0.5 mm (1/48 in.), so this value was used in the thermal finite element analysis. To maintain consistency between the conducting and insulating states of the shifting fins prototype, the same small air spaces were also added to the insulating configuration finite element model of the device.

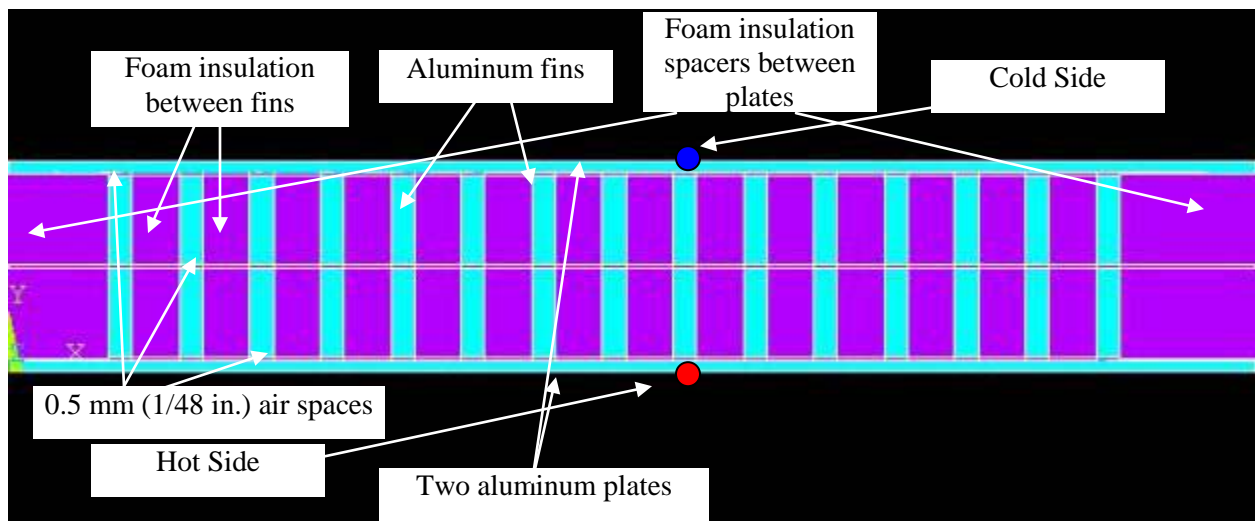


Figure 140: Conducting State of Shifting Fins Prototype Constructed in FEA Software.

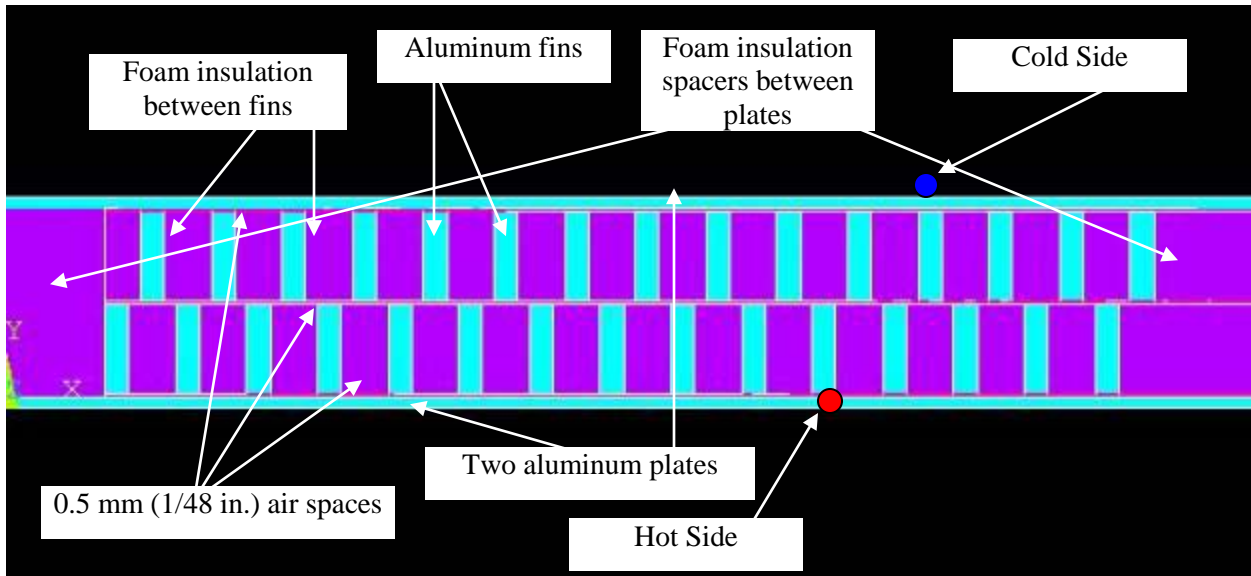


Figure 141: Insulating State of Shifting Fins Prototype Constructed in FEA Software.

A close-up view of the small air spaces at the interface between the lower and upper fins in the device's conducting state is also given in Figure 142.

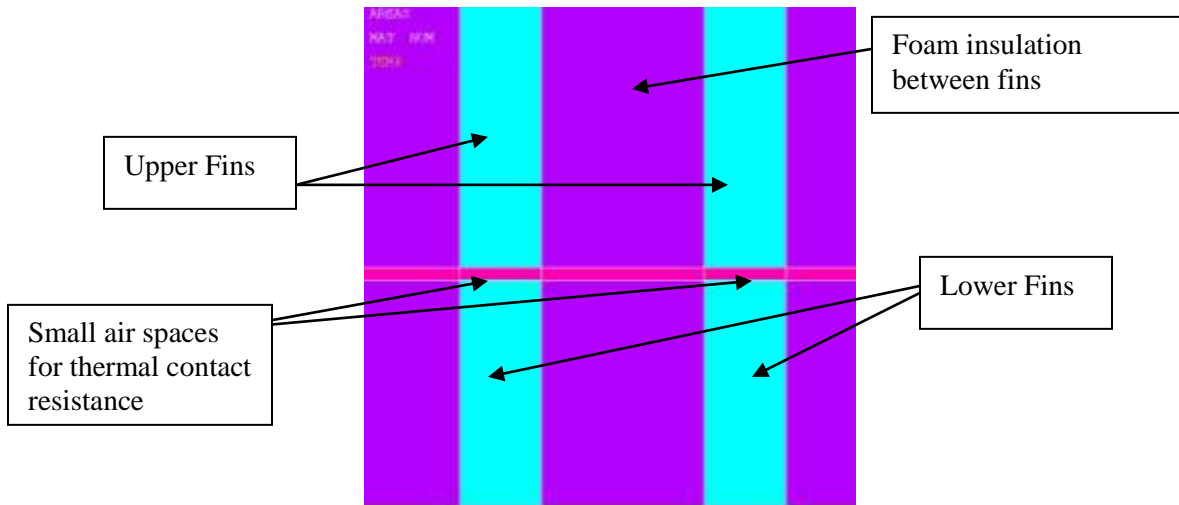


Figure 142: Close-Up View of Air Spaces Added at Interface between Contacting Fins.

Three different materials were utilized to construct the shifting fins prototype with insulation between fins in the finite element model: aluminum alloy 6061, the foam polyisocyanurate building insulation, and air. The material properties used in the thermal finite element analysis are listed in Table 12. The properties of air used in the FEA were for air at a temperature of 30 °C [31]. 30 °C was chosen because it was about the average temperature of the air within the test chamber, which varied between 20 - 40 °C during the constant temperature testing.

Table 12: Material Properties used in Finite Element Analysis of Shifting Fins Device.

Material Properties used in FEA					
6061 Aluminum Alloy		Polyisocyanurate Foam Insulation		Air	
Property	Value	Property	Value	Property	Value
ρ (kg/m ³)	2712.6	ρ (kg/m ³)	32	ρ (kg/m ³)	1.166
c_p (J/kg-K)	896	c_p (J/kg-K)	1400	c_p (J/kg-K)	1005
k (W/m-K)	167	k (W/m-K)	0.02163	k (W/m-K)	0.0264

5.1.2 Meshing of Shifting Fins Prototype with Insulation between Fins

After the shifting fins prototype had been constructed in the FEA software, the next step was to determine the type and size of the elements to be used in the mesh of the device. For all of the 2-D elements of the thermal finite element model, PLANE55 elements were utilized in the ANSYS 11.0 software, which are 2-D thermal conduction elements that can be used in a transient thermal analysis. Each PLANE55 element consists of four nodes with a single degree of freedom, temperature, at each node. When determining the desired size of the PLANE55 elements, the size of the elements was dependent on the minimum time step size in the transient thermal analysis [32]. In general for a transient thermal finite element analysis, using a finer mesh for the same time step size will result in improved results, while using smaller time steps for the same size mesh will give worse results [32]. In this transient analysis a very small minimum time step of 1.5 s is desired, so a very fine mesh will be needed. To solve for the maximum possible element size for accurate results for the minimum time step size of 1.5 s,

Equation 5.1 was utilized where Δ is the maximum possible conducting length of an element and α is the thermal diffusivity of an element, which is also given in Equation 5.2.

$$\alpha = \frac{k}{\rho c_p} \quad (5.1)$$

$$\text{Minimum Time Step Size} = \frac{\Delta^2}{4\alpha} \quad (5.2)$$

Since three different materials were used in the mesh for the shifting fins prototype, the maximum possible element edge length was calculated using Equation 5.1 for each of the three different materials' thermal diffusivities, and the smallest maximum possible edge length of the three materials was utilized as the edge length for all of the elements in the shifting fins prototype mesh. Using Equation 5.1 the maximum possible conducting lengths for the aluminum alloy, air, and the polyisocyanurate foam insulation were calculated to be 2.03 cm, 1.16 cm, and 0.17 cm respectively, so 0.05292 cm (1/48 in.) was chosen as the edge length for the PLANE55 elements. 0.05292 cm (1/48 in.) was chosen instead of lowest value of 0.17 cm mainly because it could be evenly divided into both the total height of the shifting fins device of 2.25 in. (5.715 cm) and the total width of the shifting fins device of 13.25 in. (0.337 m). The mesh of the shifting fins device's insulating state near the interface between the upper fins and upper plate is shown in Figure 143.

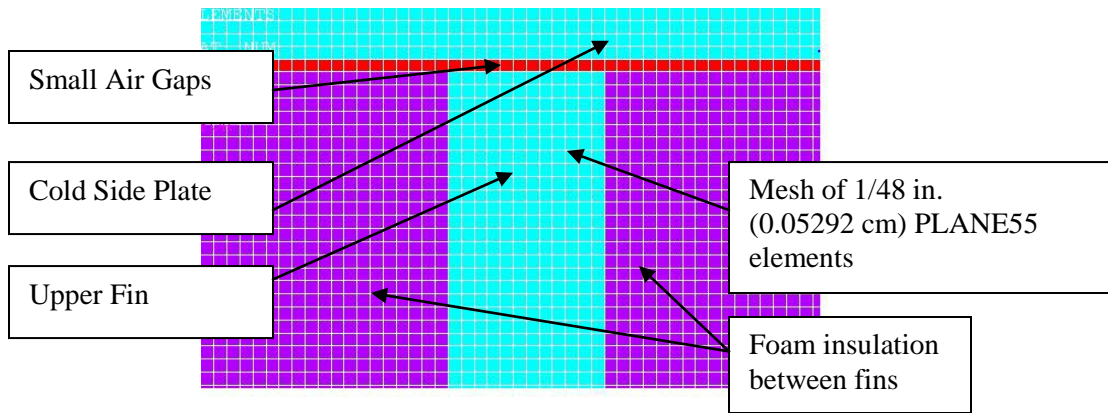


Figure 143: Shifting Fins Prototype Mesh at Interface between Upper Fins and Top Plate of Device.

5.1.3 Modeling of Hot Side Air Space in Insulation Test Chamber

In the modeling of the hot side air space used in the test chamber to heat the bottom plate of the shifting prototype, both convection and conduction heat transfer of the air from the heater to hot side place were considered. To model conduction in the hot side air space, LINK32 conductive bar elements were utilized that consisted of two nodes able to conduct heat to each other in the uniaxial direction between them with each node having a single degree of freedom, temperature. To model convection in the hot side air space, LINK34 convection elements were utilized that consisted of two nodes able to convect heat between them with the convective heat transfer coefficient, h , inputted by the user as a material property for the element. In addition, the length of the LINK34 in the model is arbitrary, since unlike conduction, the length of the element has no effect on the amount of convection heat transfer.

In the thermal FEA model of the shifting fins device in the test chamber, the hot side air space is inserted into the overall model by connecting one node of the LINK32 conduction and LINK34 convection elements directly to the bottom nodes of the bottom aluminum plate of the shifting fins device facing the hot side air space. Starting from left to right for each node of the bottom, hot side plate, the LINK32 and LINK34 1-D elements will alternate so that every other node of the hot side plate will be connected to a LINK32 element with all of the other nodes being connected to a LINK34 element. The

node at the other side of all of the LINK32 and LINK34 elements will be set to a constant temperature of 100 °F (37.78 °C) to represent the constant temperature boundary condition of the midpoint of the hot side air space. Additionally, on either side of the hot side plate where it rests on top of the foam insulation shelf, an insulated (zero heat flux) boundary condition was applied to bottom of the hot side plate.

When attaching the LINK34 1-D elements to the nodes of the hot side plate, each line attached to the hot side plate represented one LINK34 element for convection. Conversely, for the LINK32 elements each line attached the hot side plate represented many LINK32 conduction elements. For both types of 1-D elements, the length of each line attached to the hot side plate was set to a value of 0.75 in. (1.91 cm) to match the distance between the midpoint of the hot side air space and the hot side plate of the device, while the edge length of the individual LINK32 elements was kept at the same value of 1/48 in. (0.05292 cm), used for the PLANE55 elements beforehand for consistency. Figure 144 demonstrates how the LINK32 and LINK34 elements were attached to the hot side plate of the shifting fins device to model the hot side air space. Two final values needed in the model were the cross-sectional area that each LINK32 element acts over and the surface area that each LINK34 element acts over, which are essentially the same values since the area of the hot side plate serves as both the cross-sectional area for conduction and the surface area for convection. The value used for the two areas was 1/24 in. (0.106 cm), which was the distance between adjacent LINK32 elements and the distance between adjacent LINK34 elements, since the other component of the area in the 2-D model was unity. Essentially, each LINK32 or LINK34 element attached to a node of the hot side plate acts over the area of the two PLANE 55 elements on either side of that hot side plate node. A schematic that illustrates the areas over which the LINK32 and LINK34 elements act is given in Figure 145.

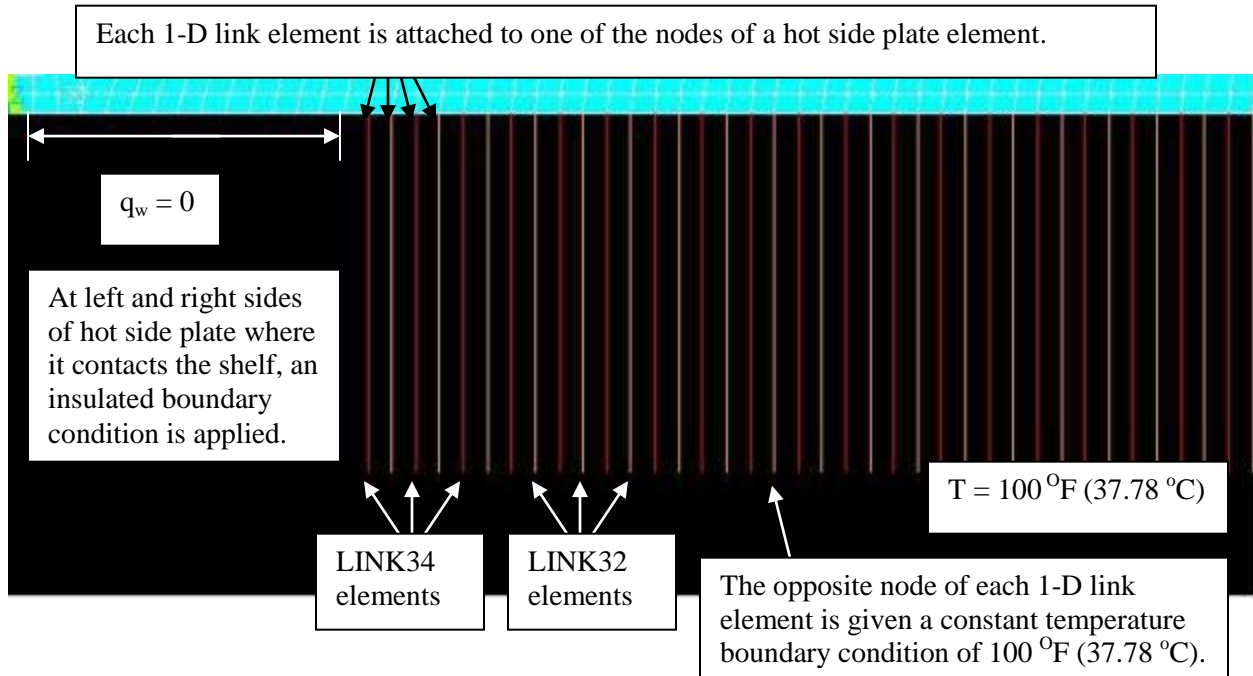


Figure 144: Schematic of How Hot Side Air Space Heating is applied to Shifting Fins Device.

An image that shows all of the LINK34 and LINK32 elements attached to the bottom of the hot side plate is given in Figure 146.

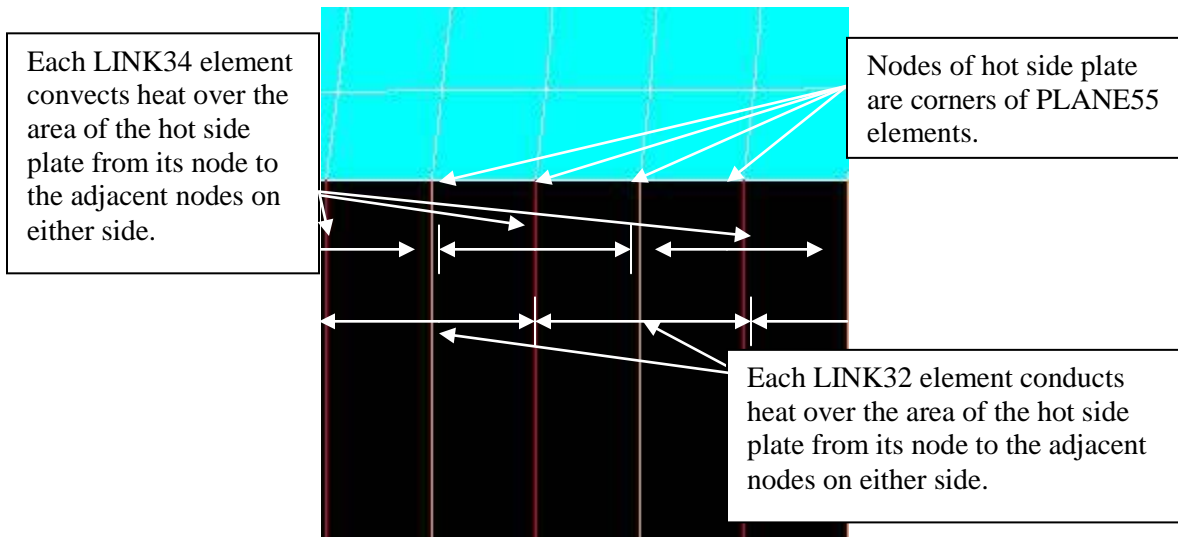


Figure 145: Areas of Hot Side Plate over which 1-D Link Elements Act.

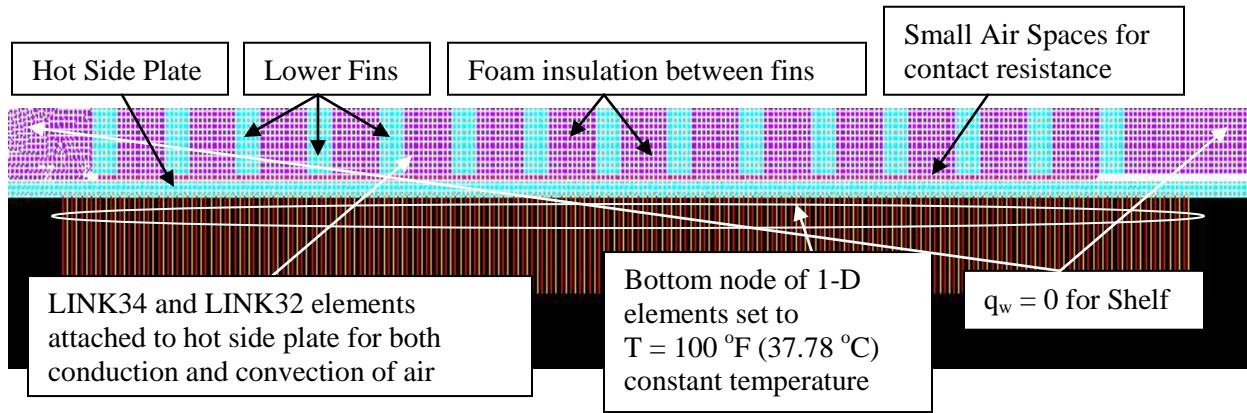


Figure 146: Hot Side Air Space and Shelf Conditions Applied to Hot Side Plate in FEA Model.

In order to calculate the convection coefficient for the LINK34 elements of the hot side air space, the equations for natural convection in an enclosure were utilized [26]. During almost the entire length of the constant temperature tests for the shifting fins prototype, a constant temperature boundary condition of 100 °F (37.78 °C) was applied to the midpoint of the hot side air space, while on the other side of the hot side air space, the hot side plate very slowly increased in temperature during the test. To calculate the convection coefficient for the constant temperature boundary condition period of the testing, equations for the Rayleigh number and the Nusselt number for natural convection in an enclosure between two horizontal plates of constant temperature were used where the Rayleigh number is simply the Grashof number multiplied by the Prandtl number as shown in Equation 5.3 [26].

$$Ra = Gr_{\delta} Pr \quad (5.3)$$

Since the temperature of the bottom plate was not actually constant but increased during the testing, several convection coefficients were calculated for different bottom plate temperatures, resulting in a hot side air space convection coefficient that was a function of the temperature of the hot side plate. To input the convection coefficient as a function of temperature into the FEA software, the convection coefficient was inputted in a tabular format.

The first step in calculating the convection coefficients for the constant temperature boundary condition for the hot side air space was to calculate several Rayleigh numbers for different hot side plate temperatures using Equation 5.4 where δ is the distance between the two horizontal constant temperature surfaces and β is given by the expression found in Equation 5.5 [26]. For the case of the hot side air space of the test chamber, a value of 0.75 in. (1.91 cm) was utilized for δ because it was the distance between the hot side plate and the constant temperature boundary condition of 37.78 °C (100 °F) at the midpoint of the chamber.

$$Ra = \frac{g\beta(37.78 - T_{Hot\ Side\ Plate})\delta^3}{\nu_{Air}\alpha_{Air}} \quad (5.4)$$

$$\beta = \frac{1}{\frac{T_{Hot\ Side\ Plate} + 37.78}{2} + 273.15} \quad (5.5)$$

Once the Rayleigh number was calculated as a function of the hot side plate temperature, the next step was to calculate the Nusselt numbers for the hot side air space for the different Rayleigh numbers. The general form for the Nusselt number for natural convection between two horizontal surfaces in an enclosure is given in Equation 5.6 where the constants C, n, and m will vary depending on the Rayleigh number determined earlier [26].

$$Nu_{\delta} = C(Ra)^n \left(\frac{L}{\delta}\right)^m \quad (5.6)$$

The calculated Rayleigh numbers varied from around 3300 to 10,600, requiring the use of two different empirical relations for the Nusselt number based on the general form of Equation 5.6 that are shown in Equations 5.7 and 5.8 with the Rayleigh number range for which each is applicable [26].

$$1700 < Ra < 7000 \quad Nu_{\delta} = 0.059(Ra)^{0.4} \quad (5.7)$$

$$7000 < Ra < 3.2 \times 10^5 \quad Nu_{\delta} = 0.212(Ra)^{1/4} \quad (5.8)$$

Finally, using the calculated Nusselt numbers the convection coefficients for the hot side air space when the midpoint of the air space is at a constant temperature were determined using Equation 5.9 [26].

$$h = Nu_{\delta} \frac{k_{Air}}{\delta} \quad (5.9)$$

The convection coefficient as a function of the hot side plate temperature is given in Table 13 for the period of the testing when the hot side air space is at a constant temperature.

Table 13: Hot Side Air Space Convection Coefficients for Constant Temperature Boundary Condition.

T _{Hot Side Plate} (°C)	h _{Hot Side Air Space} (W/m ² -K)
21.6	2.98
22.4	2.94
23.3	2.90
24.2	2.84
25.1	2.80
26.0	2.75
26.9	2.69
27.8	2.74
28.7	2.64
29.6	2.53
30.5	2.41
31.4	2.30
32.3	2.16
32.8	2.08

Although the hot side air space was at a constant temperature for the vast majority of the constant temperature tests, for the first 13 minutes of the test the heater applied a constant heat flux to the hot side air space to increase its temperature from the ambient laboratory temperature to 100 °F (37.78 °C). As a result of this different boundary condition for the hot side air space early in the test, different convection coefficients had to be calculated for the beginning of the test for the FEA model. In calculating the convection coefficients for the constant heat flux boundary condition, the first step was to calculate new Rayleigh numbers as a function of the bottom plate temperature ranging from 21.6 °C to 23.3 °C at the

very beginning of the testing. To calculate the Rayleigh numbers Equation 5.10 for free convection from inclined surfaces under constant heat flux conditions was utilized with q_w being calculated from Equation 5.11 where V is the voltage applied to the Kapton heater, I is the current applied to the Kapton heater, and A is the cross-sectional area of the hot side area space [26].

$$Ra = \frac{g\beta q_w \delta^4}{k_{Air} \alpha_{Air} \nu_{Air}} \quad (5.10)$$

$$q_w = \frac{V_{Heater} I_{Heater}}{A_{cross-sectional}} \quad (5.11)$$

Once the Rayleigh numbers were calculated, the next step was to calculate the new Nusselt numbers for the constant heat flux case using Equations 5.12 and 5.13. In Equation 5.12 the characteristic length dimension, L , for horizontal flat surfaces, such as the constant temperature horizontal surface of the hot side air space can be calculated using Equation 5.14.

$$Nu_\delta = 0.42(Ra)^{\frac{1}{4}} Pr^{0.012} \left(\frac{L}{\delta}\right)^{-0.30} \quad \begin{array}{l} q_w = constant \\ 10^4 < Ra < 10^7 \\ 10 < \frac{L}{\delta} < 40 \end{array} \quad (5.12)$$

$$Nu_\delta = 0.46(Ra)^{1/3} \quad \begin{array}{l} q_w = constant \\ 10^6 < Ra < 10^9 \\ 1 < \frac{L}{\delta} < 40 \end{array} \quad (5.13)$$

$$L = \frac{A_{cross-sectional}}{Perimeter} \quad (5.14)$$

Individually, neither Equation 5.12 nor 5.13 completely described the case of the natural convection in the hot side air space. The Rayleigh numbers obtained were in the range of 10^4 - 10^5 , which was the range of Rayleigh numbers supported by only the Equation 5.12 but not Equation 5.13, while the ratio of L/δ for the hot side air space was 4, which only fits in the range of acceptable L/δ values for Equation 5.13. Since each of the two equations for the Nusselt number only partially described the free convection of the hot

side air space, the averages of the two Nusselt numbers calculated from both Equation 5.12 and 5.13 were utilized to calculate the convection coefficients for the hot side air space. Finally, similarly to the constant temperature boundary condition period of the testing, Equation 5.9 was used to calculate the convection coefficients for the constant heat flux boundary condition time period of the testing using the new Nusselt numbers calculated from Equations 5.12 and 5.13.

At the beginning of the constant temperature tests of the shifting fins prototype in the test chamber, 46.64 W (21.2 V, 2.2 A) of power was applied to the heat source at first to allow the hot side air space to heat up very quickly to the desired constant temperature of 100 °F (37.78 °C). Once the hot side air space temperature began to approach 100 °F (37.78 °C), the power level applied to the heater was reduced to 13.27 W (11.34 V, 1.17 A) to prevent a large overshoot of the desired temperature of 100 °F (37.78 °C). To account for the constant heat flux conditions for the hot side air space under 46.64 W of power, the convection coefficient at the beginning of the testing corresponding to 21.6 °C in Table 13 was recalculated for the constant heat flux case using voltage and current levels of 21.2 V and 2.2 A to calculate q_w . Later on, to account for the constant heat flux conditions when the power level had been reduced to 13.27 W, the convection coefficient early on in the testing corresponding to 23.3 °C in Table 13 was recalculated for the constant heat flux case using voltage and current levels of 11.34 V and 1.17 A to calculate q_w . Finally, for the second temperature value of 23.3 °C in Table 13, a convection coefficient value halfway between the convection coefficients for the two different power levels was utilized to represent the reduction of power during the testing from 46.64 W to 13.27 W. The three convection coefficients as a function of temperature used for the constant heat flux portion of the FEA model for the hot side air space are given in Table 14.

Table 14: Hot Side Convection Coefficients for Constant Heat Flux Boundary Condition.

$T_{\text{Hot Side Plate}} (^{\circ}\text{C})$	$h_{\text{Hot Side Air Space}} (\text{W}/\text{m}^2\text{-K})$
21.6	24.0
22.4	20.0
23.3	15.9

After examining the convection coefficients for both the constant heat flux and constant temperature hot side air space heating conditions, the constant heat flux convection coefficients at the beginning of the test were much higher, roughly an order or magnitude, than the constant temperature convection coefficients. To prevent a very abrupt transition in convection coefficients between the two heating conditions, an assumption was made that the convection coefficients will gradually decrease from the constant heat flux values in Table 14 at the beginning of the test until the 1/3 point (120 minutes) of the constant temperature test. After that point for the last 2/3 (240 minutes) of the constant temperature test, the convection coefficients will correspond to those of the constant temperature heating condition in Table 13. During the transitional period, once the constant heat flux case for the hot side air space ends, the convection coefficients will decrease at a very steep linear rate at first, then decrease at a more gradual linear rate as a function of the hot side plate temperature until the 1/3 point of the testing. The final convection coefficients for the hot side air space used in the FEA as a function of the hot side plate temperature for both the conducting and insulating configurations of the shifting fins prototype are shown in Table 15.

Table 15: Convection Coefficients used for Hot Side Air Space in FEA of Shifting Fins Device.

	$T_{\text{Hot Side Plate}}$ (°C)	$h_{\text{Hot Side Air Space}}$ (W/m ² -K)	
First 2 hours of testing	21.6	24.00	Constant Heat Flux
	22.4	20.00	
	23.3	15.90	
	24.2	11.40	
	25.1	6.90	
	26.0	6.15	
	26.9	5.40	
	27.8	4.65	
	28.7	3.90	
	29.6	3.15	
Last 4 hours of testing	30.5	2.41	Transition Period
	31.4	2.30	
	32.3	2.16	
	32.8	2.08	

5.1.4 Modeling of Cold Side Air Space in Insulation Test Chamber

Similarly to the hot side air space, LINK32 and LINK34 elements were used in the thermal FEA of the shifting fins prototype with insulation between fins to model the conduction and convection heat transfer from the cold side plate into the cold side air space and into the top of the test chamber interior. In the same manner as for the hot side plate, the nodes of the bottom side of the LINK32 and LINK34 1-D heat transfer elements were alternately attached one-by-one left to right to the nodes of the PLANE55 elements across the entire section of cold side plate facing the cold side air space. On the opposite end of the LINK32 and LINK34 elements, the top nodes of the elements were connected to the nodes of an additional area composed of foam insulation modeled to represent the top removable wall of the test chamber. By using the LINK34 elements in the cold side air space, convection heat transfer will be able to occur in the thermal FEA between the cold side plate and the removable top wall of the test chamber, while using the LINK32 elements will enable conduction heat transfer to occur from the cold side plate through the air to the top wall of the chamber.

One major benefit of using the LINK34 1-D convection elements to model the convection heat transfer in the cold side air space is that both of the nodes of the elements are allowed to "float" with respect to the overall model of the shifting fins prototype in the test chamber without a user-specified temperature. Typically, when modeling convection in a thermal FEA the bulk temperature of the fluid causing the natural convection must be set to a constant value, but in this case using the LINK34 elements, the temperatures of the cold side plate and the top of the chamber interior on either end of the elements are determined by the overall model of the shifting fins prototype in the test chamber. As with LINK32 elements in the hot side air space, the corresponding LINK32 elements in the cold side air space were each given the same length values of 1/48 in. (0.05292 cm), while the overall length of the lines representing the LINK32 and LINK34 elements were given values of 6 in. (15.24 cm) to match the height of the cold side air space. In the top removable wall area modeled in the thermal FEA, PLANE55 elements were again used with the same element edge length of 1/48 in. (0.05292 cm) as for the elements in the shifting fins prototype. An image that illustrates how the LINK32 and LINK34 elements were used to represent the cold side air space by connecting them to the cold side plate and the removable top wall of the chamber is shown in Figure 147. An additional image that shows all of the LINK34 and LINK32 elements attached to the top of the cold side plate is also shown in Figure 148.

In order to calculate the convection coefficients for the cold side air space of the test chamber, the same equations were used as for the hot side air space for natural convection in an enclosure. Since the two sides of the cold side air space, the top of the cold side plate and the bottom of the top wall of the chamber never had a constant heat flux condition, such as for the hot side air space, only the equations for natural convection between two horizontal surfaces of constant temperature were utilized for the cold side air space. Also, as a result of the temperatures of the two sides of the cold side air space changing during the test, the convection coefficients again had to be calculated as a function of average temperature for the cold side air space, which was assumed to be the average temperature between the cold side plate of the prototype and the temperature of the top of the chamber interior. Similarly to the hot side air space, the

first step in calculating the convection coefficients for the cold side air space was to calculate the Rayleigh numbers for the range of cold air space temperatures that occurred during the testing of the

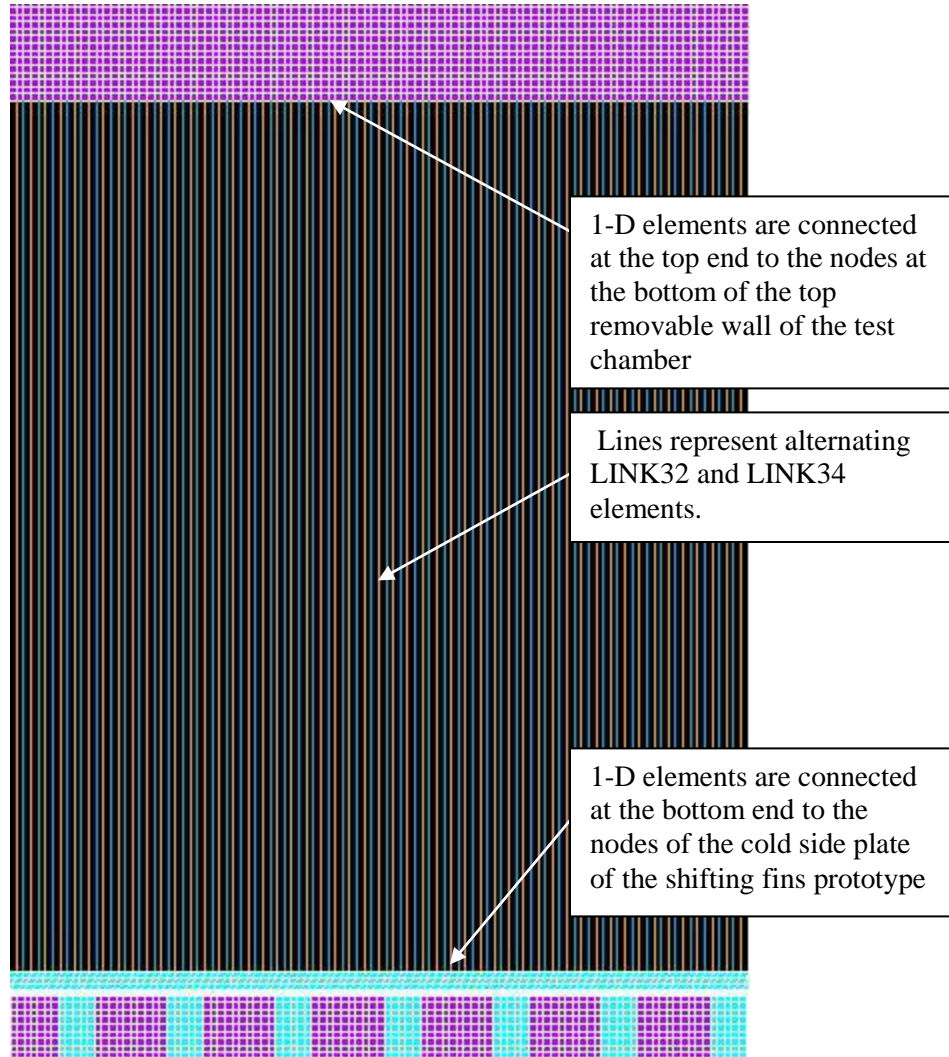


Figure 147: How LINK32 and LINK34 elements represent Cold Side Air Space in FEA Model.

shifting fins device using Equation 5.15 where β is calculated from the expression shown in Equation 5.16 [26]. For the case of the cold side air space of the test chamber, a value of 6 in. (15.24 cm) was utilized for δ because it was the distance between the cold side plate and removable top wall of the test chamber. Examining Equation 5.15 shows that the temperature differences across the cold side air space

were needed in order to calculate the Rayleigh numbers and consequently the convection coefficients for the cold side air space. To calculate the Rayleigh numbers the temperature differences from the experimental results of the constant temperature test of the conducting state of the shifting fins prototype for different average cold space temperatures were utilized.

$$Ra = \frac{g\beta (T_{Cold Side Plate} - T_{Top of Chamber Interior}) \delta^3}{\nu_{Air} \alpha_{Air}} \quad (5.15)$$

$$\beta = \frac{1}{\frac{T_{Cold Side Plate} + T_{Top of Chamber Interior}}{2} + 273.15} \quad (5.16)$$

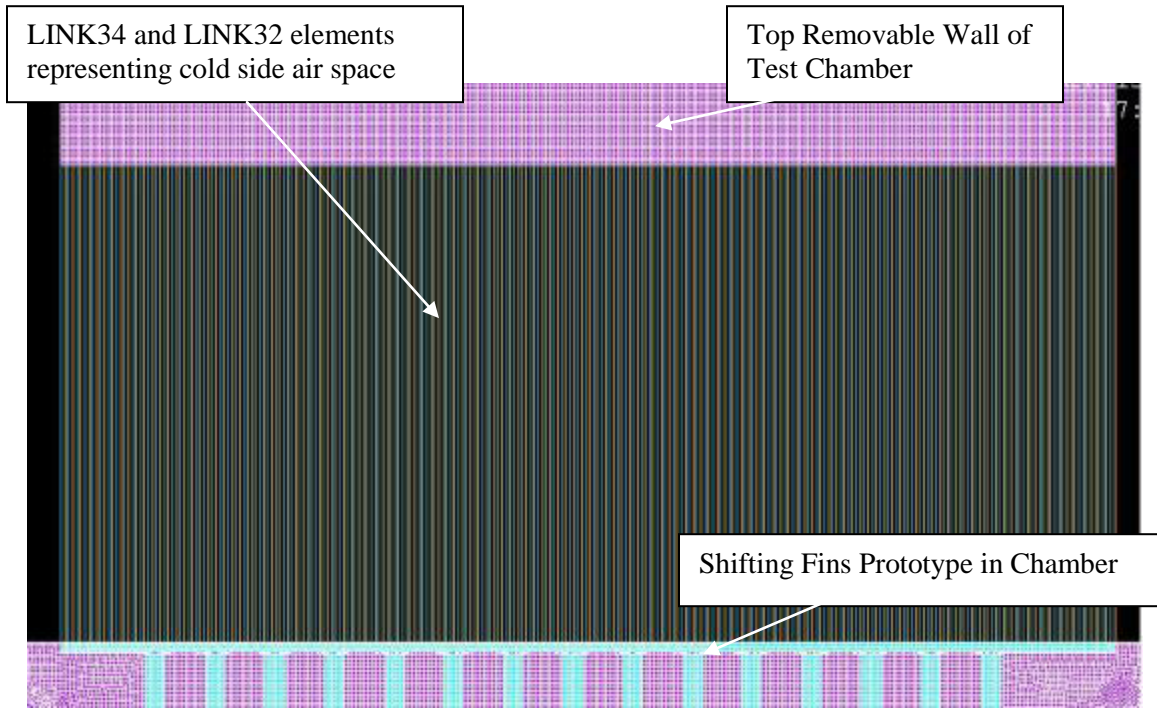


Figure 148: Cold Side Air Space Conditions Applied to Cold Side Plate in FEA Model.

After the Rayleigh numbers were calculated for the cold side air space as a function of temperature, the next step was to determine the different Nusselt numbers corresponding to each of the Rayleigh numbers. For the cold side air space the calculated Rayleigh numbers varied from around 53,000 to

700,000, requiring the use of two different empirical relations for the Nusselt number, Equation 5.8 and Equation 5.17 with the Rayleigh number range for which each is applicable [26].

$$3.2 \times 10^5 < Ra \quad Nu_{\delta} = 0.061(Ra)^{1/3} \quad (5.17)$$

Finally, using the calculated Nusselt numbers the convection coefficients for the cold side air space were determined using Equation 5.9 [26]. The convection coefficients for the cold side air space as a function of the average cold air space temperature are given in Table 16. The same convection coefficients for the cold side air space were used for both the conducting and insulating configurations of the shifting fins prototype with insulation between the fins.

Table 16: Cold Side Air Space Convection Coefficients.

$T_{\text{Cold Side Air Space, Average}} (^{\circ}\text{C})$	$h_{\text{Cold Side Air Space}} (\text{W}/\text{m}^2\text{-K})$
21.60	0.558
22.30	0.822
23.00	0.726
23.70	0.786
24.40	0.836
25.10	0.863
25.80	0.886
26.50	0.904
27.20	0.916
27.90	0.914
28.60	0.915
29.30	0.920
30.00	0.920
30.55	0.921

5.1.5 Thermal Boundary Conditions of FEA Model of Shifting Fins Prototype.

Some of the boundary conditions of the model of the shifting fins prototype in the test chamber have already been discussed. A constant temperature boundary condition of 100 °F (37.78 °C) was applied to the bottom of the hot side air space LINK32 and LINK34 elements, while an insulated constant heat flux

boundary condition of $q_w = 0$ was applied to the hot side plate where it contacted the shelf in the test chamber. At the very top of the removable top wall section of the test chamber in the finite element model, a constant temperature boundary condition corresponding to a ambient laboratory temperature of 21.6 °C at the beginning of the conducting state test or 20.4 °C at the beginning of the insulating state test was applied, since the top of the test chamber faced the outside laboratory environment. The two sides of the removable top wall section were given insulated constant heat flux boundary conditions of $q_w = 0$. On the left and right sides of the shifting fins prototype, additional sections were added that represented the side foam polyisocyanurate walls of the test chamber contacting the shifting fins prototype on either side with the same PLANE55 elements and 1/48 in. (0.05292 cm) element edge length used in the mesh of the two side walls. For the thermal boundary conditions regarding the two side walls in the FEA model, the two surfaces of the side walls contacting the outside laboratory environment were given constant temperature boundary conditions corresponding to the measured laboratory ambient temperature at the beginning of the testing, while all of the other surfaces of the side walls were given insulated constant heat flux boundary conditions of $q_w = 0$. An image of the final completed thermal finite element model of the shifting fins prototype with insulation between the fins in its conducting state in the test chamber set-up is shown in Figure 149.

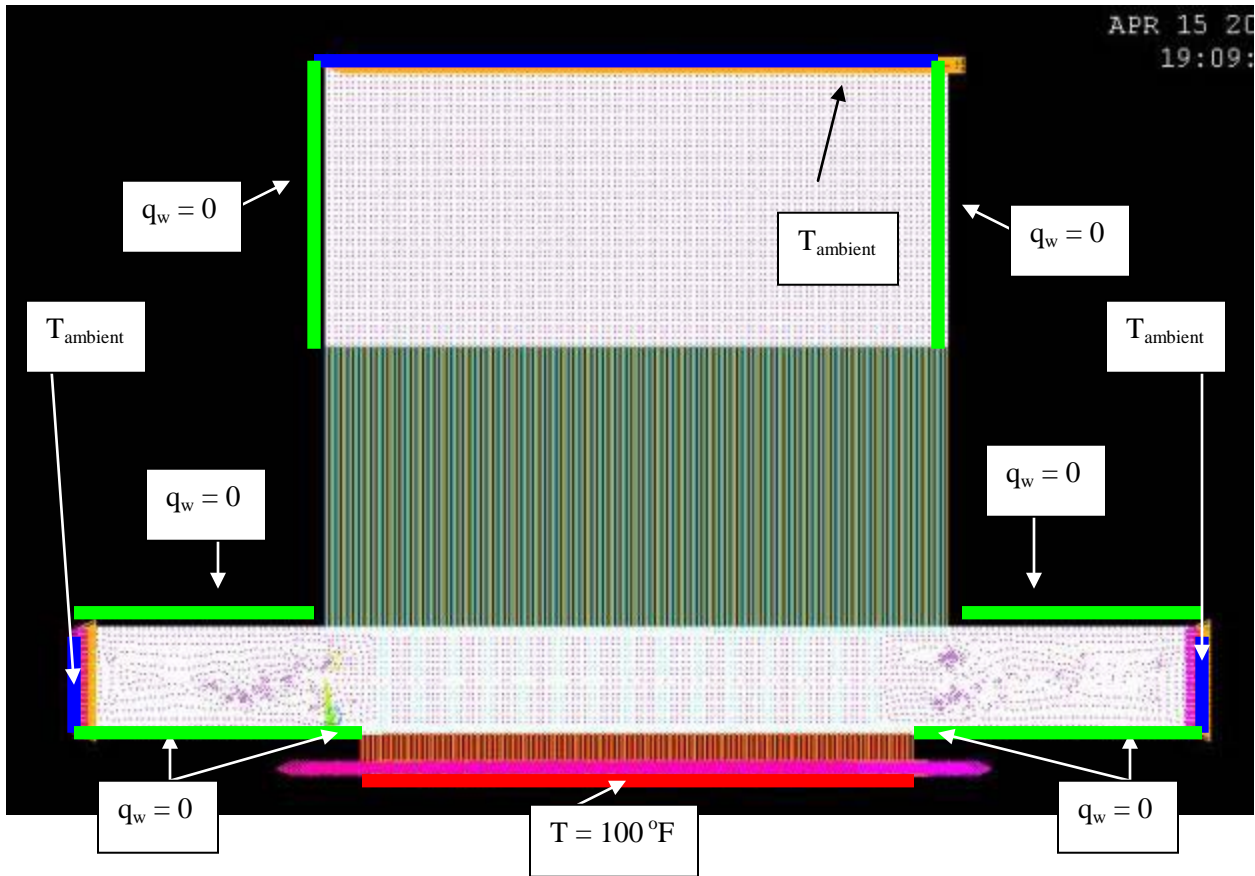


Figure 149: Final Thermal FEA Model of Shifting Fins Prototype with Insulation between Fins in Test Chamber Set-up.

5.2 RESULTS OF THE TRANSIENT FINITE ELEMENT MODELING OF THE SHIFTING FINS PROTOTYPE

Using the transient, thermal finite element model developed for the shifting fins prototype with insulation between the fins, theoretical temperature results for both the device's insulating and conducting states were obtained for the same 6 hour time duration and thermal boundary conditions as for the experimental testing of the device. Two additional parameters that needed to be set in the finite element model for the transient analysis that would not be required for a steady-state analysis were the initial temperature distribution of the model and the time step. First, the initial temperature distribution of the model was set equal to the constant value of the average test chamber temperature from the experimental results at the

beginning of either the conducting state test or the insulating state test, which was approximately equal to the ambient laboratory temperature. Thus, in the model the initial temperature distribution for the conducting configuration of the prototype was 21.6 °C, while the initial temperature distribution for the insulating configuration of the prototype was 20.4 °C.

Within the FEA software for the model of the shifting fins prototype, automatic time stepping was utilized, which allowed the program to modify the length of each time step during the 6 hour time duration depending on the number of iterations it took the model to reach convergence for the previous time step. To ensure accurate results for the transient shifting fins model, a small minimum time step value of 1.5 s was chosen, while the maximum time step value of 5 minutes (300 s) was also selected, which was still only 1/72 of the total time duration.

Once the theoretical temperature results for the insulating and conducting states of the shifting fins prototype were calculated, the theoretical results were directly compared to the results of the experimental testing of the shifting fins prototype with insulation between the fins. Earlier, during the experimental testing, the temperature values measured that were of most importance were the average hot side plate temperature, the average cold side plate temperature, and the ΔT value across the device over time. These same values were also obtained from the finite element model results by tracking the temperature of nodes in the model at the center of the hot and cold side plates facing the two air spaces over the 6 hour time duration. In addition, the temperature of the top of the chamber interior was also tracked over time for the finite element model for comparison with the experimental results for the top of the chamber interior to examine whether or not the model accurately describes the heat transfer of the shifting fins device to the cold side air space. Figure 150 gives a plot of the hot side temperature, cold side temperature, and top of the chamber interior temperature over the 6 hour time duration of the constant temperature test for the conducting state of the shifting fins prototype with insulation between fins. Likewise, Figure 151 gives a plot of the hot side temperature, cold side temperature, and top of the chamber interior temperature over the 6 hour time duration of the constant temperature test for the insulating state of the shifting fins prototype with insulation between fins.

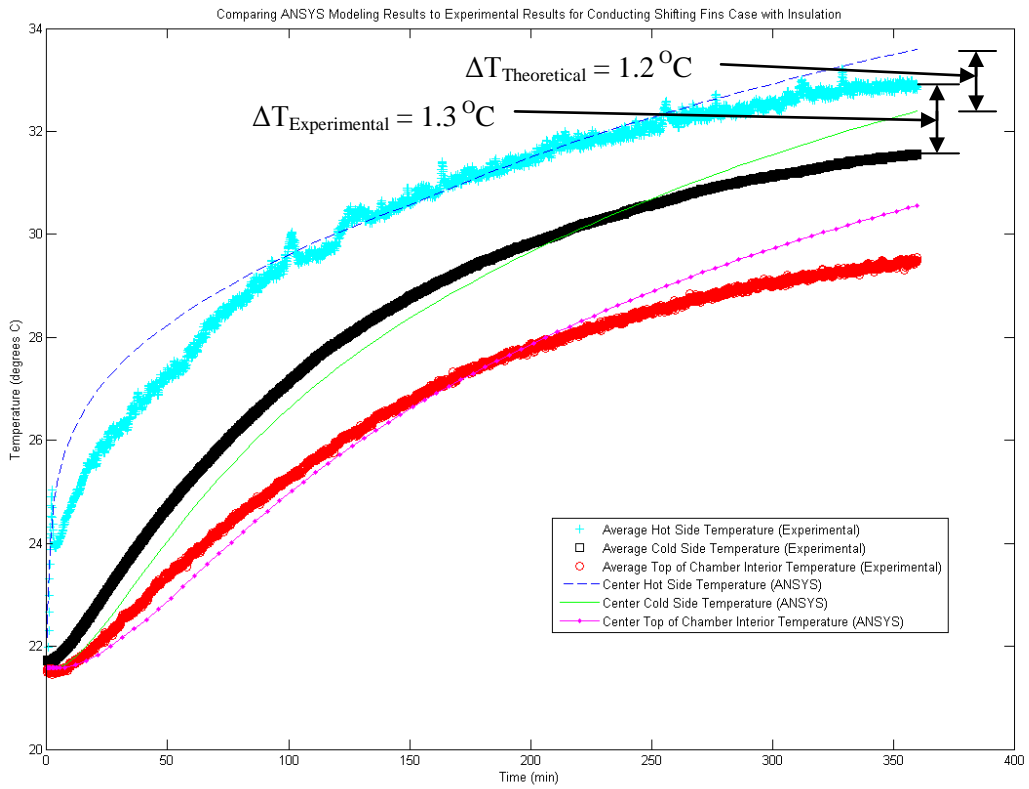


Figure 150: Comparison of Theoretical and Experimental Results for Conducting State of Shifting Fins Prototype with Insulation between Fins.

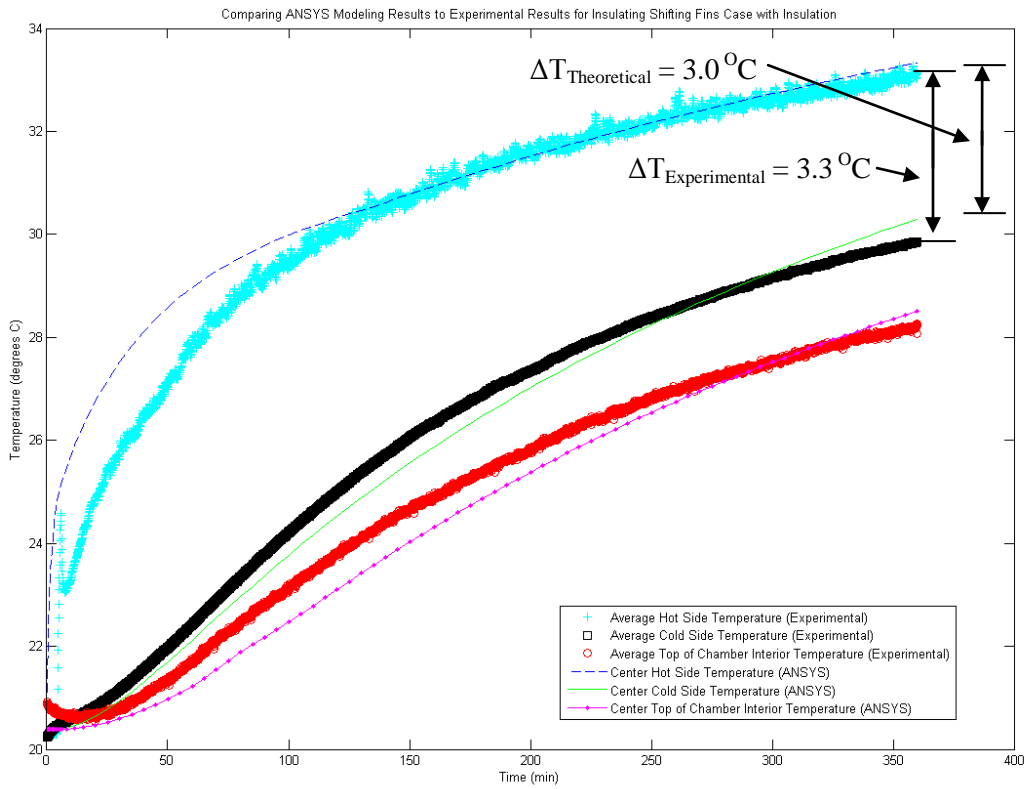


Figure 151: Comparison of Theoretical and Experimental Results for Insulating State of Shifting Fins Prototype with Insulation between Fins.

Finally, the hot side temperature, the cold side temperature, the top of the chamber interior temperature, and the ΔT value across the device are given at several points during the six hour time duration for the theoretical finite element model with the corresponding experimental temperatures values in Table 17.

Table 17: Shifting Fins Prototype with Insulation between the Fins Theoretical Results.

Constant Temperature Tests					
Conducting Configuration			Insulating Configuration		
1.5 hours into the test			1.5 hours into the test		
Measurement	Theoretical T (°C)	Experimental T (°C)	Measurement	Theoretical T (°C)	Experimental T (°C)
Hot Side Average	29.4	29.2	Hot Side Average	29.8	29.0
Cold Side Average	26.2	26.7	Cold Side Average	23.4	23.8
Top of Chamber Interior	24.6	24.9	Top of Chamber Interior	22.2	22.8
ΔT	3.2	2.5	ΔT	6.4	5.2
3 hours into the test			3 hours into the test		
Measurement	Theoretical T (°C)	Experimental T (°C)	Measurement	Theoretical T (°C)	Experimental T (°C)
Hot Side Average	31.2	31.1	Hot Side Average	31.2	31.3
Cold Side Average	29.2	29.5	Cold Side Average	26.5	26.9
Top of Chamber Interior	27.4	27.5	Top of Chamber Interior	24.9	25.4
ΔT	2.0	1.7	ΔT	4.8	4.5
At the end of the 6 hour test			At the end of the 6 hour test		
Measurement	Theoretical T (°C)	Experimental T (°C)	Measurement	Theoretical T (°C)	Experimental T (°C)
Hot Side Average	33.6	32.8	Hot Side Average	33.3	33.1
Cold Side Average	32.4	31.6	Cold Side Average	30.3	29.9
Top of Chamber Interior	30.6	29.5	Top of Chamber Interior	28.5	28.2
ΔT	1.2	1.3	ΔT	3.0	3.3

From both Figures 150 and 151 for the conducting and insulating configurations of the shifting fins prototype, the theoretical temperature results and ΔT values from the transient finite element model closely matched the experimental results over the entire length of the constant temperature tests. As a result of the close agreement between the theoretical and experimental results, it can be assumed that the transient finite element model sufficiently describes the conditions of the experimental testing of the shifting fins prototype. In addition, the theoretical results help to confirm that the experimental results for the insulating and conducting states of the shifting fins prototype were correct and that the test chamber set-up was not resulting in temperature measurement values that were unrealistic from a theoretical perspective.

5.3 OTHER VARIATIONS OF THE SHIFTING FINS PROTOTYPE MODELED

Once a theoretical model was developed that adequately described the experimental results for both the insulating and conducting states of the shifting fins thermal semiconductor with insulation between the fins, the same general model was used to analyze the performance of several other fins-related smart insulation concepts that were not experimentally tested. The three additional cases modeled consisted of a device that had the lower and upper fins contact at their sides instead of vertically, another device that had the fins fold inward from a stowed, horizontal position to contact vertically, and a final device that used lower and upper fins that both folded and contacted at their sides. For the theoretical modeling of all three variations of the original shifting fins prototype, the same thermal boundary conditions, hot side air space convection coefficients, cold side air space convection coefficients, meshing characteristics, time step size, and six-hour time duration were used as for the original model of the shifting fins prototype. The initial condition for the three additional cases was given a value of 21.6 °C, which was the initial temperature condition for the conducting state of the original shifting fins prototype model. The only differences between the models of the three additional fins-related devices and the original shifting fins prototype model were the changes in the geometry and fin arrangement for the different devices.

5.3.1 Shifting Fins with Side Contact Device Theoretical Model

The first additional fins-related concept that was modeled was the shifting fins with side contact device. The main advantage the new modified device had over the original shifting fins prototype was the additional contact surface area in the device's conducting state between the lower and upper fins of the device when the fins contacted at their sides instead of vertically. Within the original shifting fins prototype, the lower and upper fins of the device only contacted vertically over their ¼ in. (0.635 cm) widths, but for the new shifting fins with side contact design, the lower and upper fins of the device contact over much larger heights at their sides of 1 in. (2.54 cm), increasing the contacting surface area

between the lower and upper fins by a factor of four. By increasing the contact surface area between the lower and upper fins in the modified device's conducting state, the conduction heat transfer over the new design should greatly improve. Figures 152 and 153 show the conducting and insulating configurations of the shifting fins with side contact device constructed in the FEA software.

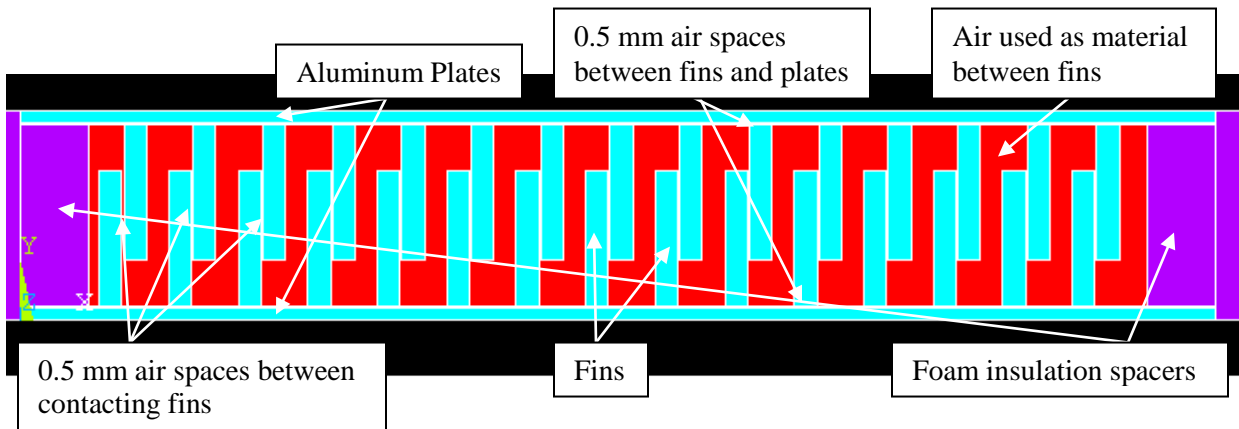


Figure 152: Conducting State of Shifting Fins with Side Contact Device Constructed in FEA Software.

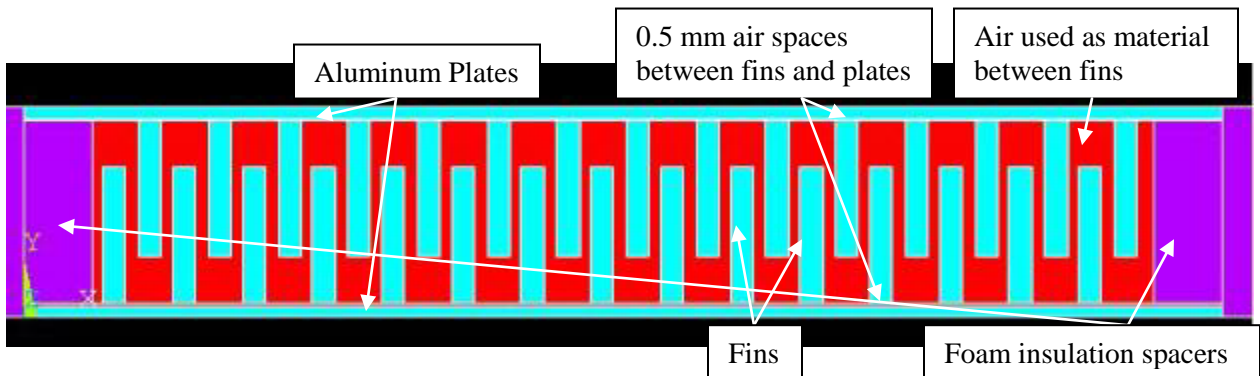


Figure 153: Insulating State of Shifting Fins with Side Contact Device Constructed in FEA Software.

As shown in Figures 152 and 153, a few changes were made in the design of the shifting fins with side contact model compared to the original shifting fins prototype besides having the fins contact at their

sides instead of vertically. First, the height of the fins was increased from an original value of 1 in. (2.54 cm) to a value of 1.5 in. (3.81 cm) for the shifting fins with side contact device in order to achieve a new contact surface area with dimensions of 1 x 13.25 in. (2.54 x 33.66 cm). Second, small air spaces of 0.5 mm were added into the model between the lower and upper fins contacting at their sides to simulate thermal contact resistance at the interfaces between the contacting fins. Finally, for the shifting fins with side contact device air was utilized as the material between the fins instead of the foam polyisocyanurate building insulation material, but convection heat transfer of the air between the fins of the device between the device's hot and cold sides was not considered in the model for simplification.

Plots of the theoretical temperature results calculated using the model of the shifting fins with side contact device are shown in Figures 154 and 155 for the device's conducting and insulating states respectively, while Table 18 gives the results of the shifting fins with side contact device at several different time intervals during the six-hour time duration.

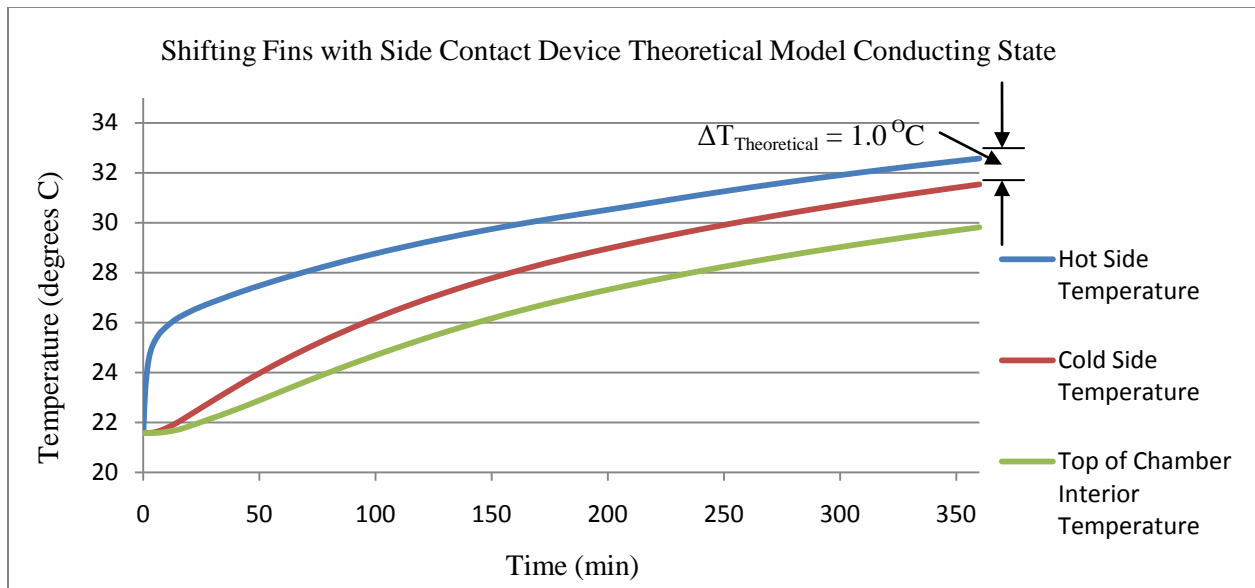


Figure 154: Shifting Fins with Side Contact Device Theoretical Results for Conducting State.

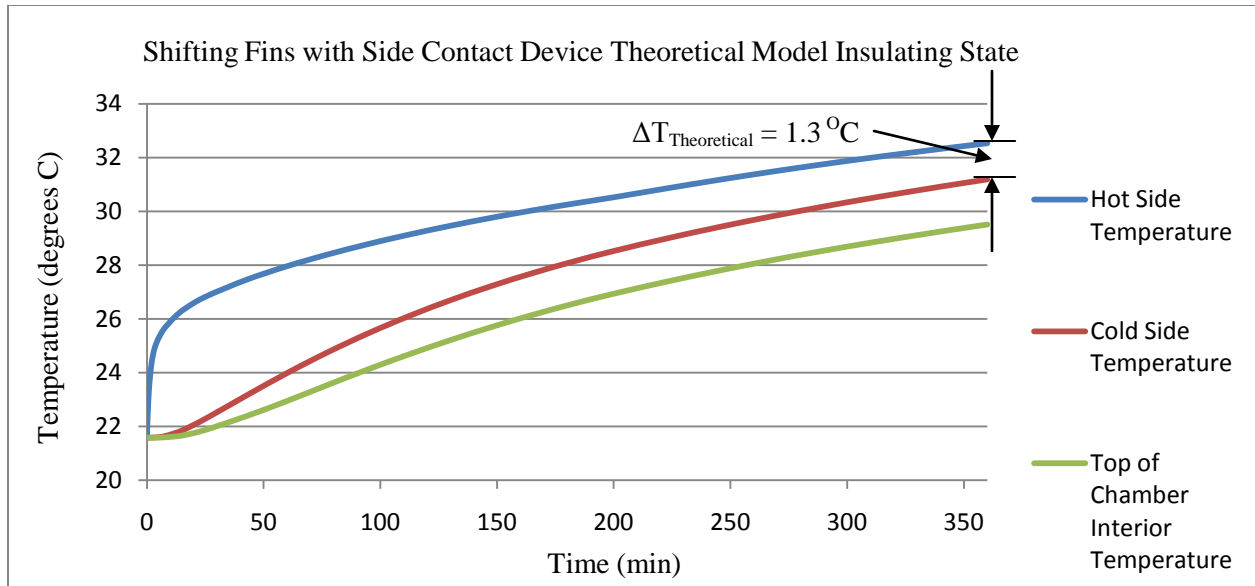


Figure 155: Shifting Fins with Side Contact Device Theoretical Results for Insulating State.

Table 18: Shifting Fins with Side Contact Device Theoretical Results.

Constant Temperature Tests					
Conducting Configuration			Insulating Configuration		
1.5 hours into the test			1.5 hours into the test		
Measurement	Theoretical T (°C)	% of Benchmark	Measurement	Theoretical T (°C)	% of Benchmark
Hot Side Average	28.6		Hot Side Average	28.8	
Cold Side Average	26.0		Cold Side Average	25.5	
Top of Chamber Interior	24.5		Top of Chamber Interior	24.1	
ΔT	2.6	27.3	ΔT	3.3	34.6
3 hours into the test			3 hours into the test		
Measurement	Theoretical T (°C)	% of Benchmark	Measurement	Theoretical T (°C)	% of Benchmark
Hot Side Average	30.3		Hot Side Average	30.3	
Cold Side Average	28.6		Cold Side Average	28.1	
Top of Chamber Interior	27.0		Top of Chamber Interior	26.6	
ΔT	1.7	18.7	ΔT	2.2	24.1
At the end of the 6 hour test			At the end of the 6 hour test		
Measurement	Theoretical T (°C)	% of Benchmark	Measurement	Theoretical T (°C)	% of Benchmark
Hot Side Average	32.6		Hot Side Average	32.5	
Cold Side Average	31.5		Cold Side Average	31.2	
Top of Chamber Interior	29.8		Top of Chamber Interior	29.5	
ΔT	1.0	11.3	ΔT	1.3	14.6

Comparing the results of Table 18 to the results for the shifting fins thermal semiconductor with insulation between the fins, the shifting fins with side contact device did not perform well as a smart insulation device. Increasing the contact surface area between the lower and upper fins only slightly improved the performance of the shifting fins device with the ΔT value for its conducting state decreasing from 13.4% of the ΔT value for the benchmark insulation test piece for the shifting fins prototype with insulation between the fins to 11.3% of the ΔT value for the benchmark insulation test piece for the shifting fins with side contact device. Although the shifting fins with side contact device's conducting state had slightly improved performance, the new device's insulating state had significantly decreased performance compared to the shifting fins prototype with insulation between fins. The ΔT value

simulated at the end of the constant temperature test for the shifting fins with side contact device was only 14.6% of the benchmark insulation test piece's ΔT value, which was less than half the 34.5% of the benchmark insulation test piece's ΔT value simulated for the shifting fins device with insulation between fins.

5.3.2 Folding Fins with Vertical Contact Device Theoretical Model

After the modeling of the shifting fins with side contact device had been completed, the next fins-related design modeled was the folding fins with vertical contact device. In this device the conducting configuration of the design was very similar to the conducting arrangement of the basic shifting fins thermal semiconductor. The insulating state of the folding fins with vertical contact device, however, is much different from that of the basic shifting fins prototype in that it consists of lower and upper fins in a horizontal, folded in, stowed position with a 1.5 in. (3.81 cm) air gap between the lower and upper fins to nearly eliminate any conduction heat transfer. Figures 156 and 157 show the conducting and insulating configurations of the folding fins with vertical contact device constructed in the FEA software.

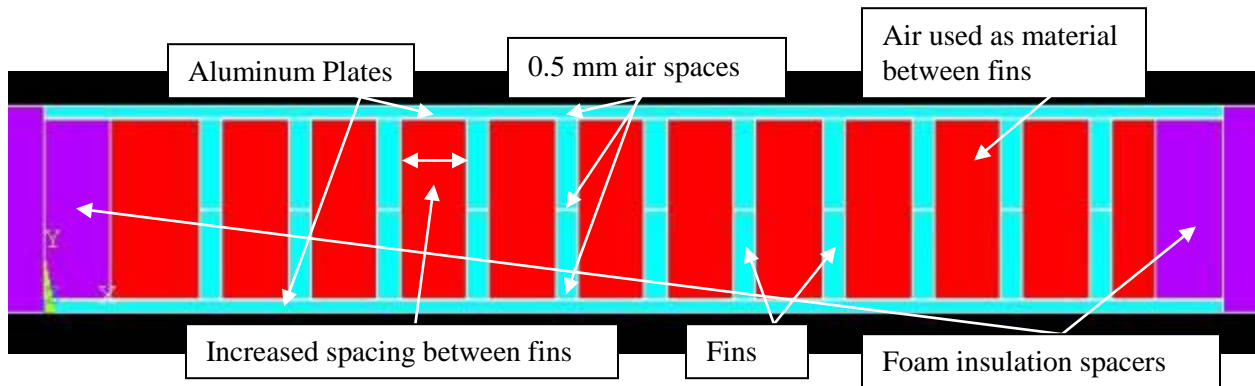


Figure 156: Conducting State of Folding Fins with Vertical Contact Device Constructed in FEA Software.

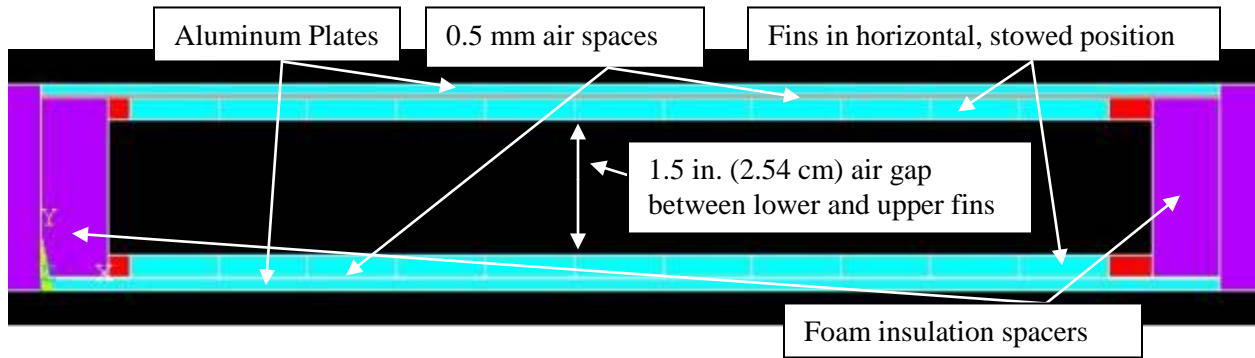


Figure 157: Insulating State of Folding Fins with Vertical Contact Device Constructed in FEA Software.

As shown in Figure 156, in the design of the folding fins with vertical contact device, the spacing between the fins in the device's conducting state had to be increased from an original center-to-center distance of 0.75 in. (1.91 cm) to 1 in. (2.54 cm) to allow enough space for the fins to fold to their stowed positions for the device's insulating state. As a result of the increased fin spacing, the overall number of fins in the folding fins with vertical contact device had to be decreased to 22 from 30 fins for the original shifting fins device. Also, as for the shifting fins with side contact device, air was utilized as the material between the fins for the folding fins with vertical contact device, but convection heat transfer of the air between the fins of the device between the device's hot and cold sides was again not considered in the model for simplification.

During the modeling of the insulating state of the folding fins with vertical contact device, alternating LINK34 and LINK32 1-D convective elements were again utilized to model the both convection and conduction heat transfer across the 1.5 in. (2.54 cm) air gap between the hot and cold sides of the device. An image that illustrates how the LINK32 and LINK34 elements were used to model the convection and conduction across the air gap from the hot side to the cold side by connecting them to the horizontal, stowed lower and upper fins on each side of the air gap is shown in Figure 158. In order to calculate the

convection coefficients for the convection across the air gap as a function of temperature, the same type of procedure that was followed for the shifting fins prototype earlier was used.

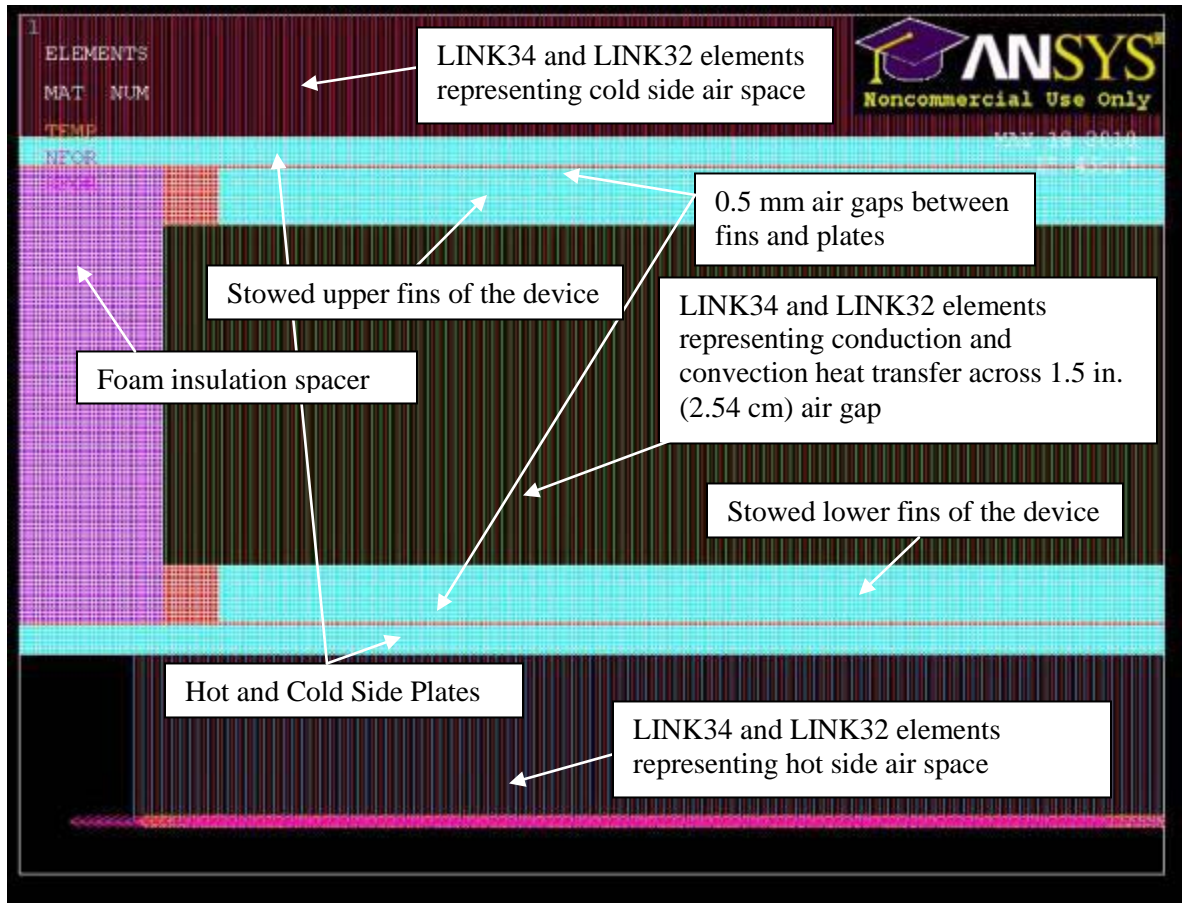


Figure 158: How LINK32 and LINK34 elements Modeled Conduction and Convection across Air Gap.

First, Rayleigh numbers were calculated for the 1.5 in. (2.54 cm) air gap using the equations for natural convection between two constant temperature surfaces in an enclosure used beforehand for the calculation of hot and cold side air space convection coefficients [26]. As a result of the temperatures of the two sides of the air gap in the folding fins with vertical contact device changing during the test, the Rayleigh numbers had to be calculated as a function of the average temperature for the air gap, which was assumed to be the average temperature between the cold and hot side plates of the device. Using Equation 5.18 the Rayleigh numbers were calculated for the air gap between the hot and cold sides of the device

with β determined in Equation 5.18 from the expression found in Equation 5.19. A value of 1.5 in. (3.81 cm) was utilized for δ in Equation 5.18 because it was the distance across the air gap between the hot and cold sides of the device. Examining Equation 5.18 shows that the temperature differences across the 1.5 in. (2.54 cm) air gap were needed in order to calculate the Rayleigh numbers and consequently the convection coefficients for the air gap in the folding fins with vertical contact device. To calculate the Rayleigh numbers the temperature differences from the experimental results of the constant temperature test that consisted simply of two 13.25 x 13.25 in. (0.337 x 0.337 m) aluminum alloy 6061 plates with 1/8 (0.318 cm) thickness with a 2 in. air gap in between them for different average air gap temperatures were utilized.

$$Ra = \frac{g\beta (T_{Hot Side Plate} - T_{Cold Side Plate})\delta^3}{\nu_{Air} \alpha_{Air}} \quad (5.18)$$

$$\beta = \frac{1}{\frac{T_{Cold Side Plate} + T_{Hot Side Plate}}{2} + 273.15} \quad (5.19)$$

Once the Rayleigh numbers were calculated for the air gap of the folding fins with vertical contact device as a function of temperature, the next step was to determine the different Nusselt numbers corresponding to each of the Rayleigh numbers. For the air gap between the hot and cold sides of the device, the calculated Rayleigh numbers varied from near 0 to around 37,600, requiring the use of two different empirical relations for the Nusselt number, Equation 5.7 and Equation 5.8 with the Rayleigh number range for which each is applicable [26]. Finally, using the calculated Nusselt numbers the convection coefficients for the air gap of the folding fins with vertical contact device were determined using Equation 5.9 [26]. The convection coefficients for the 1.5 in. (2.54 cm) air gap of the folding fins with vertical contact device as a function of the average air gap temperature are given in Table 19.

Table 19: Convection Coefficients for Air Gap in Folding Fins with Vertical Contact Device.

$T_{\text{Air Gap, Average}} (^{\circ}\text{C})$	$h_{\text{Air Gap}} (\text{W}/\text{m}^2\text{-K})$
21.3	0.01
22.1	1.41
22.9	1.66
23.7	1.82
24.5	1.92
25.3	1.98
26.1	2.02
26.9	2.04
27.7	2.02
28.5	2.00
29.3	1.97
30.1	1.91
30.9	1.87
31.7	1.80

Plots of the theoretical temperature results calculated using the model of the folding fins with vertical contact device are shown in Figures 159 and 160 for the device's conducting and insulating states respectively, while Table 20 gives the results of the folding fins with vertical contact device at several different time intervals during the six-hour time duration.

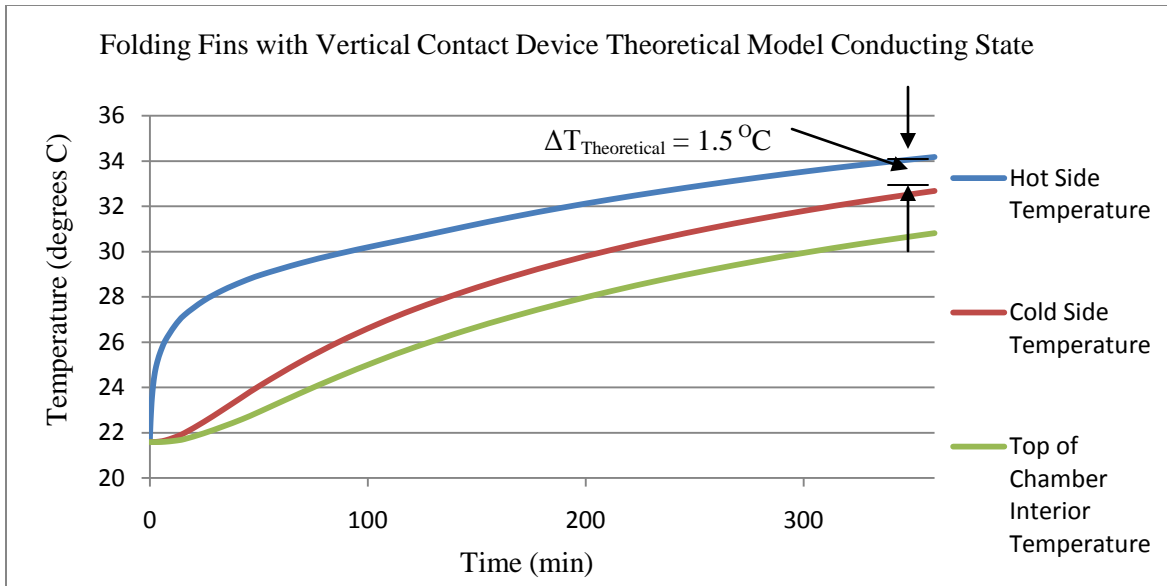


Figure 159: Folding Fins with Vertical Contact Device Theoretical Results for Conducting State.

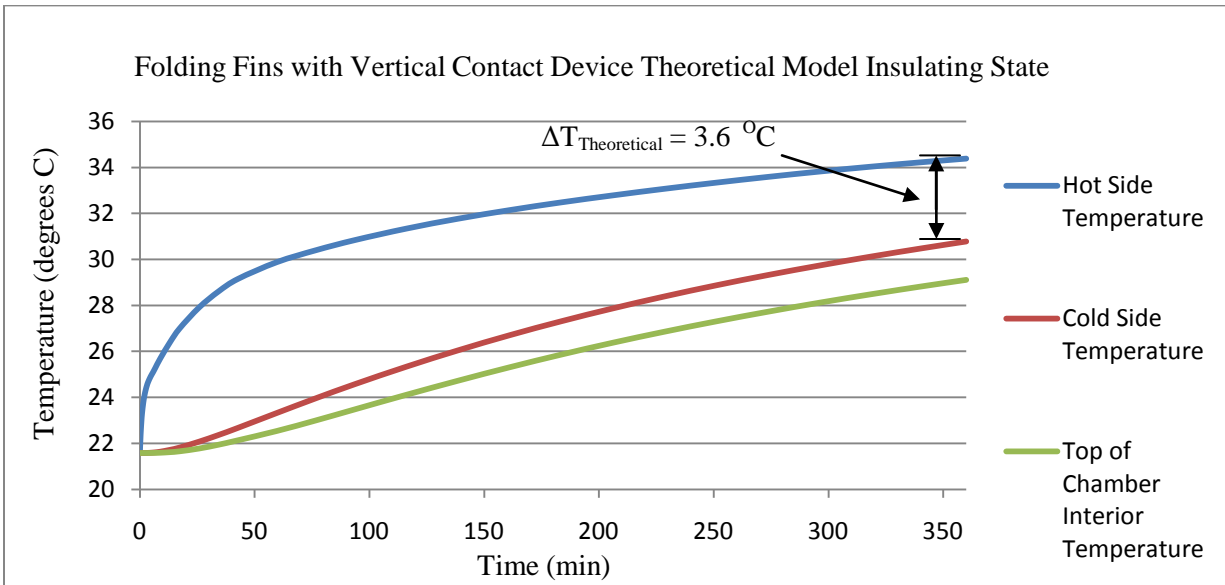


Figure 160: Folding Fins with Vertical Contact Device Theoretical Results for Insulating State.

Table 20: Folding Fins with Vertical Contact Device Theoretical Results.

Constant Temperature Tests					
Conducting Configuration			Insulating Configuration		
1.5 hours into the test			1.5 hours into the test		
Measurement	Theoretical T (°C)	% of Benchmark	Measurement	Theoretical T (°C)	% of Benchmark
Hot Side Average	29.9		Hot Side Average	30.8	
Cold Side Average	26.0		Cold Side Average	24.6	
Top of Chamber Interior	24.5		Top of Chamber Interior	23.5	
ΔT	3.9	40.9	ΔT	6.3	66.1
3 hours into the test			3 hours into the test		
Measurement	Theoretical T (°C)	% of Benchmark	Measurement	Theoretical T (°C)	% of Benchmark
Hot Side Average	31.9		Hot Side Average	32.5	
Cold Side Average	29.5		Cold Side Average	27.3	
Top of Chamber Interior	27.7		Top of Chamber Interior	25.9	
ΔT	2.4	26.3	ΔT	5.2	57.0
At the end of the 6 hour test			At the end of the 6 hour test		
Measurement	Theoretical T (°C)	% of Benchmark	Measurement	Theoretical T (°C)	% of Benchmark
Hot Side Average	34.2		Hot Side Average	34.4	
Cold Side Average	32.7		Cold Side Average	30.8	
Top of Chamber Interior	30.8		Top of Chamber Interior	29.1	
ΔT	1.5	16.9	ΔT	3.6	40.5

From the results of Table 20, the modeling of the folding fins with vertical contact device predicts that a folding fins with vertical contact prototype will have slightly better performance than the shifting fins thermal semiconductor with insulation between the fins, since a slightly larger change in the ΔT value occurs for the folding fins with vertical contact device when the device is actuated from its conducting state to its insulating state. As the folding fins with vertical contact device was changed between low and high heat transfer states, its ΔT value at the end of the constant temperature tests was able to vary from 16.9 – 40.5% of the benchmark insulation test piece’s ΔT value compared to a range of ΔT between 13.4 – 34.5% of the benchmark insulation test piece’s ΔT value for the shifting fins device with insulation between fins. Furthermore, an actual folding fins with vertical contact device would likely

have even greater performance in its conducting state than predicted by the model from the convection occurring in the air between the fins across the prototype from its hot side to its cold side. Due to the complexity of the convection of the air between the fins of the device, the convection was not incorporated into the folding fins with vertical contact device's conducting state during the modeling, but convection was included for the modeling of the insulating state of the device, since it involved the much simpler convection case of an air gap between two constant temperature surfaces. During the testing of the original shifting fins prototype, using air between the fins of the device instead of insulation reduced the ΔT value from 13.4% to 8.8% of the benchmark insulation test piece's ΔT value from the convection of the air between the fins. Similar improvement in the conducting state of the folding fins with vertical contact device from the convection of the air between fins across the device would result in a folding fins with vertical contact device with significantly improved performance over the shifting fins device with insulation between fins.

5.3.3 Folding Fins with Side Contact Device Theoretical Model

The final fins-related case modeled using the FEA software was the folding fins with side contact device, which essentially combined the two previous concepts modeled by having a smart insulation prototype with greater contact surface area as a result of the fins contacting at their sides instead of vertically and with folding fins to create a 1.5 in. (2.54 cm) air gap to inhibit conduction heat transfer in the device's insulating state. Figure 161 shows the conducting configuration of the folding fins with side contact device constructed in the FEA software. For the insulating state of the folding fins with side contact device, the results of the modeling of the folding fins with vertical contact device were utilized, since the insulating configurations of both devices with the fins in a stowed, horizontal position have the same basic geometry and fin arrangement.

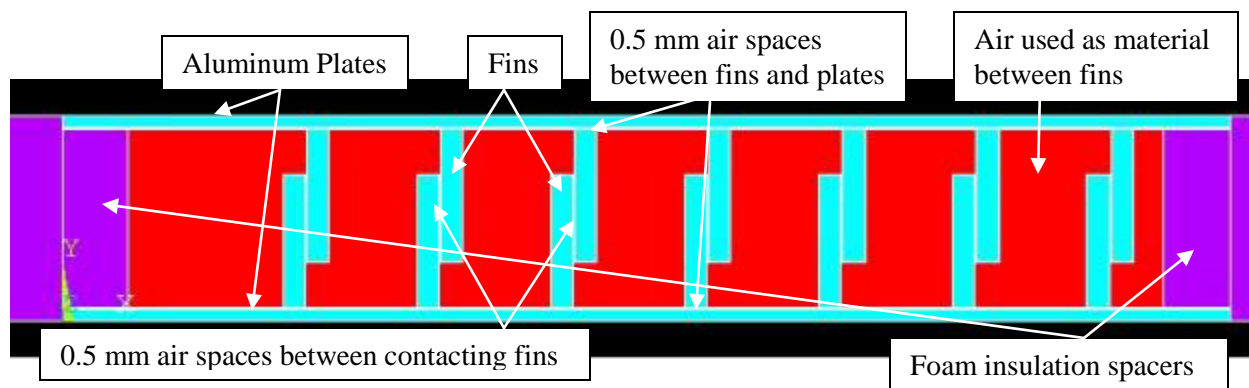


Figure 161: Conducting State of Folding Fins with Side Contact Device Constructed in FEA Software.

Figure 161 shows that the conducting state of the folding fins with side contact device is very similar to the conducting state of the shifting fins with side contact device modeled earlier. The only difference between the two types of smart insulation devices is the much greater fin spacing that was needed for the folding fins with side contact device to allow the fins to fold into their stowed, horizontal configuration for the device's insulating state. In the design of the folding fins with side contact device, the spacing between the fins in the device's conducting state had to be increased from an original center-to-center distance of 0.75 in. (1.91 cm) to 1.5 in. (3.81 cm), which resulted in the overall number of fins in the folding fins with side contact device being decreased to 14 from 30 fins for the shifting fins with side contact device. In Figure 162, a plot is given of the theoretical temperature results calculated using the model of the conducting state of folding fins with side contact device, while Table 21 gives the results of the folding fins with side contact device at several different time intervals during the six-hour time duration.

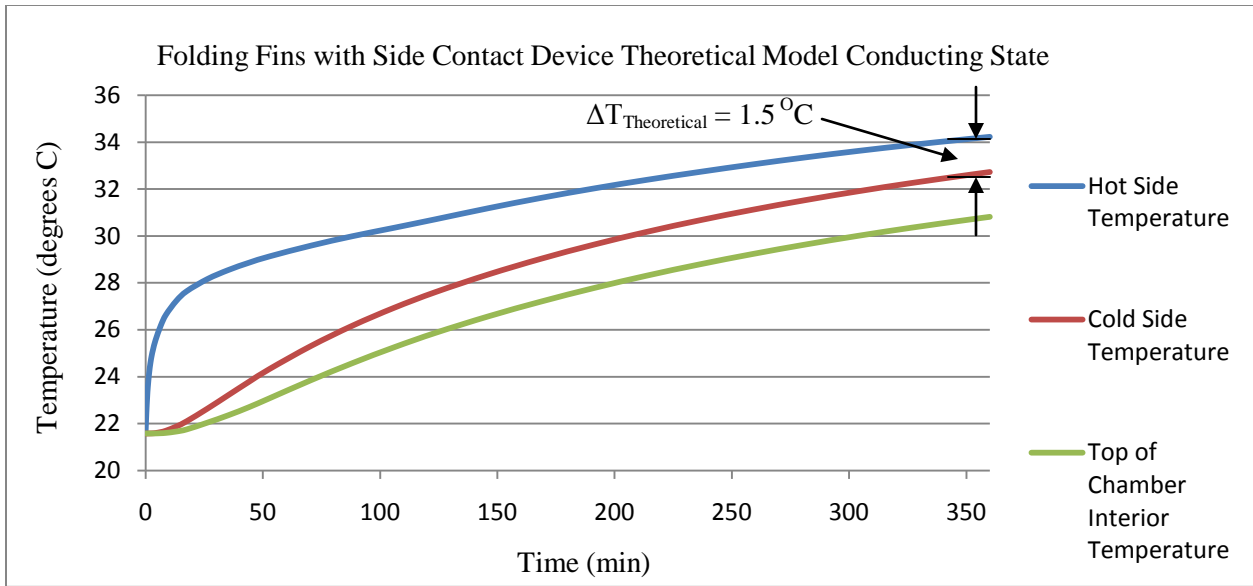


Figure 162: Folding Fins with Side Contact Device Theoretical Results for Conducting State.

Table 21: Folding Fins with Side Contact Device Theoretical Results.

Constant Temperature Tests					
Conducting Configuration			Insulating Configuration		
1.5 hours into the test			1.5 hours into the test		
Measurement	Theoretical T (°C)	% of Benchmark	Measurement	Theoretical T (°C)	% of Benchmark
Hot Side Average	30.0		Hot Side Average	30.8	
Cold Side Average	26.2		Cold Side Average	24.6	
Top of Chamber Interior	24.6		Top of Chamber Interior	23.5	
ΔT	3.8	39.8	ΔT	6.3	66.1
3 hours into the test			3 hours into the test		
Measurement	Theoretical T (°C)	% of Benchmark	Measurement	Theoretical T (°C)	% of Benchmark
Hot Side Average	31.8		Hot Side Average	32.5	
Cold Side Average	29.3		Cold Side Average	27.3	
Top of Chamber Interior	27.5		Top of Chamber Interior	25.9	
ΔT	2.5	27.4	ΔT	5.2	57.0
At the end of the 6 hour test			At the end of the 6 hour test		
Measurement	Theoretical T (°C)	% of Benchmark	Measurement	Theoretical T (°C)	% of Benchmark
Hot Side Average	34.2		Hot Side Average	34.4	
Cold Side Average	32.7		Cold Side Average	30.8	
Top of Chamber Interior	30.8		Top of Chamber Interior	29.1	
ΔT	1.5	16.9	ΔT	3.6	40.5

The folding fins with side contact device had almost exactly the same performance as the folding fins with vertical contact device after reviewing the results of Table 21 with both devices having the same possible variation of ΔT between their conducting and insulating states. Among the three additional fins-related cases that were analyzed using the original theoretical, finite element model developed from the shifting fins prototype with insulation between fins, both of the folding fins devices were predicted to have much better performance than the shifting fins with side contact device modeled and slightly better performance than any of the previous shifting fins devices that were experimentally tested. Overall, however, for all of the different fins-related devices that were tested or modeled, the back-to-back plates

with fins prototype had the best performance as a smart insulation device and remains the best candidate to further pursue in the future.

6.0 CONCLUSION AND FUTURE WORK

6.1 CONCLUSION

Many different concepts for variable insulation devices were considered for use as smart insulation in buildings, and the two best ideas were chosen for actual fabrication and experimental testing after a careful examination of which concepts had the best combination of low-cost, easy implementation, feasibility, and short-term payoff. One of the ideas revolved around a thermal semiconductor using contacting/non-contacting fins to make or break a thermal conduction path, while the other idea focused on an inflatable thermal semiconductor with a honeycomb-like structure filled with air to inhibit conduction and convection when inflated. After the smart insulation concepts had been selected, several different variations of the shifting fins and inflatable smart insulation devices were designed and fabricated in the laboratory, and an insulation test chamber was constructed for running experiments on the smart insulation devices under testing conditions similar to what the insulation would encounter in a real-world building setting. Each of different smart insulation prototypes was tested under both constant heat flux and constant temperature conditions so that the devices could be compared to each other to determine which had the best performance as a smart insulation device.

From the experimental testing proof-of-concept was achieved for smart insulation devices, since a change in thermal conductivity was measured for all of the different thermal semiconductors when they were switched between their conducting and insulating states. Once testing was completed the best two smart insulation designs were found to be the back-to-back with outward facing fins device and the NOVUS inflatable thermal semiconductor with aluminum plates. Both of these designs show the best

ability to change from a very low conductance state to a very high conductance state and vice versa. To further improve the insulator state of the back-to-back plates with fins device, the fins should be designed so that they can be folded inward to a horizontal, stowed position in the device's insulator state, which will decrease the heat transfer through the device in that state by reducing the effective surface area of the fins, while not decreasing the performance of the device in its conductor state. Likewise, for the insulator states of the NOVUS inflatable thermal semiconductors, reducing the volume of the device's chambers of air will also decrease the heat transfer through the devices in their insulating configurations, while having no effect on the devices' performance in their conducting configurations. Finally, to enable the device's insulator state to achieve or exceed the performance of the benchmark conventional insulation test piece, an additional layer of conventional insulation could be added on top of the smart insulation that would be present for both the smart insulation's conducting and insulating states. Although this will decrease the performance of the conducting states of the smart insulation devices, it will also allow the smart insulation devices to function as well as conventional building insulation in their insulating states, while still allowing the smart insulation devices to function as much better conductors than conventional insulation in their conducting states.

To confirm the validity of the results of the experimental testing, a theoretical model was developed of the shifting fins prototype with insulation between the fins. Using finite element analysis software, a transient, thermal model of the insulating and conducting configurations of the shifting fins prototype with insulation between the fins was formulated with the shifting fins device in the model under the same type of conditions imposed in the insulation test chamber experimental set-up. Reviewing the results of the theoretical finite element model showed very close agreement between the calculated theoretical temperature results of the model and the actual measured experimental temperature results for the device. As a result of this close agreement, using the transient finite element model other types of smart insulation devices not originally experimentally tested were also examined to evaluate their performance and to determine if any other smart insulation concepts should be fabricated for additional testing.

6.1 FUTURE WORK

To continue to advance the development of smart insulation technologies, one of the first steps will need to be a new detailed simulation study involving the use of variable insulation in buildings to calculate the possible energy and cost savings of smart insulation. While a previous simulation study by the Department of Energy conducted in 1990 does exist on this topic, building energy simulation software has improved greatly in the past twenty years with the development of software, such as EnergyPlus, and several shortcomings of the original study could be addressed in a new building insulation simulation. Using the results of the new simulation study and the experimental testing of the smart insulation prototypes, a cost-benefit analysis of the smart insulation concepts compared to conventional building insulation, such as fiberglass, will also need to be conducted in order to examine the amount of energy and cost savings weighed against any additional costs of implementing the smart insulation concepts.

Also, the practicality of the smart insulation concepts fabricated and tested in an actual building setting should be examined further. In particular, a more detailed examination of how to implement smart insulation in the roofs of buildings should be pursued, since the roof area was earlier determined to be the best location for smart insulation. Once this analysis is completed, an additional analysis involving the placement of the smart insulation concepts in the exterior walls for an entire building can be added on top of the roof smart insulation implementation analysis done earlier. Finally, through larger scale experimental testing or more detailed finite element modeling, the actual conditions the smart insulation concepts will encounter if implemented in a building for the different periods of a day, different seasons of a year, or cloudy vs. sunny conditions should be more accurately simulated.

BIBLIOGRAPHY

- [1] Allen Chen. Closing in on Zero-Energy Buildings. *EETD News*. Vol. 8, No. 2, Lawrence Berkeley National Laboratory, Fall 2009. <http://eetd.lbl.gov/newsletter/nl29/>, January 2010. [Active].
- [2] Thomas F. Potter and Adrian Tuluca. Identification of Building Applications for a Variable-Conductance Insulation. National Renewable Energy Laboratory, ACEEE 1992 Summer Study on Energy Efficiency in Buildings, Pacific Grove, CA, August 30-September 5, 1992.
- [3] Donald A. Neeper and Robert D. McFarland. Some Potential Benefits of Fundamental Research for the Passive Solar Heating and Cooling of Buildings. Technical report, Los Alamos National Laboratory, Department of Energy, LA-9425-MS, August 1982.
- [4] Donald A. Neeper. Impacts of Research Efforts on New and Existing Buildings. Los Alamos National Laboratory, Solar Buildings: Realities for Today, Trends for Tomorrow, Washington, D.C., March 18-20 1985.
- [5] H.P. Bovenkerk. Insulating Structures with Variable Thermal Conductivity and Method of Evacuation, U.S. patent number 3167159, January 26, 1965.
- [6] Theodore Xenophou, System of Using Vacuum for Controlling Heat Transfer in Building Structures, Motor Vehicles, and the Like, U.S. patent number 3968831, July 13, 1976.
- [7] Steven D. Burch, Thomas F. Potter, Matthew A. Keyser, Michael J. Brady, Kenton F. Michaels. Reducing Cold-Start Emissions by Catalytic Converter Thermal Management. Technical Report. National Renewable Energy Laboratory, Department of Energy, NREL/TP-473-7025, January 1995.
- [8] Steven D. Burch, Richard C. Parish, Matthew A. Keyser. Thermal Management of Batteries Using a Variable-Conductance Insulation (VCI) Enclosure. National Renewable Energy Laboratory, Intersociety Energy Conversion Engineering Conference, Orlando, FL, July 31-August 4, 1995.
- [9] Steven J. Eickhoff and Chunbo Zhange. Variable Resistor System, U.S. patent number 2008/0203081, Honeywell International, Inc., August 28, 2008.
- [10] H.E. Riordan. Device for Controlling Temperature by Heat Conduction, U.S. patent number 3225820, December 28, 1965.
- [11] Thomas F. Potter. Variably Insulating Portable Heater/Cooler, U.S. patent number 5813454, Varitec Thermal, L.L.C., September 29, 1998.

- [12] Nickolaus Laing. Building Plates with Controllable Heat Insulation, U.S. patent number 3920953, November 18, 1975.
- [13] IBM Technical Disclosure Bulletin. Variable Thermal Resistance Insulator, 1979-2009. <http://www.priorartdatabase.com/IPCOM/000067768>, August 2009. [Active].
- [14] M.A. Al-Nimr, K.R. Asfar, T. T. Abbadi. Design of a Smart Thermal Insulation System. *Heat Transfer Engineering*. Vol. 30, No. 9, August 2009.
- [15] Atsushi Ochi, Toru Mori, Yuichi Shimikawa, Yoshimi Kubo, Akira Okamoto, Yasuyuki Nakamura, Sumitaka Tachikawa, Akira Ohnishi, Kazunori Shimazaki. Variable Thermal Emittance Radiator Using Metal-Insulator Phase Transition in $\text{La}_{1-x}\text{Sr}_x\text{MnO}_3$. *Japanese Journal of Applied Physics*. Vol. 41, No. 11B, 2002.
- [16] J. van Es and M. Bsibsi. VARIable Effective Surface Radiator Executive Summary. Technical Report, National Aerospace Laboratory of the Netherlands, VARES-TN-010-NLR-Issue 01, December 2006.
- [17] Randy Roguski. Greenhouse Experiment to Use Liquid Crystal Windows, Cleveland.com, January 8, 2008. http://blog.cleveland.com/business/2008/01/greenhouse_experiment_to_use_1.html, August 2009. [Active].
- [18] Smart Greenhouse Uses Liquid Crystal. Presstime Bulletin. *Photonics Spectra*. June 2008. <http://www.photonics.com/Article.aspx?AID=33868>, August 2009. [Active].
- [19] Ingeborg and Nickolaus Laing. Variable Insulation Means Utilizing Convection Generators, U.S. patent number 3814175, June 4, 1974.
- [20] Donald L. Davis, Adolph J. Strohlein, Jr.. Inflatable Heat Barrier, U.S. patent number 4301626, Effective Conservation Systems, Inc., November 24, 1981.
- [21] Wongee Chun and Kuan Chen. Test Results of a Bi-Directional Thermodiode System for Solar Energy Utilization. *Solar Energy*. Vol. 73, No. 4, October 2002.
- [22] W. Chun, Y. J. Ko, H. J. Lee, H. Han, J. T. Kim, K. Chen. Effects of Working Fluids on the Performance of a Bi-Directional Thermodiode for Solar Energy Utilization in Buildings. *Solar Energy*. Vol. 83, No. 3, March 2009.
- [23] H. A. Fine and D. L. McElroy. Assessment of the Energy Conservation Potential of Active (Variable Thermal Resistance and Switchable Absorptance) Building Thermal Insulation Systems. Technical Report, Oak Ridge National Laboratory, Department of Energy, ORNL/TM-11425, June 1990.
- [24] Thermal Conductivity of Some Common Materials. The Engineering ToolBox. http://www.engineeringtoolbox.com/thermal-conductivity-d_429.html, February 2010 [Active].
- [25] Properties of Metals-Thermal. Engineers Edge. http://www.engineersedge.com/properties_of_metals.htm, February 2010 [Active].

- [26] J.P. Holman. *Heat Transfer: Ninth Edition*. McGraw-Hill, New York, NY, 2002.
- [27] Thermal Contact Resistance. kxcad.net.
http://www.kxcad.net/SolidWorks/COSMOSWorks_online_help/AnalysisBackground/ThermalAnalysis/Thermal_Contact_Resistance.htm, February 2010 [Active]
- [28] About Cork: Properties. Cork Institute of America.
<http://www.corkinstitute.com/properties.html>, February 2010 [Active]
- [29] D. L. Caskey. Reflective Barriers for Reducing Home Roof Heat Loss. Technical Report, Department of Energy, DOE/R6/10952—T1, August 1980.
- [30] ASM Aerospace Specification Metals, Inc.
<http://asm.matweb.com/search/SpecificMaterial.asp?bassnum=MA6061T6>, May 2009 [Active].
- [31] Air Properties. The Engineering ToolBox.
http://www.engineeringtoolbox.com/air-properties-d_156.html, May 2009 [Active].
- [32] ANSYS Thermal Analysis Guide. ANSYS Release 10.0, August 2005.